An Evaluation of Different Material Line Insulators under High Voltage AC and Bipolar DC Excitation in a Marine Polluted Environment

by
Gerton Nicolaas Jacobus Mouton

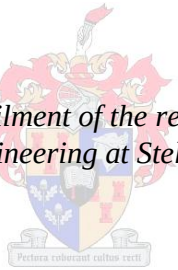

Thesis presented in partial fulfilment of the requirements for the degree Master of Science in Engineering at Stellenbosch University

Supervisor: Prof. HJ Vermeulen
Department of Electrical & Electronic Engineering

December 2012

Declaration

By submitting this thesis electronically, I declare that the entirety of the work contained therein is my own, original work, that I am the sole author thereof (save to the extent explicitly otherwise stated), that reproduction and publication thereof by Stellenbosch University will not infringe any third party rights and that I have not previously, in its entirety or in part, submitted it for obtaining any qualification.

Gerton Nicolaas Jacobus Mouton

December 2012

Abstract

The worldwide increase in the popularity of high voltage direct current (HVDC) power transmission application has led to questions regarding the performance of high voltage alternating current (HVAC) insulators when energized under HVDC excitation. These questions have led researchers conduct numerous research projects worldwide. A particular question NamPower (the power utility in Namibia) has faced is: how do these insulators perform and age when energized under HVDC excitation in heavily polluted environments? This question was only partly answered by some insulator ageing tests conducted under laboratory conditions for HVDC excitation. However, the natural ageing tests on insulators, which are preferred, have to date been confined predominantly to HVAC excitation voltages. Thus, this research was initiated to investigate the natural ageing performance of insulators under both HVAC and HVDC excitations, when subjected to harsh marine pollution environments.

This research project involved performance and ageing tests on three identical sets of line insulators made from different insulator materials, energised under HVAC and both polarities HVDC excitations respectively. The tests were conducted at Koeberg insulator pollution test station (KIPTS), which is a natural marine pollution insulator test station located near Cape Town, along the west coast of South Africa, approximately 50 m from the sea. The set of insulators consisted of EPDM silicone alloy rubber, HTV silicone rubber, RTV silicone rubber coated porcelain, Porcelain and Glass insulators. The HVAC excitation voltage was chosen as 12.7 kV r.m.s. phase-to-ground and it was decided to use a HVDC excitation voltage equal to this value.

The research results showed that the insulators made from HTV silicone rubber performed better than the insulators made from EPDM silicone alloy rubber under all excitation voltages. It is also showed that RTV silicone rubber coated porcelain insulators performed better than Glass and Porcelain insulators under all excitation voltages.

Opsomming

Die wêreld wye toename in gewildheid van hoë spanning gelyk stroom (HSGS) krag transmisie aplikasie het gelei na vrae oor die effektieweteit van hoë spanning wissel stroom (HSWS) insolators in HSGS aplikasies. Hierdie vrae het gelei na baie navorsings projekte. Een vraag waarmee NamPower (die krag voorsienings maatskapy in Namibia) gekonfronteer was, was hoe gaan die insolators wat onderworpe is aan ’n HSGS toevoer reageer in ’n baie besoedelde omgewing. Hierdie vraag was slegs gedeeltelik beantwoord deur verouderings toetse op insolators wat gedoen is in ’n labaratorium met ’n HSGS toevoer. Inteendeel, die meeste natuurlike verouderings toetse op insolators, soos verkies, is meestal gedoen met ’n HSWS toevoer. Om hierdie rede was hierdie navorsing begin om natuurlike verouderings toetse te doen op insolators onderworpe beide aan HSWS en HSGS toevoere binne ’n marien besoedelde omgewing.

Hierdie navorsings projek gaan oor prestering en verouderings toetse op drie, identiese, transmissie lyn insolator stelle, wat onderskeidelik onderworpe was aan HSWS en beide polariteite HSGS toevoere. Die toetse was gedoen by Koeberg insolator besoedeling toets stasie (KIBTS) wat naby Kaapstad geleë is langs die weskus van Suid Africa omtrent 50 m van die see. ’n Stel toets insolators bestaan uit EPDM silikon allooi rubber, HTV silikon rubber, RTV silikon rubber bedekte porselein, Porselein en Glas insolators. Die HSWS waarde waarmee die insolators getoets was, was 12.7 kV w.g.k., fase-na-grond, en dit was besluit om ’n HSGS waarde gelyk aan hierdie spannings waarde te gebruik.

Die navorsings resultate wys dat insolators wat gemaak is met HTV silikon rubber presteer beter as insolators wat met EPDM silikon allooi rubber gemaak is onder al die verskillende toevoere. Dit wys ook dat RTV silikon rubber bedekte porselein presteer beter as Porselein en Glas insolators onder al die verskillende toevoere.

Acknowledgements

- I herewith want to thank my Lord and Savior, Jesus Christ, for providing me this opportunity and for giving me the wisdom and strength to finish this project.
- A special thank you to Prof. H.J. Vermeulen, my supervisor, for his guidance and support throughout this project.
- The valuable contributions of Dr. J.P. Holtzhausen, Dr. W.L. Vosloo and Mr. P.J. Pieterse are highly appreciated.
- A sincere gratitude towards Mr. D. Mvayo (Lucky), Mr. R. Watson (Robbie), Mr. R. Davey and Atang for your technical guidance and assistance at KIPTS during the long day and night observations.
- Thank you to Mr. R. Jooste and Mr. P.J. Mouton, for your assistance with the finer language editing conducted on this thesis.
- A special, heartfelt, thank you, to my wife Noleen, for all the sacrifices that she made so that my dream could become a reality. Your love, support and encouragement is truly appreciated.
- To Daniel, my son, thank you for your unconditional love and joy that you provided during stressful times, and thank you that you were willing to share me with the Notebook during the long days and nights writing this thesis.
- My other family and friends; your words of encouragement and support was sincerely appreciated.
- A profound acknowledgement to NamPower for providing financial sponsorship for the project and to ESKOM for allowing us to do the research at KIPTS.

Nomenclature

AC	Alternating Current
ATH	Aluminium Tri-Hydrate
CIGRE	Conseil Internationale des Grandes Reseaux Electriques (*International Council for Large Electric Systems*)
CLI	Caprivi Link Interconnector
DBC	Dry band Corona
DBD	Dry band Discharge
DC	Direct Current
DDDG	Directional Dust Deposit Gauge
DDG	Dust Deposit Gauge
DDGIN	Dust Deposit Gauge Index Non-soluble
DDGIS	Dust Deposit Gauge Index Soluble
EPDM	Ethylene Propylene Diene Monomers
EPM	Ethylene Propylene Monomers
EPR	Ethylene Propylene Rubber
ESDD	Equivalent Salt Deposit Density
ESKOM	Formerly “ESCOM” for Electricity Supply Commission
FRP	Fibreglass Reinforced Plastic
HC	Hydrophobicity Classification
HTV	High Temperature Vulcanized
HVAC	High Voltage Alternating Current
HVDC	High Voltage Direct Current
ICP-AES	Inductive Coupled Plasma-optical Analytical Emission Spectrometry
IC	Ion-exchange Chromatography
IEC	International Electrotechnical Commission
IGBT	Insulated Gate Bipolar Transistor
KIPTS	Koeberg Insulator Pollution Test Station
LSR	Liquid Silicone Rubber
NamPower	Namibia Power Corporation

NSD	Non-soluble Deposit
NSDD	Non-soluble Deposit Density
OLCA	Online Leakage Current Analyser
r.m.s.	Root Mean Square
RTV	Room Temperature Vulcanized
SAPP	Southern African Power Pool
SCD	Specific Creepage Distance
SD	Spot Discharge
SEM	Scanning Electrode Microscope
SES	Site Equivalent Salinity
SIR	Silicone Rubber
SPS	Site Pollution Severity
TGA	Thermal Gravimetric Analysis
USCD	Unified Specific Creepage Distance
UV-B	Ultraviolet B
VSC	Voltage Source Controlled
WDC	Water Drop Corona

Table of Contents

List of Figures

List of Tables

Chapter 1: Introduction

1.1 Project background and motivation

In the light of power shortages affecting countries across Southern Africa, NamPower, the power utility in Namibia, embarked on many projects to provide additional power to communities across Namibia. One such project was the building of a ±350 kV bipolar high voltage direct current (HVDC) transmission line connecting the Namibian and Zambian electricity power grids, which would enable Namibia to import power from the Southern African Power Pool (SAPP). This transmission line is commonly referred to as the Caprivi Link Interconnector (CLI) and it consists of a 952 km overhead line and two converter stations [1]. The converter stations are located at the Zambezi 330 kV substation, close to Katima Mulilo in the Caprivi region, and the Gerus 400 kV substation, close to Otjiwarongo in the northern central region of Namibia. Each of the converter stations uses an insulated gate bipolar transistor (IGBT) based, voltage source controlled (VSC) switching mechanism.

The CLI project will be constructed in two phases, of which the first phase was commissioned on 15 November 2010 by His Excellency Dr. Hifikepunye Pohamba, Namibia's president. The two phases are:

- Phase 1 – the construction of a HVDC transmission line with a 300 MW mono-polar transmission mode and a metallic or earth return, which operates at negative 350 kV direct current (DC) voltage.
- Phase 2 – the upgrade of the 300 MW mono-polar transmission mode to a 600 MW bipolar transmission mode.

Reliable power transmission is one of NamPower's main objectives and the correct selection, dimensioning and maintenance of insulators play an important part in achieving that objective. It is known that natural ageing tests on insulators, to date, have been predominantly confined only to HVAC excitation voltages and these ageing tests provide valuable information regarding the correct selection, dimensioning and maintenance of insulators. Thus, to gain insight into the correct selection, dimensioning and maintenance of the insulators on the HVDC CLI transmission line, NamPower started a research program to

investigate the effects of both HVDC polarities on different insulator materials and different creepage distances.

The research program was conducted in two phases. The first phase consisted of two different laboratory tests. The first test was done according to the incline plain test method as described in the IEC 60587 standard using a test voltage of 4 kV (r.m.s.). During this test several polymer insulator materials were compared in terms of their resistance to erosion and tracking when energised by HVAC and both polarity HVDC excitation voltages. These results were published in reference [2]. The second test was done according to the tracking wheel tester (TWT) methodology as described in the IEC 61302 standard. During this test, polymer insulators from different suppliers were tested with HVAC and both polarities HVDC excitation voltages. The ageing performance of the different insulators per excitation voltage was compared in terms of peak leakage current, visual observations of surface degradation and hydrophobicity properties. These results were published in reference [3].

The second phase was done as a joint venture between NamPower, Eskom (the power utility of South Africa) and the University of Stellenbosch. NamPower financed the research and provided the personnel, while Eskom provided the test facility and the University of Stellenbosch provided the academic excellence. During this phase, natural ageing tests were conducted on power line insulators at Koeberg insulator pollution test station (KIPTS) located near Cape Town, South Africa, along the west coast approximately 50 m from the sea. KIPTS was selected as the test station, because it is an internationally recognised natural marine pollution insulator test station and it is located relatively close to Namibia. The objectives of these tests were:

- To investigate the effects of creepage distance on high temperature vulcanized (HTV) silicone rubber power line insulators under HVAC and both polarities HVDC excitations, when subjected to natural marine pollution conditions as experienced at KIPTS. All of these insulators were sourced from the same manufacturer, made from the same material but have different creepage distances. The effects of the different creepage distances were compared in terms of leakage current, visual observation of surface degradation, hydrophobicity properties and night time electrical discharge activities. These results were published in reference [4].
- To investigate the effects of different material line insulators under HVAC and both polarities HVDC excitations, when subjected to natural marine pollution conditions as

experienced at KIPTS. The effects of the different insulator materials were compared in terms of the visual material degradation, peak leakage currents, hydrophobicity properties and the starting sequence of electrical discharge activity. These results are published in this thesis. Preliminary results were also presented and published at the Southern African Universities Power Engineering Conference (SAUPEC 2011) in Cape Town, June 2011 and also at the International Symposium on High Voltage Engineering (ISH 2011) in Germany, August 2011 [5, 6]. A brief description of this project follows in the next section.

1.2 Project description

This research project involved the performance and ageing testing of three identical sets of line insulators, made from different insulator materials, energised under HVAC and both polarities HVDC excitations respectively. The tests were conducted at KIPTS, which is a natural marine pollution insulator test station and the objectives of the project were to:

- Design and build a bipolar HVDC source. This source was designed and built by the University of Stellenbosch. Please refer to section 3.2.1.2 for more detail.
- Determine the site pollution severity (SPS) index and climatic conditions at KIPTS, in order to put the results of the research in context.
- Determine which insulator material performed better under HVAC and both polarities HVDC excitation voltages, respectively, in terms of visual material degradation, peak leakage currents, hydrophobicity properties and the starting sequence of electrical discharge activity.
- Determine which excitation voltage performed better per specific insulator material in terms of visual material degradation, peak leakage currents and the starting sequence of electrical discharge activity.

Equivalent salt deposit density (ESDD) and directional dust deposit gauge (DDDG) measurements were used to determine the SPS index at KIPTS. To determine the climatic conditions at KIPTS, the temperature, Relative Humidity, Ultra Violet - B (UV-B) radiation, wind speed, wind direction and rainfall were continuously measured and recorded on an online leakage current analyser (OLCA), for the duration of the project.

The same set of insulators, which consisted of five line insulators made from different insulator materials, was installed per excitation voltage, for testing purposes. The set of insulators tested, consisted of the following insulators:

- Ethylene, propylene, diene monomers (EPDM) silicone alloy rubber composite long rod insulator.
- High temperature vulcanized (HTV) silicone rubber composite long rod insulator.
- Room temperature vulcanized (RTV) silicone rubber coated porcelain long rod insulator.
- Porcelain long rod insulator.
- Glass cap-and-pin insulator.

The RTV silicone rubber coated porcelain, Porcelain and Glass insulators were installed and energized on the day on which the project commenced, where the EPDM silicone alloy rubber and HTV silicone rubber insulators were installed and energised at a later date as explained in section 3.3. This difference in energizing dates, subsequently, led to a split in the comparison of insulator material performance per excitation voltage. The EPDM silicone alloy rubber and HTV silicone rubber insulators performances were compared and the RTV silicone rubber coated porcelain, Porcelain and Glass insulators performances were compared per excitation voltage. Their performances were measured in terms of peak leakage currents, visual material degradation, hydrophobicity properties if applicable, and the starting sequence of electrical discharge activities. The same performance criteria were used to compare the effects of the different excitation voltages per insulator material.

The peak leakage currents were measured and recorded via Hall Effect current sensors on an OLCA. Visual material degradation was determined through visual inspections of the insulator surfaces. The hydrophobicity properties of the insulator surfaces were determined by judging the hydrophobic (water repellent) or hydrophilic (easy wetted) characteristic of the insulator surfaces, in accordance with the STRI guide 1 procedure. Electrical discharge activity observations were conducted with a CoroCAM1 and 0-lux Sony camcorder during night-time, after 22h00.

The results presented in this thesis are expected to serve as a basis in the analyses of different insulator material performances under HVAC and both polarities of HVDC excitations and the analyses of the effects of the different excitation voltages per insulator material.

1.3 Thesis outline

The thesis is structured as follows:

- **Chapter 2** provides a literature review concerning the different types and characteristics of line insulators, their flashover performances, in particular, their pollution flashover performance, and the degradation of insulators caused by environmental and electrical stresses.
- **Chapter 3** gives a description of the test arrangement, the design of the HVDC excitation source, the test insulator samples and all the test instruments used during the research process.
- **Chapter 4** provides detailed discussions of all the procedures and methodology used during this research, in order to achieve all the objectives set for the research.
- **Chapter 5** contains all the results obtained during the research process, and the interpretation of the results is also provided. The results are presented in a comparative manner, in terms of the performance of the different insulator materials per excitation voltage and the performance of the different excitation voltages per insulator material.
- **Chapter 6** provides the final conclusions and recommendations.

Chapter 2: Literature Review

2.1 Overview

The methodology used in this chapter provides a brief literature review of insulators in general but a more in-depth review of transmission line insulators. Transmission line insulators were used during this project and the author thought it appropriate to provide a more in-depth review of it. The review was done by researching the following topics:

- The history of insulators: How they came to existence and; how they evolved until the present day.
- Different types and characteristics of insulators in existence today.
- Flashover performance of insulators.
- Insulator degradation.

2.2 Historical synopsis of the development of insulators

The first insulators were developed around the year 1835, where they were used for telegraph lines and made of annealed glass or "dry-pressed" porcelain [7]. For this, please refer to Figure 2-1.

Figure 2-1: Telegraph porcelain insulators [7]

With the beginning of power transmission lines in 1882, the telegraph insulators were scaled up, in line with higher voltage and mechanical loading usage ratings for the power transmission line industry. These higher rating requirements revealed shortcomings in both the material and design of the insulators in use at that time. "Dry-press" porcelain insulators, for example, suffered from punctures because of the material porosity [7]. This led to the development of wet-process porcelain in 1896, which was soon followed by the use of a vacuum extrusion process to eliminate air from the porcelain insulating body, which is virtually the same as the material used today [7].

Another shortcoming that insulators had to overcome concerned the mechanical demands on transmission lines, e.g. the weight of the conductor cables. Insulators in general are placed under tension loads on transmission lines, but porcelain and glass materials are much stronger under compression loads than tension loads [8]. Thus, designs such as cap-and-pin were developed to put the dielectric material under a compression load, while the insulator as a whole is under tension load [8]. Glass insulators also went through several developments regarding the choice of manufacturing materials and the introduction of "toughening" in the 1930s [8].

The first composite insulators made of polymeric materials with the long rod design, appeared in the late 1960s and the first test installations were done in the 1970s [9]. As with the ceramic and glass insulators, the first designs had numerous problems, especially due to material ageing effects [7]. With continuous improvements to the design of materials and shape (form factor), polymer insulators became a matured product since the 1980s and are today generally accepted and used in large numbers on transmission lines [10].

The design and manufacturing of insulators was a trial-and-error process; rather than an orderly progression [7]. The insulator design and manufacturing process of porcelain and glass insulators stabilized in the 1950s and 1960s respectively [7]. Great advances were made in the development of polymer insulators regarding its reliability in the 1980s and 1990s [7]. Presently most manufacturers have fairly stable (settled) designs.

Pin insulators, the direct descendent of telegraph porcelain insulators, are still in use today though their usage is limited to distribution lines [7]. The first successful porcelain cap-and-pin insulators were introduced in 1909 and glass cap-and-pin insulators in 1930 [8]. Pedestal

post insulators were introduced in the 1910s and long rod insulators in the 1920s [8]. Porcelain post insulators were introduced in the 1940s and polymer post insulators during the 1980s [8].

2.3 Different types and characteristics of insulators

In today's market there are many different types of insulators available; each having its specific place and use in the electricity supply industry. This section provides an overview of the fundamental physical parameters of insulators, different insulator materials, and basic insulator types available, including the fundamental profile designs and their intended applications.

2.3.1 Fundamental physical parameters of insulators

The physical shape and dimensions of an insulator determine its electrical and mechanical capabilities and can be characterised by the parameters discussed in this section [9]. These parameters also play an important part in the design phase of a transmission line system as indicated in the discussions below.

2.3.1.1 Connecting length

Connecting length, also known as section length, refers to the shortest distance between the connecting points of the life and earthed (grounded) hardware; ignoring any stress control rings but include intermediate metal parts along the length of the insulator [7]. Please refer to Figure 2-2.

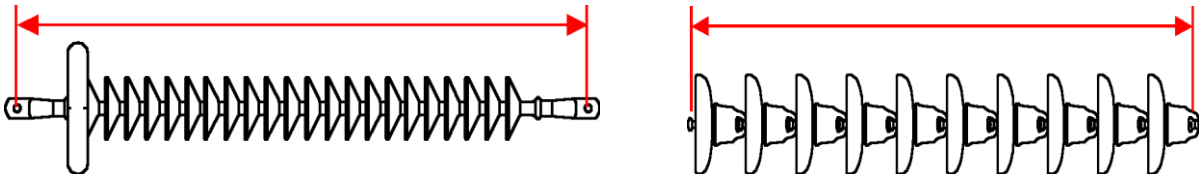

a) Long rod insulator b) Cap-and-pin insulator string

Figure 2-2: Definition of connecting length [7]

2.3.1.2 Dry arc distance

Dry arc distance is defined as the shortest distance in the air, external to the insulator, between those parts which normally have the operating voltage between them [7, 11]. Please refer to Figure 2-3. The dry arc distance is important because it determines the power frequency and impulse flashover voltages of the insulator when it is clean [9]. Therefore, to meet the electrical requirements of the system, an adequate dry arc distance must be chosen which would dictate the physical length of the insulator to be used at a given voltage level [9].

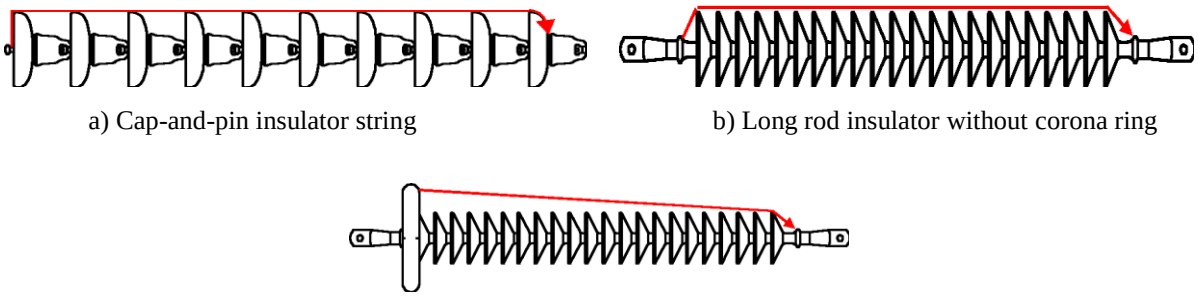

a) Cap-and-pin insulator string

b) Long rod insulator without corona ring

c) Long rod insulator with corona ring

Figure 2-3: Definition of dry arc distance [7]

2.3.1.3 Puncture distance

Puncture distance is defined as the shortest distance through the insulating material between those parts which normally have the operating voltage between them [7]. The provision of adequate puncture distance is very important because this ensure that the insulator undergoes no permanent damage if confronted with overvoltage, especially steep-fronted lightning impulses [9]. Please refer to Figure 2-4.

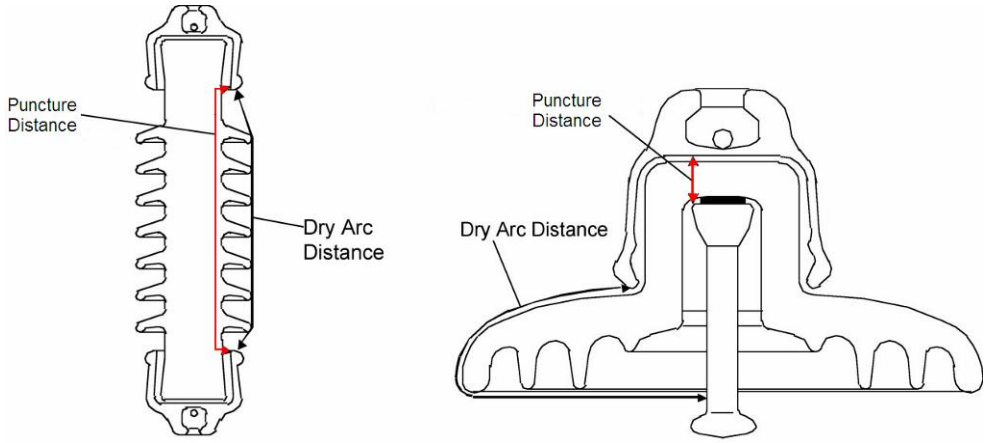

Figure 2-4: Comparison between puncture distance and dry arc distance [7]

2.3.1.4 Creepage distance

The creepage distance, also known as leakage distance, is defined as the shortest distance or the sum of the shortest distances along the surface of an insulator between two conductive parts which normally have the operating voltage between them [11]. The surface of cement or any other non-insulating jointing material is not regarded as forming part of the creepage distance [11]. If high-resistance materials are applied on the insulating section of the insulator, it is considered to be a good insulating surface and thus the distance over this surface is included in the creepage distance of the insulator [11]. Please refer to Figure 2-5.

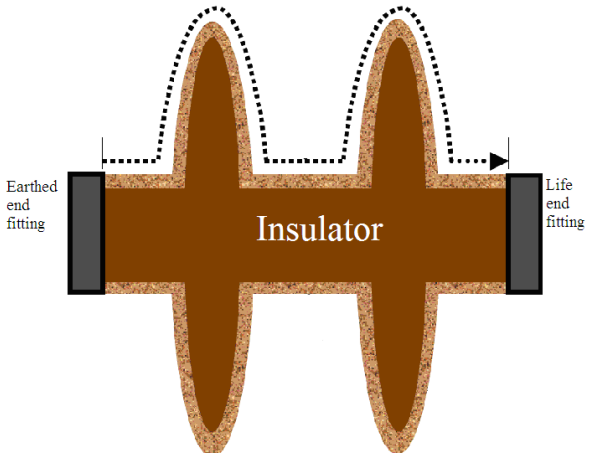

Figure 2-5: Illustration of the definition of creepage distance [12]

Creepage distance is an important parameter in instances where the insulator surfaces are polluted, because it determines the pollution flashover voltage of an insulator [12]. Since there is a direct relationship between the pollution flashover voltage of an insulator and its creepage length, the concept of specific creepage distance is commonly used [7]. In the first edition of the IEC 60815 (1986) publication, specific creepage distance (SCD) was defined as the creepage distance of the insulator divided by the phase-to-phase value of the maximum voltage for the equipment [13]. With this definition, it was difficult to compare specific creepage distance values of three phase systems with single phase AC and DC systems [9]. This led the IEC to introduce the unified specific creepage distance (USCD) concept, which is defined as the creepage distance of the insulator divided by the r.m.s. value of the highest operating voltage across the insulator [13]. The unit of both concepts is mm/kV and expressed as a minimum value [13].

2.3.1.5 Protected creepage distance

Protected creepage distance is defined as the part of the creepage distance, on the lightened side of the insulator, which would fall in the shadow if a light were projected on the insulator at 90°, or 45° in special cases, to the longitudinal axis of the insulator [7]. This refers to the part of the creepage distance that is not easily accessible to natural cleaning. Please refer to Figure 2-6.

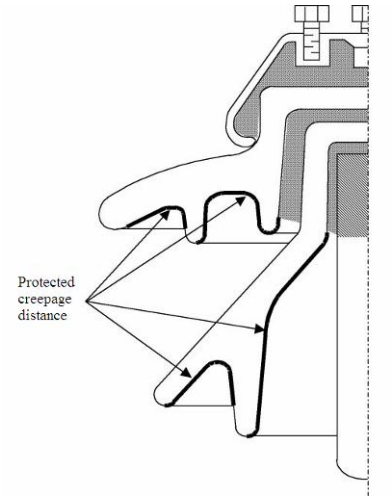

Figure 2-6: Protected creepage distance [7]

2.3.1.6 Form factor

The pollution flashover characteristic of an insulator is dependent on the surface resistance (R_{pol}) of an electrolytic pollution layer on an insulator [12] and the form factor (F_f) of an insulator is directly related to the surface layer resistance of a uniformly distributed electrolytic pollution layer on an insulator, as given by equation (2-1) [12].

$$R_{pol} = \frac{F_f}{\sigma_s} \tag{2-1}$$

where

R_{pol} is the surface layer resistance of the electrolytic pollution layer measured in MΩ,

F_f is the Form factor value

and

σ_s is the surface conductivity of the uniformly distributed electrolytic pollution layer on the insulator measured in µS.

Thus, the form factor value of an insulator plays an important role in the pollution flashover performance of an insulator. The form factor value of an insulator is determined by equation (2-2) and graphically displayed in Figure 2-7 [7].

$$F_f = \int_0^L \frac{dl}{2\pi \cdot r(l)} \tag{2-2}$$

where

L is the total creepage distance of insulator measured in mm

and

$r(l)$ is the radius of insulator at position l along the insulator creepage path, measured in mm.

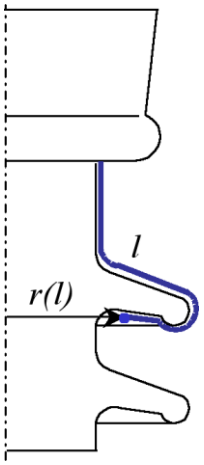

Figure 2-7: Graphical representation of the form factor equation [7]

2.3.1.7 Classification of insulators

Insulators are divided into two classes according to its design [9].

- Class A: All insulators or insulator units with a minimum puncture distance of half the dry arc distance of the respective insulator or insulator unit. Insulators categorised as class A are considered to be unpuncturable [9].
- Class B: All insulators or insulator units with a puncture distance less than half the dry arc distance of the respective insulator or insulator unit. Insulators categorised as class B are considered to be puncturable [9].

Please refer to Figure 2-4 for a graphically interpretation of the above.

2.3.2 Insulator types

In this section a brief discussion of the most used outdoor insulator types is given. The different types are used in different places in the electrical supply system, e.g. overhead lines or substations.

2.3.2.1 Pin insulator

A pin insulator is a rigid insulator consisting of an insulating part and a pin [9]. The insulating part may consist of one or more pieces permanently connected to each other, where the pin is either separable, or fixed permanently to the insulating part [9]. Pin insulators are made from porcelain, glass or resin and fall under the class B classification [9]. They are used on overhead lines up to 50 kV [9]. Please refer to Figure 2-8 for an example.

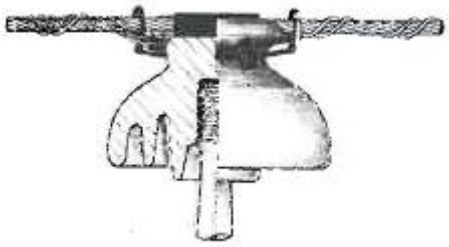

Figure 2-8: Example of a pin insulator [9]

2.3.2.2 Cap-and-pin disc insulator

A cap-and-pin disc insulator consists of an insulating part (dielectric shell) that looks like a disc or a bell, cemented to connecting devices (metal end fittings), which resemble a cap on the outside and a pin on the inside [7, 9]. The shape of the cap-and-pin insulator is designed to put the dielectric material under a compression stress during normal loading conditions [8]. Either porcelain or toughened glass is used as the dielectric material for cap-and-pin insulators [8]. Cap-and-pin insulators fall under the class B classification and are used on overhead lines [9]. Please refer to Figure 2-9 for a graphical representation of a cap-and-pin insulator.

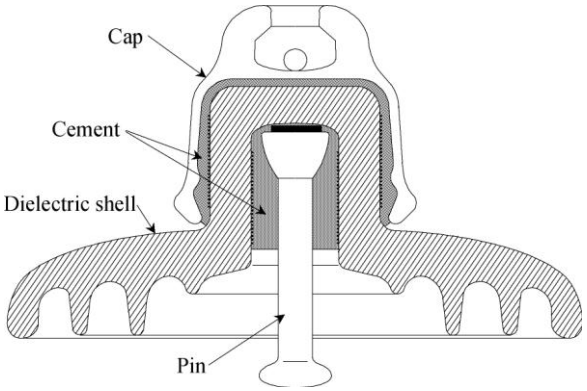

Figure 2-9: Cap-and-pin disc insulator [7]

The design of caps are mainly of the socket or clevis type and are manufactured from malleable cast iron, ductile iron or steel by using a casting or forging process [9]. The above-mentioned material is galvanized to protect it from corrosion [9]. Pin designs are mainly of the ball or tongue type and are manufactured from heat-treated, medium carbon steel using a forging process [9]. The pins are also galvanized to protect it from corrosion [9]. A zinc ring can be fitted at the edge of the cap and a zinc sleeve on the pin for HVDC line insulators to act as a sacrificial electrode to combat electrolytic corrosion [14].

2.3.2.3 Long rod insulator

A long rod insulator consists of an insulating part that has a cylindrical core with sheds, and with internal or external metal end fittings at the ends of the insulator [7]. The external metal end fittings are cemented to the insulating part as illustrated in Figure 2-10 [7].

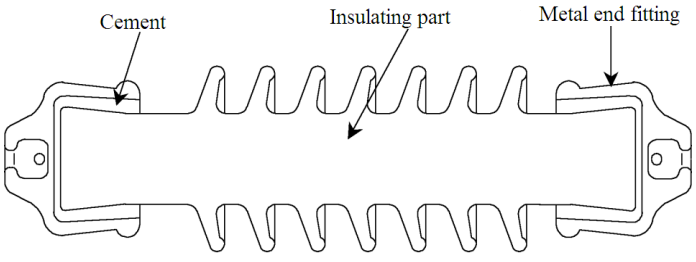

Figure 2-10: Long rod insulator [7]

The insulating part is made from porcelain or resin material [9]. Long rod insulators fall under the class A classification and are used on overhead lines.

2.3.2.4 Composite long rod insulator

A composite long rod insulator consists of a core and polymer housing, which are the two insulating parts of the insulator, and metal end fittings [9]. The insulator is designed to be used only in tension load configurations [9]. Fibre glass strains are used to manufacture the core and silicone rubber or ethylene propylene rubber is used to manufacture the polymer housing [7]. Composite long rod insulators fall under the class A classification and are used on overhead lines [9]. Please refer to Figure 2-11.

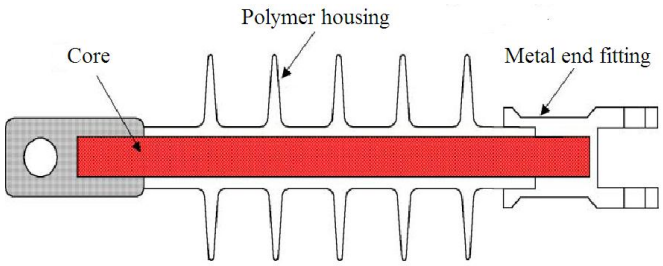

Figure 2-11: Composite long rod insulator [7]

2.3.2.5 Line post insulator

Line post insulators consist of an insulating part which consists of one or more pieces permanently connected, and a metal end fitting base to be mounted on a supporting structure [9]. Some line post insulators have a cap as well [9]. The insulating part is made of porcelain, toughened glass or resin material [9]. Line post insulators fall under the class A classification and are used on overhead lines. Please refer to Figure 2-12 for an example.

Figure 2-12: Line post insulator [9]

2.3.2.6 Composite line post insulator

Composite line post insulators consist of a load–bearing, cylindrical, insulating solid core, polymer housing and metal end fittings attached to the core [9]. Fibre glass strains are used to manufacture the core and silicone rubber, or ethylene propylene rubber is used to manufacture the polymer housing [7]. The metal end fitting on the earthed side of the insulator uses a rigid or bendable base made from ductile iron, rolled steel or aluminium, where the metal end fitting on the energized side uses either a horizontal clamp top or a drop tongue to attach the conductor to the insulator as shown in Figure 2-13 [7]. It falls under the class A classification and is used on overhead lines.

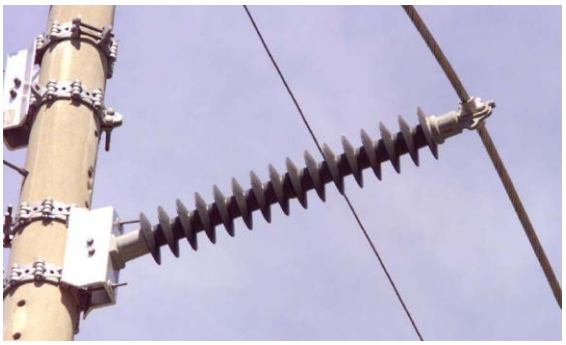

Figure 2-13: Composite line post insulator with horizontal clamp top and bendable base [7]

2.3.2.7 Station post insulator

A station post insulator consist of an insulating part of one or more pieces permanently assembled and metal end fittings to be mounted on supporting structures by means of one or more bolts [9]. The end fittings are usually made of galvanised, malleable or ductile iron [9]. The insulating part is made from porcelain, toughened glass, resin or composite material [9]. Station post insulators fall under the class A classification and are used in substations as equipment and bus bar support [9]. Please refer to Figure 2-14 for an example.

Figure 2-14: Station post insulator [9]

2.3.2.8 Pedestal post insulator

A pedestal post insulator is a post insulator with metal end fittings that consist of a cap which partly embraces the insulating part as well as a pedestal cemented into a recess in the insulating part [9]. There are normally tapped holes in the cap and plain holes in the flange of the pedestal so that it can be mounted on a supporting structure with bolts [9]. The insulating part is made from porcelain or toughened glass material [9]. Pedestal post insulators fall under the class B classification and are used in substations as equipment and bus bar support [9]. Please refer to Figure 2-15 for an example.

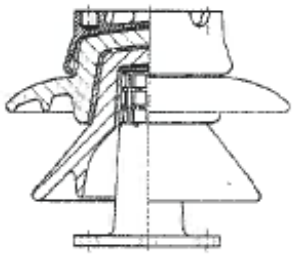

Figure 2-15: Pedestal post insulator [9]

2.3.2.9 Bushing

A bushing is used to pass one or several conductors through a partition such as a wall or tank whilst simultaneously insulating them from the partition [9]. The insulating part is made from porcelain, resin or composite material [9]. Bushings fall under the class B classification and are used in substation apparatus such as transformers [9]. Please refer to Figure 2-16 for an example.

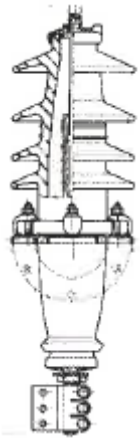

Figure 2-16: Bushing [9]

2.3.2.10 Apparatus (hollow) insulator

Apparatus insulators have hollow bodies, from end to end, and are intended to be used in electrical equipment such as instrument transformers, surge arresters and circuit breakers [9]. It falls under the class B classification and its insulating part is made from porcelain, resin or composite material [9]. It is sometimes equipped with metal flanges made from malleable iron, ductile iron or aluminium for porcelain insulators or made from cast or machine aluminium for composite insulators [9]. Please refer to Figure 2-17 for an example.

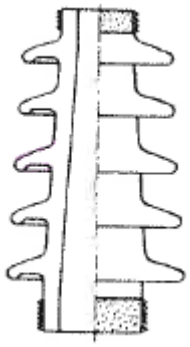

Figure 2-17: Apparatus (hollow) insulator [9]

2.3.2.11 Typical applications of transmission line insulators

Cap-and-pin, long rod and composite long rod insulators are used in I-string, V-string and dead-end configurations, as shown in Figure 2-18 (a), (b), (c) [7]. The insulators are placed under tension loads through these configurations by connecting the conductor to the transmission line towers. Porcelain or composite long rod insulators can also be used as phase spacers, however, special consideration should be granted for this application because it may apply compressive forces over the insulators, due to conductor movements as shown in Figure 2-18 (d) [7, 15].

a) Cap-and-pin insulators in I-suspension.

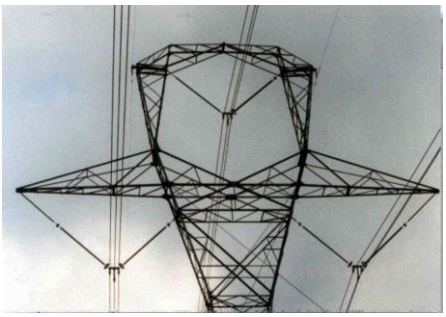

b) Composite long rod insulators in V-suspension

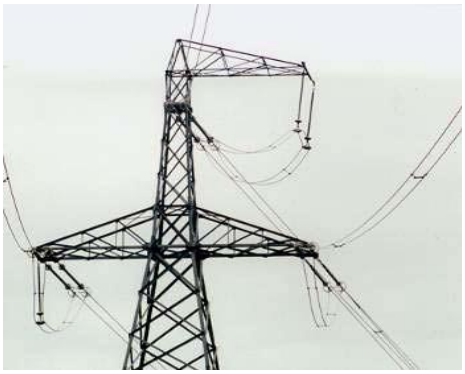

c) Composite long rod insulators in strain or dead end

d) Composite long rod insulators as phase spacers

Figure 2-18: Example of transmission line applications [7]

Porcelain and composite post insulators are used to connect conductors to single pole structures as Figure 2-19 (a) shows [7]. This is an attractive configuration, because it reduces the structure footprint, and, in some cases leads to a reduction in the required right-of-way area [7]. Post insulators can also be used in conjunction with long rod insulators to form a brace post or horizontal V configuration as shown in Figure 2-19 (b) [7]. This configuration is used to obtain stronger mechanical structures to support the conductors [7].

a) Composite line post insulator

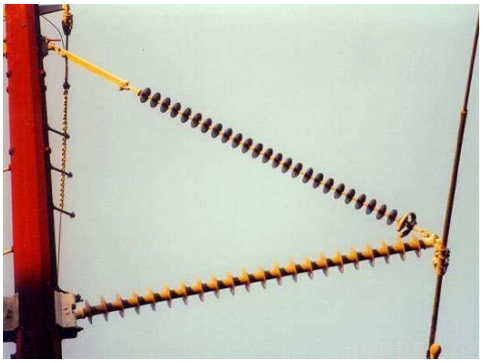

b) Brace post or horizontal V configuration

Figure 2-19: Example of line post insulators [7]

2.3.2.12 Different insulator profiles

The term insulator profile refers to the specific shape of an insulator. From experience it is known that different rates of accumulation of pollution in the same environment can be experienced on different insulator shapes as well as on different orientations of the same insulator shape [13]. Some insulator shapes are more effective than others, depending on the type of pollution which they experience [13]. In Table 2-1 different shapes of insulators are shown, as well as a short description of the pollution type that the given insulator would be most effective for.

2.3.3 Insulator materials

The materials used to make the dielectric part of insulators have to be excellent dielectric materials, capable of withstanding high electrical stresses over a long period of time [9]. Further it should withstand severe environmental factors such as ultraviolet radiation, contamination and lightning overvoltage and it must have sufficient tensile, compressive and cantilever strength to support the loads applied to it [9].

The experiences of early years of the first DC lines prove that specific dielectric materials for ceramic and glass insulators are needed for HVDC (High Voltage Direct Current) applications [14]. The unidirectional electric fields of HVDC applications have severe effects on the integrity of dielectric materials originally made for HVAC (High Voltage Alternating Current) applications as they cause unidirectional currents, which cross the dielectric body through an ionic migration process of alkalis such as NA+ [14]. This ionic current is different from surface leakage current and causes a temperature increase in the dielectric material and subsequently a local decrease of resistivity on the dielectric body, resulting in a higher ionic current, which generates another temperature increase [14]. This process repeats itself until the dielectric puncture or shatters; the visible consequence of a thermal runaway process [14]. The unidirectional current going through the body of the dielectric can cause some form of depletion on the atomic structure of the material, reducing the material's electrical and/or thermo mechanical and electromechanical properties [14]. To provide a solution for the abovementioned conditions, standard IEC 61325 made it mandatory to use only high resistive dielectric materials in HVDC glass and ceramic insulator manufacturing [14].

Table 2-1: Typical profiles with its effective pollution type [13]

Standard profiles Standard profiles are effective for use in "very light" to "medium" polluted areas where a long creepage distance or an aerodynamically effective profile is not required	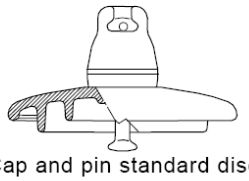 Cap and pin standard disc insulators	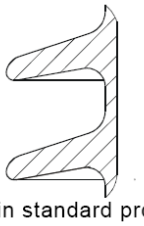 Porcelain standard profile, long rod insulators , post insulators, hollow insulators
Aerodynamic or open profiles Aerodynamic or open profiles prove to be beneficial in areas where the pollution is deposited onto the insulator by wind, such as deserts, heavily polluted industrial areas or coastal areas which are not directly exposed to salt spray. This type of profile is especially effective in areas that are characterized by extended dry periods. Open profiles have good self-cleaning properties and are also more easily cleaned under maintenance	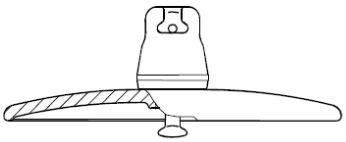 Aerodynamic disc insulators 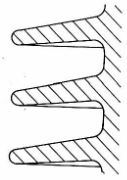 Porcelain long rod insulators, post insulators, hollow insulators	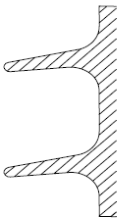 Polymeric long rod insulators, post insulators, hollow insulators
Anti fog profiles The use of anti fog profiles with steep sheds or deep under-ribs are beneficial in areas exposed to a salt water fog or spray, or to other pollutants in the dissolved state. These profiles may also be effective in areas with a particulate pollution precipitation containing slow dissolving salts. They can also be effective in areas with low NSDD and slow dissolving salts	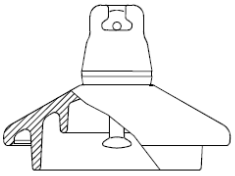 Steep anti-fog disc insulators 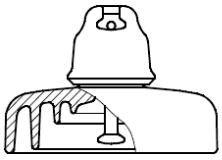 Deep under-ribs disc insulators 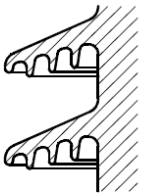 Deep under-ribs on porcelain long rod insulators, post insulators, hollow insulators	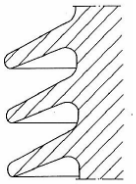 Steep porcelain long rod insulators, hollow insulators, post insulators 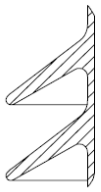 Steep polymeric long rod insulators, hollow insulators, post insulators 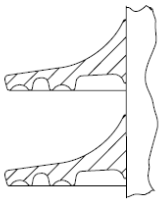 Under-ribs on polymeric long rod insulators, hollow insulators, post insulators

Table 2-1 (continued)

Alternating shed profiles		
Alternating shed arrangements are in general feasible for all profiles, although steep sheds are less beneficial. They offer increased creepage distance per unit length without penalising performance in heavy rain or icing. Similar benefits to open profiles are also provided by simple alternating profiles	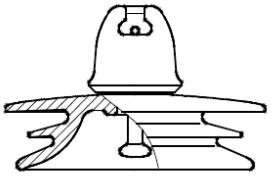 Alternating shed disc insulators	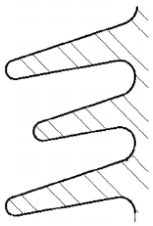 Porcelain long-rod insulators, post insulators, hollow insulators 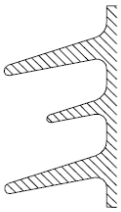 Polymeric long rod insulators, post insulators, hollow insulators

Currently, there is no international standard that covers composite insulators for HVDC applications, due to insufficient knowledge of their specific performance over time and how the material ages under different environmental and electrical stress conditions [14]. A detailed description of common materials used in insulator manufacturing is given below.

2.3.3.1 Porcelain

Electrical porcelain is made from clay and inorganic materials such as feldspar and quarts [9]. Quarts may be replaced by alumina to have better mechanical characteristics [9]. After a firing process in a kiln the porcelain consists of various oxide and silicate crystals in a glassy matrix which is completely resistant to moisture [9]. The insulators are normally glazed to provide a smooth surface which allows natural washing by rain and forms a compressive outer-layer which limits surface crack formation and increases its mechanical strength [9].

During the manufacturing of DC porcelain insulators, special care must be given to achieve a cohesive structure of crystals with a minimal content of micro cracks. This is achieved by selecting specific particle sizes of the porcelain raw materials [14]. These micro cracks are more harmful in HVDC applications than in HVAC applications [14].

The main advantages of porcelain are [9]:

- Immunity to degradation by environmental factors i.e. ultraviolet radiation and aggressive pollutants because of its inert inorganic nature.
- Resistance to damage caused by surface partial discharges and leakage current activity.
- Ability to be easily formed into variety of shapes for different applications.
- High compressive strength.

The main disadvantages of porcelain are [9]:

- Vulnerability to breaking, chipping and cracking due to its brittle nature.
- Risk of damage by electrical puncture which is very difficult to locate.
- Low tensile and cantilever (bending) strengths.
- Possibility of glaze damage and cracking of the porcelain, due to thermal effects of power arcs.

2.3.3.2 Toughened glass

Glass is made by a gradual solidification process of a melted mixture consisting of silica, limestone, dolomite, feldspar and soda ash in specific proportions [9]. During the toughening process of toughened glass insulators, the insulator outer surface cooling is accelerated while the inner part cools slowly [9]. The difference in cooling rate creates a permanent compressive pre-stressing in the outer layer to prevent the formation of surface micro-cracks and crack propagation [9]. Toughened glass has higher mechanical strength than annealed glass, which makes it the material of choice in high voltage glass insulator manufacturing [9].

DC toughened glass insulators are manufactured with dielectric material with a resistivity of 100 times greater than AC toughened glass insulator dielectric material at normal service conditions [14].

The main advantages of toughened glass are [9]:

- Resistance to ultraviolet radiation and other environmental damages.
- High dielectric strength and resistance to electrical puncture.
- Good compressive strength.
- Easy identification of faulty units due to shatter tendency when damaged.

The main disadvantages of toughened glass are [9]:

- Limited use for only certain applications, due to its mechanical characteristics.
- Susceptibility to leakage current erosion, which can lead to shattering.
- The fact that it is an ideal target for vandals due to its tendency to shatter.

2.3.3.3 Epoxy resin

Epoxy resin insulators are made from various types of heavy filled polymeric resins e.g. cycloaliphatic or bisphenol epoxies, polyester or polyurethane [9]. The filler content is typically 60 to 70% and it is added to improve the tracking and erosion performance of the formulations [9]. Prior to the late 1960s, epoxy resins were used indoor only [9]. The newer units have better resistance to the effects of ultraviolet radiation. However, material degradation may still occur, due to surface partial discharge activity because of its organic nature [9]. Thus, it will not be a good choice of material for insulators in highly polluted environments.

The main advantages of epoxy resin are [9]:

- They can be moulded in many different forms for a variety of applications.
- The embedment of metal fittings during the moulding process eliminates the need for attaching external fittings.

The main disadvantages of epoxy resin are [9]:

- Possibility of severe leakage current erosion.
- Electrical weakness at mould line may result in material degradation.
- Use is limit to medium voltages on overhead lines.

Currently there are no international standards specifying directions regarding dielectric material for epoxy resin DC insulators; therefore the same insulators are used for AC and DC applications.

2.3.3.4 Polymer composites

The term composite refers to an insulator that consists of metal end fittings, a core which carries the mechanical load of the insulator and shielded from the environment by a polymer housing [7]. The terms "core" and "polymer housing" will be discussed in detail later in this section.

The main advantages of polymer composites are [9]:

- High tensile strength-to-weight ratio.
- Improved performance in highly polluted areas by the silicone rubber types.
- They are an unattractive target for vandals and very resistant to projectile damage.

The main disadvantages of polymer composites are [9]:

- Erosion on polymer housing due to leakage currents if incorrect material and/or dimensioning are used.
- Possible electrical weakness at the mould line for moulded constructed insulators.
- Deflection under load in certain applications.
- Special care needed in design and manufacturing to eliminate entrance of moisture at the interface between core, polymer housing and metal end fittings.

Currently there are no international standards specifying directions regarding dielectric material for composite polymer DC insulators; therefore the same insulators are used for HVAC and HVDC applications.

The main aspects of polymer composites are discussed in detail below.

2.3.3.4.1 The core

The core is a fibreglass reinforced plastic (FRP) rod, which consists of axially aligned glass fibres in a resin matrix [7]. The fibres are typically 5 to 25 µm in diameter and correspond to 75 – 80% of the total weight of the rod [16]. Normal electric glass fibres (E type) are often used but special corrosion resistant glass fibres (E-CR type) are also finding increasing use [17]. The term "corrosion resistant" refers to the ability of the glass fibres to resist stress corrosion cracking (brittle fracture) by reducing the level of boron in the fibres [17]. It should

be noted that although corrosion resistant glass fibres reduce the possibility of failure due to brittle fractures, it is still vulnerable to other failure modes such as flash-under (tracking along or through the core leading to flashovers) and destruction of the core by discharge activity [7]. The resin matrix consists of a hydrolysis-resistant resin, usually of the epoxy, polyester or vinyl-ester type [7]. The core has very high tensile strengths but low compression, torsion and cantilever strengths [7]. Furthermore, it is a very good electrical insulator as long as it is dry and uncontaminated [7]. Please refer to Figure 2-20 which is a scanning electrode microscope (SEM) image of the core cross section, showing the glass fibres in the resin matrix [7].

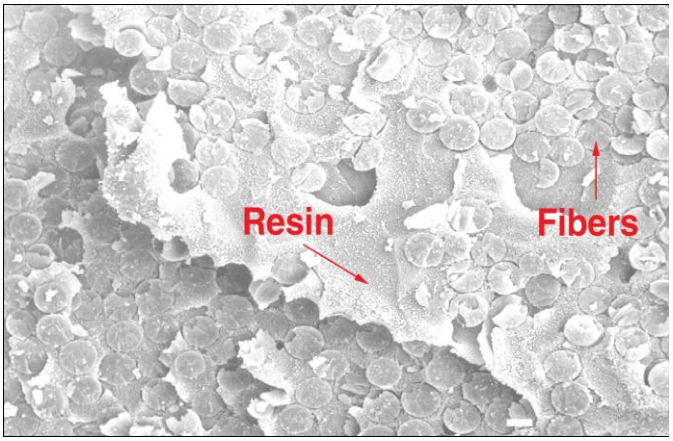

Figure 2-20: SEM image of the fibres in resin matrix [7]

2.3.3.4.2 Polymer housing

The function of the polymer housing is to seal the core, in order to protect it from electrical discharges and environmental factors such as UV radiation and moisture, and to provide sufficient creepage distance in order to comply with the power frequency pollution flashover voltage requirement [7]. The housing consists of sheds and sheath sections as shown in Figure 2-21.

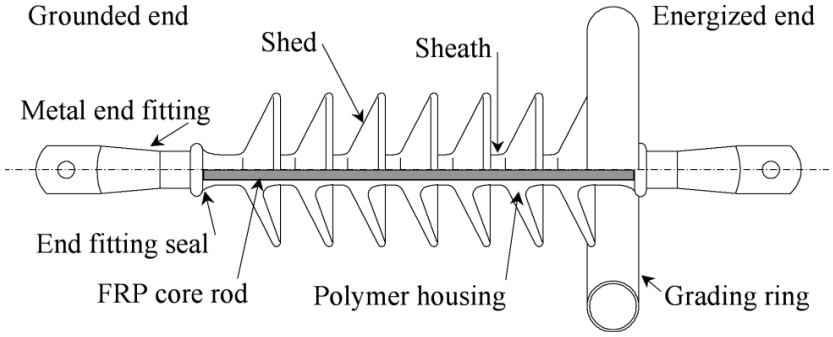

Figure 2-21: Basic components of a composite insulator [7]

The housing of a transmission line polymer insulator is normally made of ethylene propylene rubber (EPR) or silicone rubber (SIR), while distribution line polymer insulator housings may utilize other materials as well, such as cycloaliphatic epoxy or ethylene vinyl acetate [7]. The composition of the abovementioned materials and their manufacturing process varies between different manufacturers and these differences have effects on the long term performance of the insulators [7]. Therefore, one should be careful not to make assumptions regarding the performance of insulators simply by considering the family of rubbers the housing are made of.

2.3.3.4.2.1 EPR material

The first generation of EPR insulators used ethylene and propylene monomers (EPM) [7]. Today, however, most of the EPR insulators are made of ethylene, propylene and diene monomers (EPDM) [7]. The chemical structure of EPRs consists of a backbone of organic carbon molecules and side groups consisting of hydrocarbon elements as indicated in Figure 2-22 [7].

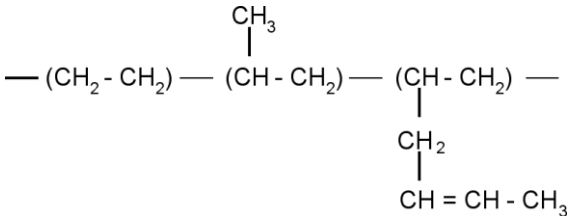

Figure 2-22: Chemical structure of EPR [7]

Thus, the carbon content of EPDM is very high and therefore it is critical to protect it from degradation. The by-product of a degradation process such as surface discharges on a high carbon based material is carbon and it may form a conductive path or track [7]. One method of protecting EPDM rubbers is to add large quantities of inorganic fillers, e.g. Aluminium Tri-

hydrate (ATH), to the EPDM rubbers during the manufacturing process [18]. ATH protects EPDM rubbers against tracking when subjected to surface discharge activities, by forming a moisture layer which, in turn, cools the discharge activity [19].

Various additives are added to EPDM rubbers during manufacturing to improve their performance. Some of the additives are listed below [7]:

- Inorganic powders such as ATH to improve resistance to discharges, arcing and tracking.
- UV stabilizing agents such as zinc oxide and titanium oxide.
- Colouring agents.

If a small amount of silicon oil is added to EPDM rubbers during manufacturing, the formulation is called an alloy [18].

EPDM rubbers have hydrophobic properties in the beginning but they tend to lose these properties very quickly when they are energized and exposed to the environment [7]. Hydrophobicity is a very important characteristic of insulators. It refers to the manner water interacts with the surface of insulators. The surface may either be hydrophobic, in other words, repelling water to form droplets, or hydrophilic, in other words, attracting water to forms a continuous water film on the surface of the insulator. This concept will be discussed in more detail in section 4.6.1.

2.3.3.4.2.2 Silicone rubber material

The tree groups of silicon rubber materials used in insulators manufacturing are [9]:

- High temperature vulcanized (HTV).
- Room temperature vulcanized (RTV)
- Liquid silicone rubbers (LSR)

For all three groups, the base silicone material is mixed with silica flour during manufacturing to give it sufficient mechanical strength [9]. Mineral filler, usually ATH, is also added to improve resistance to discharges, arcing and tracking [7]. The quantity of filler material in comparison to silicone rubber, and the form in which it is added, is an on-going research area [19]. Several more additives are added such as colouring agents [9].

The chemical structure of silicone rubber consists of an inorganic silicon-oxygen (Si-O) backbone with two organic side groups attached to the silicon atom as shown in Figure 2-23 [18]. A methyl group (CH_3) is normally used in high voltage applications, but other organic side groups such as phenyl or vinyl may also be present [7]. The chains can be of very different lengths [9]. Silicon rubbers are largely characterised by the polymer's chain length and types of side groups present [9].

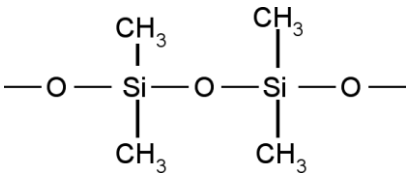

Figure 2-23: Chemical structure of silicone rubber [18]

Silicone rubber has highly hydrophobic surfaces and this is considered to be an important characteristic, because it prevents the surface from becoming completely moist, thus preventing leakage currents from flowing during pollution events [7]. Silicone rubber also has a unique characteristic whereby lightweight silicon molecules migrate to the rubber surface and encapsulate pollution on the surface, resulting in the transfer of hydrophobic characteristics to the pollution layer [9]. There are conditions whereby silicone rubber may temporary lose its hydrophobic properties, such as when an insulator is covered by pollution and subject to significant levels of discharge activity over a long period of time [20, 21]. Silicone rubber has another unique characteristic: it can regain its hydrophobic state within 24 to 48 hours after the removal of the factors causing the loss of hydrophobicity [7].

2.3.3.4.3 Processes used to apply polymer housing to the core

There are different manufacturing processes used to apply the polymer housing to an insulator core. These processes are briefly discussed below.

2.3.3.4.3.1 Injection and compression moulding

The housing can be injected over the core in one or several shots [9]. This provides a one-piece housing that is directly and chemically bonded to the core and metal end fittings [9]. The housing can also be compression moulded onto the core, which also provides a one-piece housing that is directly and chemically bonded to the core but not to the metal end fitting [22]. An end fitting seal has to be added in a separate operation, in order to seal the interface

between the polymer housing, metal end fitting and the core rod [22]. This method provides a minimum number of interfaces between the polymer housing and the core [9]. However, special care needs to be taken to centre the core and to prevent the mould line becoming a pollution trap and degrading, due to material in-homogeneity [9]. Please refer to Figure 2-24.

a) Injection moulding without seal b) Compression moulding with seal

Figure 2-24: Examples of injection and compression moulding process [22]

2.3.3.4.3.2 Extrusion

This technique consists of extruding a sheath onto the core and slipping separate moulded sheds over the sheath and bonding it onto the sheath [22]. The end fitting seal has to be added in a separate operation [22]. This construction allows for flexibility in design, by varying the quantity and positions of the sheds to suit the application, without capital cost having additional moulds [22]. Please refer to Figure 2-25.

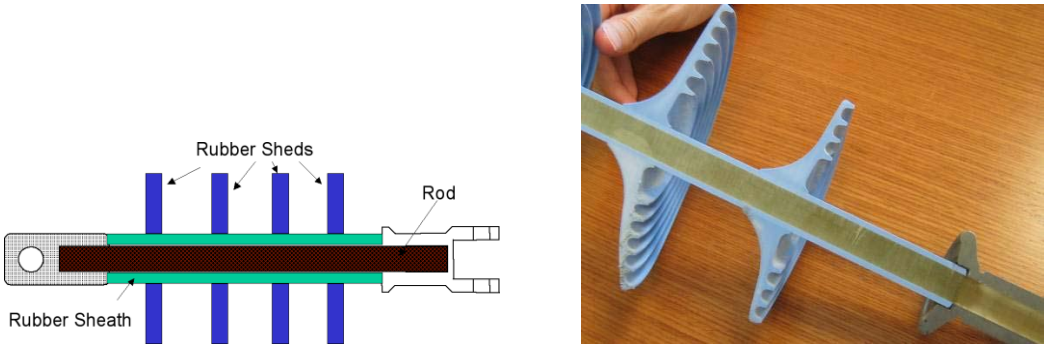

Figure 2-25: Examples of extrusion process [22]

2.3.3.4.3.3 Un-bonded sheds

This technique consists of sliding single or group shed/sheath units, which are moulded separately, over the core [22]. No bonds exist between the housing and the core. Grease, which is normally made from an active silicone gel, fills the interface between the rubber and the core [22]. The pressure between the housing and the metal end fittings, created by the

elasticity of the housing, forms the seal [22]. This technique is easy to use but creates many interfaces to the core and grease leakage may also occur [22]. Please refer to Figure 2-26

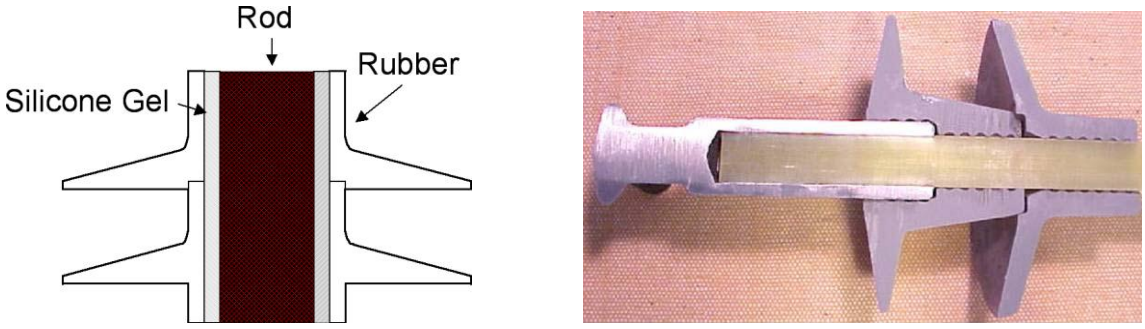

Figure 2-26: Examples of un-bonded sheds manufacturing process [22]

2.3.3.4.4 Metal end fittings

Metal end fittings serve two functions; the first function being to provide the means to attach the core to the earthed structure and to the live conductor [7]. The second function is to form a ceiling system to prevent moisture from entering the core and core-rubber interface [7]. The materials used to manufacture metal end fittings for transmission line composite long rod insulators are hot dipped galvanised forged steel or ductile iron [7]. Aluminium alloy is not used, because it has a lower melting point than the arc root temperature of a power arc, but it is sometimes used on distribution line long rod composite insulators [16]. Malleable iron, ductile iron or aluminium alloy are used to manufacture metal end fittings for line and station post insulators [9]. The flanges of hollow composite insulators are made by cast or machined aluminium [9].

There are quite a lot of metal end fittings available on the market for composite long rod insulators, but the most common types are ball, socket, oval eye, Y-clevis, tongue and clevis [9]. Please refer to Figure 2-27 for an example of the metal end fittings.

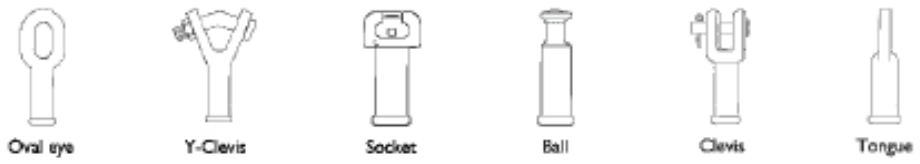

Figure 2-27: Metal end fittings for composite long rod insulators [9]

These metal end fittings are preferably, swaged or crimped onto the core [22]. Please refer to Figure 2-28 for an illustration that demonstrates this process. However, this process should

be done very carefully not to over-compress during manufacturing which can cause stress concentrations and core fractures, or under-compress, which can result in a mechanically weak insulator, which can fail due to pull-out [23].

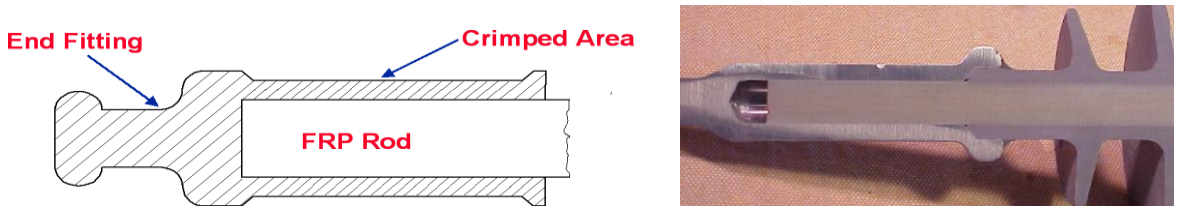

a) Schematic of crimped (swaged) end fitting b) Dissection of crimped (swaged) end fitting

Figure 2-28: Illustration of crimped (swaged) process [22]

2.3.3.4.5 End fitting seal

The region between the metal end fitting, polymer housing and core is one of the most vulnerable on a polymer composite insulator [7]. This region is protected from the environment by an end fitting seal [7]. The function of the end fitting seal is to prevent moisture and pollution from entering the core, which can lead to the eventual failure of the insulator [7]. Different end fitting seals are used, either individually, or as a combination of the following [22]:

- Direct bonding of the polymer housing to the metal end fitting.
- Single or double O-rings.
- A compression seal between the metal end fittings and polymer housing.
- A metal connection piece over the polymer housing and metal end fitting.
- An external or internal sealant applied in the interface region. In some cases, a metastable sealant is used, which does not cure fully and remains spongy, to accommodate different expansion coefficients of materials used in the sealing interface.

Please refer to Figure 2-29 for an example of the different end fitting seals.

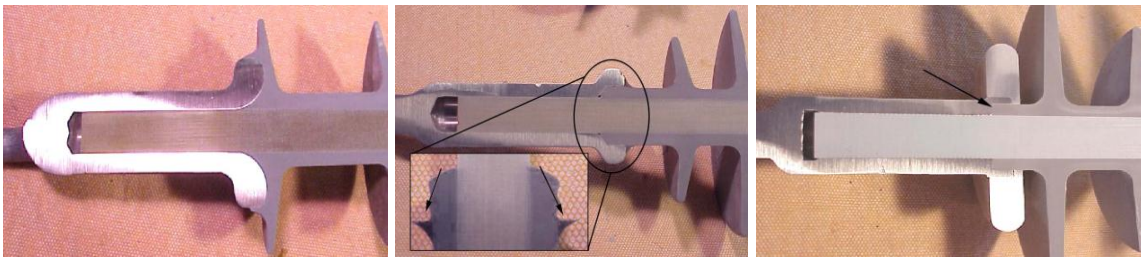

a) Direct bonding b) O-ring c) Compression seal

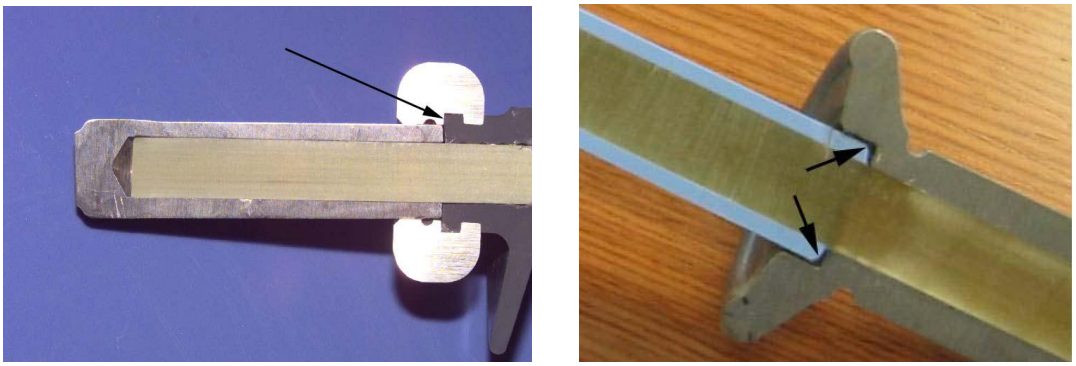

d) Metal connection piece e) Metastable sealant

Figure 2-29: Examples of end fitting seals [22]

2.3.3.4.6 Electric field grading methods

The electric field (E-field) within the rubber and core material and in the air close to the surfaces of polymer housing, metal end fittings, earthed hardware and corona rings needs to be controlled, because it affects both the short and long term performance of polymer composite insulators [20, 21]. It can be controlled using one or more of the following E-field grading methods, depending on the manufacturer and application of the insulator [7]:

- Geometric design and dimensioning of metal end fittings. In this method the metal end fitting is normally large and curved as illustrated in Figure 2-30 (a).
- Attaching E-field grading devices that have large dimensions and curved edges, as shown in Figure 2-30 (b).
- Attaching corona rings, also known as grading rings, at the energised and/or earthed ends of the insulator as illustrated in Figure 2-30 (c) and (d). Corona rings are dimensioned by considering the system voltage, hardware geometry, structure dimensions, conductor bundle configuration, insulator parameters and manufacturer recommendations. Other aspects that also need to be considered are the power arc withstanding capability and attachment process of corona rings.

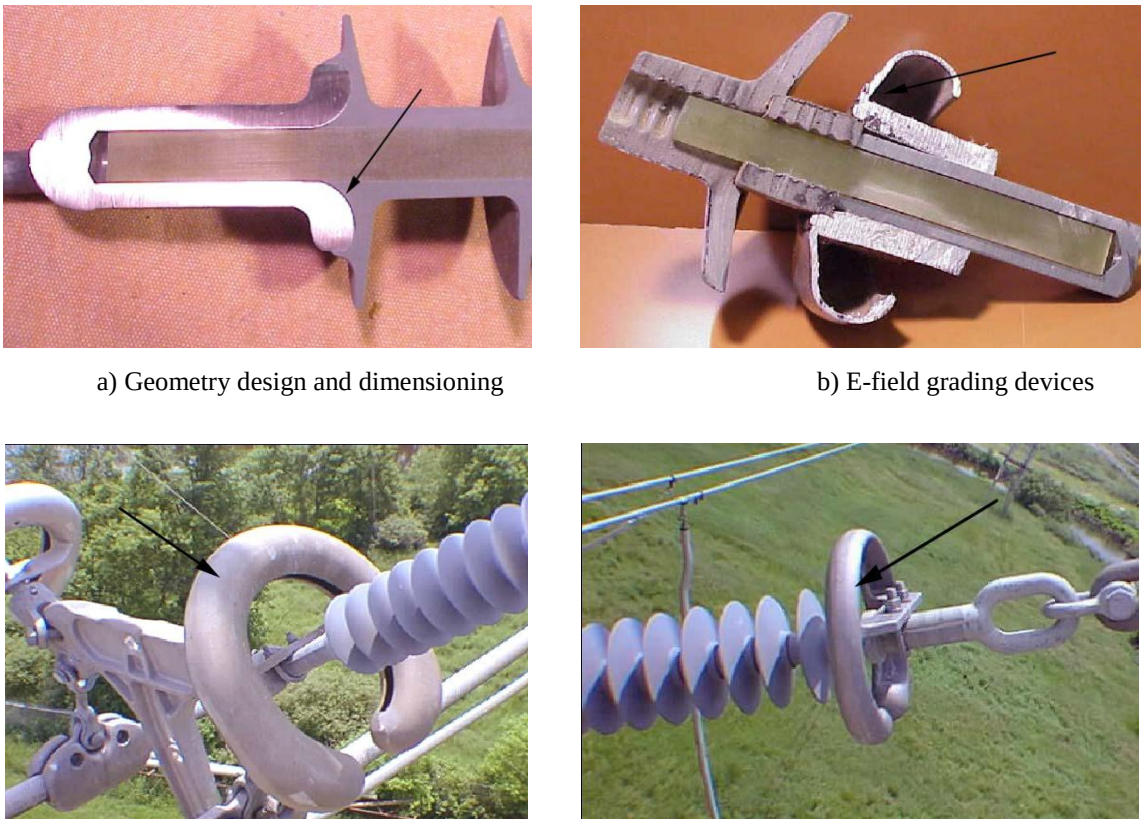

a) Geometry design and dimensioning

b) E-field grading devices

c) Corona ring on energised end

d) Corona ring earthed end

Figure 2-30: E-field grading methods [7]

2.4 Flashover performance of insulators

Air, at atmospheric pressure, is the main dielectric used in high voltage networks, because it is a good insulator and self-restoring, provided the electrical stress is kept below the ionisation threshold [9]. Air, however, has no mechanical properties such as supporting the weight of an overhead high voltage conductor. Thus, various insulators have been developed over time, to perform the dual functions of mechanical support and electrical insulation of the line from the supporting hardware [9].

The design of an insulator is very complex, if one takes into account all the stresses it must withstand, e.g. mechanical, electrical and environmental stresses [9]. These three stresses are interlinked, but only the effects of electrical and environmental stresses on insulators will be discussed in this section.

The effects of the electrical and environmental stresses on the insulator will be discussed in relation to:

- The withstand voltages of insulators during dry and wet conditions.
- Lightning and switching impulse overvoltage.
- Pollution flashover process.

The first two topics will be discussed briefly, whereas the third topic will be discussed in more detail because the pollution flashover characteristics of insulators were actively researched in this project.

2.4.1 Dry and wet withstand voltage

An insulator must be able to withstand the operating voltage and overvoltage of the system under both dry and wet conditions [9]. The dry arc distance of the insulator determines the dry surface withstand voltage and also to a large extent the wet surface withstand voltage [9].

2.4.2 Lightning and switching impulse overvoltage

An insulator must be able to withstand lightning and switching impulse overvoltage [9]. The dry arc distance of the insulator determines both the lightning and switching impulse flashover voltages [9]. At system voltages below 300 kV, lightning impulse flashovers are more dominant because switching impulse voltage levels are not high enough to cause flashovers [9]. Switching impulse flashovers are more critical at system voltages of 300 kV and above because they are directly related to the system voltage [9].

2.4.3 Pollution flashover process

Pollution related outages came to the fore front during the 1930s, a few years after the introduction of power transmission lines, and it led to the development of many insulator monitoring techniques, e.g. leakage current monitoring, which are still in use today [7]. The reason it came to the fore front is that the presence of an electrolytic pollution layer reduces the withstand voltage of insulators significantly, which leads to unexpected flashovers [9]. These unexpected flashovers caused major problems in power system reliability, which led to the initiation of many projects aimed at researching the performance of insulators under polluted conditions [7]. The aim of this continuous research was to understand the pollution

flashover process and to find insulators that are able to withstand the different pollution conditions to which they are subjected [9].

Flashovers on transmission line systems are normally the result of airborne pollution that is deposited on the surface of insulators [7]. However, it should be noted that the pollution on the insulator surfaces is not a problem in its dry state; it only becomes a problem when it is moistened and the salts within dissolve to form a conductive layer on the insulator surface [7]. The pollution may come from the sea, desert, agriculture, industrial or construction activities. One of the most common pollutants is sea-salt, sodium chloride, which may cause problems on transmission line insulators located in coastal regions [7]. A wide variety of pollution substances e.g. gypsum, sulphuric acid, fly ash and cement may be present on insulator surfaces in agriculture and industrial regions [7]. In some instances, the pollution may contaminate the insulator in its dissolved state, e.g. saltwater fog; or the pollution in its dry state may reduce the dielectric strength of the insulator e.g. when carbon or metallic pieces are present on the insulator surface [7].

In general, the presence of conductive layers on an energised insulator surface leads to the flow of leakage currents on the insulator surface. This leads to a temperature increase of the conductive layer in the high current density areas, which leads to the conductive layer evaporating and the forming of dry spots (dry bands) in those areas. When the dry bands are formed, the voltage distribution over the insulator becomes non-uniform with most of the voltage stress concentrated over the dry bands [12]. This high voltage concentration over the dry band may cause a spark-over, which is called a partial discharge [12]. Depending on the conductivity of the pollution layer, the partial discharge may grow to span the whole insulator, leading to a flashover [12]. This process can be summarized by three main processes with several sub processes as shown in Table 2-2. The three main processes are [7, 24]:

- Build-up of pollution on insulator surfaces.
- Insulator wetting.
- Partial discharge activity and development of flashovers.

Although the flashover processes are indicated as individual items in Table 2-2, they combine into one seamless process [7].

Table 2-2: General principles of the pollution flashover process [7]

	Description and Mechanisms	Influencing Factors	
	1.Clean Insulation surface	None	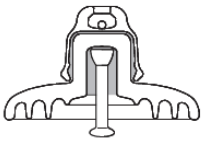
Contaminant Build-up	2. Contamination Deposited a. Airborne particles b. Salt spray c. Under dry conditions, surface remains a good insulator	- Aerodynamic properties - Surface properties - Contamination type - Electric field (mainly dc)	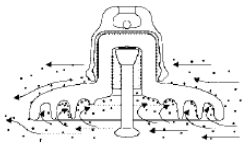
	3. Cleaning (removal of contamination) a. Rain b. Wind	- Insulator profile - String orientation - Precipitation type and intensity	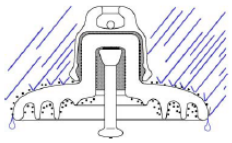
Wetting	4. Wetting of Contamination Layer a. Condensation b. Fog c. Rain d. Absorption e. Chemical Diffusion	- Contamination type (e.g., salt solubility) - Insulator profile - Surface properties - Wetting type	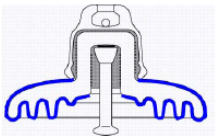
Discharge Activity and Flashover	5. Formation of Dry Bands a. Leakage current flows on surface b. Increased heating in regions of high current density c. Dry bands form in regions of increased heating	Surface resistance • Humidity of air • Rate of rainfall • Level of contamination - Distribution of contamination - Insulator geometry	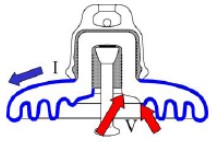
	6. Dry Band Arcing a. Dry bands interrupt leakage current flow b. Full voltage across dry bands c. Air/surface cannot maintain potential difference d. Arcs form across dry bands e. Leakage currents surge when arcs form	- Surface properties - Degree of wetting - Level of contamination - Size of dry band	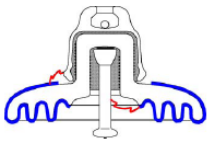
	7. Growth/Quenching of Dry Band Arcs a. Dry band arcs sustained if surface resistance of entire string is low enough b. Increased heating at arc roots dries out contamination, increasing dry band size and hence arc length c. Surface resistance decreases with increases in arc lengths, resulting in increased leakage current magnitudes c. Arc grows and may self-extinguish as gap bridged becomes too large for arc to maintain itself. d. Arcs may be quenched by precipitation	-Surface Resistance • Rate of precipitation • Humidity • Amount and type of contamination • Surface properties - Insulator profile	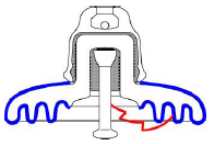
	8. Flashover a. If dry band arcs bridge a critical length of insulator, flashover occurs b. Multiple arcs may join (coalesce) c. Single arc may grow entire length	-Surface Resistance • Rate of precipitation • Humidity • Amount and type of contamination • Surface properties - Insulator profile	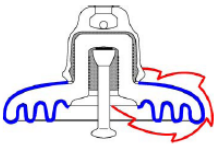

2.4.3.1 The build-up of pollution on insulator surfaces

There are two types of pollution that may build up on the surface of an insulator, which may lead to a flashover [13]. The first type pollution, Type A, is a solid pollution deposited on the insulator surface which consists of non-soluble and soluble components [13]. The soluble component becomes conductive when moistened and can be divided into high soluble salts, e.g. salts that dissolve easily in water like sea-salt (NaCl), and low solubility salts, e.g. salts that hardly dissolve in water, like gypsum [13]. The non-soluble component is divided into a group that retains water e.g. sand, dust and clay, which reduces the insulator's flashover voltage, and another group that is hydrophobic e.g. oily and greasy substances, which enhance the insulator's flashover voltage [13].

The second type pollution, Type B, is pollution in liquid form with electrolytes and very little or no non-soluble component, deposited on the surface of the insulator [13]. This pollution is already conductive in its deposited state. Examples of it include seawater spray close to the coast, or gases in a solution e.g. SO_2, H_2S or NH_3 close to chemical plants, or crop spray and acid rain [13].

2.4.3.1.1 Mechanisms of pollution deposition

There exist several mechanisms to deposit solid and liquid pollution on insulator surfaces. The first mechanism is called 'aerodynamic action' whereby pollution particles in the air, may be carried over great distances by the wind [25]. When this pollution-air combination comes into contact with an insulator, the air is deflected around the insulator body, but the particles in the air are not deflected by the same portion and are deposited on the insulator [8]. Denser particles like sand are deposited onto the side of the insulator that faces the wind direction, because they are not sufficiently deflected by the airflow [8]. The less dense particles will follow the airflow more closely and will only be deposited in areas where the airflow makes small curvatures (vortexes) such as on the leeward side of the insulator, or between shed under-ribs as shown in Figure 2-31 [8]. Aerodynamic action is, with a few exceptions, the dominant mechanism for the depositing of pollution [26].

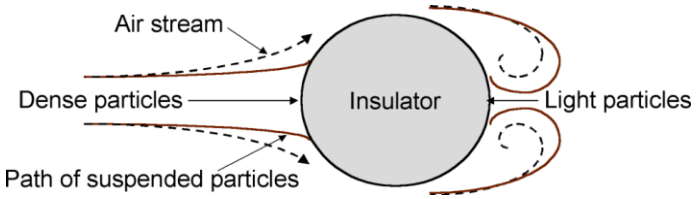

Figure 2-31: Pollution deposit by aerodynamic action [8]

Another method is pollution deposit by gravitation [7]. This method will occur under low wind or still conditions, when the pollution particles in the air settle on a horizontal surface, because of gravitational forces [7]. This pollution deposition method may be dominant in areas close to a pollution source [7].

A third method of pollution deposit is via the heating effect of leakage currents during conductive fog conditions [7]. The heating effect of the leakage current evaporates the water from a wet electrolytic layer on the insulator surface and leaves a salt residue behind, which are normally concentrated around the areas with the highest leakage current density [7].

Pollution may also be deposited on the insulator surface by electric field forces on charged particles [7]. The method is almost negligible under AC energization, because of the alternating polarity of the electric fields [7]. It is more prominent under DC energization [7]. This method will occur on DC energized insulators, under low wind or still conditions [27]. During the conditions mentioned above, the electric field forces are much stronger than the gravitational forces when the electric field strength is high, and is comparable to the gravitational forces when the electric field strength is low [27]. This method of pollution deposition may be dominant for charged particles moving in still air, in the presence of a strong DC electric field [27]. When the wind is strong, the aerodynamic action pollution deposit method is dominant [27]. However, if there are deep ribs under the shed, the wind will be obstructed and vortexes may be formed [27]. The velocity of the wind and particles within the wind would drop significantly and provide a change for the electric field forces to deposit the particles on the insulator surface [27].

2.4.3.1.2 Natural cleaning of surface pollution

The surfaces of insulators are naturally cleaned by precipitation and strong winds [7]. High intensity rain is very effective in removing pollution from the surfaces of insulators. The exposed surfaces that come into direct contact with the rain are more effectively cleaned in

comparison with protected creepage areas [28]. In desert areas, strong winds may carry large sand particles that may remove the pollution from the insulator side that faces the direction of the wind, through a sandblasting effect [7]. The extent of pollution removal depends on the intensity and duration of the cleaning event [7]. Thus, the level of pollution deposited varies over time with the highest level occurring before a cleaning event starts [7].
Liquid pollution is characterised by the fast build-up of electrolytes [7]. It can be so fast that a clean insulator can build up sufficient pollution to flashover in a single event [7]. Thus, natural cleaning has little influence in the flashover process of liquid pollution [7].

2.4.3.1.3 The effects of insulator properties on the accumulation of pollution

As realized from the above discussions, the level and distribution of pollution is a complex interaction between the environment and the insulator. This process is influenced by the profile, surface properties and installation orientation of the insulator [7].

The use of different insulator profiles is dictated by specific pollution environments. For instance, an open aerodynamic profile is more beneficial in an environment where there is a risk of long-term build-up of airborne pollution [7]. This is due to less pollution deposited on this type of profile and the pollution is accessible to natural cleaning processes [7]. In cases where there is a risk of fast pollution build up events, e.g. a conductive fog event, the anti-fog profile is more effective, because a large part of the insulator surface is protected from fast pollution accumulation [7]. Likewise, when there is a risk of gravitational pollution deposition, profiles with large horizontal surfaces should be avoided [7].

Insulator surface properties are also important in determining the amount of pollution deposited on the surface. For example, smooth surfaces accumulate less pollution than rough surfaces and dry surfaces accumulate less pollution than damp surfaces [7]. Silicone rubber insulator surfaces accumulate more pollution than glass and ceramic insulator surfaces, due to the presence of silicone oils on silicone insulators [29].

As mentioned above, the installation orientation of insulators has also an effect on the accumulation of pollution. Vertically oriented insulator strings (I-strings) accumulate more pollution than angled insulator strings (V-strings) or horizontally oriented strings (dead ends), because there are larger protected areas on the underside of the I-string insulators where

natural cleaning is less effective [7]. However, horizontally oriented insulator strings facing to or from a well-defined pollution source, may accumulate more pollution, due to the larger areas where airborne pollution deposition may occur [30].

2.4.3.2 Insulator wetting processes

It is commonly known that pollution related flashovers happen when the insulator is wetted during drizzle, fog and/or high humidity conditions [7]. The wetting of the insulator may be caused by one or a combination of the four known wetting processes, which are described as follow [31]:

- Free water droplets in the air - during rainy or foggy conditions - collide with the insulator surface and wet the surface. The distribution of the wetness on the insulator surface depends on the insulator profile and the size of the droplet. Smaller droplets tend to wet the underside of the insulator surface because they are more influenced by air movement around the insulator.
- Insulator surface pollution absorbs water molecules from the air via a deliquescence process, if the pollution particle is a salt, or absorption if it is a non-soluble material. For typical pollution layers, the deliquescence process occurs when the partial vapour pressure of the surrounding air is higher than the vapour pressure of the salt. For sea salt (NaCl), it occurs when the relative humidity is approximately 75%. The distribution and amount of wetting is dependent on the type of salt and non-soluble material present on the insulator.
- Insulator surface is moistened by condensation which occurs when the immediate surrounding air temperature of the insulator surface is equal or lower than the dew point temperature.
- Polluted surfaces are moistened more severely than clean surfaces because the polluted surfaces have a higher condensation rate, due to chemical diffusion processes.

The rate at which moisture forms on the surface of a polluted insulator may vary from light - during fog, to heavy - during rain. It may further reach the insulator surface gently, as during a light drizzle or violently, as during heavy rainfall. Natural cleaning becomes more effective, as the rate of wetting increases [7].

When the wetting of the dry pollution on an insulator surface occurs, the soluble pollution gradually dissolves to form a thin conducting liquid film on a hydrophilic insulator surface, or droplets on a hydrophobic insulator surface [7]. As the wetting continues, a redistribution of pollution on the insulator surface may take place and some of the pollution may leach, by dripping off the insulator [7]. Thus, the surface resistivity of the insulator first decreases as the salt dissolves and then increases after a while due to the leaching effect. The minimum surface layer resistance, i.e. maximum conductivity, and the time when it occurs, depends on the solution characteristics of the pre-deposited pollution layer, such as the solubility and the speed at which it changes into a solution [32]. The following statements illustrate it more clearly:

- The impact of the wetting rate on the surface layer conductivity is greater for low-soluble salts than for high-soluble salts, as proven in laboratory tests [33].
- The amount and type of the non-soluble pollution plays a role in the wetting process because non-soluble pollution binds water to the insulator surface, which may lead to the formation of a highly conductive layer on the surface of the insulator [7].
- The time it takes to reach maximum conductivity on an insulator surface, and the value of it, depends on the hygroscopic and hydrophobic properties of different inert material [34].

From the above statements, it is clear that conductivity on an insulator surface depends on a complex process that includes the amount of wetting, the chemical composition of the soluble and non-soluble pollution and the material and shape of the insulator itself [7]. Thus, critical wetting can be defined as a wetting rate that is fast enough to wet the pollution layer effectively for the flashover process to take place and yet slow enough not to wash the pollutants from the insulator surface [7]. In general, it can be stated that a low wetting rate, such as fog, is critical for fast dissolving salts such as NaCl and a heavy wetting rate, such as rain, is critical for slow dissolving salts such as gypsum [7].

During wet pollution conditions, such as conductive fog, the pollution is deposited in a solution state. For this type of pollution, the conductivity of the solution itself is important because higher solution conductivity leads to a greater flashover risk [7].

2.4.3.3 Partial discharge activity and development of flashovers

An important part of the pollution flashover process is the formation of a conductive layer on an insulator surface. The presence of a conductive layer leads to a non-uniform voltage distribution over the surface of the insulator and to the inception of discharge activity [7]. This discharge activity may develop into a flashover, if the conductivity of the pollution layer, the wetting conditions, and the surface properties of the insulator allows [7]. The discharge development is the same for solid and liquid pollution types, but differs significantly on hydrophilic (glass and porcelain) and hydrophobic (silicone) insulators [7]. The discharge development process on hydrophilic and hydrophobic insulators will be discussed in detail in this section.

2.4.3.3.1 Discharge development on hydrophilic insulators

The discharge development process on a single polluted insulator will be explained in accordance with the simplified diagram in Figure 2-32 [35].

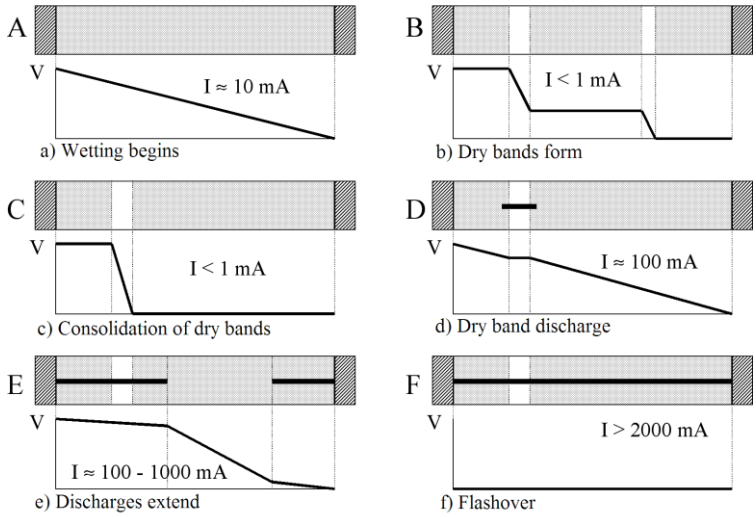

Figure 2-32: Typical steps and their associate voltage distributions in the discharge development of polluted insulators [35]

As the wetting increases, the impedance of the insulator reduces and changes from mostly capacitive, at the start of the wetting, to mostly resistive (Figure 2-32 (a)) [35]. This drop in impedance leads to an increase in leakage current and subsequently the formation of dry bands in the areas where the current density is the highest, due to localized heating [35]. The dry bands block the flow of leakage current, which results in the relocation of the applied voltage directly over the dry bands (Figure 2-32 (b)) [35]. The shift of the applied voltage to

over the dry bands leads to the formation of corona activities at the dry bands, which contribute to the drying of the conductive film and thus increases the size of the dry bands [35].

The rate at which dry bands form and are extinguished, depends on the intensity of the wetting process and drying effect of the leakage current [35]. During rainfall conditions, it may not be possible to form dry bands until after the rain, because of the intense wetting action [35]. When a dry band is established, the leakage current value drops, allowing the wetting action to overcome the drying effect of the leakage current [35]. This may lead to the re-wetting of the smaller dry bands and the forming of only one dominant dry band, which is maintained by the heating effect of corona activity. (Figure 2-32 (c)) [36].

During the occasional dry band discharge activity (Figure 2-32 (d)) the voltage distribution becomes more linear [35]. Exactly how the dry band discharge activities develop into a flashover is not fully understood yet, but it is known that for a single cap-and-pin insulator, the arc develops from the high voltage electrode [7]. The flashover is a result of the growth of the dry band discharge to span the whole insulator length (Figure 2-32 (e) and (f)) [7]. At an advanced stage of dry band discharge development, a flashover is determined by the breakdown strength of the pollution layer, which absorbs most of the applied voltage [35]. It is also known that the flashover probability becomes very high if the insulator leakage current approaches a certain threshold value [12]. This value is defined as in the maximum peak leakage current one cycle before flashover [12], as

$$I_{\max} = \left(\frac{S_{CD}}{15.32} \right)^2 \tag{2-3}$$

where S_{CD} represents the specific creepage distance of the insulator.

2.4.3.3.2 Discharge development on hydrophobic polymer insulators

The development of discharge on hydrophobic polymer insulators is distinctively different from that on hydrophilic insulators such as glass and porcelain insulators [7]. Leakage current observations of hydrophobic insulators show a continuous low level current with occasional single high current peaks [37]. This is in contrast with the gradual build-up of current and densely spaced high current peaks for hydrophilic insulators [7]. The main reason

for the difference is that on hydrophobic insulator surfaces, it is not possible to form a continuous conducting layer [7].

On hydrophobic insulator surfaces, droplets form when the surface is wetted by, e.g. fog, condensation or rain. Salts present on the surface of the insulator diffuse into the droplets to make it conductive [7]. The water from some of the drops also migrates into the dry pollution to form a damp, high resistive layer [7]. Thus, the insulator is covered with a high resistance damp layer with conductive droplets scattered over it. The leakage current of the insulator reaches a stable, low value, once an equilibrium is reached between water evaporation (due to the heating effect of the leakage current) and the reduction of surface resistance (due to wetting) [38].

The electric field on the edges of the scattered water droplets is enhanced as shown in Figure 2-33 due to the high permittivity of water (ε_r = 80) [20].

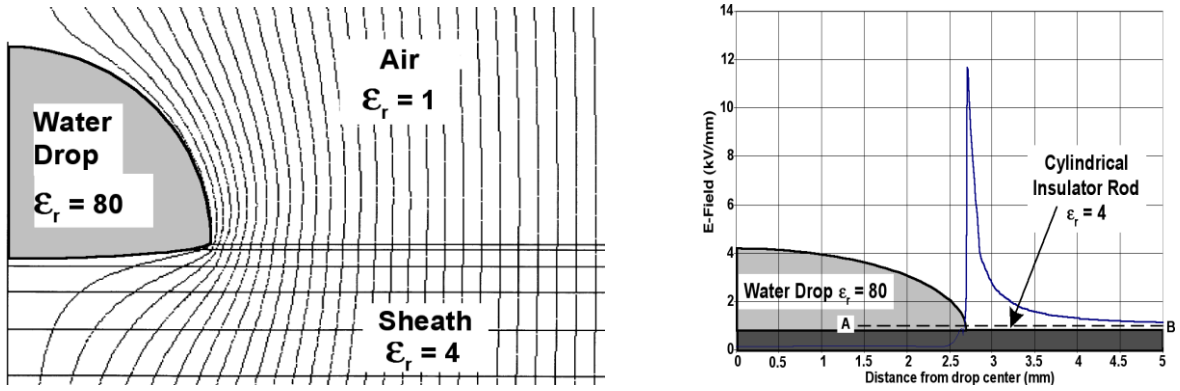

a) Equipotential lines surrounding a water drop

b) E-field surrounding a water drop

Figure 2-33: Results of finite element modelling showing an enhancement of E-field surrounding a water drop on a polymer insulator surface [20]

If the electric field surrounding the water droplets is enhanced above a critical value, corona activity will be present on the edges of the water droplet [20]. This critical value of the electric field is a function of the water droplet size and the hydrophobicity level of the rubber housing [7]. It will decrease when the water droplet size increases and/or when the hydrophobicity level decreases [7]. Furthermore, the critical value required for water droplet corona on the sheath and sheds differs due to differences in electric field orientation on the water drops [7]. Single droplet experiments have shown that water drops on the sheath

requires a critical value greater than 4 kV/cm and water drops on the shed requires a value greater than 8.5 kV/cm, depending on the hydrophobicity level [7].

Research has verified that the presence of water drop corona may result in localized temporary loss of hydrophobicity on hydrophobic insulators [20, 21]. This loss can be attributed to the chemical by-products of corona and to the presence of moisture on the surface of the insulator [39]. The temporary loss of hydrophobicity results in the forming of water patches in the areas with lower hydrophobicity levels. These surface water patches are separated by dry regions, or bands, which may be bridged by localized arcs, due to the high electric field present on the edges of the water patches [40]. The energy and temperature of these localized arcs are significantly higher than that of water drop corona and may result in additional areas where temporary loss of hydrophobicity is experienced [41]. Over time, this process continues to affect larger regions [7].

The activity described above, is initially located at the energized end of the insulator, which is the region with the highest electric field, and causes this area to be dried out more in comparison with the rest of the insulator [37]. This forms a high resistance area at the energized end of the insulator, which effectively prevents the leakage current from flowing and forms a highly non-uniform field, concentrated at the ends of the high resistance area, which may initiate a streamer breakdown process [37]. If the streamer spans a long enough high resistance area, a condition may arise wherein the wet section of the insulator is overstressed and the streamer may develop into a flashover [7]. This flashover process is generally characterized by the absence of leakage current, which lasts until the breakdown of the high resistance section, leading to high current pulses [7].

2.5 Insulator degradation

Degradation of insulators occurs due to several factors which are listed below:

- Manufacturing defects that include any fault that result from an inadequate manufacturing and assembly process or inadequate quality control [42].
- Improper handling of insulators during storage, installation and maintenance [7].
- Service induced damage or deterioration, due to incorrect dimensioning of the insulator for the pollution environment where it is installed [9]. This may lead to severe discharge activity or mechanical overload conditions [9]. Deterioration of

correctly dimensioned insulators may also occur due to ageing caused by environmental and electrical stresses [43].

- Vandalism caused by human activity such as gunshots and throwing of rocks [43].
- Damaged caused by rodents and birds through gnawing and pecking respectively [43].

Only the degradation to insulators caused by service induced damage or deterioration will be discussed in this section, because it was the only degradation factor observed during the course of the project and it would be of great academic benefit and insightful to compare the results of this project to theory. Furthermore, the degradation of insulators will be discussed by referring to the following topics:

- Degradation of glass insulators.
- Degradation of porcelain insulators.
- Degradation of composite insulators.

2.5.1 Degradation of glass insulators

Good quality glass insulators can be used in service for more than 30 years without any sign of electrical and mechanical deterioration [7]. However, it is known that a small number of units shatter spontaneously within a short time period after installation [7]. This is caused by the inclusion of impurities in the raw materials used to manufacture the glass which were left in the glass; not weeded out by the thermal shock tests at the end of the glass shell manufacturing process [9].

Glass insulators are highly resistant to electrical punctures [7]. However, if they do puncture, the glass would shatter, because of the residual tensile stress in the glass, caused by the toughening process [8]. Thus, no hidden punctures can exist on glass insulators. Punctures and shattering of the glass may be caused by the following:

- Concentration of electrical discharges under a thick layer of pollution may cause localized heating, possibly resulting in a thermal puncture [7].
- Steep-fronted electrical impulse caused by lightning and switching flashovers [9].
- Erosion of the glass surface is caused by partial discharge activity across dry bands in the pin area, confined to highly polluted environments; or sand blast activity, confined to desert environments [9]. Please refer to Figure 2-34 for an example of erosion around the pin area. If the erosion is deep enough to penetrate the toughened layer, it

may lead to the disturbance of internal mechanical forces which may cause the glass shell to shatter [9].

- Thermal run-away process of glass insulators manufactured for HVAC applications, installed in a HVDC system [44]. The thermal run-away process may lead to a redistribution of internal mechanical forces that may eventually shatter it [44].

Figure 2-34: Example of erosion in pin area of a glass disc insulator due to partial discharge activity

Glass insulators may also degrade by mechanical deterioration, caused by sparks near the cap and pin areas, which may damage the galvanized material and open the cap and pin to corrosion [14]. Corrosion can reduce the diameter of the pin to a point where it is sufficiently weakened to drop the line as shown in Figure 2-35 [7, 9]. Corrosion on the cap does not have such a detrimental effect, due to the physical size of the cap. Additionally, swelling of the pin inside the cement may cause internal mechanical stresses which may lead to insulator breakage [9].

Figure 2-35: Example of corrosion on the pin of a cap-and-pin glass insulator [7]

2.5.2 Degradation of porcelain insulators

An electrical puncture, which may be caused by a steep-fronted lightning impulse, thermal run-away process or long term high electric field stressing, may be a possible mechanism of

degradation of porcelain insulators of the class B type [8]. An electrical puncture on a porcelain insulator looks like a pinhole through the porcelain shell, from the cap to the pin [7]. The air breakdown inside the puncture channel may be intermittent, which may cause several line faults where pin insulators and single cap-and-pin strings are used and the causes of these line faults are very difficult to locate [9]. Where one disc in a string of several is punctured, no problems may be encountered, because the remaining undamaged insulators are sufficient to withstand the line voltage [9].

Another possible mechanism of degradation is cracking or breakage, caused by thermal stress [9]. Porcelain insulators are very susceptible to damage caused by rapid thermal changes or uneven heating [9]. Thus, the heat of power arcs may cause damage to the glazed surfaces, shed breakage and cracks in the sheath of long rod insulators, leading to a complete mechanical failure [9]. Cracks may also form by mechanical overloading and mechanical stresses created by ion movement in HVDC application and swelling of cement [7]. Please refer to Figure 2-36.

Figure 2-36: Example of a crack on a porcelain shell [7]

Corrosion can also damage the pin, as with glass cap-and-pin insulators, leading to a mechanical failure, which may cause the dropping of the overhead conductor [9]. Dropping of an overhead conductor may also happen when a long rod insulator loses its cap, due to improperly formulated lead antimony cement, or during a mechanical separation of the cap and pin hardware of a cap-and-pin insulator [7, 9].

2.5.3 Degradation of composite insulators

Life expectancy is the most important, but also the most uncertain parameter of composite insulators, for both users and manufacturers [45]. Further, it should be understood that any polymer material used to manufacture composite insulators will age, over time, but it is important that it does not drop the line or permit an electrical flashover [45]. The ageing and service conditions of composite insulators may differ with respect to polymer material formulations, filler type percentages, vintage, manufacturing quality, insulator profile design, operating electrical stress, service environment conditions, and, installation and handling [45].

In this section, the ageing of composite insulators is categorized according to the degree of severity. The first group is categorized under the term deterioration, which is defined as cosmetic or superficial ageing that has occurred on the composite insulator, as a direct result of exposure to the service environment, electrical stress, mechanical loading or careless handling [45]. This degree of ageing severity is not expected to cause a significant reduction in the insulator's performance and/or longevity [45]. Deterioration does not significantly reduce the thickness of the polymer housing that prevents moisture from entering the core, or reduce the creepage distance by more than 10% [45]. The second group is categorized under the term damage, which is defined as changes to the composite insulator that have occurred as a consequence, or progression of, deterioration and/or external influence, including careless handling [45]. This degree of ageing severity may have a negative impact on the insulator's performance and/or longevity [45].

2.5.3.1 Deterioration

The following visual observations are categorized as deterioration; examples of each observation can be seen in Figure 2-37 [45].

- Chalking: The appearance of a rough or powdery surface due to the exposure of filler particles from the housing material.
- Colour changes: Change in the colour of the housing material.
- Crazing: Consists of micro fractures with depths of approximately 0.01 to 0.1 mm on the surface of housing material.
- Metal end fitting corrosion: Deterioration of metal end fittings due to a chemical reaction with the environment e.g. rusting.

- Grease leakage: Escape of grease from sheath-shed or sheath-sheath interfaces, onto the sheath or shed surface.
- Light erosion: Superficial, irreversible and non-conducting degradation of the surface of the insulator, which occurs by loss of material which does not penetrate deeper than 1 mm [45]. This can be uniform or localized.
- Minor de-bonding: Separation of different parts of the insulator, which do not decrease the creepage distance significantly i.e. by more than 10% or reduce the thickness of sheath by 1 mm.
- Minor splitting or cutting: Minor breakage, tearing or cracks in polymer housing, which may have resulted in removing of material which does not decrease the creepage distance significantly i.e. by more than 10% or reduce the thickness of sheath by 1 mm.

a) Chalking

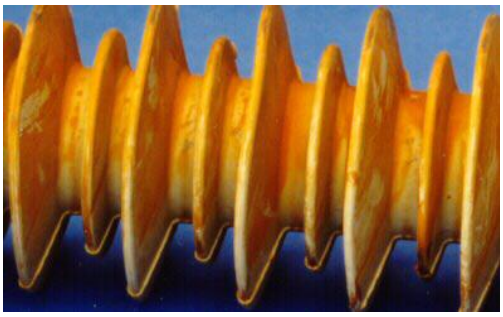

b) Colour changes

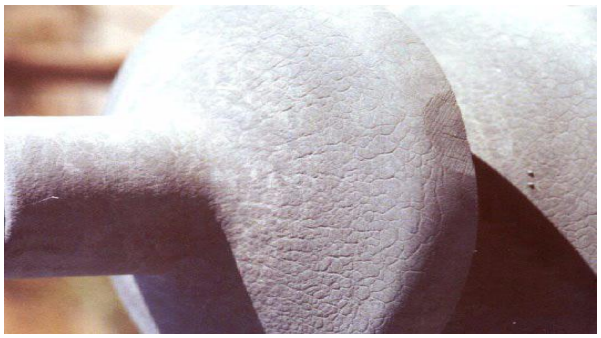

c) Crazing

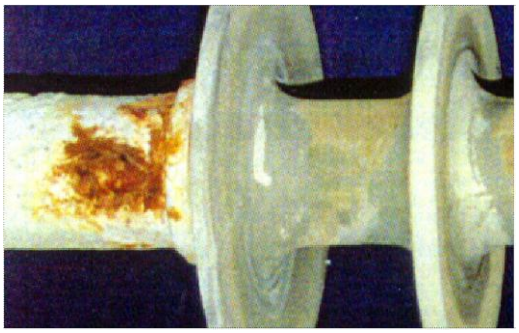

d) Metal end fitting corrosion

e) Grease leakage

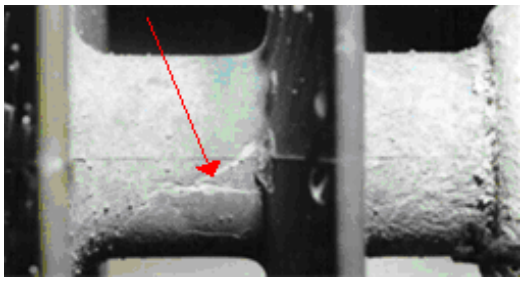

f) Light erosion

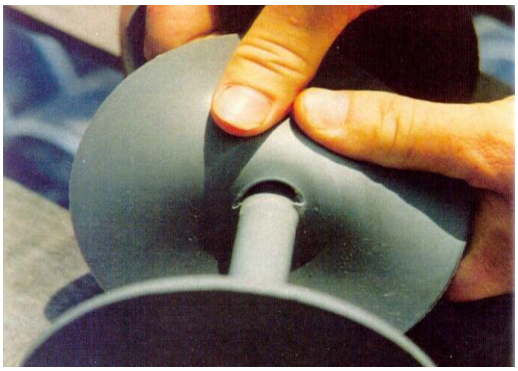

g) Minor de-bonding

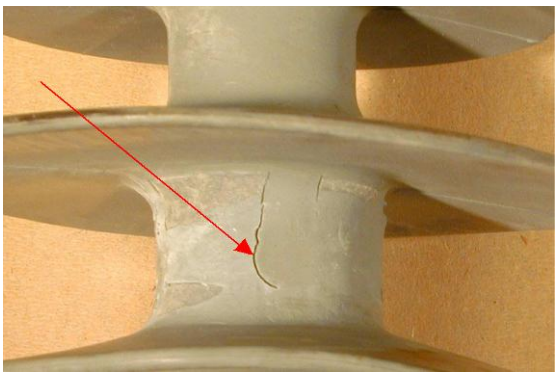

h) Minor splitting or cutting

Figure 2-37: Examples of deterioration category [45]

2.5.3.2 Damage

The following visual observations are categorized as damage and examples of each observation can be seen in Figure 2-38 [45].

- De-bonding: Separation of different parts of a composite insulator which significantly reduces the creepage distance, i.e. greater than 10%, or thickness of sheath by more than 1 mm.
- Peeling: Bonding loss of the metal end fitting seal.
- Power arc damage: Damage caused by high current and temperature concentration at the metal end fitting, caused by an electrical flashover.
- Puncture: A hole in the insulator sheath or shed.
- Splitting or Cutting: A break, tear or crack in the polymer housing which may have resulted in the removal of material, and which reduced the creepage distance by more than 10%, or the thickness of the sheath by more than 1 mm.
- Erosion: Irreversible and non-conducting degradation of the insulator surface, which occurs with major loss of material, significantly reducing the thickness of the sheath and creepage distance. It may occur uniformly or locally.
- Tracking/Carbonising: Irreversible degradation, by formation of conductive paths starting and developing on the surface of an insulating material. These tracks look like carbon tracks that cannot easily be removed and are conductive, even when dry.
- Core exposure: Uncovering of the core to the environment by erosion, tracking, puncture, splitting or careless handling.
- Mechanical failure of the core: Breakage of the core rod of an insulator, due to erosion or tracking, so that the mechanical load can no longer be supported.
- Brittle fracture: It's a type of mechanical failure, characterized by a smooth surface mostly running perpendicular to the axis of the core or, (sometimes) stepwise formations of smooth surfaces, or, fibres and resin break on the same plane or a clean fracture surface, or, normally a small residual fracture section which is generally fibrous.

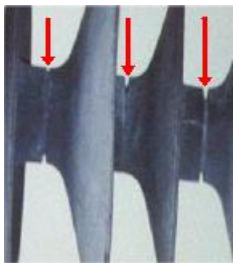

a) De-bonding

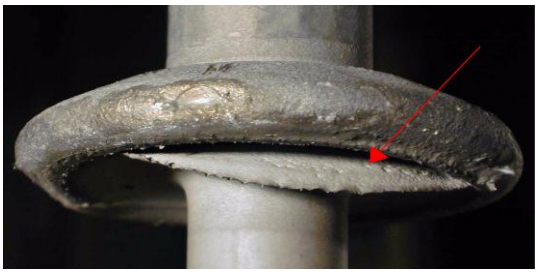

b) Peeling

c) Power arc damage

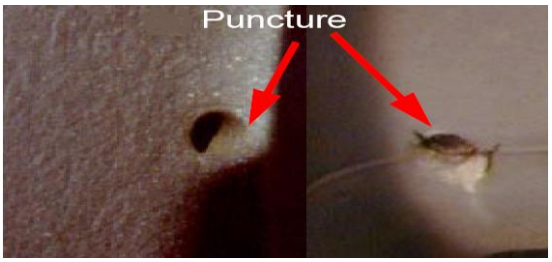

d) Punctures

e) Splitting/Cutting

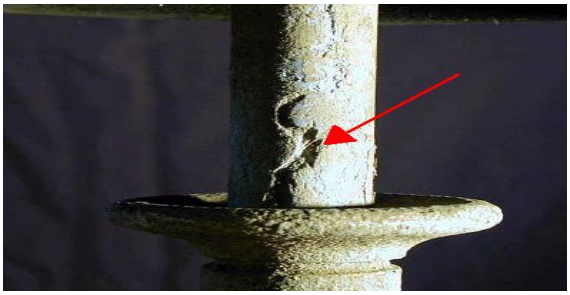

f) Erosion

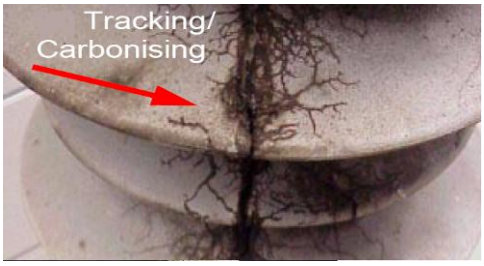

g) Tracking

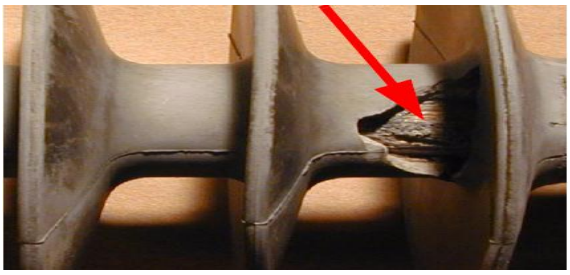

h) Core exposure due to splitting

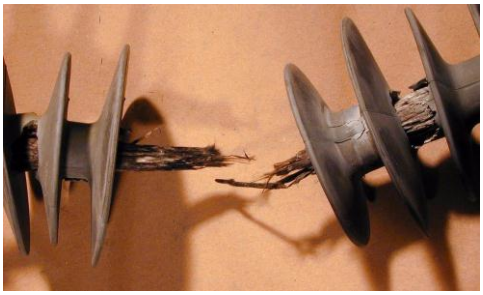

i) Mechanical failure

j) Brittle fracture

Figure 2-38: Examples of damage category [45]

Chapter 3: Design and choice of test apparatus

3.1 Overview

To achieve the objectives set in chapter 1, a test site was needed, insulator samples to be tested were needed and instruments that assist with the tests were needed. In this chapter a detailed description of the test site, insulators and test instruments selected, will be given.

3.2 Koeberg insulator test station (KIPTS)

KIPTS was selected to conduct the research. This is a marine natural ageing insulator test facility located near Cape Town, South Africa, along the west coast. It is located about 50 m from the ocean shore and is characterized by hot, dry summers, cold wet winters, mist banks, strong winds and heavy marine pollution [12]. The term 'summer' in this project refers to the months October to March and 'winter' refers to months April to September.

The pollution index at KIPTS is to the order of 2000 µS/cm, which is quantitatively high if one considers that Macey rated a pollution index greater than 850 µS/cm as 'very heavy' [12]. Furthermore, results of previous tests have shown that material degradation and ageing modes at KIPTS after a one year period, have proven to be more severe than those experienced in the IEC 5000-hour accelerated ageing test [12]. Also, field experience of flashovers on power lines in this area proved that the area is severe [12]. Due to the above reasons KIPTS was selected to perform natural, accelerated, ageing tests on the sample insulators chosen for this project.

An environmental study was done of the area surrounding KIPTS and the following pollution sources were identified [12]:

- The Atlantic ocean to the west. Wave action, winds from the sea and periodic mist banks bring moisture, salt particles and organic matter such as plankton to KIPTS.
- The breakwater wall of the Koeberg nuclear power plant northwest of KIPTS causes local salt mist banks to occur.

- Agricultural area in the east consisting of wheat fields and vineyards causes occasional field fires and the following pollution events: Ploughing, harvesting and crop spraying.
- Industrial area north east of KIPTS emits burned diesel, coal and heavy fuel oil (HFO) particles in the air.
- Lime plant to the south.
- Industries south east of KIPTS such as a fertilizer plant and an oil refinery plant are responsible for severe particle emissions.
- Sand dunes surrounding KIPTS may cause sand pollution.

Although the survey was conducted a couple of year ago, the area did not change much in terms of possible pollution sources; thus the abovementioned data is considered to be valid for today.

KIPTS has a long history of insulator pollution tests. The first version of KIPTS was built in 1975 and was ready for operation in 1977 [12]. It consisted of only an 88 kV test voltage [12]. This version of KIPTS was closed and demolished in 1986 and it was rebuilt in 1994, with a 22 kV and 66 kV test voltages. Since then, KIPTS grew in size, until the present day. It currently consists of 5 test voltages: 11 kV, 22 kV, 33 kV, 66 kV and 132 kV [5]. Presently, it is also an internationally recognized natural ageing insulator test station.

A test rig with 22 kV alternating current (AC) voltage was designed and built within the premises of KIPTS by Dr. W. L. Vosloo for his PhD research project during the year 2000 [12]. The same test rig, augmented to include high voltage positive polarity direct current (DC+) and high voltage negative polarity direct current (DC-) voltages, was utilised in this project. The design of the test rig will be discussed next.

3.2.1 Design of test rig

The test rig consists of a support structure with three radial arms, designed to support 30 insulators in total, and an electrical supply network which consists of a 50 kVA delta-star power transformer which energizes the AC voltage arm and a 50 kVA star-star supply transformer which energizes the DC voltage arms, via two DC converters as indicated in Figure 3-1.

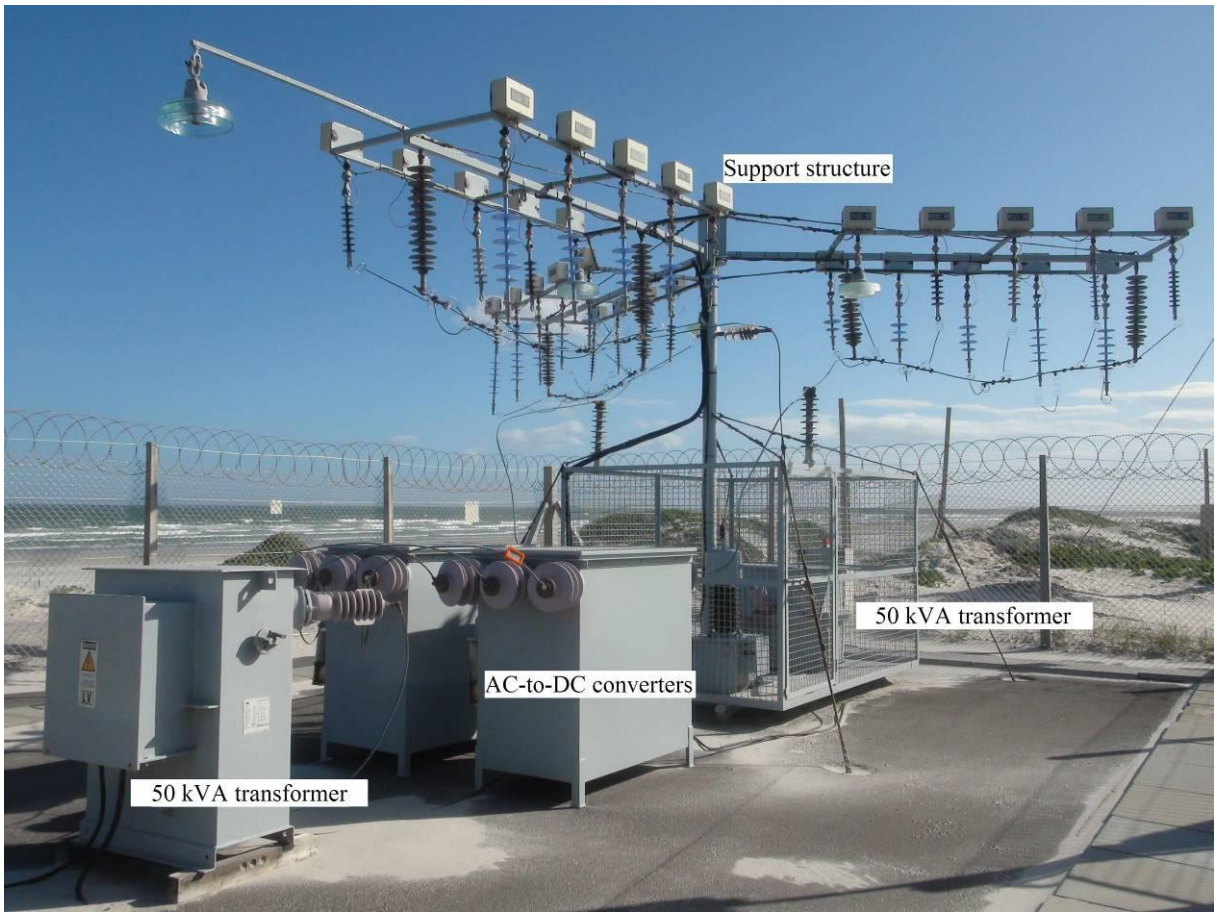

Figure 3-1: Photo of test rig

3.2.1.1 Support structure

The support structure consists of three radial, horizontal, supporting arms which are equally spaced and mounted on a vertical pole. Ten insulators can be installed on one supporting arm and each one of the three supporting arms is supplied by a different high voltage source, namely AC, DC+ and DC-. Please refer to Figure 3-2 for a non-scale top view drawing of the support structure.

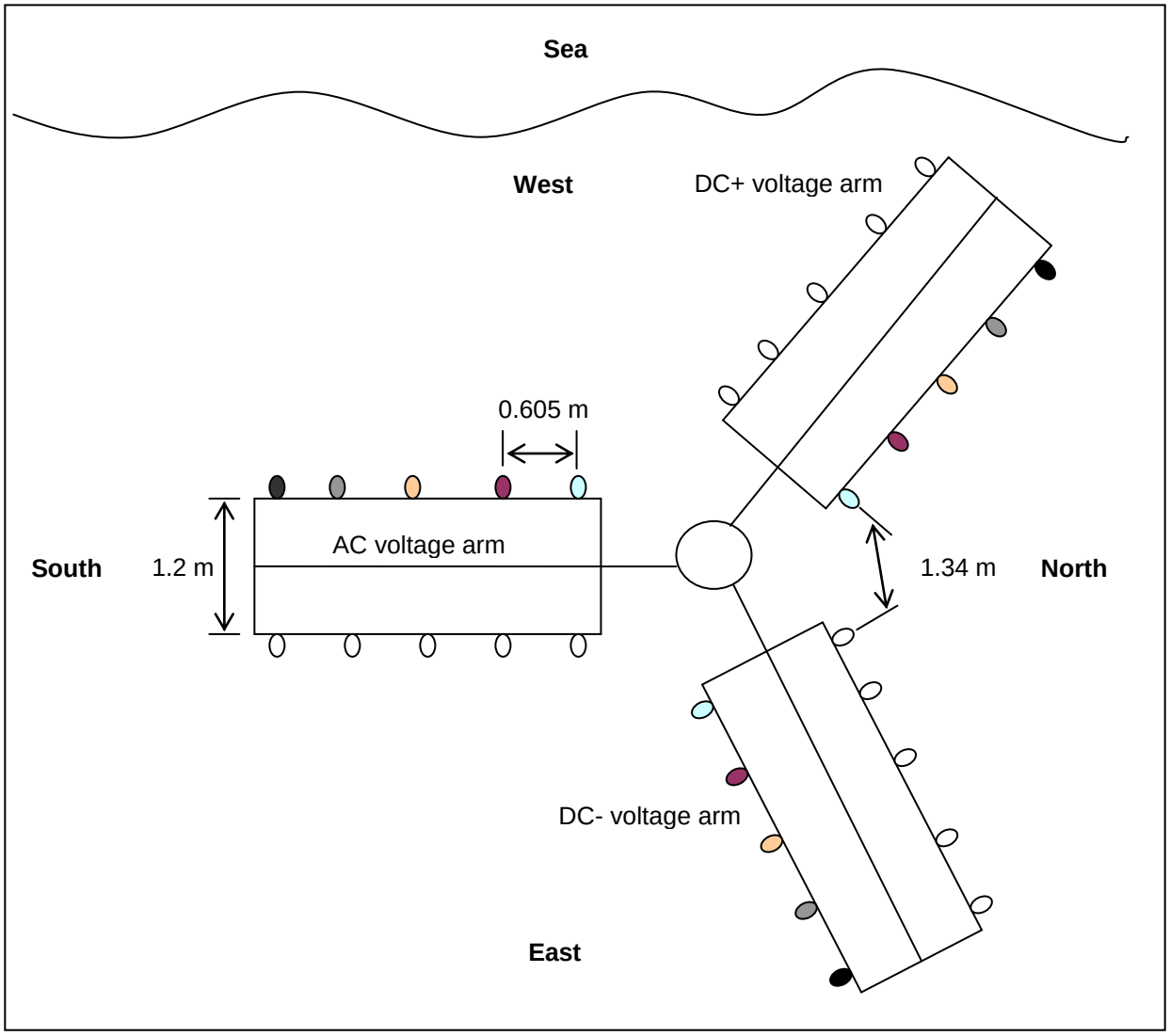

Figure 3-2: Non-scale top view of support structure

The small circles on the drawing represent the positions of all the insulators tested during this research project. The circles filled with colour represent the positions of the insulators whose results are discussed in this document. Each colour represents a different insulator material, as discussed in section 3.3. The support structure is symmetrical, thus the distance measurements given in the drawing are the same for all the corresponding position's measurements. For example, all the insulators on one side of a support arm are spaced equally with a distance of 0.605 m and the insulators on opposite sides of a support arm are spaced 1.2 m from each other. The shortest distance between insulators on neighbouring supporting arms, is 1.34 m.

The distance from ground to the radial, horizontal, supporting arms is 3.54 m. The bus bars are installed in the middle of each supporting arm with a vertically distance of 0.82 m below the supporting arms. The bus bars are connected to the supporting arms with composite long rod insulators.

Each insulator position has a weather-proof enclosure mounted on top of it, to house a current sensor for the purposes of leakage current measurement. In order to measure the leakage current, each test insulator was isolated from the support arm with a stand-off insulator as seen in Figure 3-3.

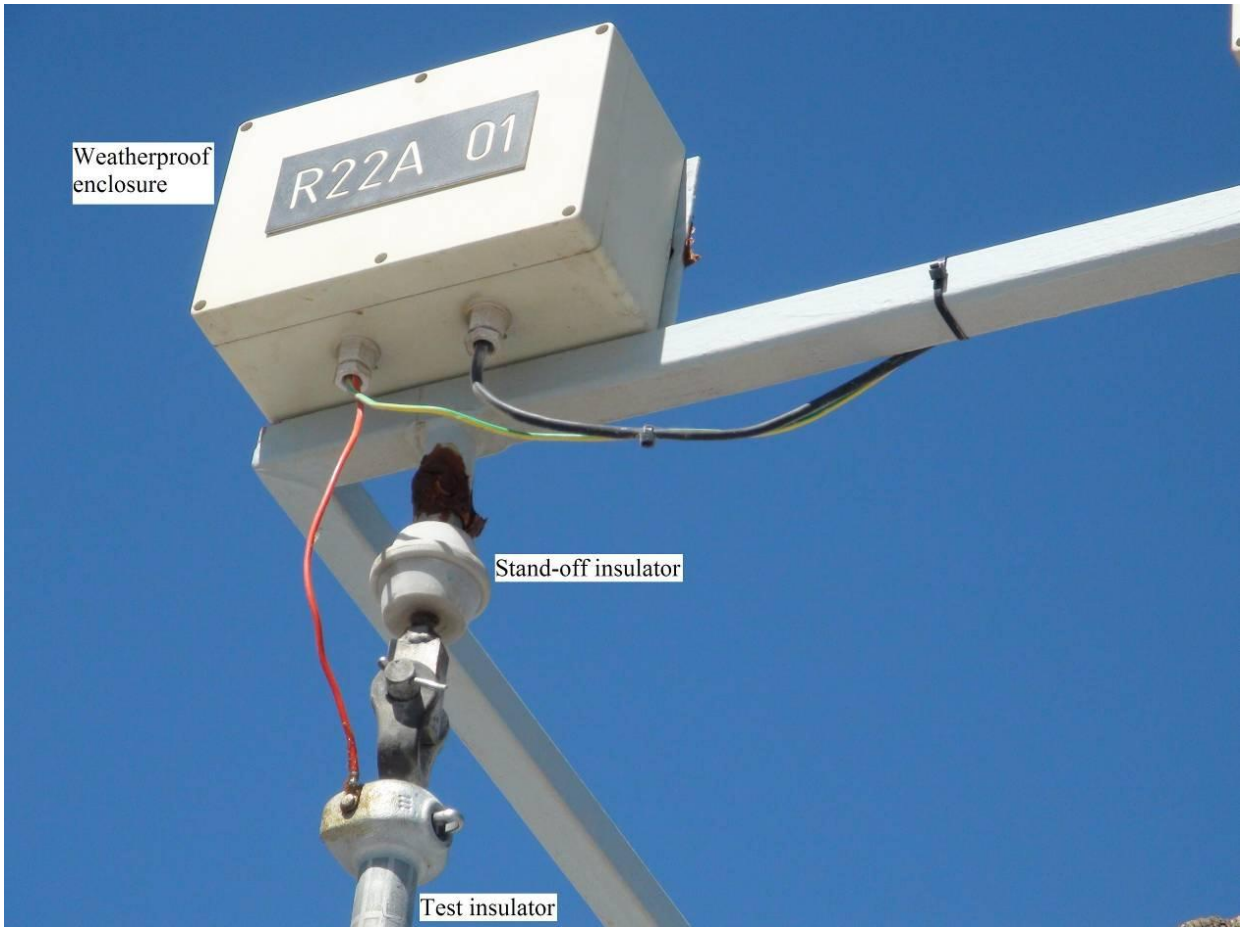

Figure 3-3: Photo of stand-off insulator

The test insulator is connected to the bus bar with a 'pigtail' connector, consisting of a copper tube and coiled stainless steel wires at the ends of the copper tube, which act as springs, and an explosive fuse, called a mace fuse. The mace fuse explodes, and thus disconnecting the test insulator from the bus bar, when it conducts a minimum current of 750 mA, which protects the test rig from an over current condition. The tension force within the coiled wires

of the pigtail connector pulls the connector from the bus bar when the fuse explodes and hence isolates the test insulator from the live bus bar. Please refer to Figure 3-4 for an example of the pigtail connector and mace fuse.

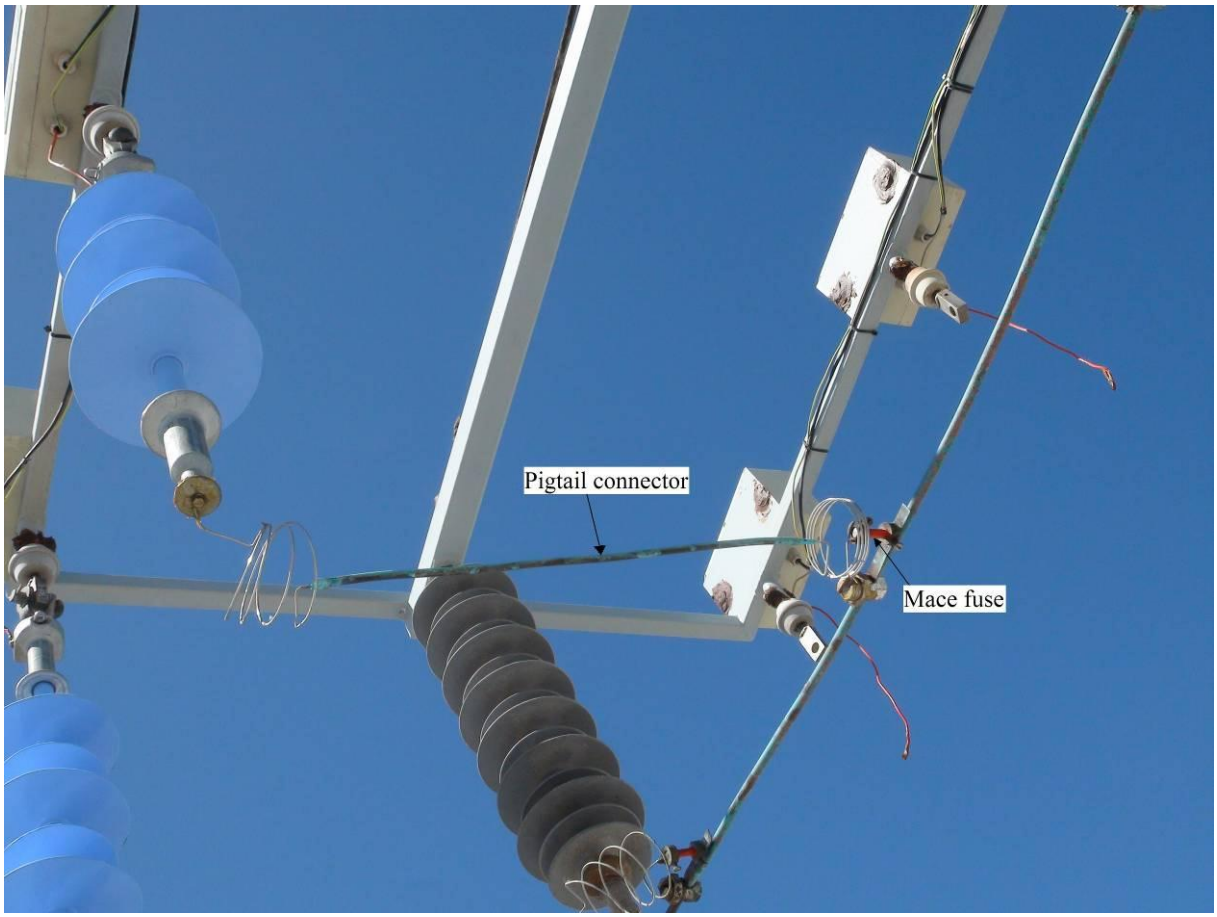

Figure 3-4: Photo of pigtail connector and mace fuse

3.2.1.2 Electrical power supply network

The test rig receives 400 V, three phase power from a municipal cubical outside KIPTS through a 400 V, four core, underground cable [6, 46]. Figure 3-5 indicates the three phases as L1, L2 and L3 respectively. The underground cable is terminated on the main contactor which is located in a weather-proof enclosure at the test rig and controlled through the user interface panel of the control box, located in the control room of the test station [46]. As seen in Figure 3-5, the main contactor controls the power throughput to both the transformers. A common earth return is used and it is connected to the station earth [46].

As indicated in Figure 3-5, the AC arm of the test rig receives its power from one phase of the secondary phases of the 50 kVA, 22 kV, delta-star three-phase transformer, which was the

original transformer when the test rig was commissioned [12]. The other two phase terminals on the secondary side of the transformer are left redundant and insulated, and the star point on the secondary side is connected to the station earth [46]. The operating voltage on the AC arm is 12.7 kV r.m.s. phase-to-ground and it is measured by the Online Leakage Current Analyser (OLCA) via a voltage transformer (VT) as shown in Figure 3-5 [46]. Please refer to Table 3-1 for the technical specifications of abovementioned transformer.

Table 3-1: Technical specifications of 50 kVA, 22 kV, delta-star, three phase transformer [46]

Manufacturer	Power Engineers
Type / connection	Delta / Star (Dyn)
Power rating	50 kVA
Primary voltage (LV)	400 V
Secondary voltage (HV)	22 kV
Primary current	72 A
Secondary current	1.3 A
Short circuit impedance (Z_{pu})	1.5%
R/X ratio	0.48
Insulating / cooling medium	Mineral Oil

The 50 kVA, 16.3 – 24 kV, multi tap, star-star three phase transformer supplies power to both AC to DC converters as seen in Figure 3-5 [6, 46]. All three secondary phase terminals of the transformer are connected to the input bushings of both AC to DC converters and the star point on the secondary side of the transformer is connected to the station earth [6]. It has a five-position off-load tap changer which varies the input voltage value to the converters and hence the output DC voltage value [6, 46]. Please refer to Table 3-2 for a list of the different voltage values for each tap setting.

Table 3-2: Voltage values of tap settings [46]

Tap position	Percentage	HV line voltage	No load DC voltage
1	130.5%	24 kV	19.6 kV
2	119.5%	22 kV	18.0 kV
3	100.0%	18.4 kV	15.0 kV
4	94.0%	17.3 kV	14.1 kV
5	88.5%	16.3 kV	13.3 kV

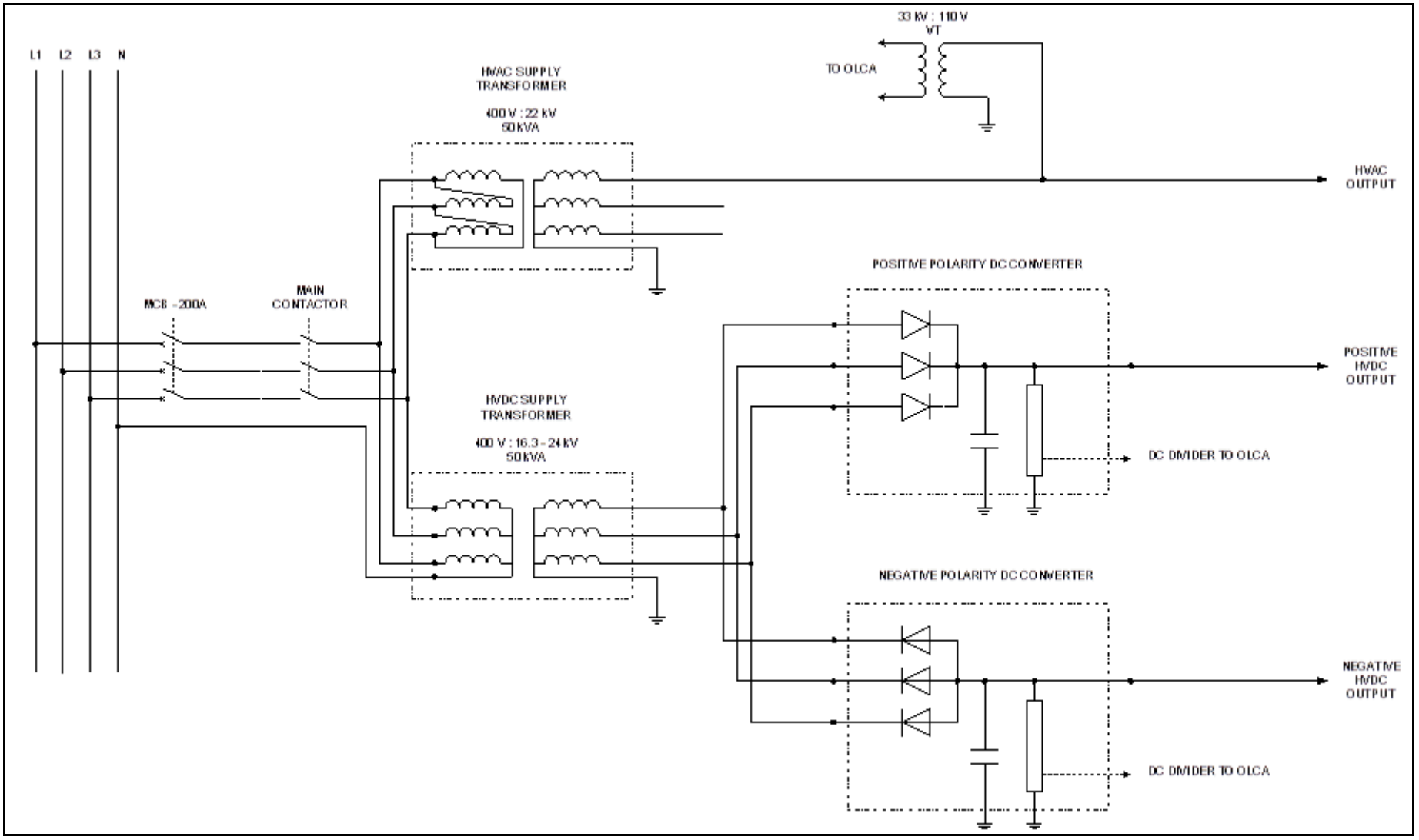

Figure 3-5: Power circuit diagram [46]

The reason for the different tap positions is to have the ability to change the DC voltage value to different values of the AC test rig arm voltage i.e. from phase-to-neutral r.m.s. value (12.7 kV) up to phase-to-neutral peak value (18 kV) [6]. For this project it was decided to use a DC voltage value equal to the phase-to-ground r.m.s. value of the AC test arm voltage [6]. The reason for selecting the DC voltage value equal to the AC phase-to neutral r.m.s. value was because of previous laboratory test done at the University of Stellenbosch, in relation to the comparison of the performance of different insulator materials under different voltage excitations (AC, DC+, DC-). Tap position number 5 was chosen because it gives a DC voltage value of 13.3 kV, which is closest to the AC test arm phase-to-neutral r.m.s. voltage value of 12.7 kV. Ideally, it would have been preferred if the DC voltage value and AC phase-to-neutral r.m.s. voltage value were exactly the same; however, the difference is so small that the 13.3 kV is considered as an appropriate DC voltage value. The OLCA measured the DC output voltages via a capacitive compensated resistive divider as shown in Figure 3-5 [46]. Please refer to Table 3-3 for the technical specifications of the abovementioned transformer.

Table 3-3: Technical specifications of 50 kVA, 16.3 – 24 kV, star-star, three phase transformer [46]

Manufacturer	Powertech Transformers
Type / connection	Star / Star (YNyn0)
Power rating	50 kVA
Primary voltage (LV)	400 V
Secondary voltage (HV)	16.3 – 24 kV
Primary current	72 A
Secondary current	1.6 A (at 100% tap – 18.4 kV)
Short circuit impedance (Z_{pu})	2%
R/X ratio	Unknown
Insulating / cooling medium	Mineral Oil

Each of AC-to-DC converters consist of three rectifier modules connected in a 3-pulse arrangement as well as two smoothing capacitors connected in parallel, which are enclosed by air-filled metal tanks, vented by silica gel breathers [6, 46]. The capacitive smoothing technique was preferred instead of an inductive filter, because of the transient nature of test insulator leakage currents [6]. A rectifier module consists of multitude diodes and a voltage equalizing network, housed in a stainless steel tank, filled with oil [46]. Please refer to Table 3-4 for the technical specifications of the converter units and to Table 3-5 for the technical specification of the capacitor.

Table 3-4: Technical specifications of AC-to-DC converters [46]

Manufacturer	University of Stellenbosch
Rectifier type	3 pulse with star point grounded
Smoothing	Capacitor bank
Input voltage	16.3 – 24 kV Three phase AC
Output voltage	±13.3 – ±19.6 kV DC
Primary phase current	1.2 – 1.8 A
Secondary maximum continuous current	±2 A
Peak stored charge at 19.6 kV	3.3 kJ
Insulating / cooling medium	Main tank air. Diodes and capacitors Mineral Oil
Nominal rectifier module voltage rating	40 kV maximum reverse voltage
Nominal rectifier module current rating	1 A
Peak rectifier module current rating 5 minutes	5 A
Peak rectifier module current rating 1 minute	40 A
Surge rectifier module current rating (10 ms)	300 A

Table 3-5: Technical specifications of capacitor [46]

Manufacturer	Westingcorp
Nominal voltage rating	30 kV DC
Capacitance	8.75 µF
Fusing	None
Discharge resistance	4.6 MΩ
Insulating medium	Mineral transformer oil

3.3 Insulator samples

A set of ten insulators were tested per excitation voltage, i.e. AC, DC+ and DC-, during this project. Five of the set of ten insulators were manufactured from the same material, by the same manufacturer, with the same profile, but with different creepage distances. The results for these insulators were compiled in reference [4].

The remaining five insulators of the set of ten were manufactured with different materials, in order to determine the influence of material on insulator performance in heavy polluted coastal environments, for different excitation voltages. These results are reported in this thesis. The different insulator materials tested during this research were DC toughened glass, Porcelain, Room Temperature Vulcanized (RTV) silicone rubber coated porcelain, High Temperature Vulcanized (HTV) silicone rubber and Ethylene Propylene Diene Monomers (EPDM) silicone alloy rubber.

Originally, all the insulators with different materials had the same creepage length and profile, except for the glass insulator. However, a week before the start of this research, a brown residue layer was discovered on the HTV silicone rubber and EPDM rubber insulator samples. It was decided not to use these samples during the research, because of the unexplained residue on their surfaces. A new set of insulator samples for these materials had to be found. The original manufacturer had no spare units available and a new set of HTV silicone rubber and EPDM silicone alloy rubber insulators from a different manufacturer were introduced. They had an identical profile, but a different creepage distance as the set of insulators that were replaced. Furthermore, the EPDM rubber insulators were replaced with EPDM silicone alloy rubber insulators.

During the planning phase of the research, it was considered important for the porcelain and RTV silicone coated porcelain insulators to have the same profile and creepage distance as the original HTV silicone rubber and EPDM rubber insulators. Due to this requirement, special porcelain insulators were manufactured and, because of the cost involved in the manufacture of the insulators, a supply phase-to-phase voltage of 22 kV was chosen as the basis excitation voltage for the project [12]. With the introduction of the new set of HTV and EPDM silicone alloy rubber insulators, it was decided not to manufacture other porcelain insulators with the same creepage distance as the new set, because of the cost and time involve in manufacture of these.

The new set of insulators was not available for the planned switch-on date. However, it was decided to proceed with the commencement of the project as planned. The reason for this was that a direct comparison between all the different insulator materials is no longer an option because of the different creepage distance of the new set of insulators. The project commenced on 03 February 2011 and the new set of HTV silicone and EPDM silicone alloy rubber insulators was installed on 16 May 2011.

Due to the different creepage distances and installation dates among the different insulator materials, it was decided to compare the performance of the HTV silicone rubber and the EPDM silicone alloy rubber insulators for each excitation voltage as one comparison. Both of these insulators have the same manufacturer, profile, creepage distance and installation date. The second comparison was between the porcelain and RTV coated porcelain insulators with the glass insulator as reference for each excitation voltage. The porcelain and RTV coated

porcelain insulators have the same profile, creepage distance and installation date. However, the glass insulator has a different profile and creepage distance, but the same installation date as the porcelain and RTV coated porcelain insulators. A third comparison was done to observe the effect of each excitation voltage, i.e. AC, DC+ and DC-, per insulator material.

Please refer to Table 3-6 for the main characteristics of the set of insulators reported on in this thesis. The different fill colours in the heading row of Table 3-6 refer to the different colours used in Figure 3-2, which indicate the relative positions of the insulators on the support structure of the test rig.

The unified specific creepage distance (USCD) in Table 3-6 was calculated by dividing the creepage distance of the insulator with the r.m.s. value of the highest operating voltage across the insulator. The highest operating voltage for AC excitation was calculated as 10% above the nominal phase-to-neutral r.m.s. voltage. Thus,

$$\begin{aligned} U_M &= 12.7 \times 1.1 \\ &= 13.97\ kV. \end{aligned} \tag{3-1}$$

The highest operating voltage for DC excitation is defined by the converting station and initial decisions taken in the insulation coordination of the line [14]. Typical values in the field vary between 3% and 6% above the nominal voltage of the line [14]. For this project a 5% value above the nominal voltage of the line were chosen as the highest operating voltage for DC excitation. Thus,

$$\begin{aligned} U_M &= 13.3 \times 1.05 \\ &= 13.97\ kV. \end{aligned} \tag{3-2}$$

The U_M value for AC and DC excitations is the same and hence the USCD values in Table 3-6 are applicable to insulators energised by both AC and DC voltages. The different alphabetic letters in the Manufacturer row in Table 3-6 represent different manufacturers and the filler content of all the polymer insulators were determined by means of a Thermal Gravimetric Analysis (TGA) performed on virgin material samples. The filler content percentage value of the RTV coated porcelain insulator was obtained from a MSc. thesis [47], where its author used the same RTV coating material and manufacturer as used during this research. It was not possible to determine the filler content during this research because there was no spare insulator available to obtain it from.

Table 3-6: Characteristics of the set of test insulators reported in this document

	EPDM silicone alloy rubber	HTV silicone rubber	RTV silicone rubber coated porcelain	Porcelain	DC toughened glass
Creepage distance [mm]	665	665	580	580	550
USCD [mm/kV]	47.6	47.6	41.5	41.5	39.4
Arcing distance [mm]	315	315	295	295	320
Connecting length [mm]	440	440	460	460	170
Form factor	6.86	6.86	4.68	5.37	1.10
ATH filler content [%]	48.03	49.5	14*	Not applicable	Not applicable
Manufacturer	W	W	X	Y	Z
Profile	Composite long rod	Composite long rod	Standard long rod	Standard long rod	Anti-fog cap-and-pin

The following code will be used from hence forth when reporting the results for a specific insulator:

- The first part of the code will represent the high voltage type, i.e., AC+ for AC voltage positive cycle, AC- for AC voltage negative cycle, DC+ for DC positive polarity voltage and DC- for DC negative polarity voltage.
- The second part of the code will consist of the name of the main material the insulator is made of, i.e., EPDM for EPDM silicone alloy rubber, HTV for HTV silicone rubber, RTV for RTV silicone rubber coated porcelain, Porcelain for porcelain and Glass for DC toughened glass.
- The first and second part of the code will be combined by the underscore sign, e.g., DC-_EPDM refers to the EPDM silicone alloy rubber insulator energized under the DC negative polarity voltage.

Please refer to Figure 3-6 for photographs of a set of the different test insulators evaluated in this thesis. The photographs of the porcelain and RTV silicone coated porcelain insulators

were obtained from a PhD thesis [12], where insulators with the same profile as the porcelain and RTV coated porcelain of this research, were used. The notation used in Figure 3-6 to refer to the different insulators is the same as the second part of the code explained above.

EPDM HTV Porcelain* RTV* Glass

Figure 3-6: Photographs of a set of test insulators

3.4 Test instruments

The following test instruments were used in this project to assist in capturing the data required to evaluate the test insulators:

- Online leakage current analyser (OLCA), which captures the leakage currents and weather data.
- Image-intensified, Ultraviolet-sensitive, video camera system (CoroCAM 1), which captures electrical activity on the insulator surfaces during night time observations.
- Sony camcorder (HDR-XR550E), which captures electrical activity on the insulator surfaces during night time observations and photographs of the insulator surfaces during daytime inspections.
- Greisinger GMH 3410 conductivity meter and Radwag AS 220/C/2 balance, which measure the conductivities of equivalent salt deposit density (ESDD) samples and mass of non-soluble deposit density (NSDD) samples respectively. In section 4.2 the abovementioned measurement processes are explained fully.

A detailed description of these test instruments will be given in the following paragraphs.

3.4.1 OLCA

The OLCA is a microprocessor-based, data acquisition system, designed to record leakage currents for up to nine insulators or bushings and six weather parameters simultaneously [48]. It has a three phase voltage measurement input, which measures the voltage over the insulators or bushings which allows parameters like resistive power loss to be calculated [48]. Four OLCAs were used in this project to continuously measure and record the leakage current data of 30 insulators simultaneously. The weather parameters were measured and recorded on one of the four OLCAs used for leakage current measurement.

Each OLCA has the ability to record the following parameters continuously [48]:

- Positive and negative peak value of the leakage current inputs.
- Positive and negative average value of the leakage current inputs.
- Positive and negative charge value of the leakage current inputs.
- R.M.S. values of the leakage current and applied voltage inputs.
- Power loss over each insulator.
- Mean temperature, Relative Humidity, Ultraviolet B (UV-B) radiation, wind speed, wind direction and rainfall.
- Daily peak leakage current and voltage waveforms.

The OLCA has 2 measurement ranges for the input leakage current, namely, ±500 mA r.m.s. and ±3 A peak [48]. The first range was selected for this research because it has a finer resolution and 99% of all the leakage current measurements made on the insulators for the duration of the research, were in that range. The measurement range for the voltage input varies from -400 V to +400V r.m.s. [48].

All the leakage current and voltage inputs are sampled continuously at 2 kHz simultaneously and all the weather inputs are sampled continuously at 1 Hz simultaneously [48]. The OLCA uses a 12 bit analogue-to-digital converter (ADC) to digitize the analogue input measurements [48]. Please refer to Figure 3-7 for a photograph of the OLCA.

Figure 3-7: Photograph of OLCA

The OLCA receives the analogue measurement values of the parameters, which it records, from the following devices [48]:

- AC and DC current sensors based on Hall Effect technology, which are galvanic isolated up to 3 kV, and they have a bandwidth from 0 to 200 kHz. Please refer to Figure 3-8 (a).
- A combination temperature and humidity probe. Please refer to Figure 3-8 (b).
- A combination wind speed and direction sensor. Please refer to Figure 3-8 (c).
- A tipping bucket rain gauge. Please refer to Figure 3-8 (d).
- A UV-B ultraviolet sensor. Please refer to Figure 3-8 (e).

The technical parameters of the abovementioned devices are listed in Table 3-7 and their photographs are shown in Figure 3-8 .

(a) (b) (c) (d) (e)

Figure 3-8: Photographs of OLCA measurement devices

Table 3-7: Technical parameters of measurement instruments of OLCA [48]

	Accuracy	Range	Resolution	Collecting area
Current sensor with a 1000:1 turn ratio	±0.5% of nominal primary current	0 to 25 A for nominal primary current.	No value	No value
Temperature probe	±0.3 °C	-50 °C to + 50 °C	No value	No value
Humidity probe	±2% relative humidity (RH)	0 to 100% RH	No value	No value
Wind speed sensor	±0.3 m/s	0 to 60 m/s	No value	No value
Wind direction sensor	±3 degrees	Mechanical: 360° Electrical: 355°	No value	No value
UV-B ultraviolet sensor	No value	0 to 500 µW/cm^2	No value	No value
Tipping bucket rain gauge	±2% up to 20 mm/hr.; ±3% up to 50 mm/hr.	No value	0.1 mm per tip	200 cm^2

There were some limitations on the test equipment. These limitations and their rectifying processes are summarized below:

- The OLCAs entered randomly in a non-operating state. During this state, they did not record/log any activity. The rectifying process was to access the OLCAs on a daily base to verify their operational state. If not operational, a hardware reset was required where all the OLCAs were switched off for about 30 seconds and then switched on again. The company which manufactures the OLCA was contacted for a solution, but they did not provide one.
- Some of the DC current sensors had fluctuation offsets, i.e. it shows a current measurement value even if the test rig was switched off. The rectifying process was to manually set the offsets to zero on the OLCAs before the initial start-up of test rig for this research. Thereafter they were monitored on a weekly routine when the test rig was switched off for visual observations. If there were current measurement values on any DC current sensor while the test rig was switched off, they were recorded and manually set to zero on the OLCA before the test rig was switch-on again. The reason why it happened is not known, but it is suspected that it might be caused by the

unidirectional flow of current through the sensors, generated by the DC excitation voltages.

3.4.2 CoroCAM 1

CoroCAM 1 is the entrance level product of the CoroCAM™ range and it is ideal for detecting and visualizing ultraviolet (UV) discharges on high voltage equipment at night time or indoor [49]. It produces real-time video images of corona, UV-activity from high voltage discharges, and the object where the corona/UV-activity is present [49]. Furthermore, it has a standard video output, which can be connected to a portable video recorder to record the activity [49]. It also has a user-gain-control to adjust the detector sensitivity and selectable optical UV wide band pass filters to enhance the background and quality of the corona images [49]. During this project, the CoroCAM 1 was used to record electrical activity on the insulators at night time.

The portable video recorder, used with the CoroCAM 1 during this project was the Sony GV-HD700 recorder [49]. It has S-video, composite and digital audio/video i-LINK® video inputs and multi A/V standard definition (SD) and component high definition (HD) video outputs [19]. Furthermore, it uses MiniDV cassettes and Memory Stick PRO™ storage devices [49]. Please refer to Figure 3-9 for photographs of the CoroCAM 1 and the Sony recorder.

a) CoroCAM 1 b) Sony recorder

Figure 3-9: Photographs of CoroCAM 1 and Sony recorder

3.4.3 Sony camcorder (HDR-XR550E)

The Sony camcorder was used in conjunction with the CoroCAM 1 during night time observations to make video recordings of partial discharge activities on the insulators.

Discharge activities were clearly visible on the Sony camcorder, whereas on the CoroCAM 1, they were observed as a bright white light that blurs the area of discharge. Corona activity was clearly visible on the CoroCAM 1, but not on the Sony camcorder. Furthermore, the Sony camcorder was also used to take photographs of any interesting observations made on the surface of the insulators, during daytime visual inspections.

The HDR-XR550E is a 240GB hard disc drive high definition (HD) camcorder (1920x1080 recording) [50]. It is equipped with an 'Exmor R' CMOS sensor for excellent low light performance video recording, which was required for the night time observations [50]. With the 240GB hard disc drive it can store up to 23 hours full HD movie recordings [50]. When switched to 'photo' mode it takes photographs up to 12 Mega pixels [50]. It has a Carl Zeis® Vario Tessar lens which is known for their high resolution, high contrast and excellent colour reproduction capability [50]. Furthermore, it has a 60x optical zoom and a built-in LED (light emitted diode) video light which enables video shoots in dark environments up to a distance of 1.5 m [50]. These are only few features of the many highlighted here. Please refer to Figure 3-10 for a photograph of the Sony HDR-XR550E camcorder.

Figure 3-10: Photograph of the Sony HDR-XR550E camcorder [50]

3.4.4 Greisinger GMH 3410 conductivity meter

The Greisinger GMH 3410 meter is a handheld conductivity meter with a two-electrode-conductivity-measuring cell, with an integrated temperature sensor [51]. It is primarily designed to measure the respective conductivities of soft and salt water [51]. It has four different measuring range resolutions and the device has the capability to automatically select the optimal resolution [51]. The conductivity measurement ranges and resolutions are as shown in Table 3-8.

Table 3-8: Conductivity measurement ranges

Range	Resolution
0 to 200 µS/cm	0.1 µS/cm
0 to 2000 µS/cm	1 µS/cm
0 to 20 mS/cm	0.01 mS/cm
0 to 200 mS/cm	0.1 mS/cm

Its accuracy at a nominal temperature of 25 °C for conductivity measurement is ± 0.5% of measuring value and for temperature it is 0.2% of measuring value [51]. Please refer to Figure 3-11 for a picture of the device.

Figure 3-11: Picture of GMH 3410 conductivity meter [51]

3.4.5 Radwag AS 220/C/2 balance

The Radwag AS 220/C/2 balance forms part of a series of analytical balances [52]. It has a LCD backlit display and its accuracy and reliability of measurement are determent by an internal automatic adjustment/calibration system triggered by time, air flow or temperature conditions [52]. Technical specifications of the Radwag AS 220/C/2 balance are given in Table 3-9 and a picture of it is shown in Figure 3-12.

Table 3-9: Technical specifications of Radwag AS 220/C/2 balance [52]

Maximum capacity	220 g
Minimal load	10 mg
Readability	0.1 mg
Tare range	-220 g
Linearity	±0.2 mg
Pan size	Diameter 85 mm
Stabilization time	3.5 s

Figure 3-12: Picture of Radwag AS 220/C/2 balance [52]

Chapter 4: Research procedures and methodology

4.1 Overview

The research was conducted over a one year period; from 03 February 2011 to 05 February 2012. Thus, it was conducted over a summer-winter-summer cycle, as defined in section 3.2. The objectives of this research were to determine which insulator material performed the best at a given excitation voltage (AC, DC+, DC-) and to determine which excitation voltage had the best effect on the different insulator materials. The term 'best' was defined by the following parameters where lesser or latter was conceived as better:

- The number of flashovers per insulator during the research period.
- The leakage currents flowing on the insulator surfaces.
- Service induced damage or deterioration observed on the insulators.
- Hydrophobicity properties on the surfaces of polymer insulators.
- The starting sequence of electrical discharge activity.

It was mentioned in section 2.4.3 that the performance and deterioration of insulators are dependent on the pollution severity and the climatic conditions of the area where they are installed. Thus, it was important to determine the site pollution severity (SPS) and the climatic conditions at Koeberg insulator pollution test station (KIPTS) to put the results observed in their correct context.

A detailed description of the procedures and methodologies that were followed during the research, which assisted in achieving the research objectives, will be discussed in this chapter. The procedures and methodologies followed are categorized under the following headings:

- SPS index and climate conditions at KIPTS.
- Number of flashover events per insulator.
- Insulator leakage current measurements.
- Night time electrical activity observations.
- Insulator surface inspections.

All the data obtained through the abovementioned procedures were stored on a notebook PC, an external hard disc drive and on a server at the University of Stellenbosch as backup.

4.2 SPS index and climatic conditions at KIPTS

The SPS index of a site refers to the pollution severity at that site and is generally expressed in terms of [13]:

- Equivalent salt deposit density (ESDD) and non-soluble deposit density (NSDD) measurements on reference insulators for type A pollution sites.
- Site equivalent salinity (SES) from onsite leakage current or conductance measurements on reference insulators for type B pollution sites.
- Dust deposit gauge index soluble (DDGIS) and dust deposit gauge index non-soluble (DDGIN) measurements of the pollutants collected by a dust gauges for type A or B pollution sites.

The definitions of type A and type B pollution are given in section 2.4.3.1. The accuracy of the SPS index measurements depends on the frequency of measurements and the duration of the study [13]. Due to the fact that pollution events are often seasonal and related to climate, a measuring period of least one year is necessary to take any seasonal effects in account [13]. Accuracy may be improved by using two or more methods in combination [13]. During this research the ESDD and NSDD, and DDGIS and DDGIN processes were used in combination to determine the SPS index of KIPTS and thus only these processes will be discussed in detail.

4.2.1 ESDD and NSDD measurements

Site pollution severity can be determined by measuring both ESDD and NSDD on reference insulators, which come from existing installations and/or are installed in field testing stations [13]. A separate glass cap-and-pin insulator was installed on the test rig at KIPTS at the same height as the test insulators, for ESDD and NSDD measurements. These measurements were conducted on a monthly basis. The glass cap-and-pin insulator used for ESDD and NSDD measurements is identical to the glass cap-and-pin insulators used for the research; the only difference being that it was not energized. Please refer to Figure 4-1 for a photograph of the glass cap-and-pin insulator used for ESDD and NSDD measurements.

The ESDD and NSDD measurements can be made by using a swap technique or washing technique [13]. During the swap technique the pollutants are wiped off from the insulator surface with a wet, squeezed cotton [13]. The washing technique was chosen for this research and it will be discussed in detail in the following sub-sections.

Figure 4-1: Photograph of a complete set of test insulators on the AC-voltage arm and glass cap-and-pin insulator for ESDD and NSDD measurements

4.2.1.1 ESDD measurements

ESDD is defined as the amount of sodium chloride (NaCl) which, when dissolved in demineralised water, gives the same volume conductivity as that of the natural deposit, removed from a given surface of the insulator, divided by the area of that surface, generally expressed in mg/cm^2 [13]. The following procedure was followed in removing the natural deposit from the ESDD and NSDD glass cap-and-pin insulator [13]:

- De-energise and earth the test rig by KIPTS personnel.

- Remove insulator from test rig and cover the cap and pin areas respectively with cling plastic wrap, without covering the insulator surface.
- Clean the bowl in which the insulator will be washed.
- Measure 1000 cm^3 of distilled water and pour it into the bowl. The distilled water should have a very low conductivity, e.g. in the orders of 10^{-4} S/m.
- Place the insulator on its cap in the water and wash the surface of the insulator facing the water with gentle hand strokes up to the rim.
- Pour the water into a clean container labelled 'glass top' whilst ensuring that no deposits remain in the bowl.
- Clean the bowl and put the insulator on its cap in the bowl.
- Measure 1000 cm^3 of distilled water and pour it onto the bottom side of the insulator, making sure that no water falls in the bowl.
- Wash the bottom surface of the insulator with gentle hand strokes and pour the water from the insulator into the bowl.
- Pour the water into a clean container labelled 'glass bottom' whilst ensuring that no deposits remain in the bowl.
- Remove the plastic cling wrap from the cap and pin areas, respectively, and re-install insulator on test rig.
- Remove the earth cables and re-energise test rig by KIPTS personnel.

The conductivity and temperature of the water containing the pollutants in the containers labelled 'glass top' and 'glass bottom' are measured after stirring the solutions for a few minutes [13]. The measured conductivities are corrected to conductivity ratings at 20 °C with the following equation [13]:

$$\sigma_{20} = \sigma_{\theta}[1 - b(\theta - 20)] \tag{4-1}$$

where

θ is the temperature of the measured solution (°C),

σ_{θ} is the volume conductivity of the measured solution at temperature of θ (S/m),

σ_{20} is the volume conductivity at temperature of 20 °C (S/m),

and

b is the factor depending on temperature of θ and calculated by the following equation:

$$b = -3200\times10^{-8}\theta^3 + 1032\times10^{-5}\theta^2 - 8272\times10^{-4}\theta + 3544\times10^{-2}. \quad (4\text{-}2)$$

The ESDD on the insulator surface is then calculated by the following equations [13]:

$$Sa = (5.7\sigma_{20})^{1.03} \quad (4\text{-}3)$$

with

$$ESDD = Sa \cdot V / A \quad (4\text{-}4)$$

where

Sa is salinity (kg/m^3),

σ_{20} is the volume conductivity at temperature of 20 °C (S/m),

$ESDD$ is the equivalent salt deposit density (mg/cm^2),

V is the volume of distilled water (cm^3)

and

A is the area of the insulator surface collecting pollutants (cm^2).

The average ESDD of the glass top and glass bottom solutions are calculated by the following equation [13]:

$$Average\ ESDD = (ESDD_t \times A_t + ESDD_b \times A_b) / A \quad (4\text{-}5)$$

where

$ESDD_t$ is the ESDD of the top area (mg/cm^2),

$ESDD_b$ is the ESDD of the bottom area (mg/cm^2),

A_t is the top area of the insulator surface (cm^2),

A_b is the bottom area of the insulator surface (cm^2)

and

A is the total area of the insulator surface (cm^2).

4.2.1.2 NSDD measurements

NSDD is defined as the amount of non-soluble residue removed from a given surface of the insulator, divided by the area of that surface, generally expressed in mg/cm^2 [13]. To measure the non-soluble residue, the water containing pollutants is filtered, using funnels and pre-dried, weighted filter papers [13]. The filter papers containing the pollutants are dried and

weighed [13]. Please note that the NSDD measurements took place after the ESDD measurements [13]. The NSDD is then calculated as follow [13]:

$$NSDD = 1000(W_f - W_i) / A \tag{4-6}$$

where

$NSDD$ is the non-soluble material deposit density (mg/cm^2),

W_f is the weight of the filter paper containing the pollutants under dry conditions (g),

W_i is the initial weight of the filter paper under dry conditions (g)

and

A is the area of the insulator surface for collecting pollutants (cm^2).

The average NSDD of the glass top and glass bottom solutions are calculated by the following equation [13]:

$$Average\ NSDD = (NSDD_t \times A_t + NSDD_b \times A_b) / A \tag{4-7}$$

where

$NSDD_t$ is the NSDD of the top area (mg/cm^2),

$NSDD_b$ is the NSDD of the bottom area (mg/cm^2),

A_t is the top area of the insulator surface (cm^2),

A_b is the bottom area of the insulator surface (cm^2)

and

A is the total area of the insulator surface (cm^2).

4.2.2 DDGIS and DDGIN measurements

DDGIS and DDGIN measurements are made by using a dust gauge. A dust gauge consists of four vertical tubes each having a slot milled to the side [13]. Each milled slot was arranged to phase north, south, east and west respectively [13]. At the bottom of the tubes, removable containers were attached to collect the deposits blown into the slots [13]. Please refer to Figure 4-2 for a schematic drawing of a dust gauge installation. The dimensions indicated in Figure 4-2 were used to build the dust gauge that was installed at the test rig to allow international comparison of the results. Please refer to Figure 4-3 for a photograph of the dust gauge installed at the test rig.

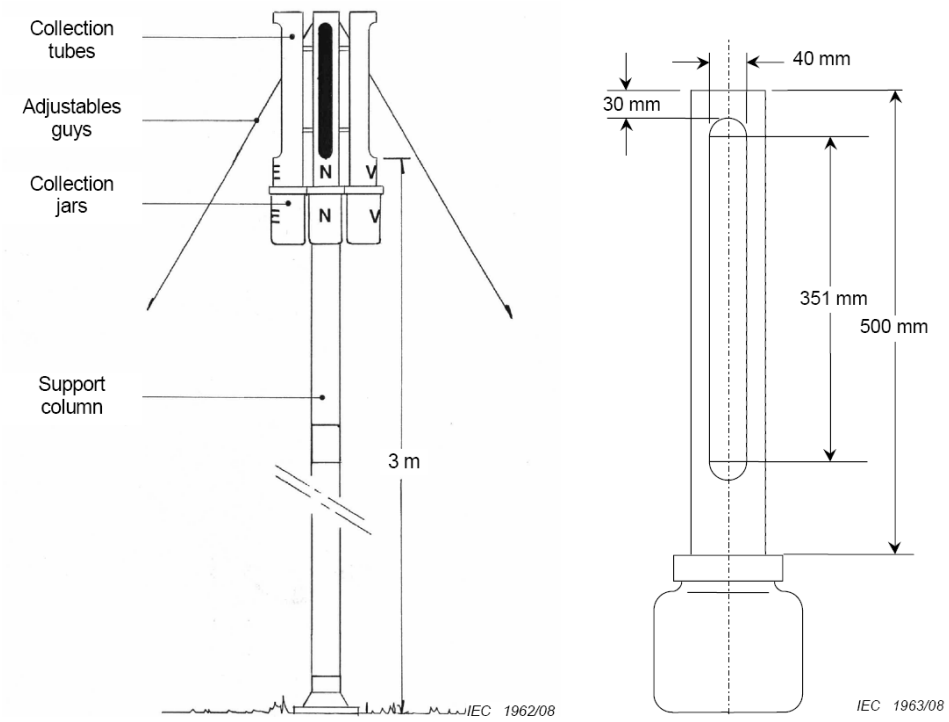

Figure 4-2: Schematic diagram of a dust gauge and a single tube with slot milled on the side with removable container [13]

Figure 4-3: Photograph of dust gauge installation at test rig

The DDGIS and DDGIN measurements were done once a month, on the same day as ESDD measurements. The following procedure was used for DDGIS and DDGIN measurements [13]:

- Rinse off the inner walls of the dust gauge tubes, using a squeeze bottle filled with demineralised water before the collection containers are removed.
- Remove the four collecting containers from the tube ends and close the containers with their lids.
- Attach four clean containers, which are labelled with the site name and compass direction, to the corresponding tube ends.

At the measurement location,

- Record the date when the collecting containers were removed.
- Add 500 ml of demineralised water to each collecting container. The conductivity of the demineralised water must be less than 5 µS/cm. If a container contains rain water, add demineralised water to increase the volume up to 500 ml. If there is more than 500 ml of rain water, no additional water is required.
- Swirl or stir the solutions until all soluble salts are dissolved.
- Measure the conductivities and temperatures of the solutions.
- If the volume of a solution is more than 500 ml, e.g. when rain water accumulated in the container, measure the volume of the solution.
- Calculate the corrected conductivity for each direction; meaning the conductivity normalized to 20 °C by using equations (4-1) and (4-2), and normalized to a volume of 500 ml and a 30-day period. The corrected conductivity is calculated by the following equation:

$$DDDG = \sigma_{20} \times \frac{V_d}{500} \times \frac{30}{D} \tag{4-8}$$

where

$DDDG$ is the directional dust deposit gauge conductivity (µS/cm),

σ_{20} is the volume conductivity at temperature of 20 °C (µS/cm),

V_d is the measured volume of the solution (ml)

and

D is the number of days the collecting containers were attached to the tubes of a dust gauge before removal for measurement (days).

- Calculate the DDGIS (expressed in µS/cm) of the month by taking the average of the four corrected directional conductivities, using the following equation:

$$DDGIS = \frac{(DDDG_{North} + DDDG_{South} + DDDG_{East} + DDDG_{West})}{4}. \quad (4\text{-}9)$$

- Filter the water containing pollutants by using funnels and pre-dried, weighted filter papers. Dry and weigh the filter papers containing the pollutants. Please note that the non-soluble deposit (NSD) measurements take place after the conductivity measurements. The NSD is then calculated as follow:

$$NSD = (W_f - W_i) \times \frac{30}{D} \quad (4\text{-}10)$$

where

NSD is the non-soluble material deposit weight (g),

W_f is the weight of the filter paper containing the pollutants under dry conditions (g),

W_i is the initial weight of the filter paper under dry conditions (g)

and

D is the number of days the collecting containers were attached to the tubes of a dust gauge before removal for measurement (days).

- Calculate the DDGIN (expressed in grams) of the month by taking the average of the four non-soluble material deposit weights by using the following equation:

$$DDGIN = \frac{(NSD_{North} + NSD_{South} + NSD_{East} + NSD_{West})}{4}. \quad (4\text{-}11)$$

At the end of the research period, a quantitative chemical analysis was conducted on the dust gauge water solutions to determine the chemical compounds of the soluble deposits collected in each of the four removable containers of the dust gauge over a two-week period. Ion-exchange chromatography (IC) and inductive coupled plasma-optical emission analytical spectrometry (ICP-MS and ICP-AES) processes were used for the chemical analysis [13].

4.2.3 Determining the site pollution severity (SPS) at KIPTS

SPS is the maximum value of ESDD and NSDD, or SES, or DDGIS and DDGIN which were measured according to the methods described above within a standard measurement interval and recorded over a minimum period of one year [13]. If the highest value of ESDD or

NSDD does not occur on the same time, the SPS is taken as a combination of these highest values [13]. The same is applicable to DDGIS and DDGIN values [13].

Site severity is characterized by five classes of pollution which are qualitatively defined as follows [13]:

- a – Very light pollution at site;
- b – Light pollution at site;
- c – Medium pollution at site;
- d – Heavy pollution at site;
- e – Very heavy pollution at site.

Figure 4-4 shows the ranges of the ESDD and NSDD values corresponding to the different SPS classes for a reference cap-and-pin insulator for type A pollution [13]. These values are deduced from field measurements, experience and pollution tests and are based on natural pollution deposits on reference insulators [13]. The transition from one SPS class to another is not sudden, thus the shaded boundaries between each class as shown in Figure 4-4 [13].

The correspondence between DDGIS and DDGIN values and SPS classes relevant to both type A and type B pollution is shown in Table 4-1 where PI implies DDGIS values and Table 4-2 where NSD implies DDGIN values.

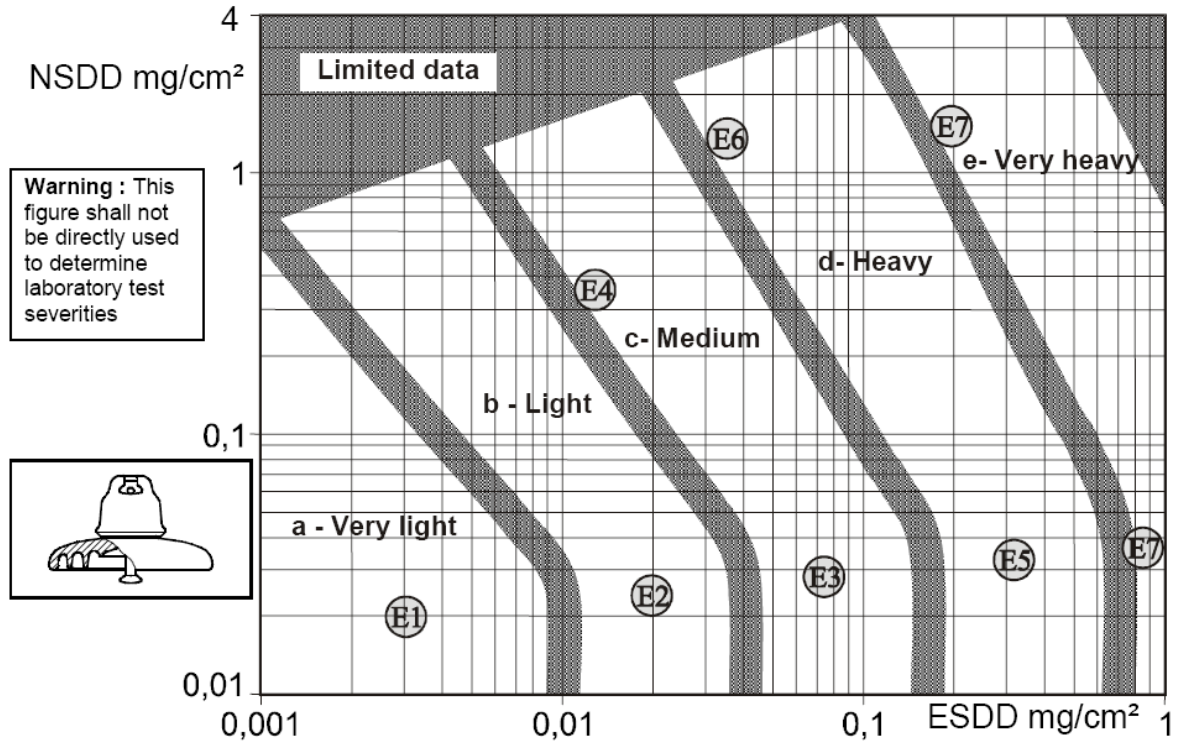

Figure 4-4: Relation between ESDD, NSDD and SPS for a reference cap-and-pin insulator [13]

Table 4-1: DDGIS values in relation to SPS classes [13]

Directional dust deposit gauge pollution index, PI (µS/cm) (take whichever is the highest)[a]		Site pollution severity class	
Average monthly value over one year	Monthly maximum over one year		
< 25	< 50	a	Very light
25 to 75	50 to 175	b	Light
76 to 200	176 to 500	c	Medium
201 to 350	501 to 850	d	Heavy
> 350	> 850	e	Very heavy

Table 4-2: Correction of SPS classes as a function of DDGIN values [13]

Directional dust deposit gauge NSD (grams) (take whichever is the highest)		Site pollution severity class correction
Average monthly value over one year	Monthly maximum over one year	
< 0,5	< 1,5	None
0,5 to 1,0	1,5 to 2,5	Increase by one class
> 1,0	> 2,5	Increase by one or two classes and consider mitigation

4.2.4 Determining climatic conditions at KIPTS

As mentioned in section 2.4.3, certain climatic conditions, especially those that are responsible to wet the insulators and transport the pollution particles to the insulators, play an important part in insulator performance. Therefore, temperature, Ultraviolet B (UV-B) radiation, rainfall, relative humidity, wind speed and wind direction were continuously measured and stored in 10 minute intervals for the duration of the research period on the OLCA as explained in section 3.4.1.

The recorded data for each measured weather parameter was divided into the different months of the research period. A monthly average, minimum and maximum values for temperature, relative humidity and UV-B radiation were calculated and plotted. The monthly average for UV-B radiation was calculated with data on daylight hours. The monthly data for wind speed and wind direction was divided into four directional groups based on the direction of the wind. The four groups are:

- NE for wind directions between 0° and 90°
- SE for wind directions between 90° and 180°
- SW for wind directions between 180° and 270°
- NW for wind directions between 270° and 360°

The number of data points per directional group is counted and divided by the total number of data point in all the directional groups, in order to determine the percentage of data points per directional group. These percentages are plotted for each month. The average and maximum wind speed for each directional group are also calculated and plotted.

A manual rain meter is used at KIPTS to measure the amount of rain. Every morning, except during weekends and public holidays, the measured amount on the manual rain meter is recorded and then it is emptied for a new measurement. The total rainfall recorded per month was calculated and plotted.

4.3 Number of flashover events per insulator

In section 3.2.1.1 it was mentioned that the test insulators were connected to the bus bar through mace fuses which explode, hence disconnecting the test insulators from the bus bar, if

it conducts a minimum current of 750 mA. Every weekday morning, test rig observations were done to determine if there were exploded fuses. If there was any, it was recorded that an insulator flashover event occurred on the insulator of which the given fuse exploded. The exploded fuse was replaced with a new fuse and the insulator was re-connected to the bus bar. If an insulator had four flashover events, it was permanently disconnected from the bus bar.

It is known that flashover currents are much higher than 750 mA, but a 750 mA fuse was chosen to protect the test rig from an over current condition and to protect the measurement equipment from damage caused by high currents. Further, as mentioned in section 2.4.3.3.1, the probability of a flashover becomes very high if the leakage current reaches a certain threshold value. This value (I_{max}) is defined as the maximum peak leakage current one cycle before flashover [12], and calculated by equation (2-3). Further, Holtzhausen proposed a permissible value of the peak leakage current as [12]:

$$I_{perm} = 0.25 \cdot I_{\max}. \tag{4-12}$$

Thus, by instituting equation (2-3) into equation (4-12) and using the mid-length test insulator USCD value,

$$\begin{aligned} I_{perm} &= 0.25 \times \left(\frac{USCD}{\sqrt{3} \times 15.32} \right)^2 \\ &= 0.25 \times \left(\frac{41.5}{\sqrt{3} \times 15.32} \right)^2 \\ &= 0.61\ A. \end{aligned} \tag{4-13}$$

Hence, leakage currents values higher than 610 mA fall outside the permissible range of the mid-length test insulator and may lead to an insulator flashover event. Thus, a fuse blow event triggered by a 750 mA leakage current was considered a good indication that an insulator flashover event might have occurred.

4.4 Insulator leakage current measurements

The leakage currents on the insulators were measured and stored on the OLCA, as explained in section 3.4.1. The positive and negative peak leakage current values were used to evaluate the performance of the insulators during this research. The daily maximum peak leakage current and supply voltage waveforms of the highest peak leakage current value recorded per

insulator, over the research period, were also used to study the build-up that led to the highest peak leakage current event.

The peak leakage current values are recorded on the OLCA, by comparing each leakage current sample with a previous peak leakage current sample stored in a register [12]. When a higher peak value is detected, the older stored register value is replaced with the new peak reading [12]. At the end of each 10 minute interval, both positive and negative peak register values are stored in the OLCA's memory and the registers are zeroed and the process is repeated for the following 10 minute intervals [12].

Charge values are measured on the OLCA by accumulating the positive and negative leakage current sample values in separate registers, until the end of the 10 minute interval [12]. The accumulated register values are then multiplied by the sampling interval, Δt, which is 0.5 ms for the OLCA, to produce positive and negative charge values for the 10 minute interval [12]. These values are stored in the OLCA's memory and the registers are zeroed and the process is repeated for the following 10 minute intervals [12]. The equation used to calculate the positive charge value is [12]:

$$Q_{ins}(pos) = \sum_{n=1}^{N} pos(i_n) \cdot \Delta t \tag{4-14}$$

where

$Q_{ins}(pos)$ is the 10 minute interval positive electrical charge value in Coulomb,

$pos(i_n)$ is the nth positive leakage current sample value in Ampere,

$T = 600\ s$,

$f = 2000\ Hz$,

$\Delta t = \frac{1}{f} = 0.0005\ s$

and

$N = f \cdot T = 1200000$.

Equation (4-14) can also be used to calculate the negative charge value by substituting the positive leakage current values with negative leakage current values.

The daily maximum peak leakage current and associated supply voltage waveforms are the actual highest peak leakage current and associated supply voltage waveforms of the day, captured over a 320 millisecond period. These waveforms consist of 640 samples each [12]. The first halve shows the pre-maximum information and the second halve shows the post-maximum information [12].

The stored data was copied from the OLCA to a computer terminal inside the control room at KIPTS on a weekly basis. The computer terminal was used to access and manage all the OLCAs. From the computer terminal, the data was copied to a portable hard disc drive on a weekly basis from where it was exported to Microsoft Excel spread sheets. On the Excel sheets, all the data points corresponding to the times when the test rig was switched off for visual observation or any other reason, were deleted, in order to eliminate any induced currents caused by switching or work done on the test rig.

Each test insulator's peak leakage current data was evaluated by dividing the data according to the calendar month in which it was measured. After that, the data for each calendar month was divided into several groups (bins) based on the value of the peak leakage current data. The bins were: 0-2 mA; 2-5 mA; 5-10 mA; 10-20 mA; 20-50 mA; 50-100 mA; 100-200 mA; 200-500 mA; 500-1000 mA. At the end of each month, the number of data points in each bin were summed and divided by the total number of peak leakage current data points captured for that month to obtain a percentage value for each bin. This process was repeated for each test insulator's peak leakage current data.

The data in the first group, 0-2 mA, was considered as general noise and the data in the second group, 2-5 mA, contained most of the DC-current offset fluctuation values as mentioned in section 3.4.1. Due to the abovementioned reasons, the first two groups were not used during the evaluation of the peak leakage current data. The other groups were used to compare and evaluate the insulator's leakage current performance.

The DC-current offset fluctuations, as mentioned in section 3.4.1, rendered the evaluation of the insulator's leakage current performance by accumulative charge calculations, impossible. The problem was that the DC-current offset fluctuation values were continuous and not intermitted, as insulator leakage current. These continuous values made the accumulative charge value very large and not representative of the actual accumulative charge value. Due

to this reason the accumulative charge value was considered as unreliable and therefore not used during evaluation.

4.5 Night time electrical activity observations

Night time electrical activity observations were conducted to determine which insulator displayed the first electrical activity and to sequence the ones that followed. It was also conducted to gain more insight on the development of a discharge activity on hydrophobic insulators and to observe if there were any differences in the development of a discharge activity for the different excitation voltages.

It was conducted with the CoroCAM 1 and Sony camcorder. These cameras were described in sections 3.4.2 and 3.4.3 respectively. These observations were done every night for the first three weeks in order to follow the progression of the electrical activity on the insulators. From thereon it was done once per week up to week 6 and then once every two weeks up to week 13.

During week 15, on 16 May 2011, the HTV silicone rubber and EPDM silicone alloy rubber insulators were installed as mentioned in section 3.3. From that point forth, the electrical activity observations for these insulators were done every night for the first three weeks. By the end of the third week all of the insulators had displayed an electrical activity. The three week period was considered sufficient for capturing the electrical activity progression on these insulators. The following observation was done six weeks thereafter; during week 23 and it was the last electrical activity observation. All the insulators were scanned and recorded during that observation. It was considered that enough observations were conducted to meet the objectives laid out for the electrical activity observations.

The electrical activity observations were started at 22h00 and continued up to 01h00 the next morning. It was found from previous work done at KIPTS that most of the electrical activity becomes visible from 22h00 onwards due to the wetting of the insulator surfaces [12]. The sequence followed during electrical activity observations was to scan and record each insulator for one minute per camera. Any electrical activity on the insulators detected by the cameras was noted down on the respective electrical activity observation form, as displayed in Annex A. At a later stage the data was transferred to Microsoft Excel sheets.

Sometimes, technical problems were experienced with the video output port of the CoroCAM 1, which prevented recording of the electrical activities on the insulator surfaces on tape. However, the insulators were scanned with the CoroCAM 1 and any activity observed, was captured on the electrical activity observation form.

The content on the CoroCAM 1 recorder tapes was digitized and separate files were generated for each one minute recorded scan of an insulator and the files were named using the following naming convention: Corocam_insulator position on support structure_date and time when scan was done.

The Sony camcorder has a build-in hard disc drive as mentioned in section 3.4.3, where the scans of the insulators were stored as separate files. The following day, after a night time observation, the data of the scans were transferred to a notebook PC and the filenames were changed using the following naming convention: Video_insulator position on support structure_date and time when scan was done.

The insulator surfaces were examined for the following electrical activity observations [12]:

- Water drop corona (WDC), referring to corona caused by water droplets on the insulator surfaces as explained in section 2.4.3.3.2. Please refer to Figure 4-5 (a).
- Spot discharge (SD), referring to discharges between water droplets and electrolytic filaments. Please refer to Figure 4-5 (b).
- Dry band corona (DBC), referring to corona within the dry band zone. Please refer to Figure 4-5 (c).
- Dry band discharge (DBD), referring to streamer, spark and/or arc discharge over the dry band zone. Please refer to Figure 4-5 (d).

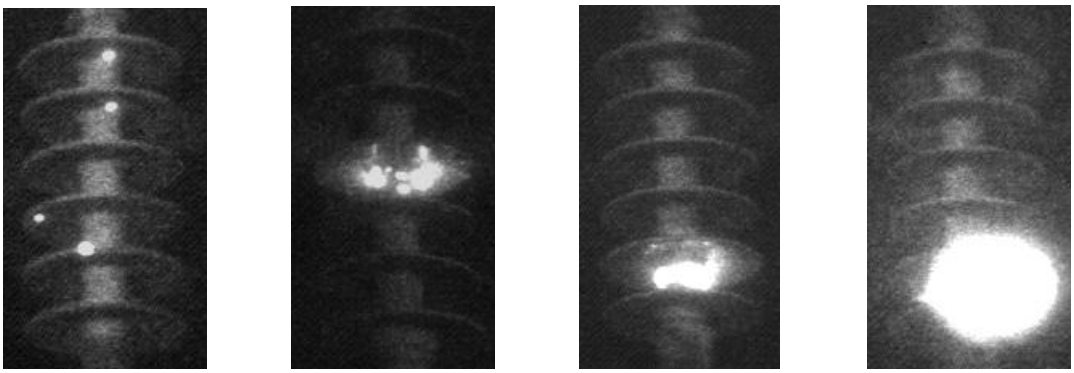

(a) (b) (c) (d)

Figure 4-5: Examples of electrical activity observations [12]

4.6 Insulator surface inspections

The electrical activity observed during night time observations and climatic conditions at KIPTS, led to the deterioration or damage of insulator surfaces. Hence, it was considered important to inspect the insulator surfaces for any signs of deterioration or damage, as this would assist in evaluating the performance of the different insulator materials. The insulator surface inspections were done without touching the insulators, so as not to disturb the natural pollution deposition process.

The insulator surface inspection process followed during this research consisted of the following steps:

- The test rig was de-energised and earthed by KIPTS personnel.
- A scaffold was built, underneath the support arm of the insulators to be inspected.
- Each insulator on the support arm was carefully inspected and every detail observed in a north, south, east and west direction on the sheaths, shed tops and shed bottoms was captured on an insulator surface inspection form as shown in Annex A. The captured observations include all of the observations listed in section 2.5, but were not limited to it.
- Any new and/or interesting observations and insulator surface deteriorations were photographed with the Sony camcorder. Details of the Sony camcorder were given in section 3.4.3.
- Wettability (hydrophobicity) classification tests were done on the polymer insulators according to STRI guide 1 [53], and the observed hydrophobicity classes were photographed. Hydrophobicity classification will be discussed later in this section.

- The scaffold was removed from underneath the support arm.
- The test rig was un-earthed and energised by KIPTS personnel.

Steps 3 to 5 were completed on one insulator before continued to a different insulator. Due to the volume of work contained in the insulator surface inspection process, only 10 insulators were inspected per day, i.e. only the insulators on one support arm. This process required the test rig to be de-energised for the whole day, from 09h30 to 16h30, thus to complete the insulator surface inspections for all three support arms per week would have required the test rig to be de-energised for 3 days per week, which is not optimal for insulator ageing tests. Hence, it was decided to rotate the insulator surface inspection process by inspecting one support arm per week.

The insulator surface inspections were weather dependent as KIPTS is an open air test station. Rain, fog, strong winds and very high relative humidity conditions (higher than 80%), were the weather conditions that did not allow visual surface inspections. Rain, fog and high relative humidity conditions wetted the insulator surfaces and made the dry band activity traces on the insulator surfaces invisible. Furthermore, rain could have damaged the camera. Strong winds created a safety concern for the people doing the inspections, as they stood on a scaffold, as well for the camera. Furthermore, during strong wind conditions, hydrophobicity classification was not possible. Due to the above reasons, it was sometimes not possible to inspect the insulator surfaces as scheduled and the inspection process was continued when weather permitted. This led to a schedule where insulator surface inspections were done once a week or every second week up to week 13 (04 May 2011) to observe the early deteriorations of the insulator surfaces. From thereon it was done once every two or three weeks up to week 43 (01 December 2011). At week 43 the insulator surface inspections were stopped, because there were no new severe surface degradations observed. A final observation was done on completion of the research project during week 53 (06 - 13 February 2012).

4.6.1 Wettability (hydrophobicity) classification

The hydrophobicity (water repellence) characteristic of polymer insulators plays an important role in the performance of polymer insulators. As mentioned in section 2.4.3.3.2, polymer insulators may temporarily lose their hydrophobic (water repellent) property, which leads to a degradation of the polymer insulator's performance. Thus, it was considered important to

know when a polymer insulator started to lose some of its hydrophobic properties for evaluation purposes. The hydrophobicity classifications were done in accordance to STRI guide 1 [53].

According to STRI guide 1, seven classes of hydrophobicity are defined, HC 1 – 7, where the first class, HC 1, corresponds to a completely hydrophobic, i.e. water repellent, surface and HC 7 corresponds to a hydrophilic, i.e. easily wetted, surface [53]. These classes provide a coarse value of the wetting status of the insulators [53].

An insulator surface area was divided into six areas where its HC ratings were determined. The six areas consist of the top, middle and bottom axial areas, for both sea side and land side facing insulator surfaces. The bottom axial area is considered the area closest to the live metal end fitting (sheath and shed 1) and the top axial area is considered the area closest to the earthed metal end fitting (the highest sheath and shed number). The six areas were further divided into shed top, shed bottom and sheath areas. Each of these areas was wetted with demineralised water by using a spray bottle capable of providing fine mist spray. Demineralised water was used in order not to add additional chemical elements on to the insulator surfaces, while conducting the hydrophobicity classification tests. The spray bottle was kept 25±10 cm away from the insulator surface while wetting it and the judgement of the hydrophobicity class was done within 10 seconds after the spraying were finished. The actual wetting appearance on the insulators was identified with one of the seven hydrophobicity classes as defined in Table 4-3 [53]. The results were captured on a hydrophobicity classification form as shown in Annex A.

Table 4-3: Criteria for hydrophobicity classification (HC) [53]

HC	Description
1	Only discrete droplets are formed. $\theta_r \approx 80°$ or larger for the majority of droplets.
2	Only discrete droplets are formed. $50° < \theta_r < 80°$ for the majority of droplets.
3	Only discrete droplets are formed. $20° < \theta_r < 50°$ for the majority of droplets. Usually they are no longer circular.
4	Both discrete droplets and wetted traces from the water runnels are observed (i.e. $\theta_r = 0°$). Completely wetted areas < 2 cm^2. Together they cover < 90% of the tested area.
5	Some completely wetted areas > 2 cm^2, which cover < 90% of the tested area.
6	Wetted areas cover > 90%, i.e. small unwetted areas (spots/ traces) are still observed.
7	Continuous water film over the whole tested area.

The contact angle (θ) between the water drops and the insulator surface must also be taken into account [53]. As seen in Figure 4-6, there exist two different contact angles, namely the advancing contact angle (θ_a) and the receding contact angle (θ_r) for water drops on an incline surface [53]. The receding contact angle is the important one in evaluating the wetting properties of an insulator, as observed in Table 4-3 [53].

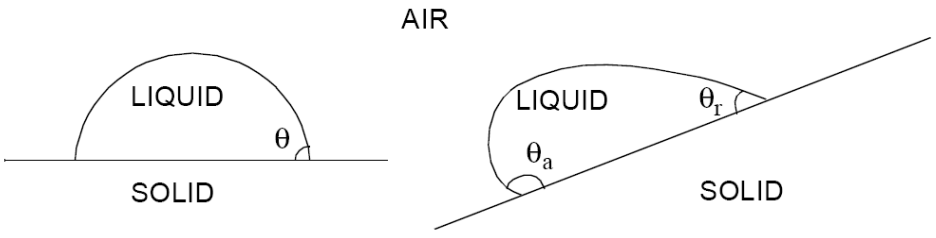

a) Horizontal plane b) Inclined plane

Figure 4-6: Definition of contact angles [53]

Photographs of typical surface examples with hydrophobicity classifications from HC 1 to HC 6 are shown in Figure 4-7.

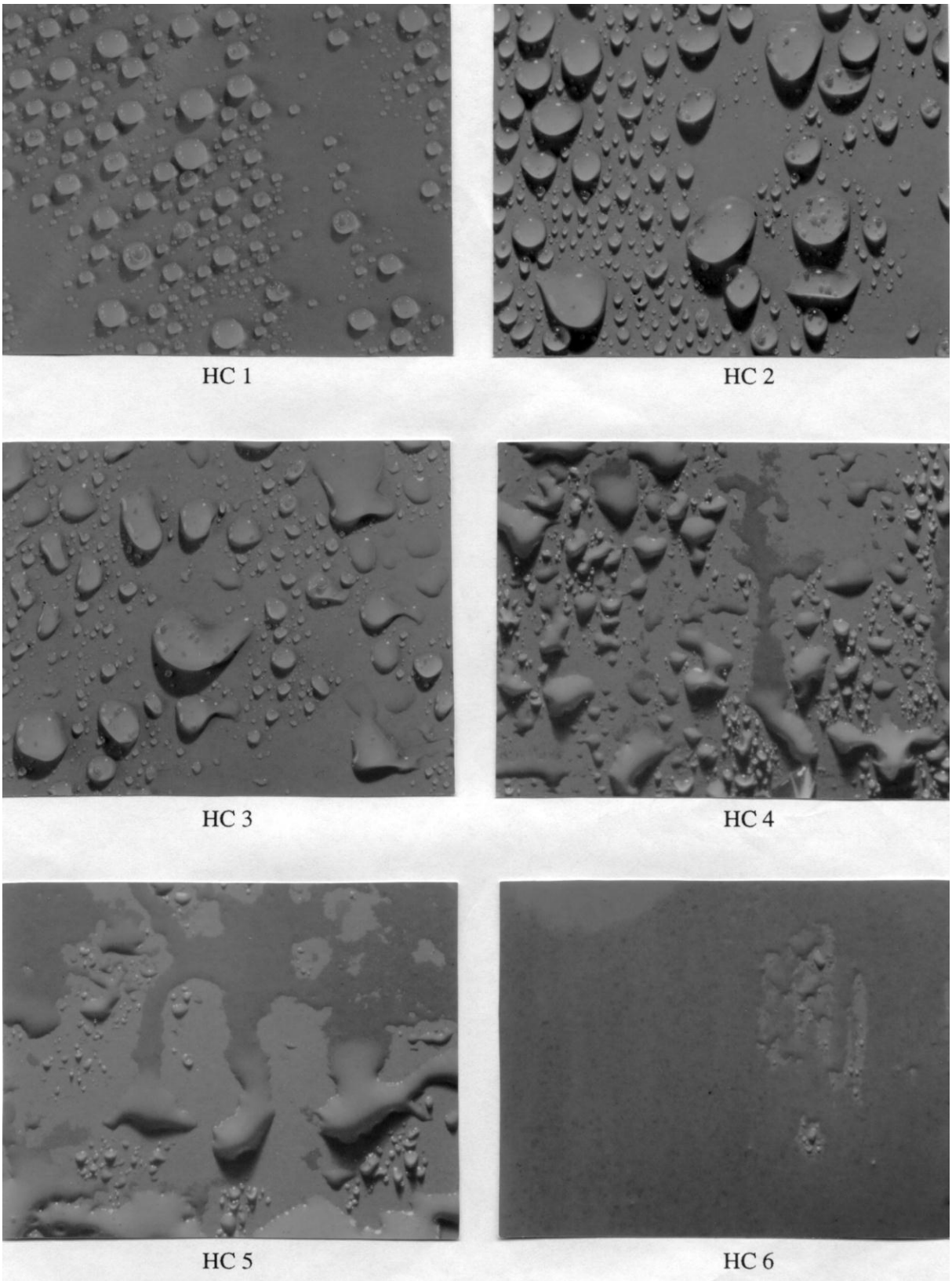

Figure 4-7: Typical examples of surfaces with hydrophobicity classification HC 1 to HC 6 [53]

Chapter 5: Results and discussions

5.1 Overview

This chapter outlines the results obtained from the one-year research project conducted and it will be presented in the following order:

- Discussions regarding monthly temperature, relative humidity, UV-B radiation, rainfall, wind speed and wind direction, to describe the climatic conditions experienced.
- Analysis of the equivalent salt deposit density (ESDD), non-soluble deposit density (NSDD), directional dust gauge index soluble (DDGIS) and directional dust gauge index non-soluble (DDGIN) measurements, to determine the site pollution severity (SPS) index of Koeberg insulator pollution test station (KIPTS).
- Discussions regarding the signs of surface degradation observed on each insulator and wettability (hydrophobicity) classifications exhibited by the polymer insulators.
- Analysis of leakage current measurements for each insulator.
- Discussions regarding the electrical activity observed during night time observations.

During the presentation of the results, the performance of the different insulator materials are also compared, in order to determine which material performed better per excitation voltage and to determine which excitation voltage performed better for each insulator material.

5.2 Climatic conditions and SPS index at KIPTS

5.2.1 Climatic conditions at KIPTS

Temperature, relative humidity, UV-B radiation, rainfall, wind speed and wind direction were the climatic conditions monitored, and measured at KIPTS as explained in section 4.2.4. The recorded data is plotted in Figure 5-1 up to Figure 5-7. The wind speed and wind direction data up to December 2011 was obtained from the Koeberg meteorological station, because there were instances over the research period where the wind speed meter at KIPTS was out

of order. The Koeberg meteorological station is about 300 m from KIPTS and the wind speed and directional meter is installed at a 10 m height.

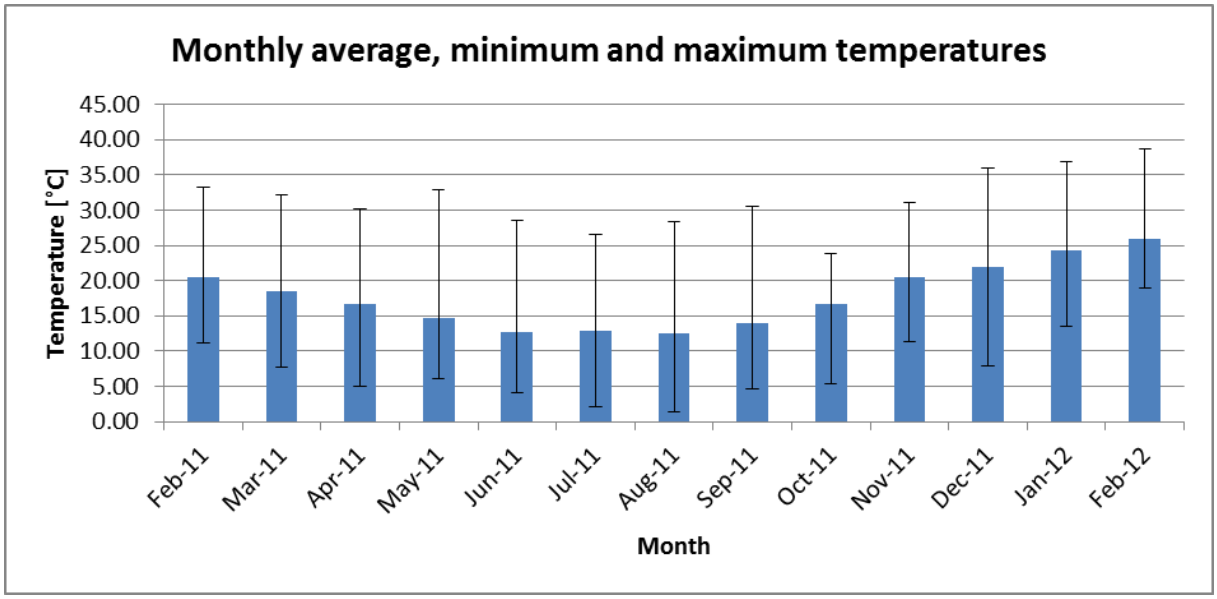

Figure 5-1: Monthly average, minimum and maximum ambient temperatures

As observed in Figure 5-1 the lowest ambient temperature of 1.39 °C was recorded in August 2011 and the maximum ambient temperature of 38.72 °C was recorded in February 2012. For the majority of the winter months (April – September) the average ambient temperature varied between 10 and 15 °C and the majority of summer months (October – March) the ambient average temperature varied between 20 °C and 25 °C.

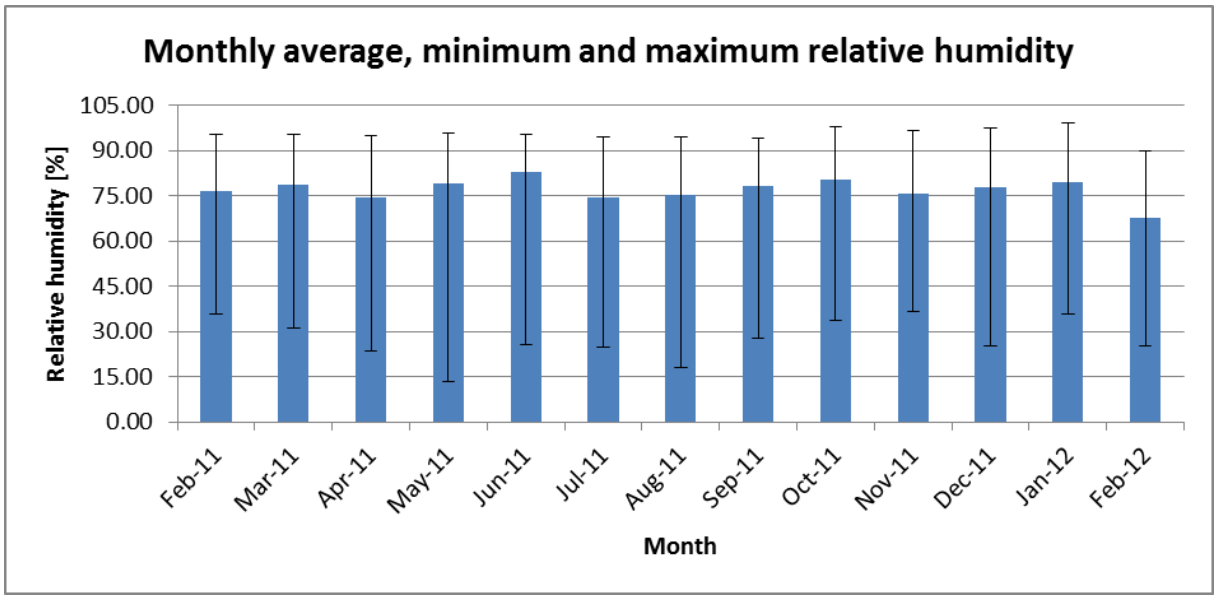

Figure 5-2: Monthly average, minimum and relative humidity

As seen in Figure 5-2 the lowest relative humidity of 13.40% was recorded in May 2011 and the maximum relative humidity of 99.13% was recorded in January 2012. For the majority of months during the research period the average relative humidity was higher than 75%. As discussed in section 2.4.3.2, a relative humidity of 75% and higher will wet the pollution layer on the insulator surface which may result in the flow of leakage currents. April 2011, July 2011 and February 2012 are the only months where the average relative humidity was lower than 75%. It is also observed that the winter months (April – September) have lower maximum and minimum relative humidity percentages than the summer months (October – March). Thus, summer months have a slightly higher relative humidity than the winter months.

The one year data of Relative Humidity were averaged over a one day period to determine which time period of a day, on average, has a Relative Humidity lower than 75%. The absolute maximum and minimum values per timeslot of the one year Relative Humidity data were also plotted in Figure 5-3. It is evident from Figure 5-3 that between 10:00 and 19:00 is the average Relative Humidity below 75% which implies dryer insulator surfaces and thus low leakage current levels. Further, the highest Relative Humidity was measured during the early morning hours (02:00 -06:00) and the lowest at midday (12:00 to 14:00). Thus, it is expected that the highest leakage current activity occurs during the early morning hours.

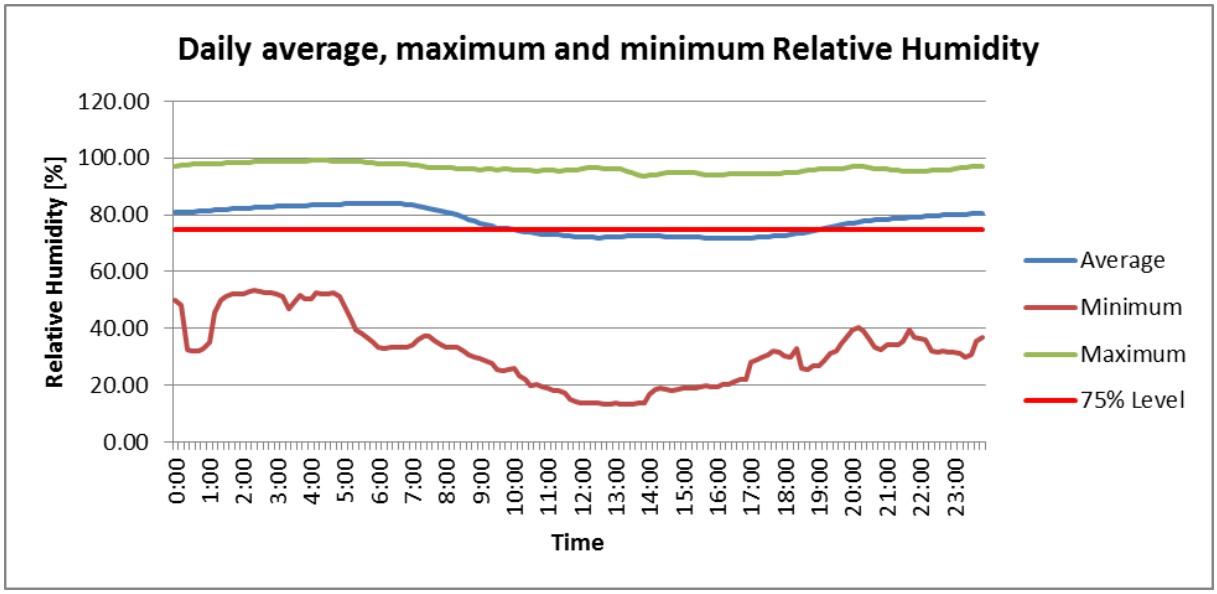

Figure 5-3: Daily average, maximum and minimum Relative Humidity

According to Figure 5-4 the highest average UV-B radiation occurs during the summer months with the highest average value of 125.81 µW/cm^2 recorded during December 2011. The maximum values plotted on the graph are outliers and thus not considered. It is not known what caused the outliers, but solar flares are expected.

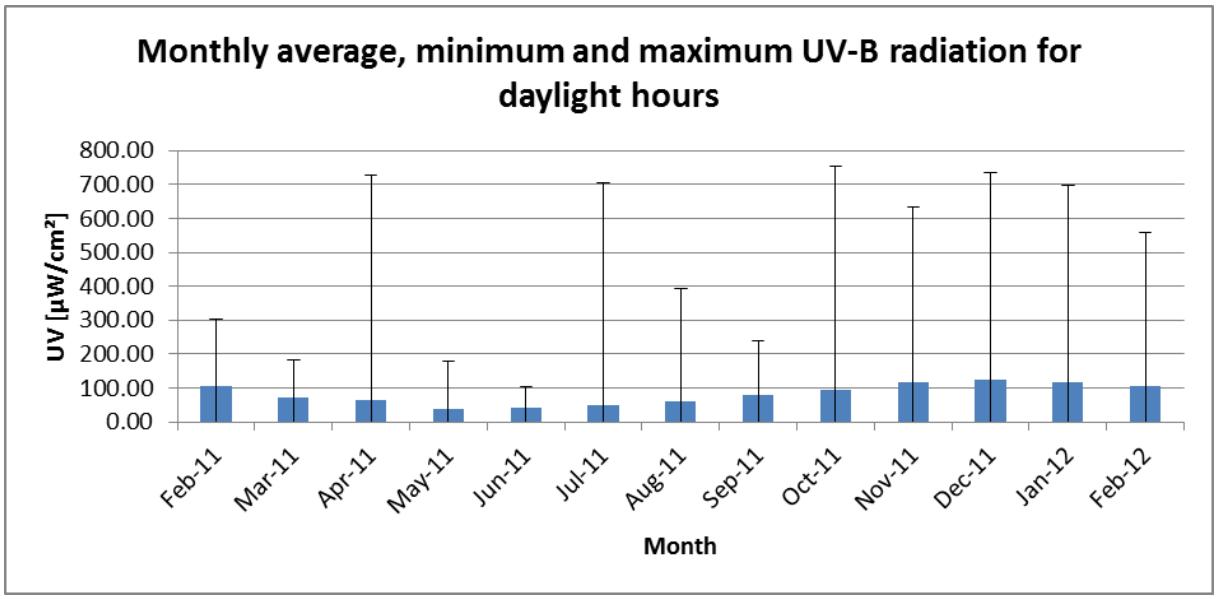

Figure 5-4: Monthly average, minimum and maximum UV-B radiation for daylight hours

UV-B radiation plays an important role in the heating of the ambient air mass, which has an influence on wind speeds and direction [12]. Furthermore, the heating of the ambient air mass surrounding the insulator surfaces during sun rise, may result in wetting of the insulator surfaces. This may happen when the temperature of the surrounding ambient air mass becomes higher than the insulator surfaces' temperature which allows condensation. They may also be wetted when the insulator surfaces temperature reaches the ambient dew point temperature, as stated in section 2.4.3.2.

UV-B radiation is also responsible for heating the insulator surfaces. During daytime, it keeps the insulator surfaces at a temperature higher than the ambient temperature, which creates a low probability state for surface wetting. The high-energy UV-B photons may also result in the ageing of polymer insulator surfaces [12]. Thus, one may expect higher wind speeds and more ageing signs on the polymer insulators during summer months because of its higher UV-B radiation averages.

With reference to Figure 5-5, KIPTS received most of its rainfall during the winter months. June 2011 received the most rain with a measured total of 91.1 mm and February 2012 received the least rain with a measured total of 0 mm. A higher rainfall for July 2011 was expected, but the dominant SE wind during July 2011, as seen in Figure 5-6, explains the low rainfall in July 2011. The SE wind is normally characterized by no rain. The rain received from May 2011 to August 2011 might have removed some of the pollution deposits from the insulator surfaces, as explained in section 2.4.3.1.2 and thus lower leakage current activity may be expected over this period. This washing effect also explains why the ESDD measurements on the glass top are lower than the glass bottom measurements during the winter months, as observed in Table 5-1.

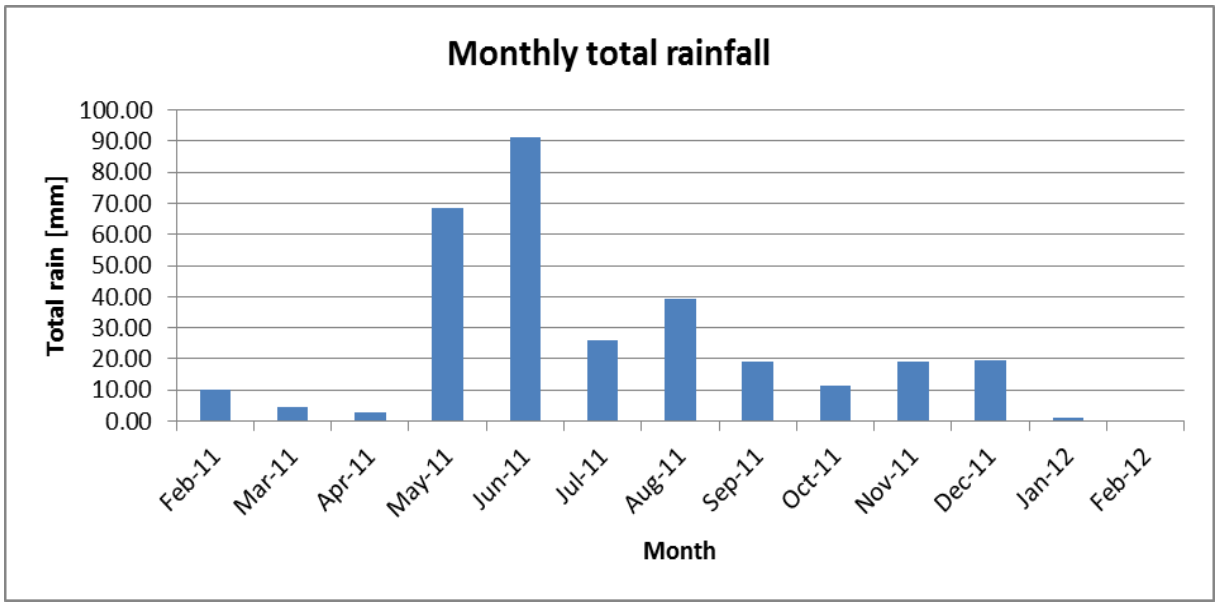

Figure 5-5: Monthly total rainfall

As seen in Figure 5-6, the predominant wind direction during the summer is SE (south-east) and followed by SW (south-west) direction. During winter the predominant wind direction is NE (north-east) and it is followed by SE (south-east) direction.

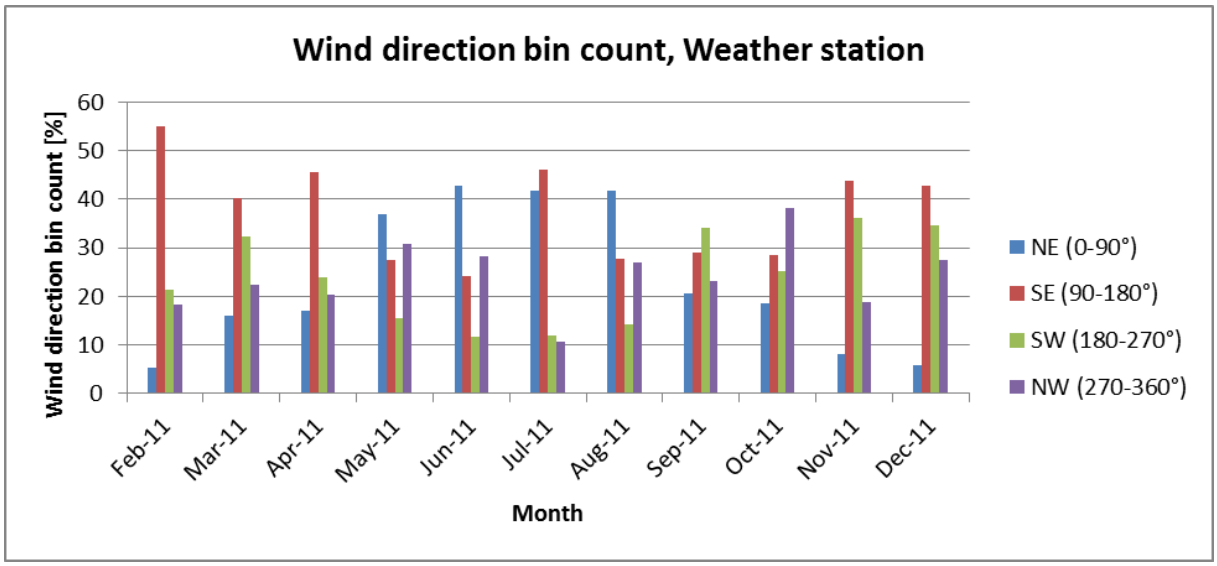

Figure 5-6: Wind direction bin count

As seen in Figure 5-7, the direction with the highest average and maximum wind speed during summer is SE and followed by SW direction. The maximum wind speed recorded during the summer months was 13.93 m/s and it was recorded during February 2011 in a SE direction. NW has the highest average wind speed during winter and it is followed by SE direction. The direction with the highest maximum wind speed during winter is SE and followed by NW direction. The highest wind speed recorded during the winter months was 14.08 m/s in a SE direction and it was recorded during July 2011. It is also noted that the average wind speed over the winter months is lower than the summer months. Thus, the expectation set in the UV-B radiation discussion earlier in this section, has come to terms.

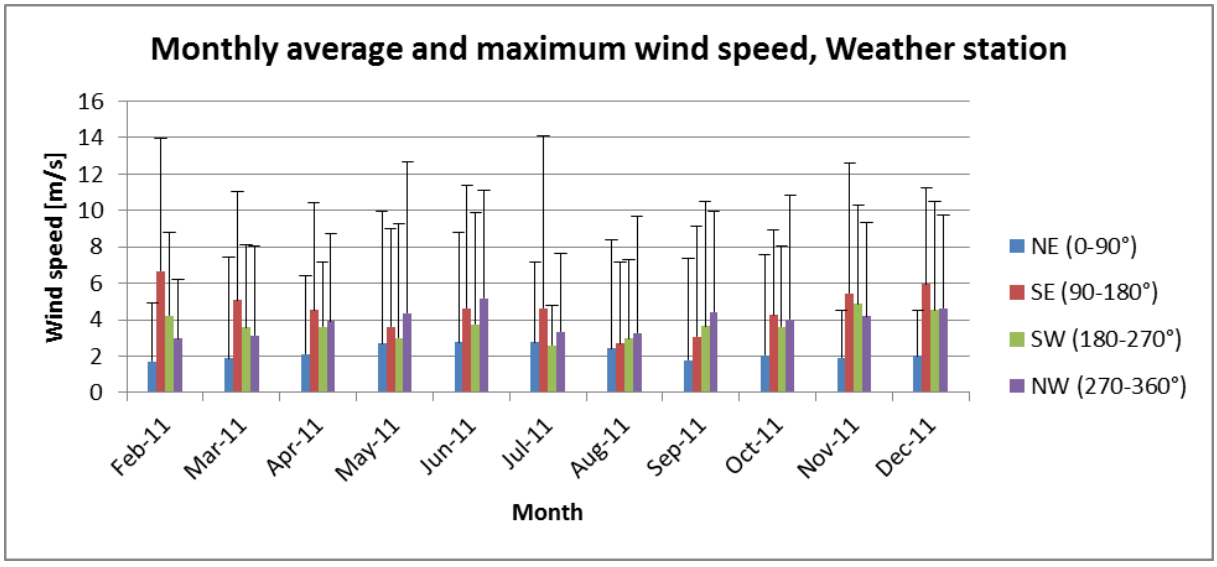

Figure 5-7: Monthly average and maximum wind speed

From the discussions above, it is clear that the South-Eastern winds are the dominant winds during summer. Pollution sources in the SE quadrant from KIPTS consist mainly from dune sand and air pollution from agricultural activities, oil refinery and fertilizer plants. The dominant source is the dune sand, which is evident from the very high non-soluble deposit (NSD) values of the south direction during summer months as indicated in Table 5-4.

If Figure 5-7 and Table 5-4 are compared, it is observed that the months with very high maximum wind speeds (higher than 11 m/s), have very high NSD values in the direction which the maximum wind speed occurred. Thus, sand pollution is affected by the maximum wind speed parameter.

If Figure 5-6 and Figure 5-5 are compared, it is observed that the three months where the wind from the NE direction was dominant in comparison to the SE direction (May, June, August), the highest rainfall was received.

5.2.2 SPS index at KIPTS

As mentioned in section 4.2, the SPS index at KIPTS were calculated by ESDD, NSDD, DDGIS and DDGIN measurement methods, but only the worst severity class, as determined by ESDD and NSDD measurements or DDGIS and DDGIN measurements will be used as KIPTS' pollution severity index as explained in section 4.2.3.

5.2.2.1 ESDD and NSDD values

The ESDD and NSDD values were measured and calculated as described in section 4.2.1 and summarized in Table 5-1 and Table 5-2 respectively.

The higher values in Table 5-1 and Table 5-2 are highlighted in grey. From Table 5-1 it is evident that during the winter months (April to September), for the majority of times, the ESDD values on the bottom of the glass disc were higher than the ESDD values on the top of the glass disc. This is due to the high rainfall during the winter months as seen in Figure 5-5, which washed away some of the soluble pollution on the glass top. The pollution on the glass bottom was protected from the rain by deep under-ribs of the glass disc. It is also observed that during the early stages of the project, for the majority of times, the ESDD values on the

top of the glass disc were higher than the ESDD values of the bottom of the glass disc. However, closer to the end of the project, the opposite was true. No explanation could be rendered for this observation.

Table 5-1: Summary of ESDD values

Date	Glass Top	Glass Bottom	Average ESDD
	ESDD [mg/cm²]	ESDD [mg/cm²]	[mg/cm²]
09 February 2011	0.052	0.024	0.033
16 February 2011	0.050	0.035	0.039
24 February 2011	0.067	0.053	0.057
03 March 2011	0.063	0.057	0.059
11 March 2011	0.118	0.065	0.081
16 March 2011	0.109	0.067	0.080
25 March 2011	0.028	0.057	0.048
05 April 2011	0.062	0.074	0.070
14 April 2011	0.088	0.048	0.060
04 May 2011	0.014	0.044	0.035
24 May 2011	0.004	0.032	0.023
07 June 2011	0.018	0.029	0.026
07 July 2011	0.033	0.049	0.044
27 July 2011	0.030	0.030	0.030
15 August 2011	0.058	0.070	0.066
29 August 2011	0.065	0.053	0.056
05 September 2011	No sample	No sample	No sample
03 October 2011	0.072	0.091	0.085
10 November 2011	0.078	0.138	0.119
29 November 2011	0.464	0.158	0.253
22 December 2011	0.099	0.115	0.110
30 January 2012	0.047	0.078	0.069

In the process of conducting the measurements for the NSDD values, it was found that sometimes the weight of the filter paper containing the pollutants was less than the weight of the previous weighted clean filter paper. This occurred when the amount of non-soluble pollutant contained on the filter paper was very small. Furthermore, the measurements were done in the order of 10^{-4} grams. During such sensitive measuring scales, many factors come into play e.g. airflow and relative humidity of the area where the measuring took place. The airflow was blocked by the sliding side and top glass panels of the balance's weighing chamber. Thus, a possible explanation is that the relative humidity of the room was different when the clean filter paper was measured compared to when the filter paper containing the pollutants was measured. This implies that the filter papers absorbed different amounts of moisture. In each case where such an incident occurred, the NSDD value in Table 5-2 was made 0.

It is evident from Table 5-2 that in most instances, the NSDD values on the top of the glass disc were higher than the NSDD values on the bottom of the glass disc. This could be explained by the aerodynamic action deposition method as described in section 2.4.3.1.1, where it states that the bigger particles like sand are deposited on the insulator surface facing the wind. The top part of the glass disc used for ESDD and NSDD measurements, faced the wind directly, whereas the majority of the bottom part of the glass disc was protected from the direct winds by its deep under-ribs.

Table 5-2: Summary of NSDD values

Date	NSDD Top [mg/cm²]	NSDD Bottom [mg/cm²]	Average NSDD[mg/cm²]
09 February 2011	0.01	0.02	0.02
16 February 2011	0.02	0.00	0.01
24 February 2011	0.32	0.06	0.14
03 March 2011	0.08	0.02	0.04
11 March 2011	0.04	0.01	0.02
16 March 2011	0.00	0.00	0.00
25 March 2011	0.00	0.00	0.00
05 April 2011	0.01	0.00	0.00
14 April 2011	0.00	0.00	0.00
04 May 2011	0.03	0.01	0.02
24 May 2011	0.01	0.02	0.01
07 June 2011	No sample	No sample	No sample
07 July 2011	0.09	0.04	0.06
27 July 2011	0.00	0.00	0.00
15 August 2011	0.00	0.00	0.00
29 August 2011	0.00	0.00	0.00
05 September 2011	0.00	0.00	0.00
03 October 2011	0.01	0.00	0.01
10 November 2011	0.01	0.02	0.02
29 November 2011	0.08	0.07	0.08
22 December 2011	0.00	0.01	0.01
30 January 2012	0.03	0.12	0.09

It is also observed from the above tables that the average ESDD and NSDD values are smaller during the winter months than the summer months (October to March). The washing effect of the winter rainfall as seen in Figure 5-5 could be a possible explanation for this observation. Also, during winter months, the average wind speed was lower than during summer months as seen in Figure 5-7, which lowers the pollution carrying capacity of the winter wind and thus a lower ESDD and NSDD value.

According to Table 5-1 the highest ESDD value measured on 29 November 2011 was 0.253 mg/cm^2 and according to Table 5-2 the highest NSDD value measured on 24 February 2011 was 0.14 mg/cm^2. By applying these values to Figure 4-4 it indicates that KIPTS has a class d, heavy pollution, SPS index.

5.2.2.2 DDGIS and DDGIN values

The DDGIS and DDGIN measurements and calculations were done as described in section 4.2.2 and summarized in Table 5-3 and Table 5-4 respectively.

Table 5-3: Summary of DDGIS values

Date	North	East	South	West	DDGIS [µS/cm]
	DDDG [µS/cm]	DDDG [µS/cm]	DDDG [µS/cm]	DDDG [µS/cm]	
09 February 2011	167.16	104.36	265.05	149.47	171.51
16 February 2011	152.97	205.60	878.30	653.49	472.59
24 February 2011	425.38	162.42	3003.90	590.05	1045.44
03 March 2011	87.03	51.79	602.12	204.40	236.33
11 March 2011	619.97	140.00	2478.50	386.29	906.19
16 March 2011	281.47	193.37	895.55	566.72	484.28
25 March 2011	456.21	222.79	1682.33	984.36	836.43
05 April 2011	334.15	310.20	854.42	466.42	491.30
14 April 2011	308.91	143.73	936.47	145.02	383.53
04 May 2011	859.67	254.09	1475.91	957.27	886.73
24 May 2011	805.42	91.87	568.10	243.74	427.28
07 June 2011	1273.37	322.70	1473.13	1574.72	1160.98
07 July 2011	1063.03	191.81	916.76	1221.23	848.21
27 July 2011	84.84	62.22	119.72	62.84	82.41
15 August 2011	650.68	122.60	834.69	644.78	563.19
29 August 2011	515.74	214.93	839.89	364.03	483.65
05 September 2011	No sample	No sample	No sample	No sample	No sample
03 October 2011	738.65	219.80	709.67	818.72	621.71
10 November 2011	305.69	158.23	302.55	434.02	300.12
29 November 2011	586.84	271.85	1532.55	2921.11	1328.09
22 December 2011	388.88	106.55	796.00	826.35	529.45
30 January 2012	406.00	247.37	868.46	931.66	613.37
Average					612.99

Table 5-4: Summary of DDGIN values

Date	NSD North [g]	NSD East [g]	NSD South [g]	NSD West [g]	DDGIN [g]
09 February 2011	0.00	0.00	2.38	0.34	0.68
16 February 2011	0.00	0.05	2.19	0.13	0.59
24 February 2011	0.82	1.95	13.57	2.27	4.65
03 March 2011	0.00	0.00	7.86	0.37	2.06
11 March 2011	0.00	0.00	6.85	0.22	1.77
16 March 2011	0.00	0.00	10.90	0.00	2.72
25 March 2011	0.00	0.00	1.00	0.00	0.25
05 April 2011	0.00	0.00	2.24	0.16	0.60
14 April 2011	0.03	0.94	2.29	0.04	0.82
04 May 2011	0.21	0.28	0.49	0.13	0.28
24 May 2011	3.63	0.33	0.21	0.57	1.18
07 June 2011	No sample	No sample	No sample	No sample	No sample
07 July 2011	0.52	0.13	1.97	0.04	0.66
27 July 2011	0.31	1.69	10.80	0.00	3.20
15 August 2011	0.40	0.01	0.00	0.02	0.11
29 August 2011	0.03	0.01	0.11	0.01	0.04
05 September 2011	0.95	0.00	0.00	0.32	0.32
03 October 2011	0.31	0.02	0.96	0.08	0.34
10 November 2011	0.05	0.01	1.00	0.19	0.31
29 November 2011	0.15	0.27	23.87	0.90	6.30
22 December 2011	0.36	0.47	25.11	1.00	6.73
30 January 2012	0.18	0.77	24.57	0.77	6.57
Average					1.91

From Table 5-3 and Table 5-4, it is evident that for the majority of times the south direction has the highest levels of conductivity and the highest mass of non-soluble pollution. Thus, a correlation exists between the high mass numbers of non-soluble pollution of the south direction, and the high conductivity measurements of the south direction as observed in Table 5-3. In the above tables the highest values are highlighted in grey. These results were expected, because there is a sand dune located adjacent to KIPTS, in a southwardly direction, and the wind blows for the majority of times from a southern direction as discussed in section 5.2.1.

Another observation is that the non-soluble pollution mass in the west direction never exceeds the non-soluble mass of the south direction; however the conductivity measurements in the west sometimes exceed the measurements for the south direction. A possible explanation is that the seawater spray coming from the sea, located about 50 m from KIPTS in a westward direction, was responsible for the high conductivity measurements in the west.

It is also observed that during winter months, the DDGIN values are smaller than the values for the summer month; however, the same observation cannot be made for the DDGIS values. A possible explanation is that during winter months the average wind speed is lower than during the summer months as seen in Figure 5-7, which lowers the big particle carrying capacity of wind, which leads to a lower DDGIN value.

According to Table 5-3 the highest DDGIS value is 1328 µS/cm and it was measured on 29 November 2011 and the average DDGIS value is 613 µS/cm. According to Table 5-4 the highest DDGIN value is 6.73 g which was measured on 22 December 2011 and the average DDGIN value is 1.91 g. By applying these values to Table 4-1 and Table 4-2 it indicates that KIPTS has a class e, very heavy pollution, SPS index

According to the ESDD and NSDD calculations KIPTS has a class d SPS index rating and according to DDGIS and DDGIN calculations KIPTS has a class e SPS index rating. When applying the definition to choose the worst SPS index rating as the site's SPS index rating, KIPTS is found to have a class e, very heavy pollution, SPS index rating.

As seen in Figure 5-8, the minimum recommended reference unified specific creepage distance (USCD) for a class e SPS is 53.7 mm/KV for glass, ceramic and polymer insulators [54, 55]. Furthermore, it is recommended that under extreme pollution conditions, as experienced at KIPTS, one should increase the USCD of the insulators above the recommended value [54, 55]. However, the USCD of the insulators used during this research, as given in Table 3-6, are smaller than the recommended minimum USCD. The insulators were selected to have smaller USCDs, in order to accelerate the ageing of the insulators over the one year research period.

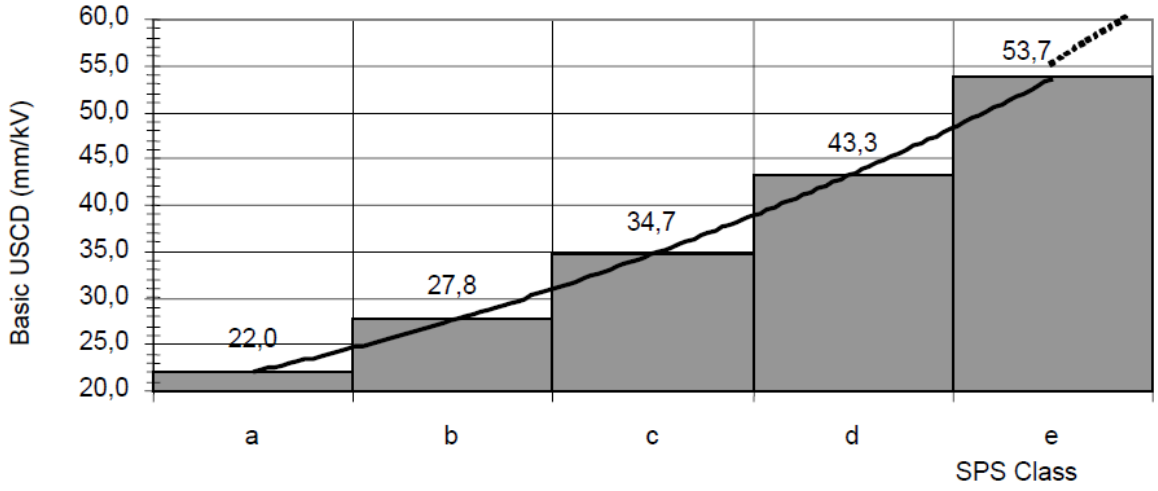

Figure 5-8: Reference USCD as a function of SPS Class for glass, ceramic and polymer insulators [54, 55]

5.2.2.3 Chemical analysis of dust gauge water solutions

At the end of the research period, a quantitative chemical analysis was conducted on the dust gauge water solutions, to determine the chemical compounds of the soluble deposits collected in each of the four removable containers of the dust gauge over a two-week period, as mentioned in section 4.2.2. The results of the analysis are split in 2 categories; cations presented in Table 5-5 and anions presented in Table 5-6. Cations were tested with inductive coupled plasma-optical emission analytical spectrometry (ICP-MS and ICP-AES) processes and anions were tested with Ion-exchange chromatography (IC) process. Furthermore, the results were compared with elements present in seawater and the information about the elements in seawater was retrieved from an internet source at www.seafriends.org.nz/oceano/seawater.htm [56].

Table 5-5: Cations present in dust gauge water solutions compared to elements in seawater

	Quality Control							
	Cert std value	Analysed	% Error	North [µg/l]	South [µg/l]	East [µg/l]	West [µg/l]	Seawater [µg/l] [56]
Al	24.68	25.14	1.87	13.73	22.60	23.20	15.34	1
As	24.68	25.04	1.48	0.08	0.55	0.03	0.15	2.6
B	24.68	26.36	6.80	32.90	56.21	27.40	38.57	4450
Ba	24.68	24.28	1.64	1.47	2.52	1.51	2.88	21
Ca	9.70	9.95	2.62	6303	24720	8516	12800	411000
Cd	9.87	9.82	0.48	0.22	0.11	0.11	0.19	0.11
Co	9.87	10.07	2.04	0.29	0.14	0.22	0.27	0.39
Cr	24.68	25.35	2.73	0.02	0.06	<0.000	<0.000	0.2
Cu	24.68	25.68	4.03	4.65	242.81	2.91	13.61	0.9
Fe	24.68	25.35	2.72	4.24	8.38	3.80	5.63	3.4
K	9.70	11.54	18.97	612.4	2848	418.5	4659	392000
Li	24.68	25.44	3.08	0.49	1.20	0.28	1.72	170
Mg	9.70	10.86	11.96	1678	6468	1234	15350	1290000
Mn	24.68	26.20	6.18	0.64	0.41	1.07	0.66	0.4
Na	9.70	10.36	6.80	14530	58360	10020	118400	10800000
Ni	24.68	26.13	5.89	0.62	0.90	0.43	0.79	6.6
P	1.94	1.98	2.11	2.7	1759	5.8	20.5	88
Pb	24.68	24.42	1.04	0.59	0.16	0.64	2.42	0.03
Se	24.68	24.11	2.29	0.04	0.22	0.54	<0.000	0.9
Si	0.97	0.98	1.16	44.9	278.4	52.5	73.4	2900
Sr	0.97	0.96	1.07	43.6	226.2	60.4	107.7	8000
Zn	0.97	1.07	9.90	19.3	9	25.7	153.2	5
V	9.87	10.70	8.36	0.10	0.74	0.10	0.14	1.9
Mo	9.87	9.53	3.42	0.25	0.76	0.22	0.35	10
Hg	1.00	0.95	4.53	0.07	0.06	0.05	0.04	0.15

Table 5-6: Anions present in dust gauge water solutions compared to elements in seawater

	North [µg/l]	South [µg/l]	East [µg/l]	West [µg/l]	Sea Water [µg/l] [56]
F	None detected	None detected	None detected	None detected	13000
Cl	27400	99900	17100	202000	19400000
NO2	None detected	None detected	None detected	None detected	Not mentioned
NO3	None detected	None detected	None detected	None detected	Not mentioned
PO4	None detected	None detected	None detected	None detected	Not mentioned
SO4	3500	11900	1600	18400	2701000

The soluble deposits originate from different sources, namely the sea, ocean sand, sand dunes surrounding KIPTS and from air pollution. The ocean sand and sand from the sand dunes

contains most of the same chemical elements as the sea, because it is frequently covered with sea spray. From the above two tables, it is evident that all of the elements detected in the dust gauge water solutions are also present in seawater. Thus, one may assume that most of the soluble deposits in the dust gauges and thus deposited on the insulators, came from the sea and surrounding sand.

The highest value of a specific element in the above two tables is highlighted in grey and it is evident from Table 5-5 and Table 5-6 that the South and West directions have the most elements with highest values. This observation is in alignment with Table 5-3, which showed that the two directions with the highest levels of conductivity are South and West.

5.3 Insulator surface conditions

The insulator surfaces were inspected as discussed in section 4.6 and the results of the inspections will be presented in this section. Signs of insulator degradation were observed in the form of light erosion, minor splitting or cutting, colour changes, glaze chipping on the porcelain insulators and metal end fitting corrosion as defined as in section 2.5. Signs of insulator damage were also observed in the form of erosion as defined as in section 2.5. Other observations were sand pollution, crazing within the pollution layer, salt crystals, dry band formations, dead insects, plant particles and grease stains. In order to compare the insulators surface performance, only the observations of surface degradation and damage were directly considered during evaluations.

Please refer to Figure 5-9 for photographs of the other observations that were not directly considered during the insulators surface performance evaluations.

Hydrophobicity tests were also conducted on the polymer insulator surfaces on the same day the insulator surfaces were inspected. A summary of the results will also be presented in this section.

a) Crazing pollution layer b) Dry band formation c) Plant particle

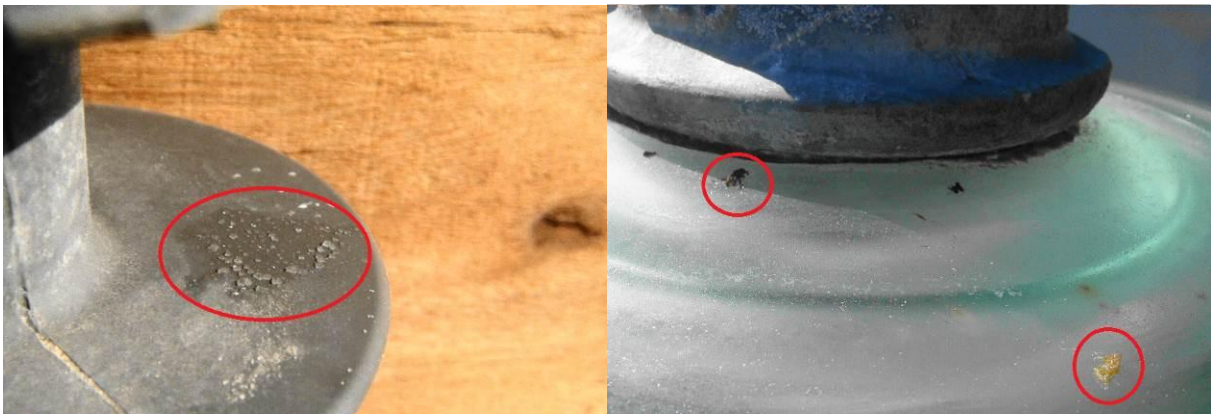

d) Salt crystals e) Dead insect and grease stain

Figure 5-9: Photographs of observations not directly considered during evaluations

5.3.1 Light erosion and erosion

In this section a detailed description of light erosion and erosion observations per insulator will be given and at the end of this section the insulators will be compared to determine which insulator material were mostly effected by light erosion and erosion. The comparison was done in terms of the number of light erosion and erosion observations per insulator, because detailed measurements of light erosion and erosion observations on the insulator surfaces in terms of width, depth and length were not possible, due to a decision not to touch the insulators, in order to prevent possible disturbances in the natural pollution deposition process.

5.3.1.1 Insulators under AC excitation voltage

In this section, light erosion and erosion observations, as observed on the different insulators excited by AC voltage, will be discussed.

5.3.1.1.1 AC_EPDM insulator

The AC_EPDM insulator was installed and energised on 16 May 2011 and the first insulator surface inspection was done on 6 July 2011. During this inspection there were no signs of light erosion. The earliest observations of light erosion were made during the third inspection cycle on 16 November 2011. The details of first occurrences of light erosion are summarized in Table 5-7. To interpret the information in Table 5-7, the following must be noted: the sheaths and sheds were counted from the live side of the insulator to the earthed side of the insulator i.e. sheath 1 is connected to the AC voltage source (bus bar) via a metal end fitting and sheath 9 is connected to the station earth via a metal end fitting.

Table 5-7: First occurrences of light erosion on the AC_EPDM insulator

First occurrences of light erosion on the AC_EPDM insulator			
Date	**Insulator position**	**Direction**	**Preceded by**
2011/11/16 (Day 185)	Mould line of 3rd sheath	East	Light pollution, dry band
	Mould line of 3rd shed bottom	East	Light pollution, dry band
	Mould line of 5th shed top	West	Light pollution, dry band
2012/02/06 (Day 267)	Mould line of 1st sheath	East	Light pollution, dry band
	Mould line of 6th shed bottom	East	Light pollution, dry band
	9th sheath	East	Light pollution, dry band
	Mould line of 7th shed bottom	West	Light pollution, dry band, salt crystals

It is evident from Table 5-7 that light erosion observations were more prominent on the mould lines, the east side of the insulator and close to the earthed side of the insulator. Furthermore, it is noted that all of the light erosion observations were preceded by light pollution and dry band formations. The dry band formations are indicative that there were electrical discharge activities at the respective areas and it could be the cause of material erosion. Please refer to Figure 5-10 and Figure 5-11 for photographs of light erosion observations on AC_EPDM insulator.

Figure 5-10: Light erosion observation on the mould line of the sheath and shed bottom of the AC_EPDM insulator

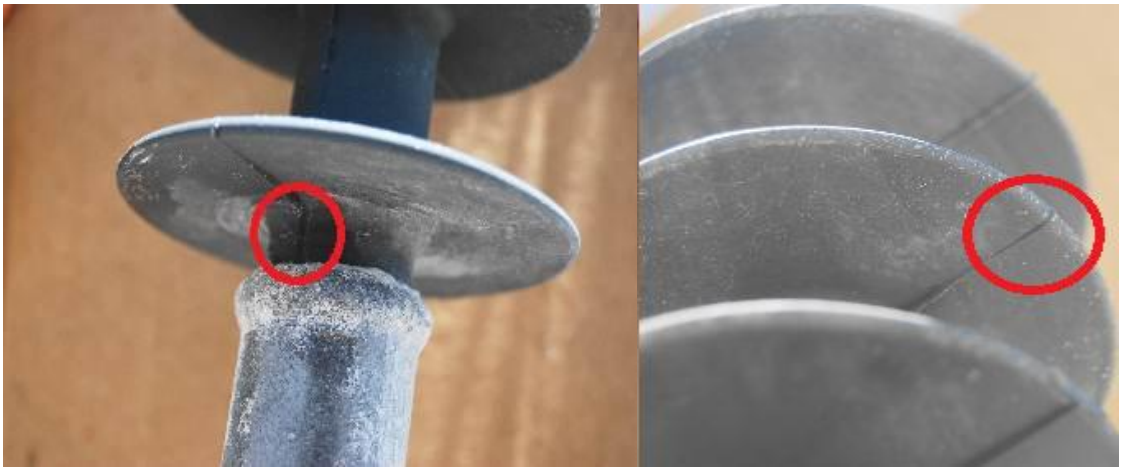

Figure 5-11: Light erosion observations on mould line of the AC_EPDM insulator

5.3.1.1.2 AC_HTV insulator

The AC_HTV insulator was installed and energised on 16 May 2011 and the first insulator surface inspection was done on 6 July 2011. During this inspection, there were no signs of light erosion observed. The earliest light erosion was observed during the third inspection cycle on 16 November 2011. To interpret the information in Table 5-8, the following must be noted: sheath 1 is connected to the AC voltage source (bus bar) via a metal end fitting and

sheath 9 is connected to the station earth via a metal end fitting. The details of first occurrences of light erosion are summarized in Table 5-8.

Table 5-8: First occurrences of light erosion on the AC_HTV insulator

First occurrences of light erosion on the AC_HTV insulator			
Date	**Insulator position**	**Direction**	**Preceded by**
2011/11/16 (Day 185)	Mould line of 8th sheath	West	Light pollution, dry band, crazing in pollution layer
2012/02/08 (Day 269)	1st sheath	South	Light pollution, dry band, crazing in pollution layer

It is evident from Table 5-8 that the light erosion observed is located more prominently, on the sheath section of the insulator. However, no conclusions can be made regarding the prominent direction and axial position of the light erosion observations on the insulator. Furthermore, it is noted that all of the light erosion observations were preceded by light pollution, dry band formations and crazing within the pollution layer. The dry band formations are indicative that there were electrical discharge activities at the respective areas and this could be the cause of material erosion. Please refer to Figure 5-12 for photographs of light erosion observations on AC_HTV insulator.

Figure 5-12: Light erosion observations on the AC_HTV insulator

5.3.1.1.3 AC_RTV insulator

The AC_RTV insulator was installed on 1 February 2011 and energised on 3 February 2011 and the first insulator surface inspection was done on 3 March 2011. During this inspection there were no signs of light erosion or erosion. The earliest light erosion observations were made during the fourth inspection cycle on 7 July 2011 and the earliest erosion observation

were made during the sixth inspection cycle on 16 November 2011. To interpret the information in Table 5-9, the following must be noted: the bottom of shed 1 is connected to the AC voltage source (bus bar) via a metal end fitting and the top of shed 6 is connected to the station earth via a metal end fitting. The details of first occurrences of light erosion and erosion are summarized in Table 5-9.

Table 5-9: First occurrences of light erosion and erosion on the AC_RTV insulator

First occurrences of light and erosion on the AC_RTV insulator			
Date	**Insulator position**	**Direction**	**Preceded by**
2011/07/07 (Day 155)	4th sheath	South	Heavy pollution, dry band, crazing in pollution layer
2011/11/16 (Day 287)	1st shed bottom	East	Medium pollution, dry band, crazing in pollution layer, colour change, dead insect

No conclusions can be made regarding the prominent direction, axial position and insulator position of light erosion and erosion observations on the insulator. Furthermore, it is noted that the light erosion and erosion observations were preceded by dry band formation and crazing within the pollution layer activities. The erosion observation was on the 1st shed bottom and it was preceded, in addition, by colour change activities, which are also a sign of material degradation. The dry band and colour change observations are indicative that there were electrical discharge activities at the respective areas and this could be the cause of material erosion. Please refer to Figure 5-13 for photographs of light erosion and erosion observations on the AC_RTV insulator.

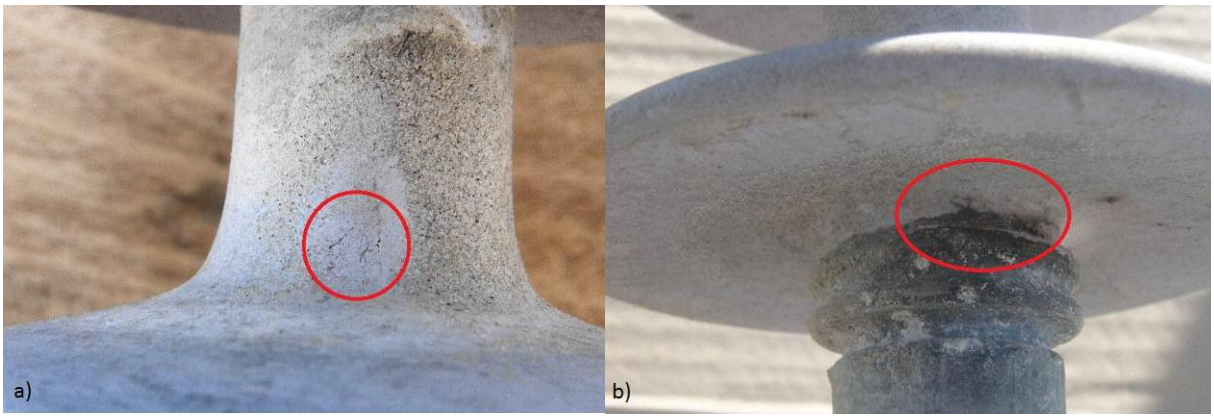

Figure 5-13: Light erosion (a) and erosion (b) observations on the AC_RTV insulator

5.3.1.1.4 AC_Porcelain insulator

No observation of light erosion or erosion was made on the AC_Porcelain insulator during the research period.

5.3.1.1.5 AC_Glass insulator

No observation of glass erosion was made on the AC_Glass insulator during the research period.

5.3.1.2 Insulators under DC+ excitation voltage

In this section, light erosion and erosion observations, as observed on the different insulators excited by DC+ voltage, will be discussed.

5.3.1.2.1 DC+_EPDM insulator

The DC+_EPDM insulator was installed and energised on 16 May 2011 and the first insulator surface inspection was done on 7 June 2011 and during this inspection, signs of light erosion were observed. The earliest erosion observation was made during the second inspection cycle on 3 August 2011. To interpret the information in Table 5-10, the following must be noted: sheath 1 is connected to the DC+ voltage source (bus bar) via a metal end fitting and sheath 9 is connected to the station earth via a metal end fitting.

The details of first occurrences of light erosion and erosion are summarized in Table 5-10, where the erosion observations were limited to the end fitting sealant. Furthermore, it is noted that the light erosion observations were more prominent on the mould lines, the middle axial section of the insulator and the east and west side of the insulator. It is also noted that most of the light erosion and erosion observations were preceded by light pollution and dry band formations. The dry band observations are indicative that there were electrical discharge activities at the respective areas and it could be the cause of material erosion. Please refer to Figure 5-14 and up to Figure 5-17 for photographs of light erosion and erosion observations on the DC+_EPDM insulator.

Table 5-10: First occurrences of light erosion and erosion on the DC+_EPDM insulator

First occurrences of light erosion and erosion on the DC+_EPDM insulator			
Date	**Insulator position**	**Direction**	**Preceded by**
2011/06/07 (Day 23)	Mould line of 2nd shed top	East	Light pollution, dry band
	Mould line of 3rd shed top	East	Light pollution, dry band
	Mould line of 4th shed top	East	Light pollution, dry band
	Mould line of 5th shed top	East	Light pollution, dry band
	Mould line of 6th shed top	East	Light pollution, dry band
	Mould line of 2dn shed top	West	Light pollution, dry band
	Mould line of 3rd shed top	West	Light pollution, dry band
	Mould line of 4th shed top	West	Light pollution, dry band
2011/08/03 (Day 80)	1st sheath, sealant	East	Light pollution, dry band
	Mould line of 5th sheath	East	Light pollution, dry band
	5th sheath	East	Light pollution, dry band
	5th shed top	East	Light pollution, dry band
	6th sheath	East	Light pollution, dry band
	7th shed top	East	Light pollution, dry band
	9th sheath, sealant	East	Light pollution, dry band
	1st sheath, sealant	West	Light pollution, dry band, rust layer
	Mould line of 1st sheath	West	Light pollution, dry band
	Mould line of 9th sheath	West	Light pollution, dry band
	9th sheath, sealant	West	Light pollution, dry band
	9th sheath, sealant	North	Light pollution, dry band
	9th sheath, sealant	South	Light pollution, dry band
2011/10/26 (Day 164)	Mould line of 2nd sheath	West	Light pollution, dry band
	7th sheath	West	Light pollution, dry band
	4th sheath	South	Light pollution, dry band
2012/02/08 (Day 269)	Mould line of 4th sheath	East	Light pollution, dry band
	Mould line of 7th sheath	East	Light pollution, dry band
	Mould line of 8th shed top	East	Light pollution, dry band
	Mould line of 3rd sheath	West	Light pollution, dry band
	Mould line of 4th sheath	West	Medium pollution, dry band
	Mould line of 5th sheath	West	Light pollution, dry band
	Mould line of 6th sheath	West	Light pollution, dry band
	Mould line of 4th shed bottom	West	Light pollution, dry band, salt crystals

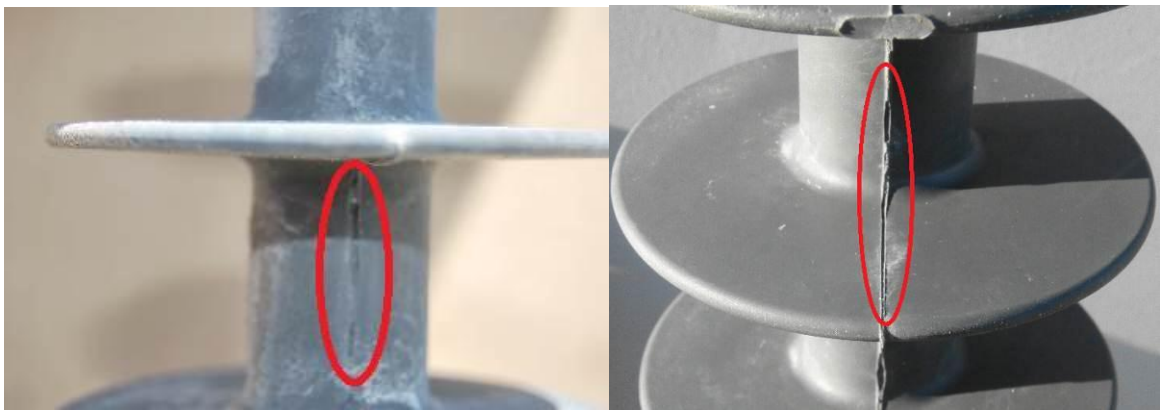

Figure 5-14: Light erosion observations on mould line of the DC+_EPDM insulator

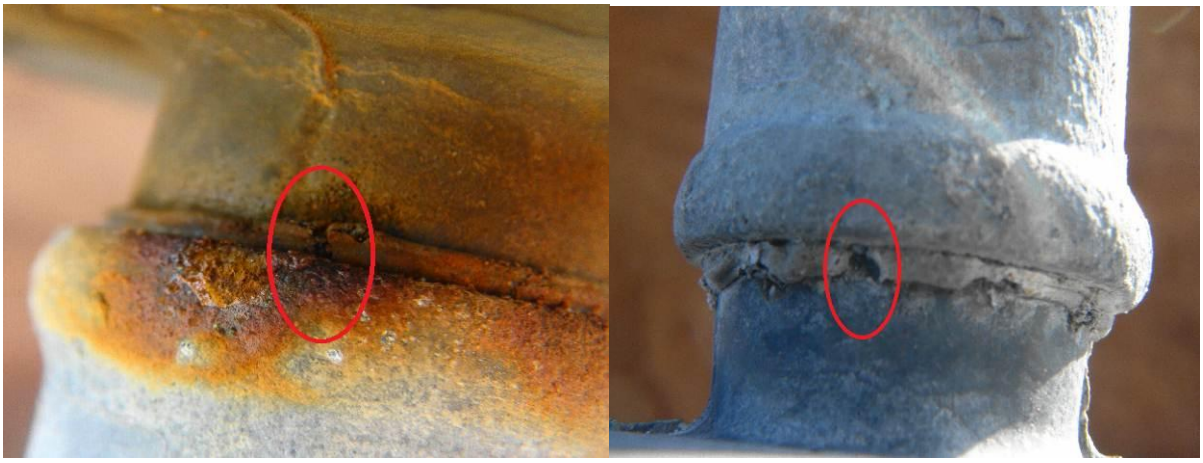

Figure 5-15: Erosion observations on sealant of the DC+_EPDM insulator

Figure 5-16: Light erosion observations on the sheaths of the DC+_EPDM insulator

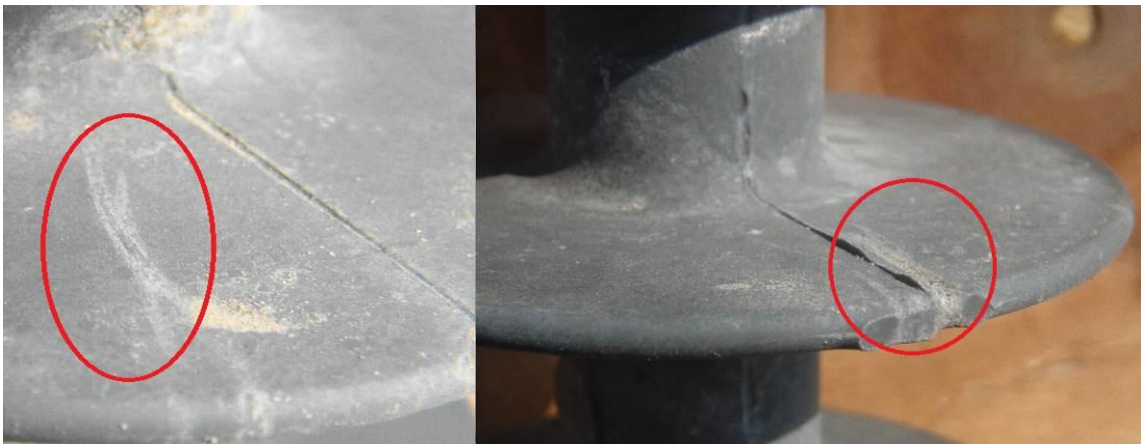

Figure 5-17: Light erosion observations on the shed tops of the DC+_EPDM insulator

5.3.1.2.2 DC+_HTV insulator

The DC+_HTV insulator was installed and energised on 16 May 2011 and the first insulator surface inspection was done on 7 June 2011. During this inspection no signs of light erosion or erosion were observed. The earliest light erosion observations were made during the second inspection cycle on 3 August 2011 and the earliest erosion observation was made during the third inspection cycle on 26 October 2011. To interpret the information in Table 5-11, the following must be noted: sheath 1 is connected to the DC+ voltage source (bus bar) via a metal end fitting and sheath 9 is connected to the station earth via a metal end fitting. The details of first occurrences of light erosion and erosion are summarized in Table 5-11, where the erosion observations were limited to the end fitting sealant.

Table 5-11: First occurrences of light erosion and erosion on the DC+_HTV insulator

First occurrences of light erosion and erosion on the DC+_HTV insulator			
Date	**Insulator position**	**Direction**	**Preceded by**
2011/08/03 (Day 80)	2nd sheath	West	Light pollution, dry band
2011/10/26 (Day 164)	1st sheath, sealant	West	Light pollution, dry band
	4th sheath	West	Light pollution, dry band
2012/02/08 (Day 269)	6th sheath	North	Light pollution, dry band, salt crystals, plant particle
	8th sheath	North	Light pollution, dry band

Furthermore, it is noted that the light erosion observations were more prominent on the sheath sections, the west side of the insulator and close to the live end fitting of the insulator. It is also noted that all of the light erosion and erosion observations were preceded by light

pollution and dry band formations. The dry band observations are indicative that there were electrical discharge activities at the respective areas and this could be the cause of material erosion. Please refer to Figure 5-18 for photographs of light erosion and erosion observations on the DC+_HTV insulator.

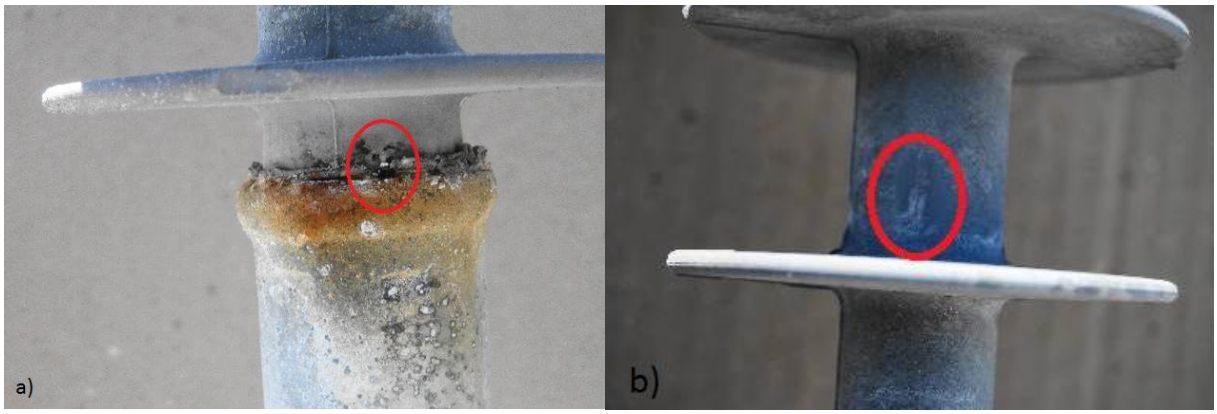

Figure 5-18: Observations of erosion on sealant (a) and light erosion on sheath (b) of the DC+_HTV insulator

5.3.1.2.3 DC+_RTV insulator

The DC+_RTV insulator was installed on 1 February 2011 and energised on 3 February 2011 and the first insulator surface inspection was done on 21 February 2011. During this inspection, no signs of light erosion or erosion were observed. The earliest light erosion observations were made during the fourth inspection cycle on 7 June 2011 and it evolved to erosion by the sixth inspection cycle on 26 October 2011. To interpret the information in Table 5-12, the following must be noted: the bottom of shed 1 is connected to the DC+ voltage source (bus bar) via a metal end fitting and the top of shed 6 is connected to the station earth via a metal end fitting. The details of first occurrences of light erosion and erosion are summarized in Table 5-12.

It is evident from Table 5-12 that the light erosion and erosion observations were more prominent on the sheath section, the south side of the insulator and close to the earthed side of the insulator. Furthermore, it is noted that most of the light erosion and erosion observations were preceded by medium pollution, dry band formation, crazing within the pollution layer and colour change activities. The colour change activities are also considered as a material degradation observation. Dry band and colour change observations are indicative that there were electrical discharge activities at the respective areas and this could be the cause of

material erosion. Please refer to Figure 5-19 and Figure 5-20 for photographs of erosion observations on the DC+_RTV insulator.

Table 5-12: First occurrences of light erosion and erosion on the DC+_RTV insulator

First occurrences of light erosion and erosion on the DC+_RTV insulator			
Date	**Insulator position**	**Direction**	**Preceded by**
2011/06/07 (Day 125)	4th sheath	West	Light pollution, dry band, colour change, crazing within pollution layer
	5th sheath	West	Light pollution, dry band, colour change, crazing within pollution layer
	2nd sheath	South	Light pollution, dry band, colour change, crazing within pollution layer
	3rd sheath	South	Light pollution, dry band, colour change, crazing within pollution layer
2011/08/03 (Day 182)	1st shed bottom	East	Light pollution, dry band, colour change, crazing within pollution layer
	5th sheath	North	Light pollution, dry band, colour change, crazing within pollution layer, salt crystals
	1st shed top	South	Light pollution, dry band, colour change, crazing within pollution layer
	5th sheath	South	Heavy pollution, dry band, colour change
2011/10/26 (Day 266)	1st shed bottom	South	Medium pollution, dry band, colour change, crazing within pollution layer, rust spots
	5th shed top	South	Medium pollution, dry band, colour change, crazing within pollution layer
	6th shed top	South	Medium pollution, dry band, colour change, crazing within pollution layer, rust spots, salt crystals
	6th shed bottom	South	Medium pollution, dry band, colour change, crazing within pollution layer, salt crystals
2012/02/08 (Day 371)	5th sheath	East	Medium pollution, dry band, colour change, crazing within pollution layer
	2nd shed top	South	Medium pollution, dry band, colour change, crazing within pollution layer

Figure 5-19: Erosion observations on shed top and shed bottom of the DC+_RTV insulator

Figure 5-20: Erosion observations on the sheaths of the DC+_RTV insulator

5.3.1.2.4 DC+_Porcelain insulator

No observation of light erosion or erosion was made on the DC+_Porcelain insulator, during the research period.

5.3.1.2.5 DC+_Glass insulator

The DC+_Glass insulator was installed on 1 February 2011 and energised on 3 February 2011 and the first insulator surface inspection was done on 21 February 2011. During this inspection, there were no signs of glass erosion observed. The earliest glass erosion observations were made during the second inspection cycle on 24 March 2011. The details of first occurrences of glass erosion are summarized in Table 5-13.

Table 5-13: First occurrences of glass erosion on the DC+_Glass insulator

First occurrences of glass erosion on the DC+_Glass insulator			
Date	**Insulator position**	**Direction**	**Preceded by**
2011/03/24 (Day 50)	Bottom	East	Light pollution, dry band
	Bottom	West	Light pollution, dry band
	Bottom	North	Light pollution, dry band
	Bottom	South	Light pollution, dry band
2011/06/07 (Day 125)	Top	West	Light pollution, dry band, salt crystals, plant particle, grease stain, dead insect

It is evident from Table 5-13 and Figure 5-22 that glass erosion observations were more prominent around the pin area on the bottom side of the insulator. As seen in Figure 5-22, there is no cement growth or swelling of the pin, which could have put a mechanical force on the glass disc leading to the formation of glass erosion. Thus, it may be assumed that the glass erosion was caused by electrical discharge activity, as indicated by the dry band formations on the glass disc preceding the glass erosion. It is also noted in Table 5-13 that the glass erosion observation on the top side of the glass insulator was preceded with a grease stain. This grease stain could have possibly come from the grease applied at the earth wire connection point on the cap, which preserves the connection point from corrosion. Please refer to Figure 5-21 and Figure 5-22 for photographs of glass erosion observations on the DC+_Glass insulator.

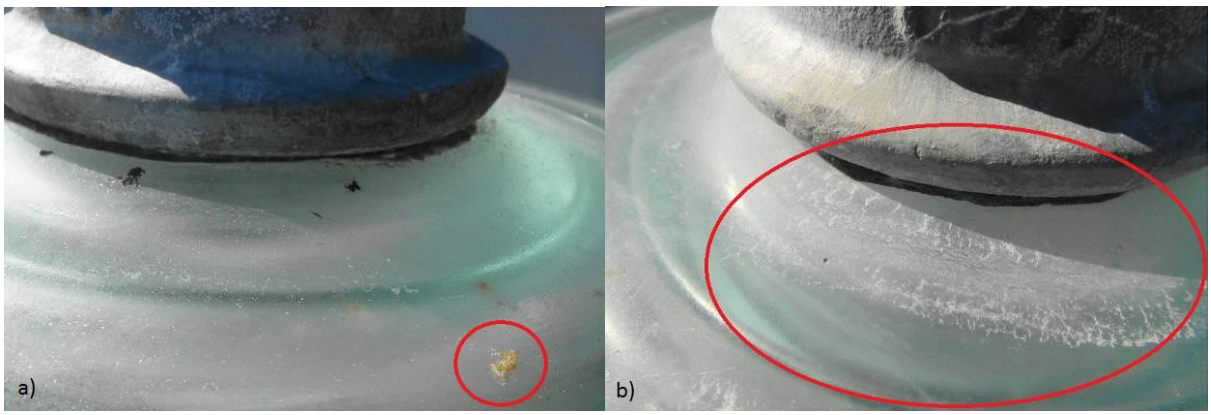

Figure 5-21: Grease stain (a) and glass erosion observations on shed top (b) of the DC+_Glass insulator

Figure 5-22: Glass erosion observations on the shed bottom of the DC+_Glass insulator

5.3.1.3 Insulators under DC- excitation voltage

In this section light erosion and erosion observations, as observed on the different insulators excited by DC- voltage, will be discussed.

5.3.1.3.1 DC-_EPDM insulator

The DC-_EPDM insulator was installed and energised on 16 May 2011 and the first insulator surface inspection was done on 19 May 2011, and during this inspection no signs of light erosion were observed. The earliest light erosion observation was made during the second inspection cycle on 26 July 2011 and the earliest sealant erosion observation was made during the same inspection cycle. To interpret the information in Table 5-14, the following must be noted: sheath 1 is connected to the DC- voltage source (bus bar) via a metal end fitting and sheath 9 is connected to the station earth via a metal end fitting. The details of first occurrences of light erosion and erosion are summarized in Table 5-14.

All the observations regarding the sealant as summarized in Table 5-14 are erosion observations. Furthermore, it is noted that the light erosion observations were more prominent on the mould line, the west and east side of the insulator and close to the live end fitting of the insulator. It is also noted that most of the light erosion and erosion observations were preceded by light pollution and dry band observations. The dry band formations are indicative that there were electrical discharge activities at the respective areas and this could be the cause of material erosion. Please refer to Figure 5-23 and Figure 5-24 for photographs of light erosion and erosion observations on the DC-_EPDM insulator.

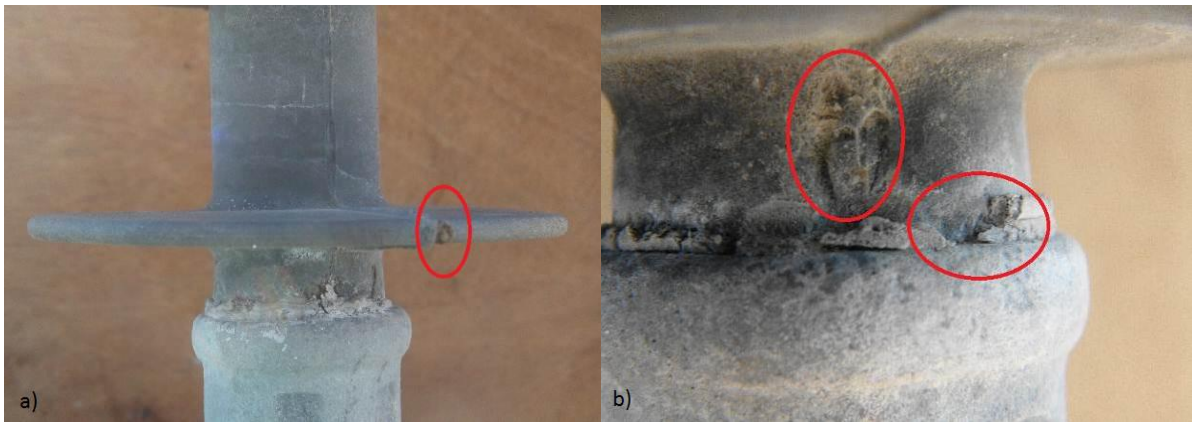

Figure 5-23: Observations of light erosion on shed rim (a) and erosion on sealant as well as light erosion on sheath (b) of the DC-_EPDM insulator

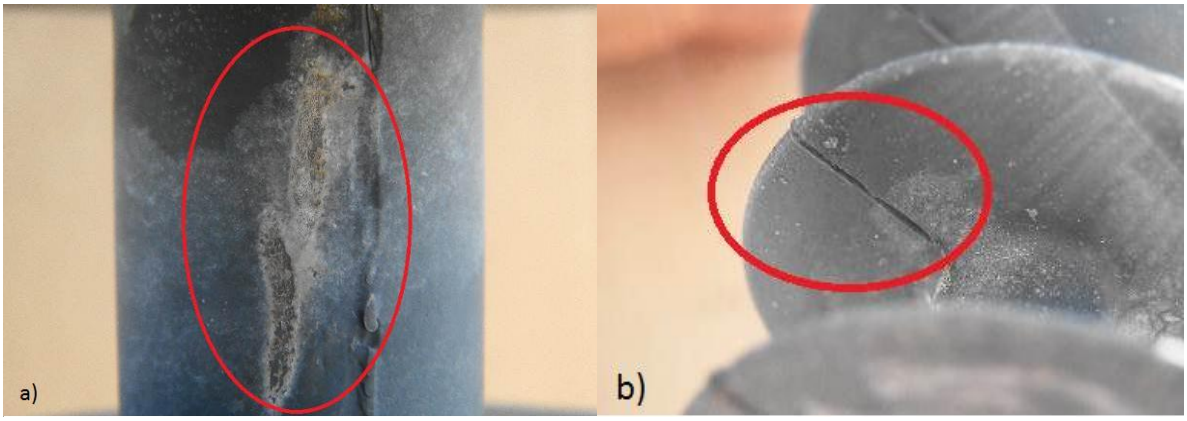

Figure 5-24: Observations of light erosion on sheath (a) and light erosion on mould line of shed bottom (b) of the DC-_EPDM insulator

Table 5-14: First instances of light erosion and erosion observed on the DC-_EPDM insulator

First instances of light erosion and erosion observed on the DC-_EPDM insulator			
Date	**Insulator position**	**Direction**	**Preceded by**
2011/07/26 (Day 72)	2nd sheath	East	Light pollution, dry band
	8th sheath	East	Light pollution, dry band
	1st sheath	West	Light pollution, dry band
	1st sheath sealant	West	Light pollution, dry band
	1st rim	West	Light pollution, dry band, salt crystals
	Mould line of 3rd sheath	West	Light pollution, dry band
	Mould line of 4th sheath	West	Light pollution, dry band
	Mould line of 5th sheath	West	Light pollution, dry band
	6th sheath	West	Light pollution, dry band
	Mould line of 7th sheath	West	Light pollution, light crazing, rust layer
	1st sheath	South	Light pollution, dry band
	1st sheath sealant	South	Light pollution, dry band
2011/09/05 (Day 113)	Mould line of 2nd sheath	East	Light pollution, dry band
	4th sheath	East	Light pollution, dry band, light crazing
	Mould line of 6th sheath	East	Light pollution, dry band
	Mould line of 6th shed top	East	Light pollution, dry band
	Mould line of 7th shed top	East	Light pollution, dry band
	Mould line of 2nd shed bottom	West	Light pollution, dry band, salt crystals
	Mould line of 5th shed bottom	West	Light pollution, dry band, salt crystals
	Mould line of 9th sheath	West	Light pollution, dry band, rust layer
	1st sheath sealant	North	Light pollution, dry band
2011/12/01 (Day 200)	3rd sheath	East	Light pollution, dry band
	Mould line on 3rd shed bottom	East	Light pollution, dry band
	Mould line on 4th shed top	East	Light pollution, dry band
	7th sheath	East	Light pollution, dry band
	Mould line on 3rd shed bottom	West	Light pollution, dry band, salt crystals
	Mould line on 4th shed bottom	West	Light pollution, dry band, salt crystals
	Mould line on 6th shed bottom	West	Light pollution, dry band, salt crystals
	Mould line on 8th sheath	West	Light pollution, dry band, rust layer
	6th sheath	South	Light pollution, dry band
2012/02/10 (Day 271)	1st rim	East	Light pollution, dry band, salt crystals
	3rd rim	East	Light pollution, dry band, salt crystals
	5th sheath	East	Light pollution, dry band
	Mould line on 7th shed bottom	West	Medium pollution, dry band, salt crystals

5.3.1.3.2 DC-_HTV insulator

The DC-_HTV insulator was installed and energised on 16 May 2011 and the first insulator surface inspection was done on 19 May 2011, and during this inspection no signs of light erosion were observed. The earliest light erosion observation was made during the third inspection cycle on 5 September 2011 and the earliest sealant erosion observation was made during the same inspection cycle. To interpret the information in Table 5-15, the following must be noted: sheath 1 is connected to the DC- voltage source (bus bar) via a metal end fitting and sheath 9 is connected to the station earth via a metal end fitting. The details of first occurrences of light erosion and erosion are summarized in Table 5-15.

Table 5-15: First instances of light erosion and erosion observed on the DC-_HTV insulator

First instances of light erosion and erosion observed on the DC-_HTV insulator			
Date	**Insulator position**	**Direction**	**Preceded by**
2011/09/05 (Day 113)	1st sheath, sealant	West	Light pollution, dry band, hair
	1st sheath, sealant	South	Light pollution, dry band
	Mould line of 2nd sheath	South	Light pollution, dry band
2011/12/01 (Day 200)	7th sheath	South	Medium pollution, dry band
	8th sheath	South	Medium pollution, dry band
2012/02/10 (Day 271)	1st sheath, sealant	North	Light pollution, dry band

From the above table it is noted that the light erosion observations are more prominent on the sheath sections, the south side of the insulator and close to the live end fitting of the insulator. It is also noted that most of the light erosion and erosion observations were preceded by light pollution and dry band formation observations. The dry band formations are indicative that there were electrical discharge activities at the respective areas and this could be the cause of material erosion. Please refer to Figure 5-25 and Figure 5-26 for photographs of light erosion and erosion observations on DC-_HTV insulator.

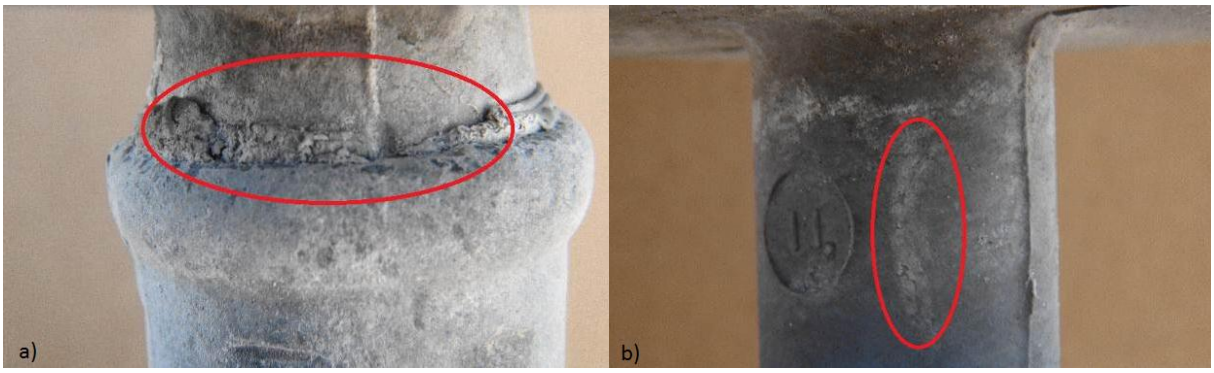

Figure 5-25: Observations of erosion on sealant (a) and light erosion on sheath (b) on the DC-_HTV insulator

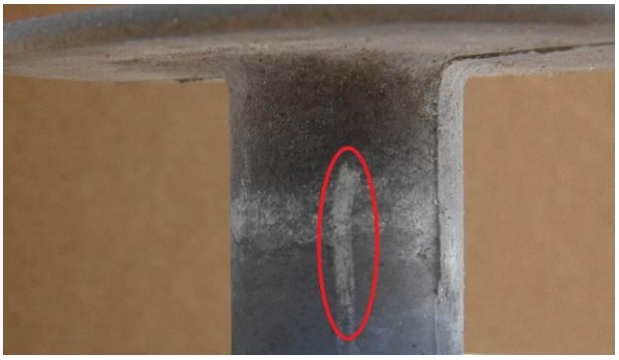

Figure 5-26: Light erosion observation on sheath on the DC-_HTV insulator

5.3.1.3.3 DC-_RTV insulator

The DC-_RTV insulator was installed on 1 February 2011 and energised on 3 February 2011 and the first insulator surface inspection was done on 12 February 2011. During this inspection, no signs of light erosion or erosion were observed. The earliest light erosion and erosion observations were made during the fourth inspection cycle on 19 May 2011. To interpret the information in Table 5-16, the following must be noted: the bottom of shed 1 is connected to the DC- voltage source (bus bar) via a metal end fitting and the top of shed 6 is connected to the station earth via a metal end fitting. The details of first occurrences of light erosion and erosion are summarized in Table 5-16.

Table 5-16: First instances of light erosion and erosion observed on the DC-_RTV insulator

First instances of light erosion and erosion observed on the DC-_RTV insulator			
Date	**Insulator position**	**Direction**	**Preceded by**
2011/05/19 (Day 106)	1st shed bottom	East	Light pollution, dry band, light crazing, colour change
	1st shed bottom	West	Light pollution, dry band, light crazing, colour change, dead insect
	1st sheath	South	Heavy pollution, colour change
	1st shed bottom	South	Heavy pollution, colour change, dry band, light crazing
2011/07/26 (Day 174)	1st sheath	North	Light pollution, dry band, light crazing, colour change
	3rd shed top	North	Light pollution, light crazing, colour change
2011/09/05 (Day 215)	4th sheath	East	Light pollution, dry band, light crazing, colour change
	1st shed top	West	Light pollution, dry band, light crazing, colour change, dead insect
	2nd sheath	South	Heavy pollution, dry band, light crazing, colour change, plant particle
2011/12/01 (Day 302)	3rd shed top	South	Heavy pollution, dry band, light crazing, colour change

From the observations listed in Table 5-16, the observation on shed 1 bottom, which was observed on 19 May 2011, and the observation on shed top 3, which was observed on 1 December 2011, are erosion observations. The other observations are light erosion observations, which are more prominent on the sheath sections of the insulator. Furthermore, the light erosion and erosion observations are more prominent on the south side of the insulator and close to the live end fitting of the insulator. It is also noted that most of the light erosion and erosion observations were preceded by light pollution, dry band formation, crazing within the pollution layer and colour change observations. A colour change activity in itself is also a sign of material degradation. The dry band and colour change observations are indicative that there were electrical discharge activities at the respective areas and this could be the cause of material erosion. Please refer to Figure 5-27 and Figure 5-28 for photographs of light erosion and erosion observations on the DC-_RTV insulator.

Figure 5-27: Erosion observations on the DC-_RTV insulator

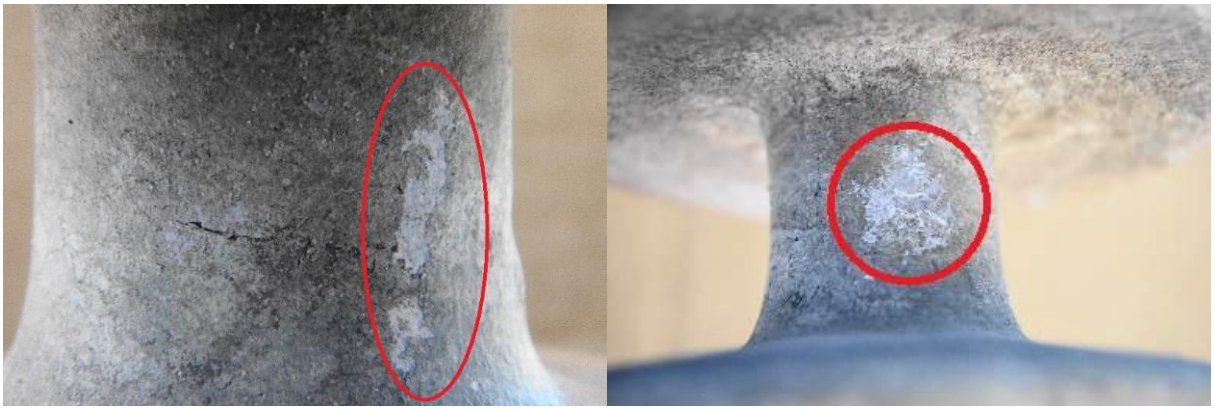

Figure 5-28: Light erosion observations on the DC-_RTV insulator

5.3.1.3.4 DC-_Porcelain insulator

The DC-_Porcelain insulator was installed on 1 February 2011 and energised on 3 February 2011 and the first insulator surface inspection was done on 12 February 2011. During this inspection, no signs of light erosion were observed. The earliest light erosion observation was made during the sixth inspection cycle on 6 September 2011. The detail of the first and only light erosion observation is summarized in Table 5-17. To interpret the information in Table 5-17, the following must be noted: the bottom of shed 1 is connected to the DC- voltage source (bus bar) via a metal end fitting and the top of shed 6 is connected to the station earth via a metal end fitting.

Table 5-17: First instance of light erosion observation on the DC-_Porcelain insulator

First instance of light erosion observation on the DC-_Porcelain insulator			
Date	**Insulator position**	**Direction**	**Preceded by**
2011/09/06 (Day 216)	1st sheath	South	Medium pollution, dry band, salt crystals

As seen in Table 5-17, the light erosion occurred on the sheath section, south direction and it was preceded by medium pollution, dry band and salt crystal observations. The light erosion was observed close to the live end fitting of the insulator. The dry band formation is indicative that there were electrical discharge activities present at the respective area and this could be the cause of material erosion. Please refer to Figure 5-27 for a photograph of the light erosion observation on the DC-_Porcelain insulator.

Figure 5-29: Light erosion observation on the DC-_Porcelain insulator

5.3.1.3.5 DC-_Glass insulator

The DC-_Glass insulator was installed on 1 February 2011 and energised on 3 February 2011 and the first insulator surface inspection was done on 12 February 2011. During this inspection there were signs of glass erosion observed. The details of first occurrences of glass erosion are summarized in Table 5-18.

Table 5-18: First instances of glass erosion observed on the DC-_Glass insulator

First instances of glass erosion observed on the DC-_Glass insulator			
Date	**Insulator position**	**Direction**	**Preceded by**
2011/02/12 (Day 10)	Bottom	South	Light pollution
2011/03/11 (Day 37)	Bottom	East	Light pollution, dry band
	Bottom	West	Light pollution, dry band
	Bottom	North	Light pollution, dry band

It is evident from Table 5-18 and Figure 5-30 that glass erosion observations were more prominent around the pin area on the bottom side of the insulator. As seen in Figure 5-30, there was no cement growth or swelling of the pin, which could have put a mechanical force on the glass disc leading to the glass erosion forming. Thus, it may be assumed that the glass erosion was caused by electrical discharge activity, as indicated by the dry band formations on the glass disc preceding the glass erosion observation. Please refer to Figure 5-30 for a photograph of glass erosion observation on the DC-_Glass insulator.

Figure 5-30: Glass erosion observation on the DC-_Glass insulator

5.3.1.4 Summary of light erosion and erosion observations

Table 5-19 was constructed from the above information to summarize the prominent areas of light erosion observations on all the insulators to determine if a pattern of prominence exists.

Table 5-19: Summary of all the prominent light erosion areas on the respective insulators

Insulator	AC	DC+	DC-
EPDM	Mould line, east, earthed section	Mould line, east and west, middle section	Mould line, west and east, live section
HTV	Sheath	Sheath, west, live section	Sheath, south, live section
RTV	No prominence	Sheath, south, earthed section	Sheath, south, live section
Porcelain	No observation	No observation	Sheath, south, live section
Glass	No observation	Around pin area, live section	Around pin area, live section

It is evident from Table 5-19 that the north side is the only direction without a prominent light erosion observation status and the south direction has the most prominent observations. This

can be explained by the sand pollution build-up on the south side of the insulators, caused by the dominant south-east wind as mentioned in section 5.2.1 and the sand dunes located to the south of KIPTS. It is expected that the sand has a high concentration of soluble salts, because it is located close to the sea and receptive to sea spray. Thus, the sand pollution build-up on the south side of the insulator may increase the moisture absorption from the air which may cause to the flow of leakage currents, dry band formations and electrical discharge activity, which may lead to surface erosion.

It is also observed that only the DC- excitation voltage has a dominant axial area of light erosion prominence, namely, close to the live end fitting, whereas the other excitation voltages have no dominant axial area of prominence. The DC- excitation voltage light erosion prominence close to the live end fitting is expected, because the electric field stresses are the strongest close to the live end fitting in a point-to-plain model, where the live end fitting is considered the point and the earthed end fitting the plain. The only explanation for the light erosion activity behaviour of the other excitation voltages, in terms of axial prominence, is that the voltage distribution and electric field stresses occur anywhere on the axial length of an insulator, when the insulator surface becomes polluted, as explained by W. Vosloo in his PhD thesis [12]. Another observation from Table 5-19 is that the light erosion positions on the insulator surfaces remain constant, irrespective of the excitation voltages applied on the insulators, i.e. for the EPDM insulators it remains on the mould line, for the HTV and RTV insulators on the sheath section and for the glass insulators around the pin area. This is an indication that the mould line on the EPDM insulator is more sensitive to material erosion caused by electrical discharge activity, because of material in-homogeneity at the mould line. Furthermore, it indicates that the HTV and RTV insulators have their highest leakage current density on the sheath sections as expected and the Glass insulators have their highest leakage current density close to the pin area. As mentioned in section 2.4.3, the area with the highest leakage current density generates dry band formations, which lead to electrical discharge activity, which causes erosion on the insulator surfaces.

In this section, the normalized totals of light erosion and erosion observations per position per insulator are also compared with each other, in order to determine which insulator per excitation voltage performed better. Furthermore, the effects of the different excitation voltages per insulator material are also compared in terms of light erosion and erosion observations. The insulator with the lesser amount of light erosion and erosion observations

is considered as the better performer. Due to the different installation dates, the EPDM and HTV insulators are compared with each other and the RTV, Porcelain and Glass insulators are compared with each other. Please refer to Table 5-20 for a comparison between EPDM and HTV insulators.

Table 5-20: Summary of light erosion and erosion observations of EPDM and HTV insulators

Summary of normalized totals of light erosion and erosion observations							
Direction	Insulator position	EPDM insulators			HTV insulators		
		AC [%]	DC+ [%]	DC- [%]	AC [%]	DC+ [%]	DC- [%]
East	Sheath	11	44	67	0	0	0
	Shed top	0	25	0	0	0	0
	Shed bottom	0	0	0	0	0	0
	Rim	0	0	25	0	0	0
	Mould line sheath	22	33	22	0	0	0
	Mould line shed top	0	75	38	0	0	0
	Mould line shed bottom	25	0	13	0	0	0
West	Sheath	0	33	22	0	33	11
	Shed top	0	0	0	0	0	0
	Shed bottom	0	0	0	0	0	0
	Rim	0	0	13	0	0	0
	Mould line sheath	0	78	67	0	0	0
	Mould line shed top	13	38	0	0	0	0
	Mould line shed bottom	13	13	75	0	0	0
North	Sheath	0	11	11	0	22	11
	Shed top	0	0	0	0	0	0
	Shed bottom	0	0	0	0	0	0
	Rim	0	0	0	0	0	0
	Mould line sheath	0	0	0	0	0	0
	Mould line shed top	0	0	0	0	0	0
	Mould line shed bottom	0	0	0	0	0	0
South	Sheath	0	22	22	11	0	33
	Shed top	0	0	0	0	0	0
	Shed bottom	0	0	0	0	0	0
	Rim	0	0	0	0	0	0
	Mould line sheath	0	0	0	0	0	11
	Mould line shed top	0	0	0	0	0	0
	Mould line shed bottom	0	0	0	0	0	0
	Average [%]	2.98	13.29	13.34	0.40	1.98	2.38

From Table 5-20, it is evident that the HTV insulators performed much better than the EPDM insulators under all three excitation voltages. Furthermore, it is observed that the AC excitation voltage performed best and the DC- excitation voltage performed worst for both EPDM and HTV insulators. However, it should be noted that the averaged, normalized light

erosion and erosion observation totals, differ slightly between DC+ and DC- excitation voltages for both EPDM and HTV insulators, as observed in Table 5-20.

Please refer to Table 5-21 for a comparison between RTV, Porcelain and Glass insulators, where it is evident that the Porcelain insulators performed better than the RTV and Glass insulators under all three excitation voltages. The Glass insulators performed worst under both DC excitation voltages and the RTV insulator performed worst under the AC excitation voltage. Furthermore, it is observed that the AC excitation voltage performed best for all the insulators and the DC+ excitation voltage performed worst for RTV and Glass insulators, whereas DC- excitation voltage performed worst for Porcelain insulators.

Table 5-21: Summary of light erosion and erosion observations of RTV, Porcelain and Glass insulators

Summary of normalized totals of light erosion and erosion observations										
Direction	**Insulator position**	**RTV**			**Porcelain**			**Glass**		
		AC [%]	**DC+ [%]**	**DC- [%]**	**AC [%]**	**DC+ [%]**	**DC- [%]**	**AC [%]**	**DC+ [%]**	**DC- [%]**
East	Sheath	0	20	20	0	0	0	0	0	0
	Shed top	0	0	0	0	0	0	0	0	0
	Shed bottom	17	17	17	0	0	0	0	100	100
	Rim	0	0	0	0	0	0	0	0	0
West	Sheath	0	40	0	0	0	0	0	0	0
	Shed top	0	0	17	0	0	0	0	100	0
	Shed bottom	0	0	17	0	0	0	0	100	100
	Rim	0	0	0	0	0	0	0	0	0
North	Sheath	0	20	20	0	0	0	0	0	0
	Shed top	0	0	17	0	0	0	0	0	0
	Shed bottom	0	0	0	0	0	0	0	100	100
	Rim	0	0	0	0	0	0	0	0	0
South	Sheath	20	60	40	0	0	20	0	0	0
	Shed top	0	67	17	0	0	0	0	0	0
	Shed bottom	0	33	17	0	0	0	0	100	100
	Rim	0	0	0	0	0	0	0	0	0
	Average [%]	2.29	16.04	11.25	0.00	0.00	1.25	0.00	62.50	50.00

5.3.2 Minor splitting or cutting

Only one minor splitting or cutting observation was recorded over the research period. Please refer to Table 5-22 for details regarding this observation and to Figure 5-31 for a photograph of it.

Table 5-22: Summary of first appearances of minor splitting or cutting observations

First appearance of minor cutting observations on the test insulators				
Insulator	**Date**	**Position**	**Direction**	**Preceded by**
AC_EPDM	2011/07/06 (Day 52)	Corner of 6th sheath and 6th shed bottom	North	Light pollution, dry band, salt crystals

Figure 5-31: Minor split or cut on AC_EPDM insulator

This observation was made during the first inspection cycle on 6 July 2011, which makes it difficult to pin point the exact date when the split or cut appeared, if it is considered that the insulator was installed and energized on 16 May 2011. The size of the minor split or cut did not grow since the day it had been observed and as discussed in section 5.3.1.4 above, the AC_EPDM insulator performed better than the DC+_EPDM and DC-_EPDM insulators in terms of light erosion and erosion observations, however no minor split or cut was observed on their surfaces. Thus, it is difficult to conclude that the minor split or cut was caused by

electrical discharge activity. A manufacturing defect is suspected as a possible cause for the creation of the minor split or cut.

5.3.3 Colour changes on insulator surfaces

Colour changes were only observed on the RTV insulators and in this section a detailed description of colour change observations per insulator will be given and at the end of this section, the insulators will be compared in order to determine which of the insulator were mostly affected by colour changes. The comparison was done in terms of the number of colour change observations per insulator, because detail measurements of the colour change observations on the insulator surfaces were not possible.

5.3.3.1 AC_RTV insulator

Signs of insulator surface colour changes were observed from the onset of the first inspection cycle. The details of first occurrences of insulator surface colour change observations are summarized in Table 5-23.

From Table 5-23, it is evident that there is no trend regarding axial position prominence on the insulator. It is also noted that most of the colour change observations were preceded by light pollution and crazing within the pollution layer observations. The dry band formation observations were not as prominent as with the light erosion and erosion observations. It is also noted that the greater majority of the observations were captured during the first two inspection cycles. Please refer to Figure 5-32 for a photograph of colour change observations on the AC_RTV insulator.

Table 5-23: First instances of colour change observations on the AC_RTV insulator

First instances of colour change observations on the AC_RTV insulator			
Date	**Insulator position**	**Direction**	**Preceded by**
2011/03/03 (Day 29)	2nd sheath	East	Light pollution
	2nd shed bottom	East	Medium pollution
	4th sheath	East	Light pollution
	5th sheath	East	Medium pollution
	5th shed bottom	East	Medium pollution
	6th shed bottom	East	Medium pollution
	2nd sheath	West	Light pollution, dry band, crazing in pollution layer
	4th sheath	West	Light pollution, crazing in pollution layer
	4th shed bottom	West	Medium pollution
	5th sheath	West	Light pollution, crazing in pollution layer
	6th shed bottom	West	Medium pollution
	2nd sheath	North	Light pollution, dry band, crazing in pollution layer
	2nd shed top	North	Light pollution, dry band, crazing in pollution layer
	2nd shed bottom	North	Light pollution, dry band
	4th sheath	North	Light pollution, crazing in pollution layer
	4th shed top	North	Light pollution
	4th shed bottom	North	Light pollution
	5th sheath	North	Light pollution, crazing in pollution layer
	5th shed bottom	North	Light pollution
	2nd shed bottom	South	Medium pollution, dry band
	4th shed bottom	South	Medium pollution, dry band
	5th shed bottom	South	Medium pollution, dry band
2011/04/05 (Day 62)	1st sheath	East	Light pollution
	1st shed bottom	East	Light pollution, salt crystals, crazing in pollution layer
	3rd sheath	East	Light pollution, plant particle
	6 shed top	East	Medium pollution, plant particle
	1st sheath	West	Light pollution, crazing in pollution layer
	1st shed top	West	Light pollution, dry band, crazing in pollution layer
	2nd shed bottom	West	Medium pollution, crazing in pollution layer
	4th shed top	West	Light pollution, dry band, crazing in pollution layer
	5th shed top	West	Light pollution, crazing in pollution layer, dead insect
	5th shed bottom	West	Medium pollution
	6th shed top	West	Medium pollution, dry band, crazing in pollution layer
	6th shed bottom	West	Medium pollution, dry band, crazing in pollution layer
	1st shed top	North	Light pollution
	1st shed bottom	North	Light pollution, dry band, salt crystals
	3rd sheath	North	Light pollution, crazing in pollution layer
	6th shed top	North	Light pollution
	6th shed bottom	North	Medium pollution, crazing in pollution layer
	1st sheath	South	Heavy pollution, dry band, crazing in pollution layer
	1st shed bottom	South	Medium pollution, dry band, salt crystals
	4th shed top	South	Medium pollution, crazing in pollution layer
	5th sheath	South	Heavy pollution, crazing in pollution layer
	6th shed top	South	Medium pollution, dry band, crazing in pollution layer

Table 5-23 continued…

First instances of colour change observations on the AC_RTV insulator			
Date	**Insulator position**	**Direction**	**Preceded by**
2011/05/04 (Day 91)	4th shed top	East	Light pollution, dry band
	4th shed bottom	East	Medium pollution, crazing in pollution layer
	1st shed bottom	West	Medium pollution, dry band, crazing in pollution layer, salt crystals
	6th shed bottom	South	Medium pollution, dry band, crazing in pollution layer
2011/07/07 (Day 155)	1st shed top	East	Light pollution, dry band, crazing in pollution layer
	3rd shed top	East	Light pollution, crazing in pollution layer
	3rd shed bottom	East	Medium pollution, crazing in pollution layer
	3rd shed top	West	Light pollution, crazing in pollution layer
	1st sheath	North	Light pollution, dry band, crazing in pollution layer
	3rd shed top	North	Light pollution, crazing in pollution layer
	3rd shed bottom	North	Light pollution, crazing in pollution layer
	1st shed top	South	Medium pollution, dry band, crazing in pollution layer
	2nd sheath	South	Heavy pollution, dry band, crazing in pollution layer
	3rd shed bottom	South	Medium pollution, crazing in pollution layer
2011/08/25 (Day 204)	5th shed top	North	Light pollution, crazing in pollution layer
2011/11/16 (Day 287)	4th sheath	South	Heavy pollution, dry band, crazing in pollution layer, material erosion
2012/02/08 (Day 371)	3rd shed bottom	West	Medium pollution, crazing in pollution layer, salt crystals, plant particle

Figure 5-32: Colour change observation on the AC_RTV insulator

5.3.3.2 DC+_RTV insulator

Signs of insulator surface colour changes were observed from the onset of the second inspection cycle. The details of first occurrences of insulator surface colour change observations are summarized in Table 5-24.

Table 5-24: First instances of colour change observations on the DC+_RTV insulator

First instances of colour change observations on the DC+_RTV insulator			
Date	**Insulator position**	**Direction**	**Preceded by**
2011/03/24 (Day 50)	2nd sheath	East	Light pollution, crazing within pollution layer
	3rd sheath	East	Light pollution, crazing within pollution layer
	4th sheath	East	Light pollution, crazing within pollution layer
	5th sheath	East	Light pollution, dry band, crazing within pollution layer
	5th shed bottom	East	Medium pollution, crazing within pollution layer, salt crystals
	6th shed top	East	Light pollution, dry band, crazing within pollution layer
	6th shed bottom	East	Medium pollution, dry band, crazing within pollution layer
	1st sheath	West	Light pollution, dry band, crazing within pollution layer
	1st shed top	West	Light pollution, crazing within pollution layer, salt crystals
	1st shed bottom	West	Light pollution, crazing within pollution layer, salt crystals
	2nd sheath	West	Light pollution, dry band, crazing within pollution layer, salt crystals
	2nd shed top	West	Light pollution, dry band, crazing within pollution layer, salt crystals
	3rd sheath	West	Light pollution, dry band, crazing within pollution layer
	3rd shed top	West	Light pollution, dry band, crazing within pollution layer, salt crystals
	4th sheath	West	Light pollution, dry band, crazing within pollution layer
	4th shed top	West	Medium pollution, crazing within pollution layer
	5th sheath	West	Light pollution, dry band, crazing within pollution layer
	6th shed bottom	West	Light pollution, dry band, crazing within pollution layer, salt crystals
	1st sheath	North	Light pollution, dry band, crazing within pollution layer
	1st shed top	North	Light pollution, crazing within pollution layer, salt crystals
	1st shed bottom	North	Light pollution, crazing within pollution layer, salt crystals
	2nd sheath	North	Light pollution, crazing within pollution layer
	2nd shed bottom	North	Light pollution, dry band, crazing within pollution layer
	3rd sheath	North	Light pollution, dry band, crazing within pollution layer
	4th sheath	North	Light pollution, dry band, crazing within pollution layer, salt crystals
	4th shed bottom	North	Light pollution, dry band, crazing within pollution layer, salt crystals
	5th sheath	North	Light pollution, dry band, crazing within pollution layer, salt crystals
	6th shed top	North	Light pollution, dry band, crazing within pollution layer, salt crystals, rust spot
	6th shed bottom	North	Light pollution, dry band, crazing within pollution layer, salt crystals
	1st sheath	South	Heavy pollution, dry band, crazing within pollution layer
	1st shed top	South	Medium pollution, crazing within pollution layer, salt crystals
	2nd sheath	South	Heavy pollution, crazing within pollution layer
	2nd shed top	South	Medium pollution, dry band, crazing within pollution layer
	3rd sheath	South	Heavy pollution, dry band, crazing within pollution layer
	4th sheath	South	Heavy pollution, dry band, crazing within pollution layer
	4th shed top	South	Medium pollution, dry band, crazing within pollution layer
	4th shed bottom	South	Medium pollution, dry band, crazing within pollution layer, salt crystals
	5th sheath	South	Heavy pollution, dry band
	6th shed bottom	South	Medium pollution, crazing within pollution layer, salt crystals

Table 5-24 continued…

First instances of colour change observations on the DC+_RTV insulator			
Date	**Insulator position**	**Direction**	**Preceded by**
2011/04/19 (Day 76)	1st shed top	East	Medium pollution, dry band, crazing within pollution layer, salt crystals, dead insect
	1st shed bottom	East	Light pollution, dry band, crazing within pollution layer, rust spot
	3rd shed bottom	East	Medium pollution, crazing within pollution layer, salt crystals, plant particle
	3rd shed bottom	West	Medium pollution, dry band, crazing within pollution layer
	3rd shed top	North	Light pollution, dry band, crazing within pollution layer, plant particle
	3rd shed bottom	North	Light pollution, crazing within pollution layer, salt crystals
	2nd shed bottom	South	Medium pollution, dry band, crazing within pollution layer
2011/06/07 (Day 125)	3rd shed top	East	Light pollution, crazing within pollution layer
	2nd shed bottom	West	Medium pollution, dry band, crazing within pollution layer, salt crystals
	6th shed top	West	Light pollution, dry band, crazing within pollution layer, salt crystals, rust spots
	2nd shed top	North	Light pollution, crazing within pollution layer, salt crystals, material defect
	1st shed bottom	South	Medium pollution, dry band, crazing within pollution layer, rust spots
	5th shed bottom	South	Medium pollution, dry band, crazing within pollution layer, salt crystals
2011/08/03 (Day 182)	1st sheath	East	Light pollution, dry band, crazing within pollution layer
	3rd shed top	South	Medium pollution, dry band, crazing within pollution layer
	5th shed top	South	Medium pollution, dry band, crazing within pollution layer
2011/10/26 (Day 266)	4th shed bottom	West	Medium pollution, dry band, crazing within pollution layer, salt crystals
	5th shed top	West	Light pollution, dry band, crazing within pollution layer, material erosion, grease stain
	5th shed bottom	West	Medium pollution, dry band, crazing within pollution layer
	5th shed bottom	North	Light pollution, dry band, crazing within pollution layer, salt crystals
	3rd shed bottom	South	Medium pollution, dry band, crazing within pollution layer, plant particle
	6th shed top	South	Medium pollution, dry band, crazing within pollution layer, material erosion, salt crystals, rust spots
2012/02/08 (Day 371)	5th shed top	East	Medium pollution, crazing within pollution layer, salt crystals
	4th shed top	North	Light pollution, crazing within pollution layer, salt crystals

From Table 5-24, it is evident that the colour change observations were more prominent close to the live end fitting of the insulator. It is also noted that most of the colour change observations were preceded by light pollution and crazing within the pollution layer observations. The dry band formation observations were not as prominent as with the light erosion and erosion observations. It is also noted that most of the observations were captured during the second inspection cycle. Please refer to Figure 5-33 for a photograph of a colour change observation on the DC+_RTV insulator.

Figure 5-33: Colour change observation on the DC+_RTV insulator

5.3.3.3 DC-_RTV insulator

Signs of insulator surface colour changes were observed from the onset of the second inspection cycle. The details of first occurrences of insulator surface colour change observations are summarized in Table 5-25.

From Table 5-25, it is evident that the colour change observations were more prominent close to the live end fitting of the insulator. It is also noted that most of the colour change observations were preceded by light pollution and crazing within the pollution layer observations. The dry band formation observations were not as prominent as with the light erosion and erosion observations. It is also noted that most of the observations were captured during the second inspection cycle. Please refer to Figure 5-34 for a photograph of a colour change observation on the DC-_RTV insulator.

Table 5-25: First instances of colour change observations on the DC-_RTV insulator

First instances of colour change observations on the DC-_RTV insulators			
Date	**Insulator position**	**Direction**	**Preceded by**
2011/03/11 (Day 37)	1st sheath	East	Light pollution, crazing within pollution layer
	1st shed bottom	East	Light pollution, crazing within pollution layer
	2nd sheath	East	Light pollution
	2nd shed top	East	Light pollution
	3rd sheath	East	Light pollution, manufacturing defect
	3rd shed top	East	Light pollution, crazing within pollution layer
	4th sheath	East	Light pollution, crazing within pollution layer
	5th sheath	East	Light pollution, crazing within pollution layer
	6th shed bottom	East	Light pollution
	1st sheath	West	Light pollution, crazing within pollution layer
	1st shed bottom	West	Light pollution, crazing within pollution layer
	2nd shed top	West	Light pollution
	3rd sheath	West	Light pollution, manufacturing defect
	3rd shed top	West	Light pollution, crazing within pollution layer
	4th sheath	West	Light pollution, crazing within pollution layer, salt crystals
	5th sheath	West	Light pollution, crazing within pollution layer
	5th shed top	West	Light pollution, crazing within pollution layer
	6th shed bottom	West	Light pollution
	1st sheath	North	Light pollution, crazing within pollution layer
	1st shed bottom	North	Light pollution, crazing within pollution layer
	2nd shed top	North	Light pollution
	3rd sheath	North	Light pollution
	3rd shed top	North	Light pollution
	3rd shed bottom	North	Light pollution
	4th sheath	North	Light pollution, crazing within pollution layer
	5th sheath	North	Light pollution, crazing within pollution layer
	6th shed bottom	North	Light pollution
	1st sheath	South	Heavy pollution
	1st shed bottom	South	Heavy pollution, crazing within pollution layer
	2nd shed top	South	Heavy pollution
	3rd sheath	South	Heavy pollution, manufacturing defect
	3rd shed bottom	South	Heavy pollution
	4th sheath	South	Heavy pollution, crazing within pollution layer
	5th sheath	South	Heavy pollution, crazing within pollution layer
	5th shed top	South	Heavy pollution, crazing within pollution layer

Table 5-25 continued…

First instances of colour change observations on the DC-_RTV insulators			
Date	**Insulator position**	**Direction**	**Preceded by**
2011/04/13 (Day 70)	2nd shed bottom	East	Medium pollution
	6th shed top	East	Medium pollution, crazing within pollution layer, salt crystals, rust spots
	1st shed top	West	Light pollution, dry band, crazing within pollution layer, dead insect
	2nd sheath	West	Light pollution, dry band, crazing within pollution layer
	2nd shed bottom	West	Medium pollution, rust spots
	3rd shed bottom	West	Medium pollution
	1st shed top	North	Light pollution, dry band, crazing within pollution layer, plant particle
	2nd sheath	North	Light pollution, dry band, crazing within pollution layer
	2nd shed bottom	North	Medium pollution, salt crystals
	5th shed top	North	Light pollution, crazing within pollution layer
	2nd sheath	South	Heavy pollution, dry band, plant particle
2011/05/19 (Day 106)	1st shed top	East	Light pollution, crazing within pollution layer
	5th shed bottom	North	Light pollution, crazing within pollution layer, plant particle
	1st shed top	South	Heavy pollution, dry band, crazing within pollution layer, dead insect
	5th shed bottom	South	Heavy pollution, plant particle
2011/07/26 (Day 174)	3rd shed bottom	East	Medium pollution
	4th shed bottom	East	Medium pollution, crazing within pollution layer
	5th shed top	East	Light pollution, crazing within pollution layer
	5th shed bottom	East	Light pollution
	4th shed bottom	West	Medium pollution, plant particle
	5th shed bottom	West	Medium pollution, crazing within pollution layer, plant particle
	4th shed bottom	North	Medium pollution, crazing within pollution layer
	3rd shed top	South	Heavy pollution, crazing within pollution layer
2011/09/05 (Day 215)	2nd shed bottom	South	Heavy pollution, crazing within pollution layer
	4th shed bottom	South	Heavy pollution, crazing within pollution layer, plant particle
2011/12/01 (Day 302)	4th shed top	North	Light pollution, crazing within pollution layer
2012/02/13 (Day 376)	4th shed top	East	Light pollution, crazing within pollution layer
	6th shed top	West	Medium pollution, crazing within pollution layer, rust layer
	4th shed top	South	Heavy pollution, dry band, crazing within pollution layer, rust layer
	6th shed bottom	South	Heavy pollution, dry band, crazing within pollution layer, dead insect, rust layer

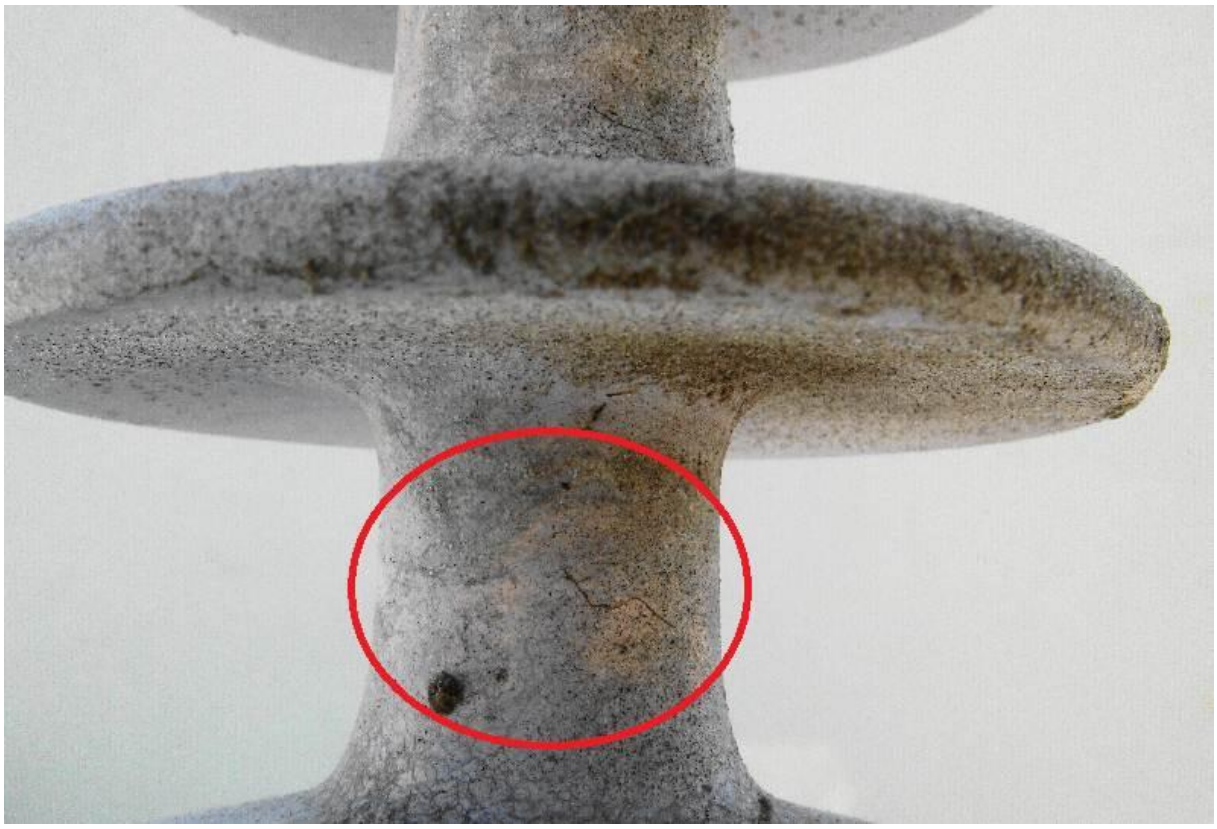

Figure 5-34: Colour change observation on the DC-_RTV insulator

5.3.3.4 Summary of colour change observations

In this section, the normalized totals of colour change observations per position on the RTV insulators, are compared with each other to determine which excitation voltage performed better. The insulator with the least number of colour change observations is considered to be the best performer. Please refer to Table 5-26 for a comparison between RTV insulators under the different excitation voltages.

It is evident from Table 5-26 that the AC excitation voltage performed best and the DC- excitation voltage performed worst, which is in contrast with the light erosion and erosion observations where the DC+ excitation voltage performed worst as mentioned in section 5.3.1.4. Table 5-27 was compiled from Table 5-26 and the discussions above for further comparisons.

Table 5-26: Summary of normalized totals of colour change observations

Summary of normalized totals of colour change observations				
Direction	**Insulator position**	**RTV**		
		AC [%]	**DC+ [%]**	**DC- [%]**
East	Sheath	100	100	100
	Shed top	67	67	100
	Shed bottom	100	67	100
West	Sheath	100	100	100
	Shed top	83	100	83
	Shed bottom	100	100	100
North	Sheath	100	100	100
	Shed top	100	83	83
	Shed bottom	100	100	100
South	Sheath	80	100	100
	Shed top	50	100	83
	Shed bottom	100	100	100
	Average [%]	90.00	93.06	95.83

Table 5-27: Summary of the prominent colour change areas on the respective insulators

Insulator	AC	DC+	DC-
RTV	Shed bottom, north, no prominent axial position	Sheath, west and south, live section	Sheath and shed bottom, east, live section

From Table 5-27 it is evident that there is no prominent direction of colour change observations for the different insulators. The common observations from Table 5-27 are:

- The shed top positions have no prominent colour change observations.
- The DC excitation voltages have prominent areas close to the live metal end fittings of the insulators.

5.3.4 Chipped glazing observations on porcelain insulators

In this section, a detailed description of the chipped glazing observations per porcelain insulator will be given and at the end of this section, the insulators will be compared in order to determine which insulator was worst affected by it. The comparison was done in terms of the number of observations per insulator, because detailed measurements of the chips on the insulator surface glazing were impossible. However, the chipping of the porcelain glazing was only observed during the last observation, where permission was granted to touch the porcelain insulator surfaces. Thus, the date when the process started is unknown.

5.3.4.1 AC_Porcelain insulator

No chipped glazing observations were made on the AC_Porcelain insulator during the research period.

5.3.4.2 DC+_Porcelain insulator

The details of first occurrences of chipped glazing observations are summarized in Table 5-28. It is evident from Table 5-28 that the chipped glazing observations were more prominent in the middle axial section and east side of the insulator. It is also noted that most of the observations were preceded by medium pollution and dry band observations. The dry band observations, as a preceding observation, were as prominent as with the light erosion and erosion observations on the polymer insulators. The dry band observations are indicative that there were electrical discharge activities at the respective areas and it could be the reason for the chipping of the glazing. Please refer to Figure 5-35 for a photograph of a chipped glazing observation on the DC+_Porcelain insulator.

Figure 5-35: Chipped glazing observation on the DC+_Porcelain insulator

Table 5-28: First instances of chipped glazing observations on the DC+_Porcelain insulator

First instances of chipped glazing observations on the DC+_Porcelain insulator			
Date	**Insulator position**	**Direction**	**Preceded by**
2012/02/08 (Day 371)	1st sheath	East	Medium pollution, dry band, plant particle
	1st shed bottom	East	Medium pollution, dry band
	2nd sheath	East	Medium pollution, dry band
	2nd shed bottom	East	Medium pollution, dry band, salt crystals
	3rd sheath	East	Light pollution, dry band
	4th sheath	East	Light pollution, dry band, dead insect
	4th shed bottom	East	Medium pollution, dry band
	5th sheath	East	Light pollution, dry band
	5th shed bottom	East	Medium pollution, dry band, salt crystals
	3rd shed bottom	West	Light pollution, dry band, salt crystals
	4th sheath	West	Medium pollution, dry band
	4th shed top	West	Light pollution, dry band
	4th shed bottom	West	Light pollution, dry band, salt crystals
	5th sheath	West	Medium pollution, dry band
	5th shed bottom	West	Medium pollution, dry band, salt crystals
	1st shed bottom	North	Light pollution, dry band, salt crystals
	2nd shed bottom	North	Medium pollution, dry band, salt crystals
	3rd shed bottom	North	Light pollution, dry band, salt crystals
	4th sheath	North	Light pollution, dry band
	4th shed top	North	Light pollution, dry band, salt crystals
	4th shed bottom	North	Medium pollution, dry band, salt crystals
	5th sheath	North	Medium pollution, dry band
	5th shed bottom	North	Medium pollution, dry band, salt crystals, plant particle
	4th shed top	South	Medium pollution, dry band, plant particle
	4th shed bottom	South	Medium pollution, dry band, salt crystals, plant particle
	5th shed bottom	South	Medium pollution, dry band, salt crystals, plant particle

5.3.4.3 DC-_Porcelain insulator

The details of first occurrences of chipped glazing observations are summarized in Table 5-29.

It is evident from Table 5-29 that the chipped glazing observations are more prominent close to the live end fitting and north side of the insulator. It is also noted that most of the chipped glazing observations were preceded by medium pollution and dry band observations. The dry band observations, as a preceding observation, were as prominent as with the light erosion and erosion observations on the polymer insulators. The dry band observations are indicative that there were electrical discharge activities at the respective areas and it could be the reason

for the chipping of the glazing. Please refer to Figure 5-36 for a photograph of a chipped glazing observation on DC-_Porcelain insulator.

Table 5-29: First instances of chipped glazing observations on the DC-_Porcelain insulator

First instances of chipped glazing observations on the DC-_Porcelain insulator			
Date	**Insulator position**	**Direction**	**Preceded by**
2012/02/13 (Day 376)	1st sheath	East	Medium pollution, dry band, plant particle
	1st shed top	East	Medium pollution, dry band
	3rd sheath	East	Medium pollution, dry band
	4th sheath	East	Medium pollution, dry band
	5th sheath	East	Light pollution, dry band
	1st sheath	West	Medium pollution, dry band, salt crystals
	1st shed top	West	Light pollution, dry band, salt crystals, dead insect
	2nd sheath	West	Medium pollution, dry band
	3rd sheath	West	Medium pollution, dry band
	4th sheath	West	Medium pollution, dry band
	5th sheath	West	Medium pollution, dry band
	1st sheath	North	Medium pollution, dry band, dead insect
	1st shed top	North	Light pollution, dry band
	2nd sheath	North	Medium pollution, dry band
	3rd sheath	North	Medium pollution, dry band
	4th sheath	North	Medium pollution, dry band
	5th sheath	North	Medium pollution, dry band
	5th shed top	North	Medium pollution, dry band
	1st sheath	South	Heavy pollution, dry band, material erosion, salt crystals

Figure 5-36: Chipped glazing observation on DC-_Porcelain insulator

5.3.4.4 Summary of chipped glazing observations

In this section the normalized totals of the chipped glazing observations per position on the Porcelain insulators are compared with each other in order to determine which excitation voltage performed better. The insulator with the least glazing chip observations is considered to be the best performer. Please refer to Table 5-30 for a comparison between the Porcelain insulators under the different excitation voltages.

Table 5-30: Summary of normalized totals of chipped glazing observations on Porcelain insulators

Summary of normalized totals of chipped glazing observations on Porcelain insulators				
Direction	**Insulator position**	**AC_Porcelain [%]**	**DC+_Porcelain [%]**	**DC-_Porcelain [%]**
		08-Feb-12 (Day 371)	**08-Feb-12 (Day 371)**	**13-Feb-12 (Day 376)**
East	Sheath	0	100	80
	Shed top	0	0	17
	Shed bottom	0	67	0
West	Sheath	0	40	100
	Shed top	0	17	17
	Shed bottom	0	50	0
North	Sheath	0	40	100
	Shed top	0	17	33
	Shed bottom	0	83	0
South	Sheath	0	0	20
	Shed top	0	17	0
	Shed bottom	0	33	0
	Average [%]	0.00	38.61	30.56

It is evident from Table 5-30 that the AC excitation voltage performed best and the DC+ excitation voltage performed worst, which is in contrast with the light erosion and erosion observations for Porcelain insulators where the DC- excitation voltage performed worst as mentioned in section 5.3.1.4. Table 5-31 was compiled from Table 5-30 and the discussions above for further comparisons.

Table 5-31: Summary of the prominent chipped glazing areas on the respective insulators

Insulator	AC	DC+	DC-
Porcelain	No observation	Shed bottom, east, middle axial section	Sheath, north, live section

It is evident from Table 5-31 that there is no prominent direction, or axial position of chipped glazing observations, for the different insulators. The only common observation is that the shed top positions have no prominent chipped glazing observations.

The heat of the power arcs could have damaged the glazed surfaces of Porcelain insulators as mentioned in section 2.5.2, thus it may be assumed that most of the electrical discharge activities occurred on the positions as summarized in Table 5-31.

5.3.5 Metal end fitting corrosion

In this section the insulators will be compared, in order to determine which metal end fitting corroded and which corroded the earliest. The comparison was done by comparing the dates a rust layer was first observed on the metal end fittings of the insulators. A further comparison was done by categorizing the amount of rust present on the end fittings, either as 'light' or 'moderate'. Please refer to Table 5-32 for a summary of the metal end fitting corrosion observations.

Table 5-32: Summary of the first time metal end fitting corrosion observations

First time metal end fitting corrosion observations						
	AC		DC+		DC-	
Insulators	Date	Position	Date	Position	Date	Position
EPDM silicone alloy	None	None	2011/08/03 (moderate) (Day 80)	Live end fitting	2011/07/26 (moderate) (Day 72)	Earthed end fitting
HTV	None	None	2011/10/26 (light) (Day 164)	Live end fitting	2011/07/26 (light) (Day 72)	Earthed end fitting
RTV coated porcelain	None	None	2011/03/11 (moderate) (Day 37)	Live end fitting	2011/02/10 (moderate) (Day 8)	Earthed end fitting
Porcelain	None	None	2011/08/15 (moderate) (Day 194)	Live end fitting	2011/03/03 (moderate) (Day 29)	Earthed end fitting
Glass	None	None	None	None	None	None

It is evident from Table 5-32 that no corrosion was observed on the metal end fittings of the insulators under AC excitation voltage. However, corrosion was observed on the live metal end fittings of all the insulators under DC+ excitation voltage, except the Glass insulator and corrosion was observed on the earthed metal end fittings of all the insulators under DC- excitation voltage except for the Glass insulator. Thus, corrosion occurred on the metal end fittings which have a relative positive voltage. It is also noted that corrosion on the metal end fittings were first observed on the insulators under DC- excitation voltage. Further, only the HTV insulators on both DC excitation voltages have a light corrosion observation, while the other insulators have moderate corrosion observations. Please refer to Figure 5-37 and Figure 5-38 for photos of the relevant corrosion observations.

a) DC-_EPDM b) DC-_HTV c) DC-_RTV d) DC-_Porcelain

Figure 5-37: Corrosion on the earthed metal end fittings of the insulators under DC- excitation voltage

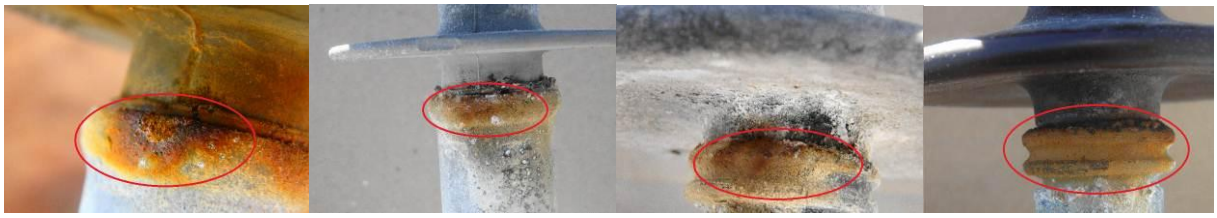

a) DC+_EPDM b) DC+_HTV c) DC+_RTV d) DC+_Porcelain

Figure 5-38: Corrosion on the live metal end fittings of the insulators under DC+ excitation voltage

The cause of corrosion of the metal end fittings, with the relative positive voltages, is an electrolytic corrosion process caused by the DC leakage currents. This process is explained in Figure 5-39 where it is illustrated that the metal end fitting with the relative positive voltage donates positive iron ions to the water electrolyte, which consists of the conducting solution layer on the surface of the insulator [57]. The positive iron ions react with hydroxide ions, which were reduced from oxygen and water, to form iron (II) hydroxide which readily undergoes oxidation to form hydrated iron (III) oxide, better known as rust [58].

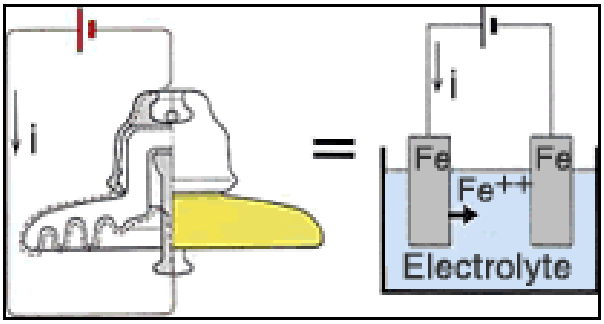

Figure 5-39: Electrolytic corrosion process [57]

The reason why the metal end fittings on the glass insulators did not corrode, was because a zinc ring was fitted at the edge of the cap and a zinc sleeve on the pin during manufacturing of

the Glass insulator. The zinc ring and sleeve act as sacrificial electrodes to combat corrosion [14]. Please refer to Figure 5-40 for an illustration of the zinc sleeve attached to the pin.

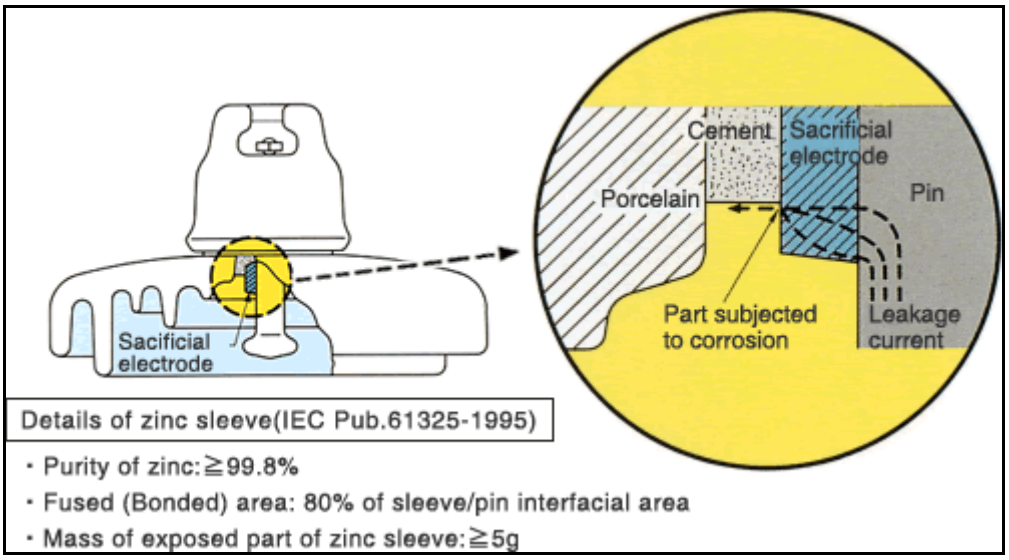

Figure 5-40: Illustration of a zinc sleeve attached to the pin of a cap-and-pin insulator [57]

It appears from the above mentioned results that hot dipped galvanizing does not provide sufficient protection for the metal end fittings against electrolytic corrosion for insulators under DC excitation voltages. A sacrificial zinc sleeve or zinc ring is thus recommended for all metal end fittings of insulators under DC excitation voltages.

A possible explanation of why the metal end fittings under DC- excitation corroded earlier than the metal end fittings under DC+ excitation is that the gravitational forces and the electrical forces worked in the same direction under DC- excitation voltage. However, the gravitational and electrical forces worked in opposing directions under DC+ excitation voltage. Thus, the resulting force on the positive iron ions is stronger under DC- excitation than under DC+ excitation, which could lead to earlier corrosion.

5.3.6 Interesting observations

The observations discussed in this section are observations of interest, which not necessarily contributed to the degradation of the insulators as the other observations discussed earlier in this chapter.

5.3.6.1 Dark layer observations

Dark layers were observed on AC_Porcelain and DC+_Porcelain insulators. Please refer to Table 5-33 for a summary of the first dark layer observations and to Figure 5-41 for photographs of it.

Table 5-33: First dark layer observations

First dark layer observations				
Insulator	**Date**	**Position**	**Direction**	**Preceded by**
AC_Porcelain	2011/05/04 (Day 91)	5th shed top	West	Medium pollution, dry band
		6th shed top	West	Light pollution, dry band
	2011/07/07 (Day 155)	5th shed bottom	West	Light pollution, dry band, salt crystals, plant particle
		5th shed bottom	North	Light pollution, dry band, salt crystals
		6th shed top	North	Light pollution, dry band, grease stain
		5th shed bottom	East	Medium pollution
DC+_Porcelain	2011/04/19 (Day 76)	6th shed top	North	Light pollution, dry band

Initially it was thought that the dark layer observations were burned fungus growths on the insulators, but at the end of the research period, samples of the dark layers were sent to a Microbiology laboratory at the University of Stellenbosch, where it was found that it was not a fungus growth. Currently it is not known what had caused the dark layers on the respective porcelain insulators. However, it is known that the dark layer observations were preceded by dry band observations as presented in Table 5-33, which indicate that there were electrical discharge activities at the respective insulator areas. Thus, a substance e.g. pollution, salt crystals, plant particles, grease stain or a combination of it could have been burned by the electrical discharge activities and formed the dark layers.

a) AC_Porcelain insulator b) DC+_Porcelain insulator

Figure 5-41: Dark layer observations

5.3.6.2 Sand pollution

In section 2.4.3.1.1, it was mentioned that DC electric field forces may assist with pollution depositing on the insulator surfaces. While taking the above mentioned in consideration, the author wanted to explore if such a tendency was present at KIPTS, by comparing, visually, the amount of sand pollution on the insulator surfaces. Ideally it would have been preferred if ESDD and NSDD measurements were taken periodically on the live insulators to compare the amount of pollution deposited on the insulators. However, due to a decision not to disturb the natural pollution deposition process on the insulator surfaces, ESDD and NSDD measurements were not possible and the only option was to do a visual comparison.

The number of sheaths, shed tops and shed bottoms covered with sand during each inspection were summed per wind direction for each insulator and divided by the total number of sheaths, shed tops and shed bottoms of the respective insulator, in order to obtain the percentage value covered by sand for each wind direction. The corresponding values of all the inspection were summed and divided by the number of inspections, in order to obtain an average value of sand pollution per insulator per direction. These values are tabulated in Table 5-34 and used to evaluate the amount of sand pollution on the insulators. Please refer to Figure 5-42 for photographs of typical sand pollution on the insulator surfaces.

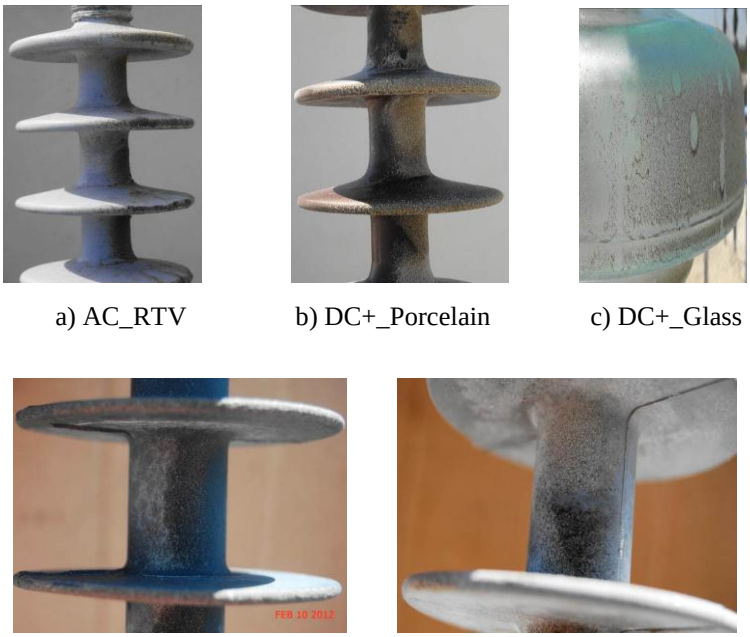

a) AC_RTV b) DC+_Porcelain c) DC+_Glass

d) DC-_EPDM e) AC_HTV

Figure 5-42: Photographs of insulators with sand deposited on their surfaces

Table 5-34: Sand pollution averages over entire research period

Sand pollution averages over entire research period				
Direction	**Insulator**	**AC Average [%]**	**DC+ Average [%]**	**DC- Average [%]**
East	EPDM	1.00	3.00	4.80
	HTV	3.00	2.00	11.20
	RTV	31.09	18.49	6.62
	Porcelain	14.29	6.72	19.85
	Glass	14.29	21.43	25.00
West	EPDM	2.00	2.00	6.40
	HTV	6.00	3.00	10.40
	RTV	26.89	12.61	20.59
	Porcelain	5.04	10.92	14.71
	Glass	7.14	28.57	25.00
North	EPDM	0.00	0.00	3.20
	HTV	5.00	0.00	6.40
	RTV	2.52	0.84	9.56
	Porcelain	6.72	5.88	15.44
	Glass	14.29	42.86	31.25
South	EPDM	16.00	9.00	12.00
	HTV	18.00	8.00	22.40
	RTV	78.99	46.22	55.15
	Porcelain	36.97	32.77	55.88
	Glass	57.14	71.43	50.00
Average total [%]		**17.32**	**16.29**	**20.29**

It is evident from Table 5-34 that the insulators energised by DC+ voltage have the least amount of sand pollution and the insulators energised by DC- voltage has the most amount of sand pollution on their surfaces. This result might proof that the electrostatic pull forces of DC- voltage are stronger than the pull forces of DC+ voltage. However, further investigation regarding this is needed before a firm conclusion may be made.

5.3.7 Wettability (hydrophobicity) classification

The hydrophobicity classification was done, as discussed in section 4.6.1, but to compare the surface conditions of the insulators, the results were divided into two groups of hydrophobicity, namely hydrophobic for a hydrophobicity classification (HC) < 5 and hydrophilic for HC ≥ 5. This was based on previous work which showed a narrow distribution of surface conductivity and a consistent flashover performance for insulator surfaces with a HC < 5 [59]. It was proven that both the surface conductivity and flashover performance deteriorated significantly for insulator surfaces with a HC above 5 [59].

The insulator surface areas which became hydrophilic were tabulated in Table 5-35 up to Table 5-37. The following code was used in the tables to identify the specific area where the surface became hydrophilic:

- The first letter of the code refers to the direction that the insulator surface faces, where L refers to land side and S refers to sea side.
- The second letter refers to the position on the insulator, where S refers to sheath, T refers to shed top and B refers to shed bottom.
- The number refers to the sheath and shed number, where 1 refers to the sheath and shed closest to the live metal end fitting and the highest number (6 or 9) refers to the sheath and shed closest to the earthed metal end fitting.
- Thus, the code LT1 would be interpreted as the insulator surface area that faces the Land side on the shed Top closest to the live metal end fitting.

Table 5-35: Hydrophilic positions on polymer insulators under DC- excitation voltage

Hydrophilic positions on Insulators			
Date	**DC- Excitation voltage**		
	EPDM	**HTV**	**RTV**
10-Feb-11	Not installed	Not installed	None (Day 8)
11-Mar-11	Not installed	Not installed	All except SB1, SS3, SB6, LB1, LS1, LS3, LT6, LB6, LS5 (Day 37)
13-Apr-11	Not installed	Not installed	All except LT1, LS1, LT3, LS3 (Day 70)
19-May-11	All (Day 4)	SS4, SS9 (Day4)	All (Day 106)
26-Jul-11	All (Day 72)	All except LS4, LS9 (Day 72)	All except ST3, SB3, LT3, LB3, LS3 (Day 174)
05-Sep-11	All (Day 113)	All (Day 113)	All (Day 215)
01-Dec-11	All	All	All
10-Feb-12	All	All	All

Table 5-36: Hydrophilic positions on polymer insulators under DC+ excitation voltage

Hydrophilic positions on Insulators			
Date	**DC+ Excitation voltage**		
	EPDM	**HTV**	**RTV**
21-Feb-11	Not installed	Not installed	ST1, SB3, ST6,SB6, LT1, LB3, LT6, LB6 (Day 19)
24-Mar-11	Not installed	Not installed	All except ST1, LT1, LB1 (Day 50)
19-Apr-11	Not installed	Not installed	All (Day 76)
07-Jun-11	All (Day 23)	All except SB1, SB4, SB8, LB1, LB4, LS4, LB8 (Day 23)	All except SB1, SB3, LT1 (Day 125)
03-Aug-11	All (Day 80)	All except SB1, SB4, LB1, LS4 (Day 80)	All except ST1, SB1, LT1, LS1, LB3 (Day 182)
26-Oct-11	All (Day 166)	All (Day 166)	All (Day 268)
08-Feb-12	All	All	All

Table 5-37: Hydrophilic positions on polymer insulators under AC excitation voltage

Hydrophilic positions on Insulators			
Date	**AC Excitation voltage**		
	EPDM	**HTV**	**RTV**
03-Mar-11	Not installed	Not installed	LT1, LT3 (Day 29)
05-Apr-11	Not installed	Not installed	All except ST1, SB1, LS3, LS5 (Day 62)
04-May-11	Not installed	Not installed	All except ST1, SS4, LS1 (Day 91)
07-Jul-11	All (Day 53)	All except SB1, SB4, SB8, SS9, LS1, LB8, LS9 (Day 53)	All except ST1, SB1, SS3, LS3 (Day 155)
25-Aug-11	All (Day 102)	All (Day 102)	All except ST1, ST3, LS3, LT6 (Day 204)
29-Nov-11	All (Day 198)	All (Day 198)	All (Day 300)
08-Feb-12	All	All	All

It is evident from Table 5-35 that the DC-_EPDM insulator lost its hydrophobicity characteristic the earliest of the insulators under DC- excitation voltage. The EPDM and

HTV insulators were installed on 16 May 2011 on all three different excitation voltage arms. The DC-_EPDM insulator surface was hydrophilic by its first inspection cycle, which was conducted on 19 May 2011. The DC-_HTV insulator surface was hydrophilic by its third inspection cycle, which was conducted on 5 September 2011. The DC-_RTV insulator surface was hydrophilic by its fourth inspection cycle, which was conducted on 19 May 2011. It regained some of its hydrophobicity characteristic by its fifth inspection cycle on 26 July 2011, but lost it again by its sixth inspection cycle on 5 September 2011. It is observed in Figure 5-5 that KIPTS received approximately 115 mm rain between the fourth and fifth inspection cycles of the DC- voltage arm. This amount of rain could have cleaned the DC-_RTV insulator surface, which could have led to the regaining of some of its hydrophobicity characteristic. Please refer to Figure 5-43 for photographs of the hydrophilic state of the polymer insulators under DC- excitation voltage.

a) DC-_EPDM insulator b) DC-_HTV insulator c) DC-_RTV insulator

Figure 5-43: Hydrophilic state of polymer insulators under DC- excitation voltage

It is evident from Table 5-36 that the DC+_EPDM insulator lost its hydrophobicity characteristic the earliest of the polymer insulators under DC+ excitation voltage. The DC+_EPDM insulator surface was hydrophilic by its first inspection cycle, which was conducted on 7 June 2011. The DC+_HTV insulator surface was hydrophilic by its third inspection cycle, which was conducted on 26 October 2011. The DC+_RTV insulator surface was hydrophilic by its third inspection cycle, which was conducted on 19 April 2011. It regained some of its hydrophobicity characteristic by its fourth inspection cycle on 7 June 2011, but lost it again by its sixth inspection cycle on 26 October 2011. It is observed in Figure 5-5 that KIPTS received approximately 70 mm rain between the third and fourth inspection cycles of the DC+ voltage arm. This amount of rain could have cleaned the DC+_RTV insulator surface, which could have led to the regaining of some of its hydrophobicity characteristic. Please refer to Figure 5-44 for photographs of the hydrophilic state of the polymer insulators under DC+ excitation voltage.

a) DC+_EPDM insulator b) DC+_HTV insulator c) DC+_RTV insulator

Figure 5-44: Hydrophilic state of polymer insulators under DC+ excitation voltage

It is evident from Table 5-37 that the AC_EPDM insulator lost its hydrophobicity characteristic the earliest under AC excitation voltage. The AC_EPDM insulator surface was hydrophilic by its first inspection cycle, which was conducted on 7 July 2011. The AC_HTV insulator surface was hydrophilic by its second inspection cycle, which was conducted on 25 August 2011. The AC_RTV insulator surface was hydrophilic by its sixth inspection cycle, which was conducted on 29 November 2011. Please refer to Figure 5-44 for photographs of the hydrophilic state of the polymer insulators under AC excitation voltage.

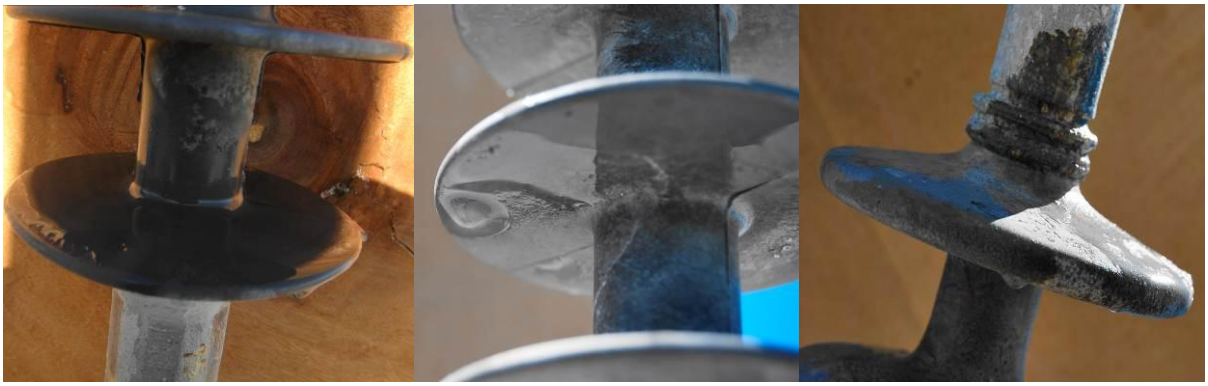

a) AC_EPDM insulator b) AC_HTV insulator c) AC_RTV insulator

Figure 5-45: Hydrophilic state of polymer insulators under AC excitation voltage

It is difficult to compare the hydrophobicity characteristic of the same insulator material across the different excitation voltages because the different voltage arms were inspected on different dates. The only possible result from cross voltage comparison is that the AC_RTV insulator lost its hydrophobicity characteristic later than the DC-_RTV and DC+_RTV insulators. Please refer to Annex B for the actual hydrophobicity classification results.

5.4 Insulator leakage currents

The actual peak leakage current values were recorded and manipulated, as discussed in section 4.4 for leakage current analysis purposes. In this section the measured results of the insulator leakage currents will be discussed, by comparing the different leakage current peak values of all the insulators energized by the same voltage type. The effect of the different voltage sources on the leakage current peak values for each insulator material will also be discussed.

The linearity of the leakage current sensors was tested prior to the start of this research project, in order to determine the linearity region of the leakage current measurements and to validate that the measurements recorded during the research period would be true and trustworthy.

The insulator leakage current section will be discussed in the following sequence:

- Results of current sensors linearity tests.
- Plots of the maximum actual leakage current peaks of all the insulators tested.
- Summary of the insulator flashover events.
- Histogram analyses of the insulator's peak leakage current values.
- Comparing the effect of the different voltage sources on the different insulator material's peak leakage current values.

5.4.1 Results of current sensors linearity tests

A variable DC power source and a variable resistor were used to inject different DC current levels into the DC current sensors. The actual value of the current injected into the current sensor was measured with a multi-meter and its reading was compared to the value measured on the online leakage current analyser (OLCA). These values are given in Table 5-38 and Table 5-39. The block diagram of the measurement arrangement used for the linearity test on the DC current sensors is displayed in Figure 5-46.

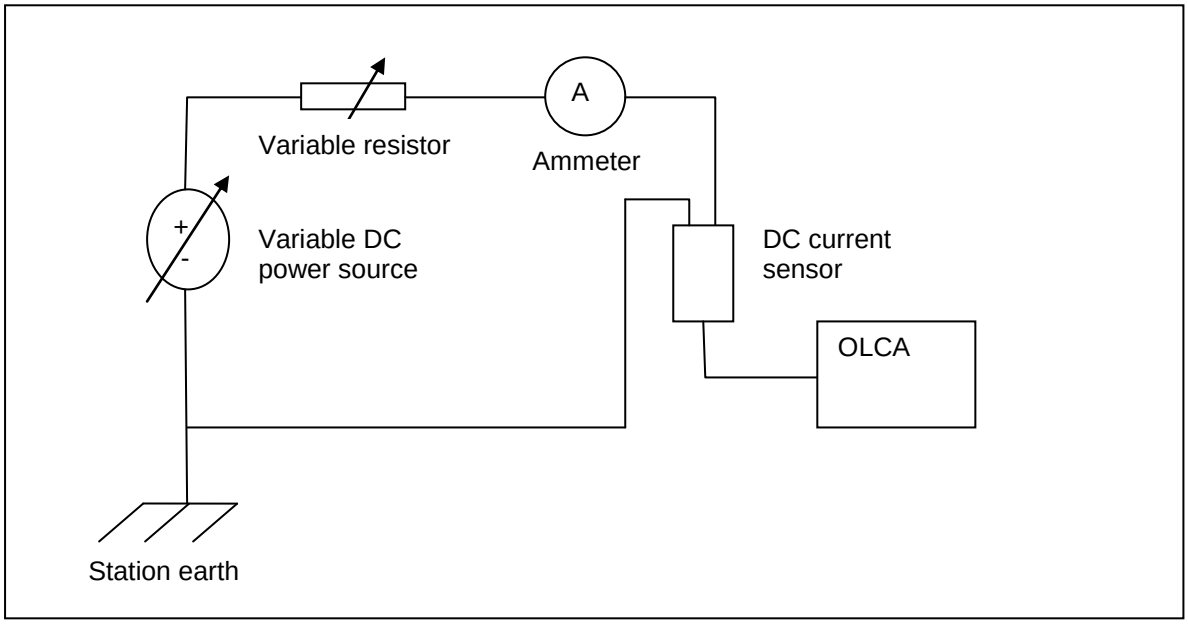

Figure 5-46: Block diagram of linearity test arrangement for DC current sensors

Different AC current levels were injected into the AC current sensors by using a variac that was connected to a 220 V (rms) AC power source via an isolating transformer, and a variable resistor. The actual value of the current injected into the current sensor was measured with a multi-meter and its reading was compared to the value measured on the OLCA. These values are given in Table 5-40. The block diagram of the measurement arrangement used for the linearity test on the AC current sensors is displayed in Figure 5-47.

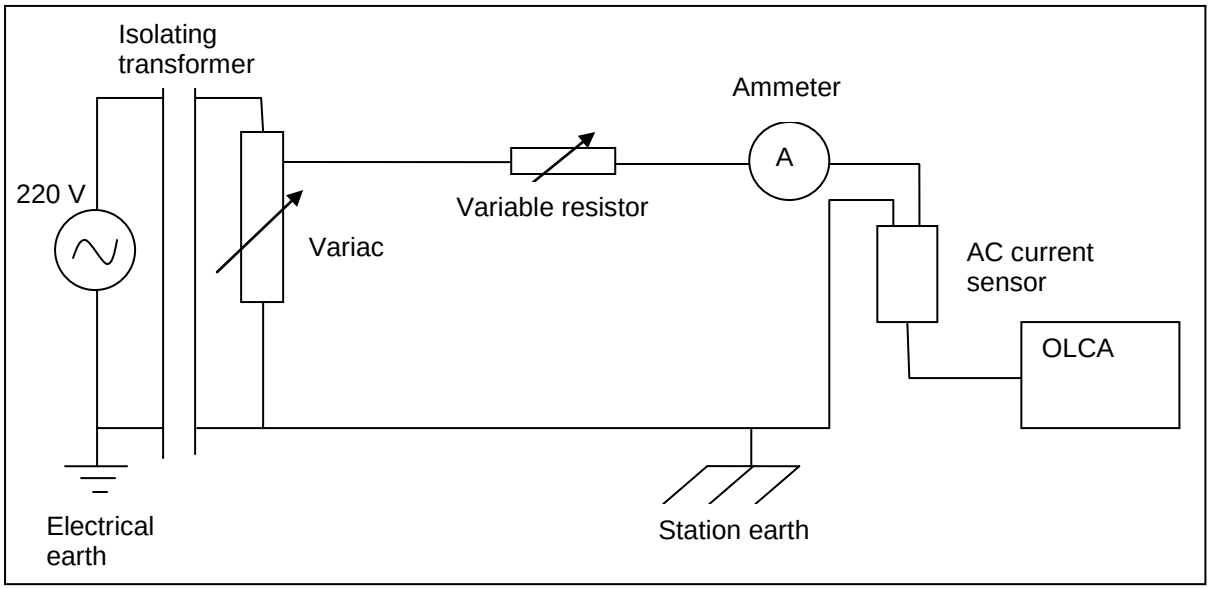

Figure 5-47: Block diagram of linearity test arrangement for AC current sensors

Table 5-38: Linearity test results of current sensors on DC+ voltage arm

Linearity test results of current sensors on DC+ voltage arm: 18 January 2011									
EPDM		HTV		RTV		Porcelain		Glass	
Multi-meter [mA]	OLCA [mA]	Multi-meter [mA]	OLCA [mA]	Multi-meter [mA]	OLCA [mA]	Multi-meter [mA]	OLCA [mA]	Multi-meter [mA]	OLCA [mA]
0	0	0	0	0	0	0	0	0	0
10.1	10.9	10.04	9.9	10.13	8.8	10.13	10.9	10.26	9.5
50.2	51	50.9	50.8	50.7	49.7	50.2	50.8	50.4	49.6
100.2	100.9	100.4	100.4	100	99	100.2	100.8	100.3	99.1
200	200.5	200.7	200.2	200	199.1	200	200.6	200.2	198.9
250	250.4	250.5	249.9	250	249.5	250.3	250.6	250.6	247.8
500	495.5	500	505.1	500	493.4	500	497	500	487.5
600	596.1	600	603.4	600	597.7	600	594.6	600	587.7
700	697.1	700	703.9	700	697.4	700	699	700	695.9
710	711.5	710	715.5	710	708	710	705	710	707.9
720	713.3	720	719.7	720	717.8	720	715.5	720	713.2
730	718.5	730	720.1	730	720.7	730	716.3	730	718.8
740	719.2	740	720.8	740	720.7	740	717.3	740	718.8
750	719.6	750	721.2	750	721	750	717.3	750	718.8
800	719.6	800	721.2	800	721.4	800	717.3	800	718.8

Table 5-39: Linearity test results of current sensors on DC- voltage arm

Linearity test results of current sensors on DC- voltage arm: 18 January 2011									
EPDM		HTV		RTV		Porcelain		Glass	
Multi-meter [mA]	OLCA [mA]	Multi-meter [mA]	OLCA [mA]	Multi-meter [mA]	OLCA [mA]	Multi-meter [mA]	OLCA [mA]	Multi-meter [mA]	OLCA [mA]
0	0	0	0	0	0	0	0	0	0
10.82	9.8	10.57	9.5	10.31	9.8	10.46	9.1	10.64	10.2
50.8	49.8	50.7	49.5	50.2	49.1	50	48.3	50.4	49.8
100.6	99.3	100.5	99.3	100.1	98.2	100.7	98.6	100.1	99.2
200.8	199	200.2	198.5	200	196.8	200.4	197.9	200.6	199.4
250.6	248.5	250.8	249	250.5	246.7	250.1	247.2	250	248.5
500	489	500	486.5	500	478.9	500	481.5	500	490.4
600	592.2	600	591	600	589.1	700	682.2	600	600.4
700	691.6	700	687.1	700	682.4	710	693.1	700	697.9
710	699.6	710	696.9	710	697.5	720	705.3	710	704.9
720	709.5	720	708.1	720	707.3	730	708.1	720	713.6
730	711.9	730	709.5	730	709.8	740	709.2	730	713.6
740	713.3	740	710.6	740	710.8	750	709.9	740	713.6
750	714.4	750	711.3	750	711.9	760	710.2	750	713.6
800	715.1	800	715.4	800	712.9	800	710.2	800	713.6

Table 5-40: Linearity test results of current sensors on AC voltage arm

Linearity test results of current sensors on AC voltage arm: 19 January 2011									
EPDM		HTV		RTV		Porcelain		Glass	
Multi-meter [mA]	OLCA [mA]	Multi-meter [mA]	OLCA [mA]	Multi-meter [mA]	OLCA [mA]	Multi-meter [mA]	OLCA [mA]	Multi-meter [mA]	OLCA [mA]
0	0	0	0	0	0	0	0	0	0
50.4	50.7	10.52	10.5	10.5	10.5	10.45	10.5	10.09	10.1
101.7	102.1	50.1	50.1	50.3	50.6	50	50.2	50.4	50.6
200.6	201.4	100.4	100.7	100.4	100.8	100.1	100.5	102.3	102.7
250.9	251.8	201.8	202.5	200	201.8	200.6	201.3	201.7	202.5
500	503.5	250.2	250.9	250.1	251.4	250.2	251.3	250.4	251.4
510	510.3	500	503.4	500	502.7	500	502.2	500	510.1
520	519	510	511.4	510	512.9	510	509.7	510	512.1
530	525.7	530	525.9	530	525.7	530	526	530	526.1
550	535.5	550	533.7	550	537.2	550	537	550	537.3
600	557	600	557.7	600	557.3	600	557.1	600	557
700	585.4	700	584.3	700	584.6	700	584.2	700	585
800	602.8	800	601.9	810	604.2	800	603.8	800	604.5

The values of Table 5-38, Table 5-39 and Table 5-40 were plotted for each current sensor and these graphs are displayed in Annex C. The graphs of the DC+_EPDM and AC_EPDM sensors are displayed below in Figure 5-48 and Figure 5-49 respectively, as typical outcomes of the linearity tests for the DC and AC sensors.

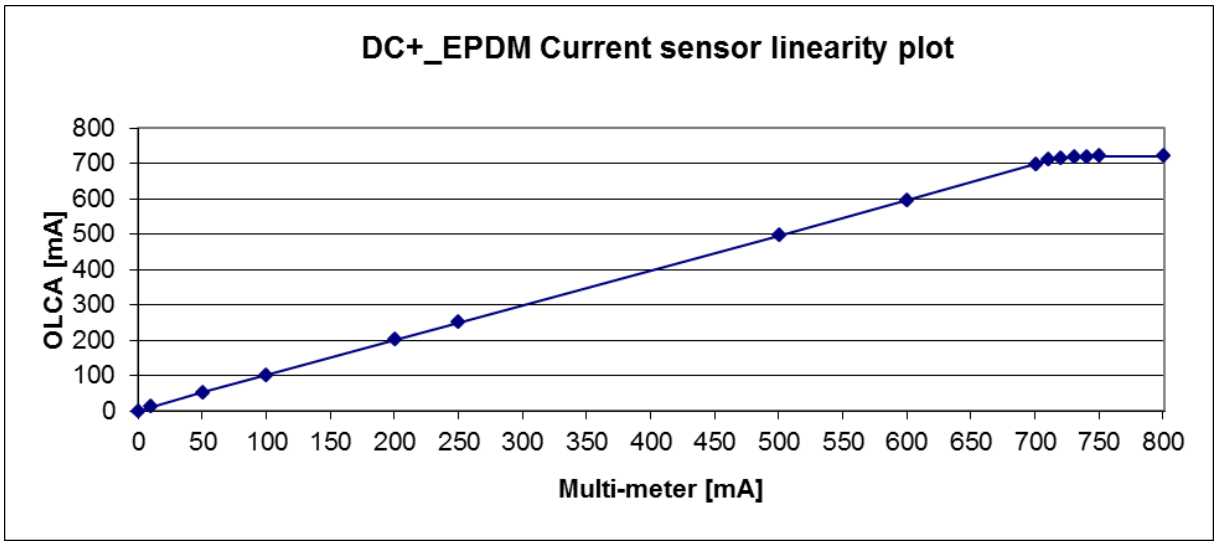

Figure 5-48: Linearity plot of DC+_EPDM current sensor

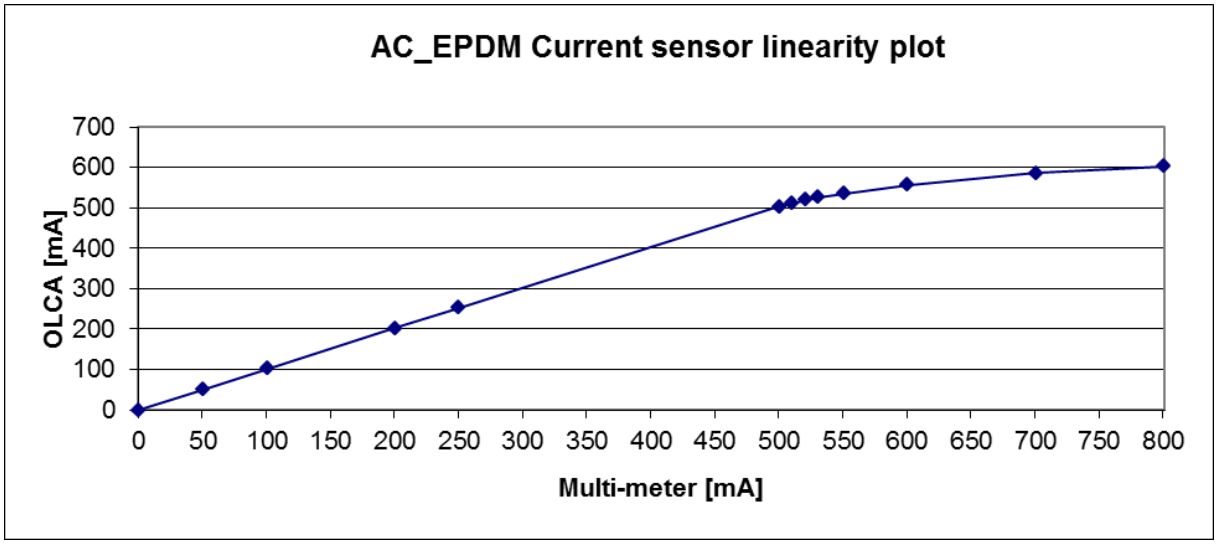

Figure 5-49: Linearity plot of AC_EPDM current sensor

It is observed from Table 5-38, Table 5-39 and Figure 5-48 that the actual DC current values measured by the multi-meter and the values measured on the OLCA differ minimally and they have a linear relationship up to 700 mA. Thus, any DC leakage current measurements on the

OLCA higher than 700 mA falls within the non-linear portion of the measurement system and the actual value might have been much higher than recorded value on the OLCA.

It is observed from Table 5-40 and Figure 5-49 that the actual AC current values measured by the multi-meter and the values measured on the OLCA, differ minimally and they have a linear relationship up to 500 mA. It should be noted that the AC current values measured during the linearity tests were r.m.s. values. This is also the reason why the linear range of the AC current sensors is smaller than the DC current sensors. The peak value of a 500 mA r.m.s. value is 707 mA which corresponds approximately to the DC linear range. Furthermore, only the peak leakage current values will be used to analyse the leakage currents flowing over the insulator surfaces, as mentioned in section 4.4. Thus, the linear range of ±700 mA will be used for both AC and DC peak leakage current measurements during the analyses of the peak leakage current measurements. Any peak leakage current measurements on the OLCA outside the ±700 mA range falls within the non-linear portion of the measurement system, thus, the actual peak leakage current value might have been much higher than the recorded value.

As mentioned in section 3.4.1, the OLCA has an input current measurement range of ±500 mA (r.m.s.). Thus, the limitation on the linear range of the measurement system is determined by the OLCA, and not the current sensors.

5.4.2 Plots of actual leakage current peaks of insulators tested

Please refer to the research period's peak leakage current plots, for all the insulators tested, in Figure 5-50 up to Figure 5-56.

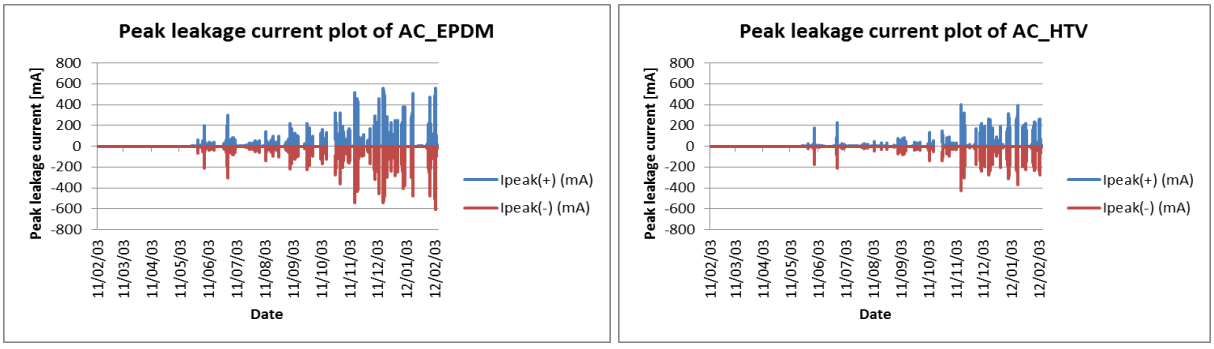

Figure 5-50: Peak leakage current plots of AC_EPDM and AC_HTV insulators

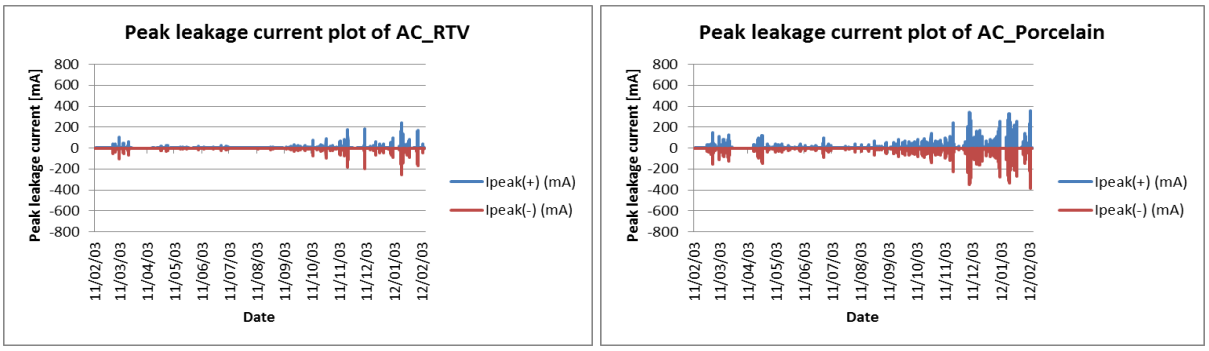

Figure 5-51: Peak leakage current plots of AC_RTV and AC_Porcelain insulators

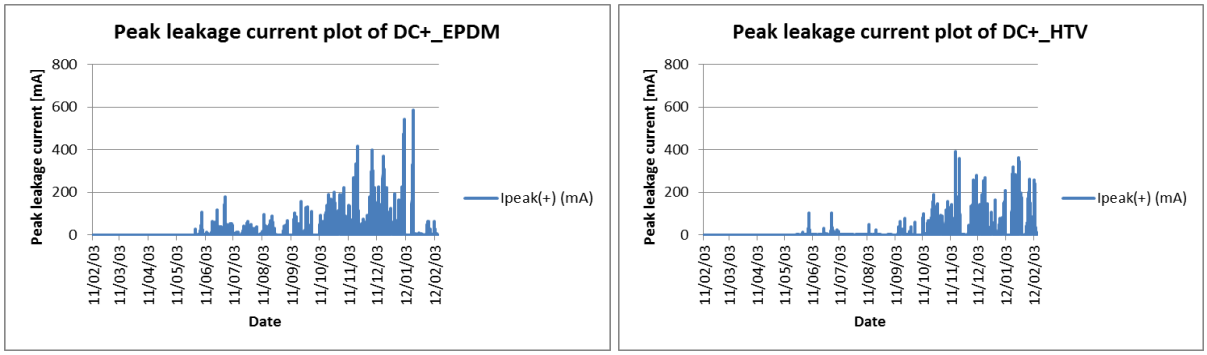

Figure 5-52: Peak leakage current plots of DC+_EPDM and DC+_HTV insulators

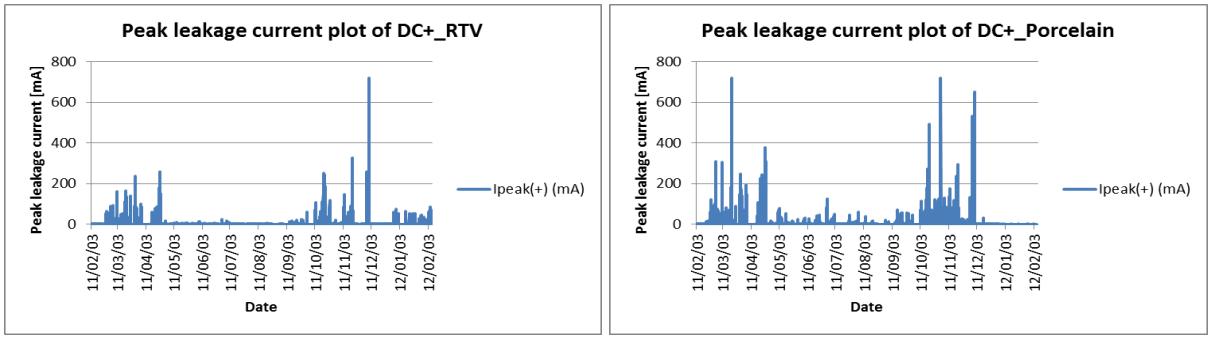

Figure 5-53: Peak leakage current plots of DC+_RTV and DC+_Porcelain insulators

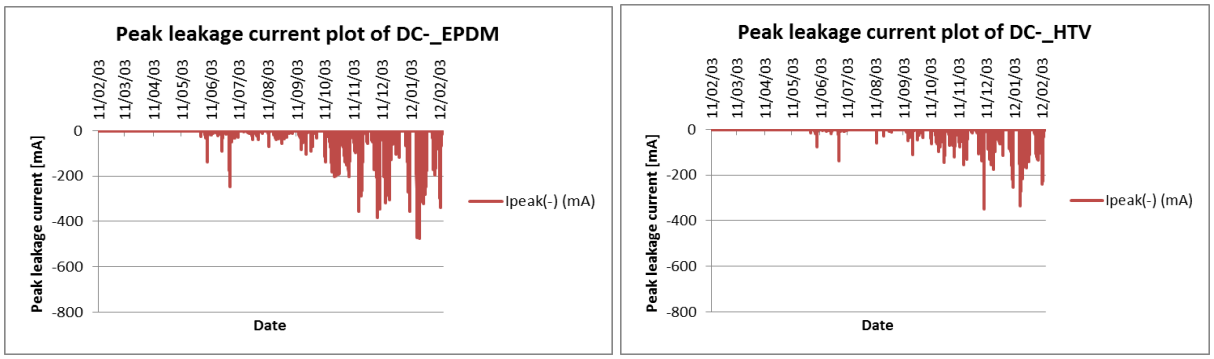

Figure 5-54: Peak leakage current plots of DC-_EPDM and DC-_HTV insulators

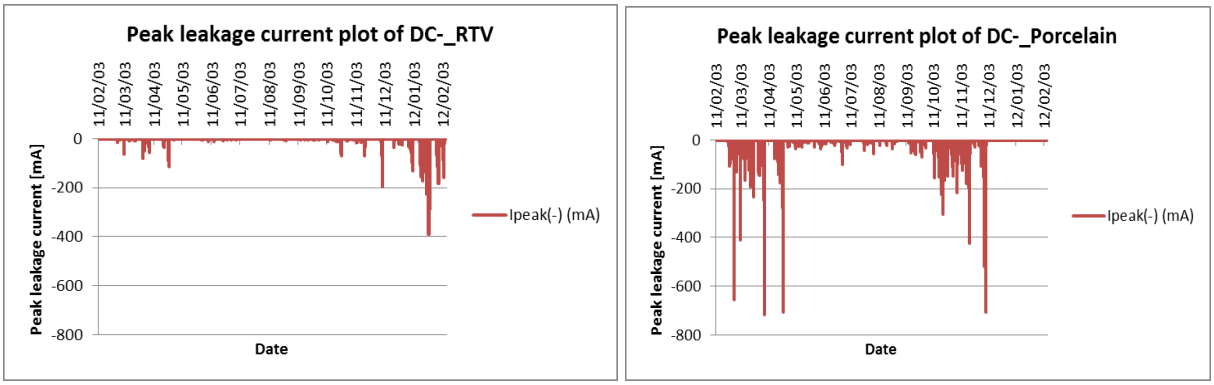

Figure 5-55: Peak leakage current plots of DC-_RTV and DC-_Porcelain insulators

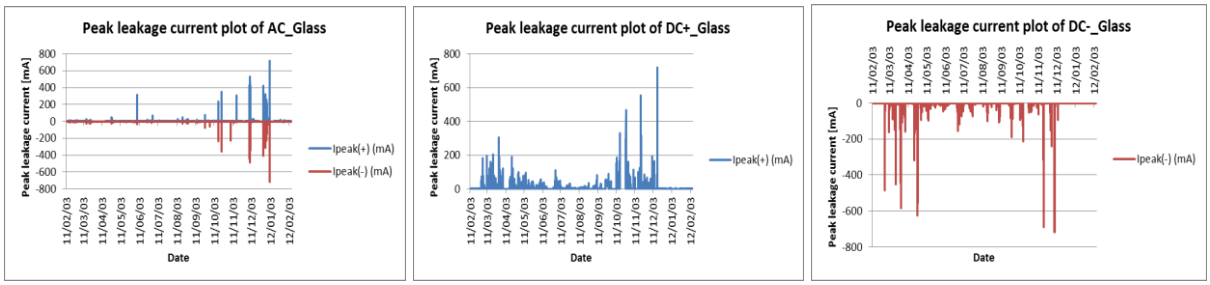

Figure 5-56: Peak leakage current plots of AC, DC+ and DC-_Glass insulators

It is evident from the above figures that the peak leakage current values of the polymer insulators (EPDM, HTV and RTV insulators) increased over time. This is an indication that the polymer insulator surfaces aged over the research period, which includes loss of hydrophobicity and material erosion as discussed in sections 5.3.1 and 5.3.7.

The AC_Glass, DC+_Glass and the AC_Porcelain insulator also followed the trend of the polymer insulators. This behaviour for the glass insulators is explainable by considering the deep under ribs on the bottom of the glass insulator. Thus, during the early stages of the research project, large scale pollution deposition on the bottom surfaces of the glass insulators, by wind, was not possible because the majority of it was blocked by the deep under ribs of the glass insulators. However, over time, some pollution was deposited on the bottom surfaces of the glass insulators which was not cleanable by natural washing e.g. rain, because it was protected from rain by the deep under ribs. Thus, the pollution deposition on the bottom surface of the glass insulators continued as time progressed, which led to the increase of leakage currents flowing on the surfaces of the insulator during insulator wetting conditions.

The high leakage currents on the DC-_Glass insulator in the beginning of the research period may be attributed to the electrostatic pull forces of the DC- voltage electric fields, which pulled the charged pollution particles to the bottom surface of the glass insulator. This assumption is in line with the assumption that was stated in section 5.3.6.2, which is that the DC- voltage electrostatic pull forces are stronger than the electrostatic pull forces of the DC+ voltage. However, more research regarding this observation is needed before a firm conclusion may be made.

The reason why the AC_Porcelain insulator followed the polymer insulator leakage current trend is not known. It is expected that the AC_Porcelain insulator should follow the DC+_Porcelain and DC-_Porcelain leakage current trends, as seen in Figure 5-53 and Figure 5-55, because porcelain insulators do not have a hydrophobicity characteristic, which requires the insulator surface to age before high leakage currents could flow.

Another interesting observation from Figure 5-50 to Figure 5-55 is that the HTV and RTV insulators, which are known to be hydrophobic in the early stages of their operational life, show a continuously low level current with occasional, singular, high current peaks during the early stages of their operational life, as described in section 2.4.3.3.2. The EPDM and ceramic insulators, which are known to be hydrophilic, show dense current peaks from the early stages of their operational life. It is observed that as the HTV and RTV insulators age and their hydrophobicity characteristics disappear, their leakage current peaks became less isolated and start to follow the same pattern as the EPDM and ceramic insulators.

The DC+_RTV and AC_Glass insulators were the only insulators that did not follow the abovementioned pattern as observed in Figure 5-53 and Figure 5-56. It is expected that the DC+_RTV insulator would have isolated leakage current peaks during the early stages of its operational life, yet it had dense leakage current peaks. No explanation could be given to justify the abovementioned behaviour. Furthermore, it is expected that the AC_Glass would have dense leakage current peaks, yet it had isolated leakage current peaks. This can be explained by the clean bottom surface of the glass disc, caused by the deep under ribs on the bottom of the glass insulator, which prevent the pollution from being deposited on it. Furthermore, the AC voltage does not have a strong electrostatic force to pull the charged pollution particles to the bottom surface of the glass disc. The clean bottom surface has a very high resistivity, even when wetted, and therefore the establishment of leakage current paths on the insulator surface happens infrequently, which results in isolated leakage current peaks.

5.4.3 Summary of insulator flashover events

An event was considered as an insulator flashover event if the protection fuse of an insulator blew, as discussed in section 4.3. Please refer to Table 5-41 for a summary of all the insulator flashover events during the research period.

It is evident from Table 5-41 that DC-_Glass and DC+_Glass insulators were disconnected from the power supply after four flashovers where the DC-_Porcelain and DC+_Porcelain insulators were disconnected from the power supply after five flashovers and they were disconnected before the Glass insulators. The DC+_EPDM had two flashover events and the DC+_RTV and AC_Glass insulators had one flashover event respectively. All of the insulators energized by DC+ voltage, except DC+_HTV insulator, had flashover events where only the ceramic insulators under DC- voltage had flashover events and only the glass insulator under AC voltage had a flashover event. It is also noticed that the DC-_Glass insulator had the first flashover event.

Table 5-41: Summary of insulator flashover events

Date exploded	Time exploded	DC-_Glass		DC-_Porcelain		DC+_Glass		DC+_Porcelain		DC+_RTV		DC+_EPDM		AC_Glass	
		Peak current [mA]	Date replaced	Peak current [mA]	Date replaced	Peak current [mA]	Date replaced	Peak current [mA]	Date replaced	Peak current [mA]	Date replaced	Peak current [mA]	Date replaced	Peak current [mA]	Date replaced
23-Feb-11	05:40:00	-483	23-Feb-11												
13-Mar-11	01:10:00							718	14-Mar-11						
13-Mar-11	01:50:00	-450	14-Mar-11												
21-Mar-11				X	21-Mar-11										
29-Mar-11	03:30:00			-716	29-Mar-11										
19-Apr-11	07:20:00			-708	19-Apr-11										
03-Oct-11						X	03-Oct-11								
12-Oct-11	03:50:00							490	13-Oct-11						
15-Oct-11	00:50:00					488	17-Oct-11								
24-Oct-11	23:50:00							715	26-Oct-11						
04-Nov-11						X	04-Nov-11								
28-Nov-11	03:00:00			-520	29-Nov-11										
28-Nov-11	21:10:00							533	29-Nov-11						
30-Nov-11	00:10:00	-717	30-Nov-11												
30-Nov-11	04:50:00			-708											
30-Nov-11	05:00:00									719.8	30-Nov-11				
30-Nov-11	05:30:00							650							
01-Dec-11				Disconnected				Disconnected							
06-Dec-11		X													
10-Dec-11	02:50:00					717.8									
12-Dec-11		Disconnected				Disconnected									
01-Jan-12	01:20:00											545	09-Jan-12		
02-Jan-12	04:20:00													716	09-Jan-12
11-Jan-12	04:20:00											588	12-Jan-12		

Note: X indicates that no peak leakage current values and time stamp data were received from an OLCA because it did not log any information.

Furthermore, on 13 March 2011 two flashover incidences occurred within the space of an hour during the early morning hours and on 30 November 2011 four flashover events occurred during the early morning hours. It is suspected that an instantaneous pollution event, e.g. conductive fog, occurred during the early morning hours of the above two dates that triggered the many flashover events. It is also observed that most of the flashovers occurred during the early morning hours, while from Figure 5-3 it is seen that the relative humidity is also the highest during early morning hours. Thus, it may be assumed that the high relative humidity conditions were a contributing factor in the realization of most of the flashover events.

5.4.4 Insulator leakage current analyses

The leakage currents will be analysed as follows:

- The absolute maximum peak leakage current values measured and recorded for each insulator over the research period will be compared amongst each other. Graphs of the actual maximum peak leakage current waveforms with their associated actual voltage waveforms will also be presented and discussed.
- A statistical method was used, which required that the 10 minute interval peak leakage current data for each insulator, be divided into different bins according to their value and the month of occurrence. The peak leakage current data points in each bin were then counted to construct histograms. The corresponding histograms of the different insulators were compared to evaluate the leakage current performance of the different insulators.

5.4.4.1 Maximum absolute peak leakage current values

The maximum absolute peak leakage current values of the EPDM insulators recorded over the research period are given in Table 5-42 where the maximum values are given in **bold** text and the symbol "-" indicates that there were no leakage current values recorded for the specific insulator and timeslot on the OLCA. The actual waveforms of the maximum peak leakage currents and their respective voltages of the EPDM insulators are shown in Figure 5-57, Figure 5-58 and Figure 5-59. Each graph represents a 320 millisecond window.

Table 5-42: Maximum absolute peak leakage current values for EPDM insulators

Maximum absolute peak leakage current values for EPDM insulators						
Date	**Time**	**AC voltage [mA]**	**DC+ voltage [mA]**	**DC- voltage [mA]**	**Rel. Humidity [%]**	**Temperature [°C]**
09-Dec-11 (Day 208)	23h45	**562**	264.95	218.32	80.7	18.7
11-Jan-12 (Day 241)	04h15	-	**588**	200.92	92.5	17.6
12-Jan-12 (Day 242)	21h30	-	3.15	**474.2**	84	23.9

It is observed from Table 5-42 that the EPDM insulator energized under DC+ voltage had the highest maximum absolute peak leakage current value of 588 mA and the insulator energised under DC- voltage had the lowest maximum absolute peak leakage current value of 474.2 mA. It is further noticed that the maximum absolute peak leakage current values occurred when the Relative Humidity at KIPTS was higher than 80% and at night or early mornings when there is no UV-B radiation rays from the sun. The UV-B radiation rays from the sun increase the temperature of the insulator surfaces, which causes evaporation and prevents condensation, which in turn prohibits the forming of a critical wetting condition on the surfaces of the insulators as explained in section 2.4.3.2. Thus, from the abovementioned observations, it may be assumed that critical wetting conditions were formed on the insulator surfaces during the timeslots indicated in Table 5-42, which allowed the flow of maximum peak leakage currents. The critical wetting conditions could have been formed by condensation, deliquescence process, rain drizzle and/or fog.

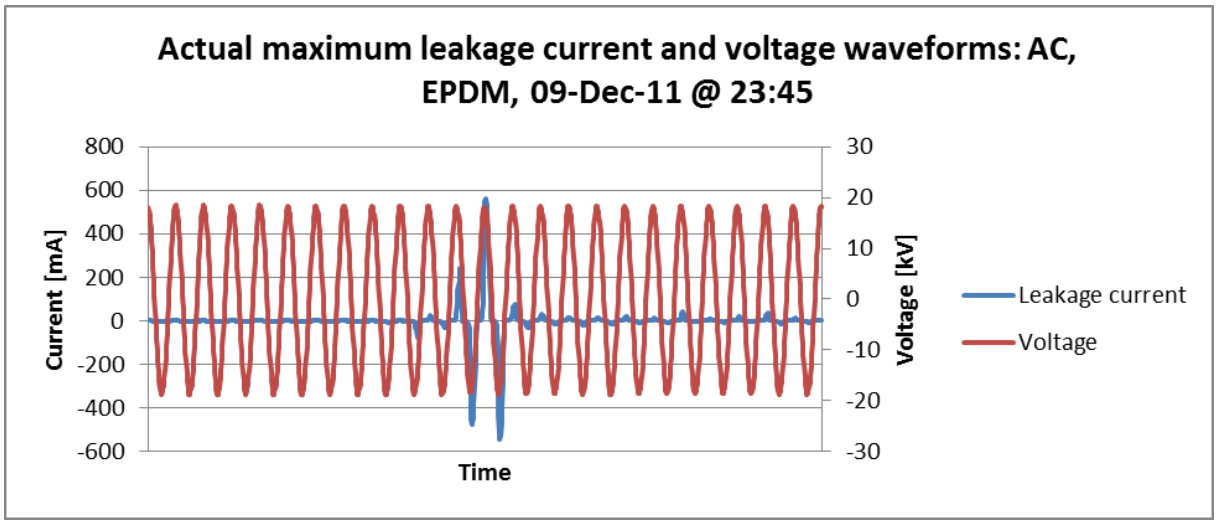

Figure 5-57: Actual maximum leakage current and voltage waveforms of the AC_EPDM insulator

It is observed in Figure 5-57 that the AC leakage current has a non-sinusoidal waveform, which implies that the AC leakage current consists of higher harmonic content as well. Furthermore, it should be noted that no fuse explosion activity occurred in this graph.

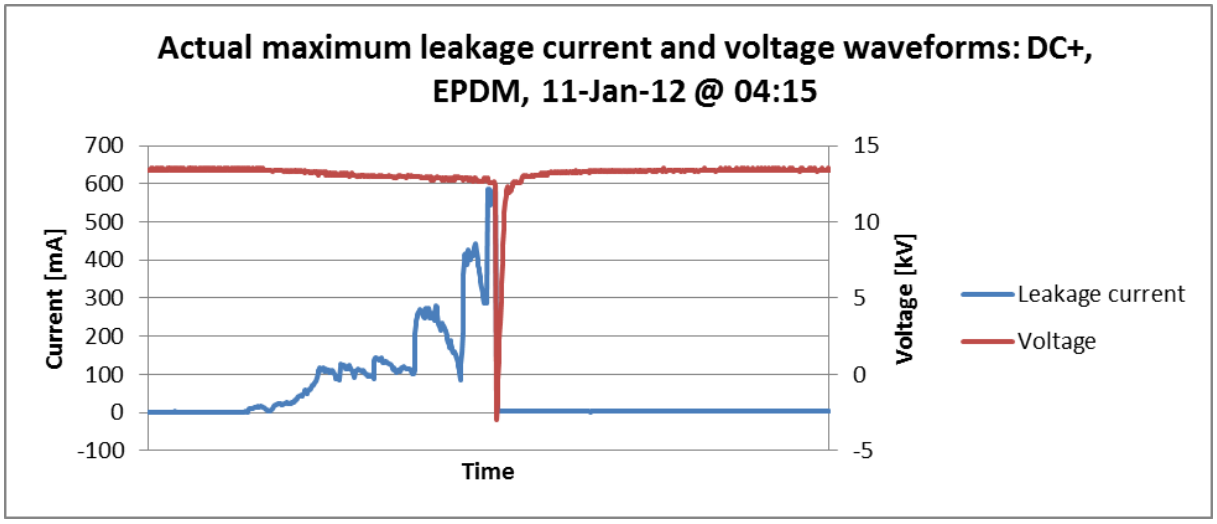

Figure 5-58: Actual maximum leakage current and voltage waveforms of the DC+_EPDM insulator

It is observed in Figure 5-58 that the leakage current of the DC+_EPDM insulator had an approximate linear increase of up to 110 mA and then it became non-linear with very steep increases. The steep increases were small in the beginning of the non-linear portion of the waveform and increase in magnitude closer to the instance when the fuse exploded. It is also observed that the steep increases were followed by approximate linear decreases. The approximate linear increase in the beginning of the graph was caused by the establishment of a leakage current path and an increase of the surface conductivity, which could be caused by continuous wetting of the insulator surface by condensation, deliquescence process, rain drizzle and/or fog. When the leakage current reached a value of approximately 110 mA, as seen in Figure 5-58, the electrolytic conductive layer on the insulator surface vaporizes at the areas with the highest leakage current density, which eventually forms dry bands. It is assumed that there exist multiple leakage current paths on the insulator surface at an instance. Thus, if a dry band forms on one leakage current path, the leakage current flowing on the insulator surface does not necessary reduce to 0 A, but decreases linearly as the conductive layer vaporise. The high voltage differences over the dry bands polarize the air and electrical discharge activities occur which are presented as steep increases in the leakage current plot in Figure 5-58. The small steep increases represent weak electrical discharge activities (small, faint discharges) and the large steep increases represent prominent electrical discharge activities (visible discharges).

In the middle of the graph, the leakage current reduces instantaneously to 0 mA. This happened because the Mace fuse exploded and opened the circuit. The transient response of the smoothing capacitor and the capacitors in parallel with the voltage divider resistors of the AC-to-DC converters reduced the system voltage to -3 kV at the moment at which the fuse exploded, as seen in Figure 5-58. The voltage, then recovers immediately to the value it had before the fuse exploded.

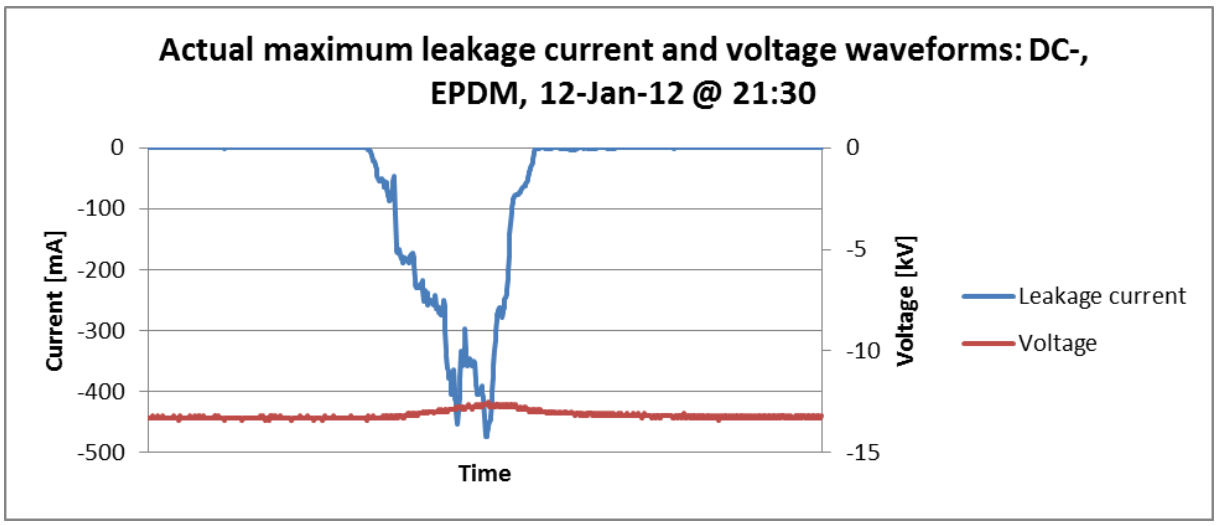

Figure 5-59: Actual maximum leakage current and voltage waveforms of the DC-_EPDM insulator

It is observed in Figure 5-59 that the leakage current of the DC-_EPDM insulator had an approximate linear waveform up to -90 mA and then it became non-linear with very steep decreases. The steep decreases were large in the beginning of the non-linear portion of the waveform, and nearby the maximum negative leakage current peak. Furthermore, it is small in the middle section between the beginning of the non-linear portion and the maximum negative leakage current peak. The steep decreases were caused by electrical discharge activities, where the small steep decreases represent weak electrical discharge activity (small, faint discharges) and the large steep decreases represent prominent electrical discharge activities (visible discharges). The steep increases in the graph represent the extinguished electrical discharge activities. Close to the end of the graph it is observed that the non-linear part of the graph ends at approximately -90 mA and increases approximately linearly to 0 mA. The approximate linear increase to 0 mA represents the drying of the leakage current path through evaporation. Furthermore, it should be noted that no fuse explosion activity occurred in this graph.

The maximum absolute peak leakage current values of the HTV insulators recorded over the research period are given in Table 5-43, where the maximum values are given in **bold** text. The actual waveforms of the maximum peak leakage currents and their respective voltages of the HTV insulators are shown in Figure 5-60, Figure 5-61 and Figure 5-62. Each graph represents a 320 millisecond window.

Table 5-43: Maximum absolute peak leakage current values for HTV insulators

Maximum absolute peak leakage current values for HTV insulators						
Date	**Time**	**AC voltage [mA]**	**DC+ voltage [mA]**	**DC- voltage [mA]**	**Rel. Humidity [%]**	**Temperature [°C]**
08-Nov-11 (Day 177)	17h30	**402.94**	389.76	154.9	90.9	20.2
08-Nov-11 (Day 177)	17h30	402.94	**389.76**	154.9	90.9	20.2
01-Dec-11 (Day 200)	03H28	218.3	278	**349**	96.3	18.2

It is observed from Table 5-43 that the HTV insulator energized under AC voltage had the highest maximum absolute peak leakage current value equal to 402.94 mA and the insulator energised under DC- voltage had the lowest maximum absolute peak leakage current value equal to 349 mA. It is further noticed that the maximum absolute peak leakage current values occurred when the Relative Humidity at KIPTS was higher than 90%. The maximum absolute peak leakage current values of the RTV insulators energized by AC voltage and DC+ voltage occurred on the same day and time, namely 8 November 2011 @ 17h30. It is believed that a special climatic condition, e.g. fog, occurred at KIPTS on that day and time, because all the HTV insulators had relative high absolute peak leakage current values whilst it was day time.

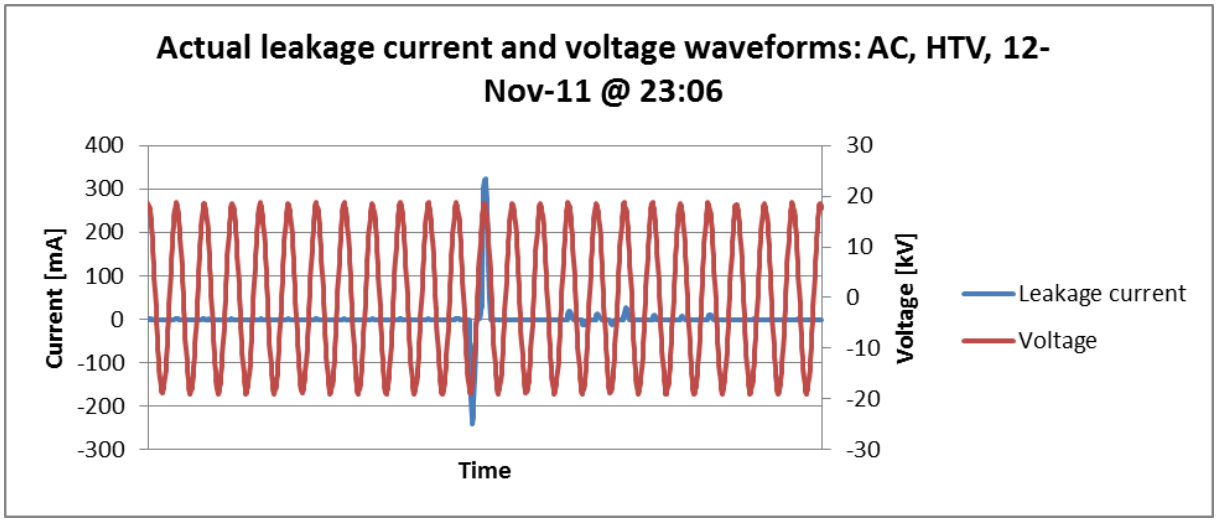

Figure 5-60: Actual leakage current and voltage waveforms of AC_HTV insulator

It is observed in Figure 5-60 that the AC leakage current has a non-sinusoidal waveform, which implies that the AC leakage current consists of higher harmonic content as well. Furthermore, it should be noted that no fuse explosion activity occurred in this graph. It should be noted that the leakage current waveform in Figure 5-60 is not the waveform of the maximum absolute peak leakage current value recorded for the AC_HTV insulator, but the second highest. The actual leakage current waveform of the maximum absolute peak leakage current value was not stored on the OLCA.

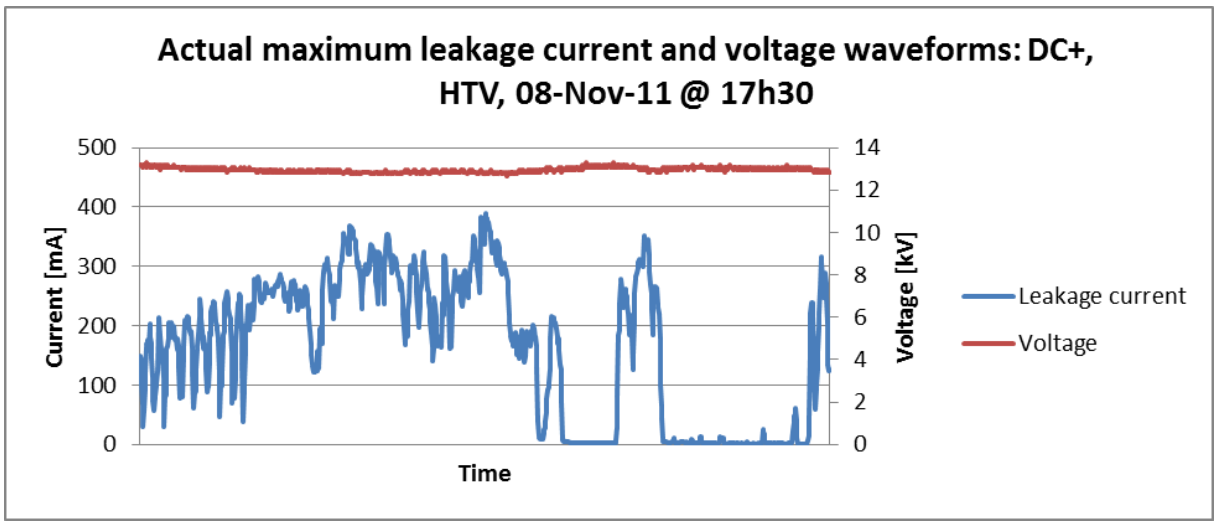

Figure 5-61: Actual maximum leakage current and voltage waveforms of the DC+_HTV insulator

It is observed in Figure 5-61 that the leakage current waveform of the DC+_HTV insulator is non-linear with very steep increases and decreases. The steep increases in the leakage current are caused by electrical discharge activities. The small steep increases represent weak electrical discharge activity (small, faint discharges) and the large steep increases represent prominent electrical discharge activities (visible discharges). The steep decreases represent extinguished electrical discharge activities. The leakage current waveform in Figure 5-61 is mostly characterized by large steep increases and decreases, thus visible discharges. Furthermore, it should be noted that no fuse explosion activity occurred in this graph.

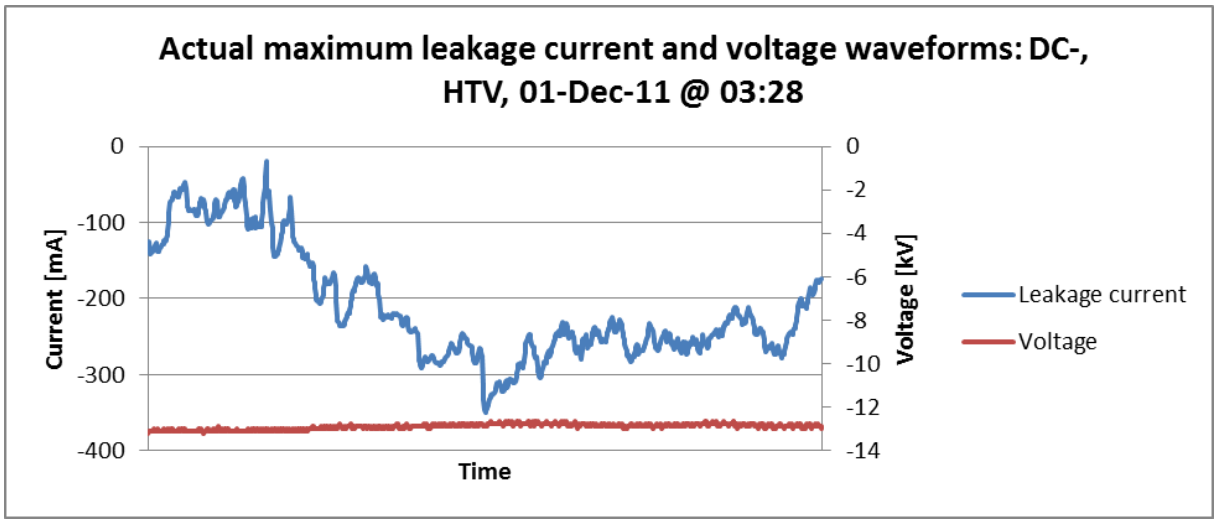

Figure 5-62: Actual maximum leakage current and voltage waveforms of the DC-_HTV insulator

It is observed in Figure 5-62 that the leakage current waveform of the DC-_HTV insulator is non-linear with very steep increases and decreases. The steep decreases in the leakage current are caused by electrical discharge activities. The small steep decreases represent weak electrical discharge activity (small, faint discharges) and the large steep decreases represent prominent electrical discharge activities (visible discharges). The steep increases represent extinguished electrical discharge activities. The leakage current waveform in Figure 5-62 is mostly characterized by small steep increases and decreases, thus small, faint discharges. Furthermore, it should be noted that no fuse explosion activity occurred in this graph.

The maximum absolute peak leakage current values of the RTV insulators recorded over the research period are given in Table 5-44 where the maximum values are given in **bold** text. The actual waveforms of the maximum peak leakage currents and their respective voltages of RTV insulators are shown in Figure 5-63, Figure 5-64 and Figure 5-65. Each graph represents a 320 millisecond window.

Table 5-44: Maximum absolute peak leakage current values for RTV insulators

Maximum absolute peak leakage current values for RTV insulators						
Date	**Time**	**AC voltage [mA]**	**DC+ voltage [mA]**	**DC- voltage [mA]**	**Rel. Humidity [%]**	**Temperature [°C]**
11-Jan-12 (Day 343)	02h26	**241**	0.7	38.9	90.2	18
30-Nov-11 (Day 301)	04h51	1.74	**719.8**	18.75	89.1	19.1
18-Jan-12 (Day 350)	04h36	7.69	0.35	**388**	84.9	26.6

It is observed from Table 5-44 that the RTV insulator energized under DC+ voltage had the highest maximum absolute peak leakage current value equal to 719.8 mA and the one energised under AC voltage had the lowest maximum absolute peak leakage current value equal to 241 mA. It should be noted that the recorded maximum absolute peak leakage current value for DC+ voltages falls within the non-linear portion ($|I_p|$ > 700 mA) of the leakage current measurement system, as explained in section 5.4.1, and that the actual absolute leakage current values might have been much higher. It is further noticed that the maximum absolute peak leakage current values occurred when the Relative Humidity at KIPTS was higher than 84% and during early mornings when there is no UV-B radiation rays from the sun. The UV-B radiation rays from the sun increase the temperature of the insulator surfaces which causes evaporation and prevent condensation, which prohibits the forming of a critical wetting condition on the surface of the insulators as explained in section 2.4.3.2. Thus, from the abovementioned observations, it may be assumed that critical wetting conditions were formed on the insulator surfaces during the timeslots indicated in Table 5-44, which allowed the flow of maximum peak leakage currents. The critical wetting conditions could have been formed by condensation, deliquescence process, rain and/or fog.

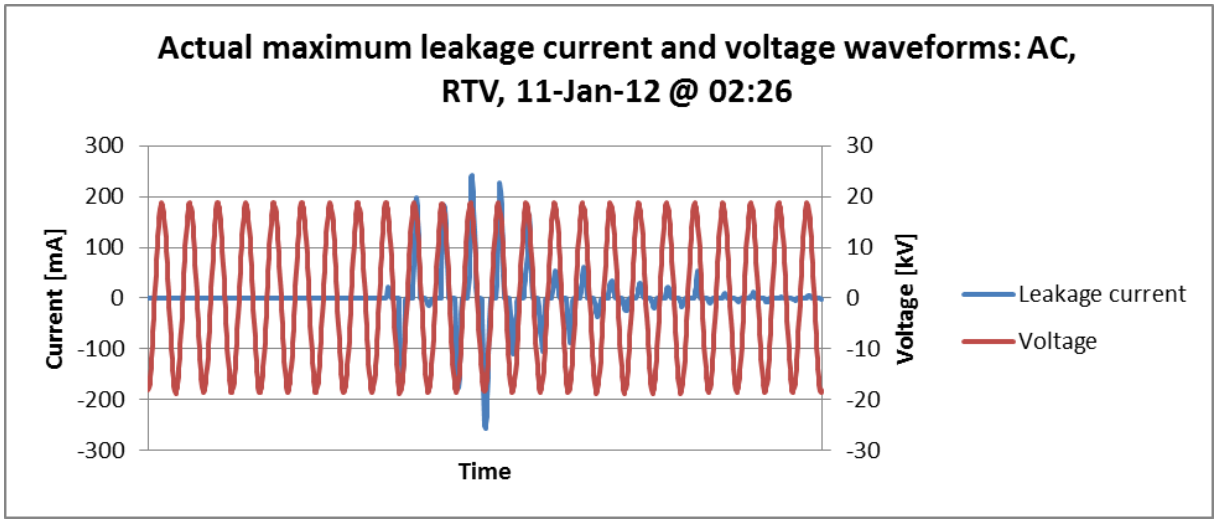

Figure 5-63: Actual maximum leakage current and voltage waveforms of the AC_RTV insulator

It is observed in Figure 5-63 that the AC leakage current has a non-sinusoidal waveform, which implies that the AC leakage current consists of higher harmonic content as well. Furthermore, it should be noted that no fuse explosion activity occurred in this graph.

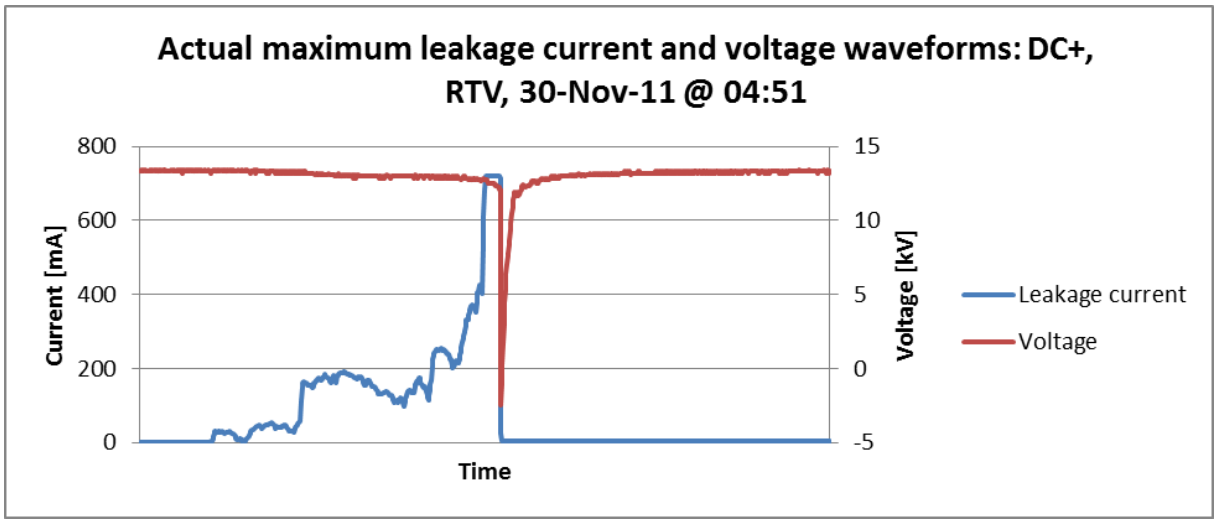

Figure 5-64: Actual maximum leakage current and voltage waveforms of the DC+_RTV insulator

It is observed in Figure 5-64 that the leakage current of the DC+_RTV insulator is non-linear with very steep increases and decreases. The steep increases were small in the beginning of the waveform and it became larger close to the instance when the fuse exploded. The steep increases in the leakage current as observed in Figure 5-64 were caused by electrical discharge activities. The small steep increases represent weak electrical discharge activity (small, faint discharges) and the large steep increases represent prominent electrical discharge activities (visible discharges).

In the middle of the graph the maximum peak leakage current saturated at 719.8 mA and then reduced instantaneously to 0 mA. This happened because the Mace fuse exploded and opened the circuit. The transient response of the smoothing capacitor and the capacitors in parallel with the voltage divider resistors of the AC-to-DC converters reduced the system voltage to -3 kV at the moment the fuse exploded as seen in Figure 5-64. The voltage then immediately recovers to the value it had prior the explosion of the fuse.

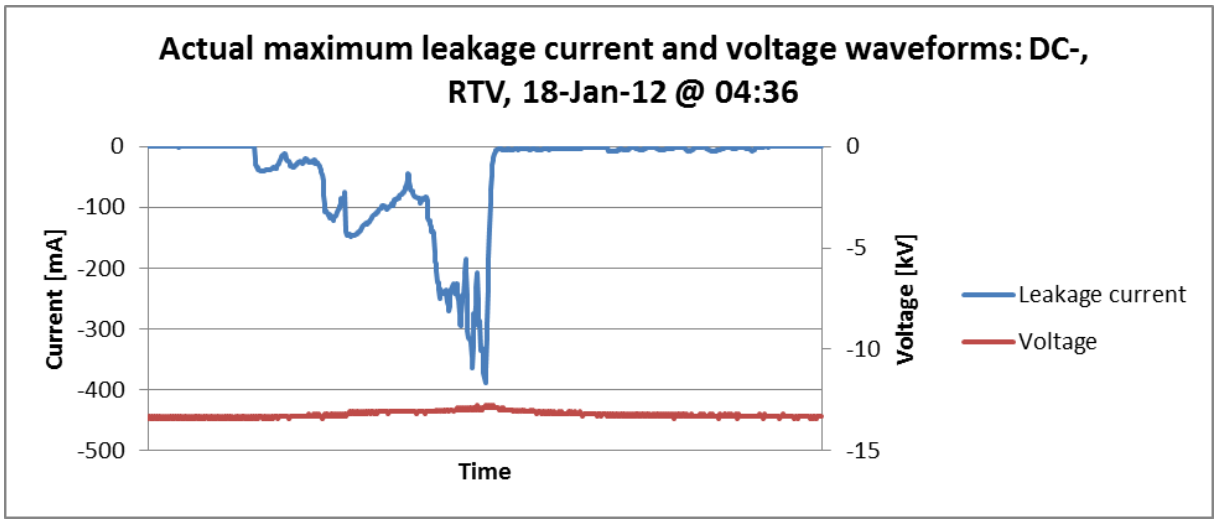

Figure 5-65: Actual maximum leakage current and voltage waveforms of the DC-_RTV insulator

It is observed in Figure 5-65 that the leakage current of the DC-_RTV insulator is non-linear with very steep decreases and increases. The steep decreases were small in the beginning of the waveform and large close to the maximum negative leakage current peak. The steep decreases in the leakage current were caused by electrical discharge activity. The small steep decreases represent weak electrical discharge activity (small, faint discharges) and the large steep decreases represent prominent electrical discharge activities (visible discharges). The steep increases in the graph represent the extinguished electrical discharge activities. Furthermore, it should be noted that no fuse explosion activity occurred in this graph.

The maximum absolute peak leakage current values of the Porcelain insulators recorded over the research period are given in Table 5-45 where the maximum values are given in **bold** text. The actual waveforms of the maximum peak leakage currents and their respective voltages are shown in Figure 5-66, Figure 5-67 and Figure 5-68. Each graph represents a 320 millisecond window.

Table 5-45: Maximum absolute peak leakage current values for Porcelain insulators

Maximum absolute peak leakage current values for Porcelain insulators						
Date	**Time**	**AC voltage [mA]**	**DC+ voltage [mA]**	**DC- voltage [mA]**	**Rel. Humidity [%]**	**Temperature [°C]**
04-Feb-12 (Day 367)	05h21	**386.5**	Disconnected	Disconnected	81.2	22.3
13-Mar-11 (Day 39)	01h01	68.68	**718**	133.23	89.2	14
29-Mar-11 (Day 55)	03h29	-	43	**716**	93.9	15.1

It is observed from Table 5-45 that the maximum absolute peak leakage current values of the Porcelain insulators energized under DC+ and DC- can both be categorized as the highest and the insulator energised under AC voltage had the lowest maximum absolute peak leakage current value equal to 386.5 mA. It should be noted that the recorded maximum absolute peak leakage current values for both DC+ and DC- voltages fall within the non-linear portion ($|I_p| > 700$ mA) of the leakage current measurement system, as explained in section 5.4.1, and that the actual absolute peak leakage current values might have been much higher. Thus, it is not possible to confirm which insulator had the highest absolute leakage current peak value, because both of these values fall within the non-linear section. It is further noticed that the maximum absolute peak leakage current values occurred when the Relative Humidity at KIPTS was higher than 81% and during early mornings when there is no UV-B radiation rays from the sun. The UV-B radiation rays from the sun increase the temperature of the insulator surfaces which causes evaporation and prevents condensation, which in turn prohibits the forming of a critical wetting condition on the surface of the insulators as explained in section 2.4.3.2. Thus, from the abovementioned observations, it may be assumed that critical wetting conditions were formed on the insulator surfaces during the timeslots indicated in Table 5-45, which allowed the flow of maximum peak leakage currents. The critical wetting conditions could have been formed by condensation, deliquescence process, rain and/or fog.

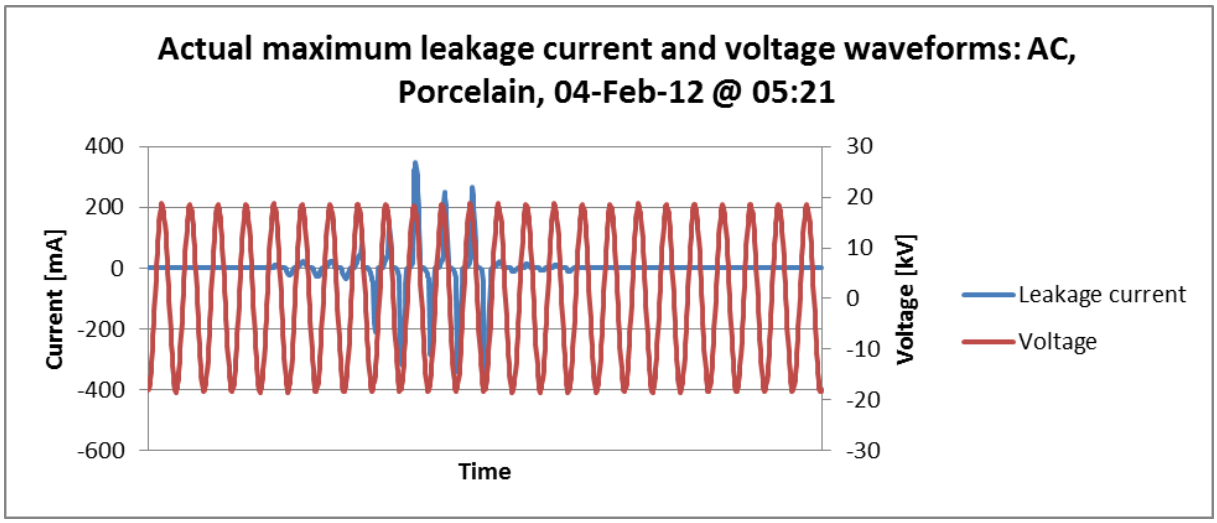

Figure 5-66: Actual maximum leakage current and voltage waveforms of the AC_Porcelain insulator

It is observed in Figure 5-66 that the AC leakage current has a non-sinusoidal waveform, which implies that the AC leakage current consists of higher harmonic content as well. Furthermore, it should be noted that no fuse explosion activity occurred in this graph.

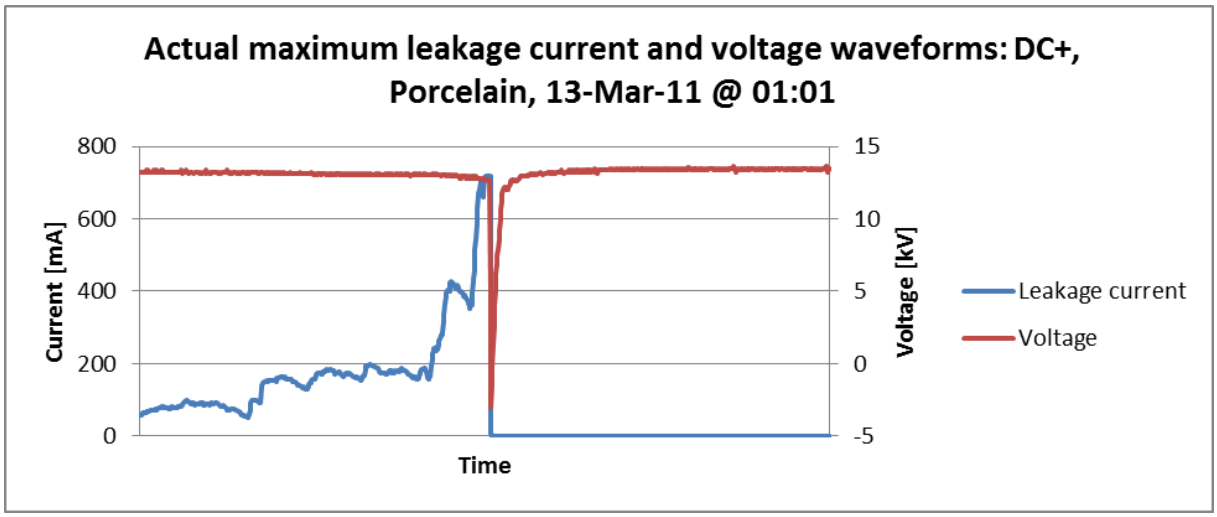

Figure 5-67: Actual maximum leakage current and voltage waveforms of the DC+_Porcelain insulator

It is observed in Figure 5-67 that the leakage current of the DC+_Porcelain insulator had an approximate linear increase of up to 110 mA, followed by an approximate linear decrease to 90 mA and then it became non-linear with very steep increases. It is also observed that the steep increases were followed by approximately linear decreases. The approximate linear increase in the beginning of the graph was caused by the establishment of a leakage current paths and an increase of the surface conductivity which could be caused by continuous wetting of the insulator surface by condensation, deliquescence process, rain drizzle and/or fog. When the leakage current reached a value of approximately 110 mA, the electrolytic conductive layer on the insulator surface vaporizes at the areas with the highest leakage current density which decreases the flow of the leakage current and eventually forms dry bands. It is assumed that there exist multiple leakage current paths on the insulator surface, at an instance. Thus, if a dry band forms on one leakage current path, the leakage current flowing on the insulator surface does not necessarily reduce to 0 A, but decreases linearly as the conductive layer vaporise. The high voltage differences over the dry bands polarize the air and electrical discharge activities occur which are presented as steep increases in the leakage current plot in Figure 5-67. The small steep increases represent weak electrical discharge activities (small, faint discharges) and the large steep increases represent prominent electrical discharge activities (visible discharges).

In the middle of the graph, the maximum peak leakage current saturated at 718 mA and then reduced instantaneously to 0 mA. This happened because the Mace fuse exploded and opened the circuit. The transient response of the smoothing capacitor and the capacitors in

parallel with the voltage divider resistors of the AC-to-DC converters reduced the system voltage to -3 kV at the moment at which the fuse exploded, as seen in Figure 5-67. The voltage recovers then immediately to the value it had before the fuse exploded.

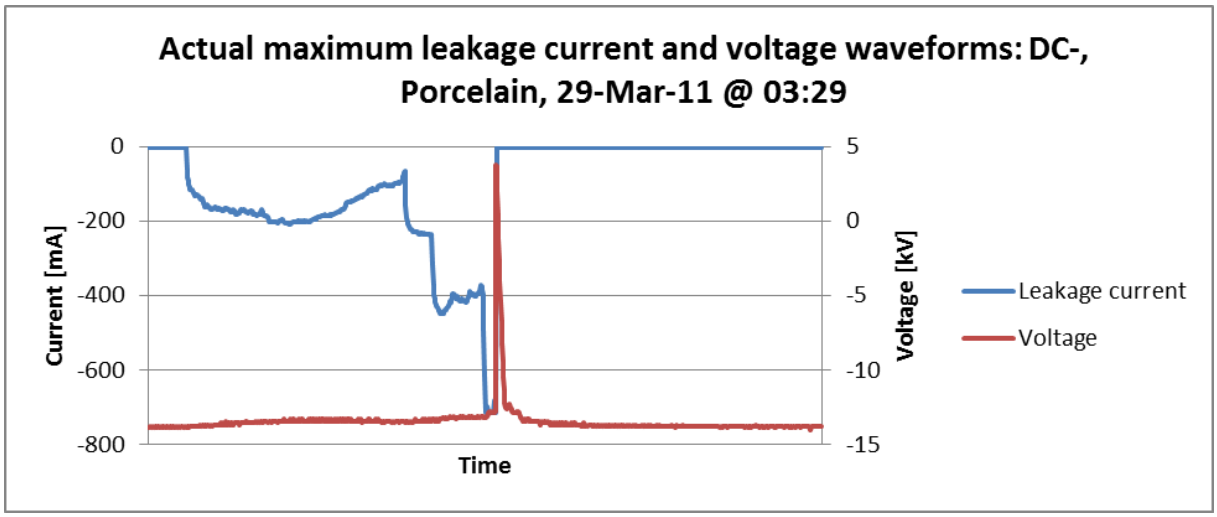

Figure 5-68: Actual maximum leakage current and voltage waveforms of DC-_Porcelain insulator

It is observed in Figure 5-68 that the leakage current of the DC-_Porcelain insulator starts with a very steep decrease to -100 mA and then decreases approximate linearly to -200 mA and then it increases approximate linearly to -100 mA. The approximate linear decrease in the middle section of the graph represents the forming of leakage current paths and an increase of the surface conductivity which could be caused by continuous wetting of the insulator surface by condensation, deliquescence process, rain drizzle and/or fog. When the leakage current reached a value of approximately -200 mA, the electrolytic conductive layer on the insulator surface vaporizes at the areas with the highest leakage current density which decreases the flow of the leakage current and eventually forms dry bands. It is assumed that there exist multiple leakage current paths on the insulator surface, at an instance. Thus, if a dry band forms on one leakage current path, the leakage current flowing on the insulator surface does not necessarily increase to 0 A, but increases linearly as the conductive layer vaporises to a value of -40 mA. The high voltage differences over the dry bands polarize the air and electrical discharge activities occur which are presented as steep decreases in the leakage current plot in Figure 5-68. The small steep decreases represent weak electrical discharge activities (small, faint discharges) and the large steep decreases represent prominent electrical discharge activities (visible discharges).

In the middle of the graph the maximum peak leakage current saturated at -716 mA and then increased instantaneously to 0 mA. This happened because the Mace fuse exploded and opened the circuit. The transient response of the smoothing capacitor and the capacitors in parallel with the voltage divider resistors of the AC-to-DC converters increased the system voltage to 3 kV at the exact moment at which the fuse exploded, as seen in Figure 5-68. The voltage recovers then immediately to the value it had before the fuse exploded.

The maximum absolute peak leakage current values of the Glass insulators recorded over the research period are given in Table 5-46 where the maximum values are given in **bold** text. The actual waveforms of the maximum peak leakage currents and their respective voltages are shown in Figure 5-69, Figure 5-70 and Figure 5-71. Each graph represents a 320 millisecond window.

Table 5-46: Maximum absolute peak leakage current values for Glass insulators

Maximum absolute peak leakage current values for Glass insulators						
Date	**Time**	**AC voltage [mA]**	**DC+ voltage [mA]**	**DC- voltage [mA]**	**Rel. Humidity [%]**	**Temperature [°C]**
02-Jan-12 (Day 334)	04h20	**716**	Disconnected	Disconnected	91.2	21.7
10-Dec-11 (Day 311)	02h42	2.8	**717.8**	Disconnected	86.8	17.9
30-Nov-11 (Day 301)	00h02	1.4	42.91	**717**	84.6	23.5

It is observed from Table 5-46 that the maximum absolute peak leakage current values of Glass insulators energized under AC, DC+ and DC- can all be categorized as the highest. It should be noted that the recorded maximum absolute peak leakage current values for AC, DC+ and DC- voltages fall within the non-linear portion ($|I_p| > 700$ mA) of the leakage current measurement system, as explained in section 5.4.1, and that the actual absolute peak leakage current values might have been much higher. Thus, it is not possible to confirm which insulator had the highest maximum absolute peak leakage current value, since all of these values fall within the non-linear section. It is further noticed that the maximum absolute peak leakage current values occurred when the Relative Humidity at KIPTS was higher than 84% and during early mornings when there is no UV-B radiation rays from the sun. The UV-B radiation rays from the sun increase the temperature of the insulator surfaces, which causes evaporation and prevents condensation which prohibits the forming of a critical wetting condition on the surface of the insulators, as explained in section 2.4.3.2. Thus, from the abovementioned observations, it may be assumed that critical wetting conditions were formed

on the insulator surfaces during the timeslots indicated in Table 5-46, which allowed the flow of maximum peak leakage currents. The critical wetting conditions could have been formed by condensation, deliquescence process, rain and/or fog.

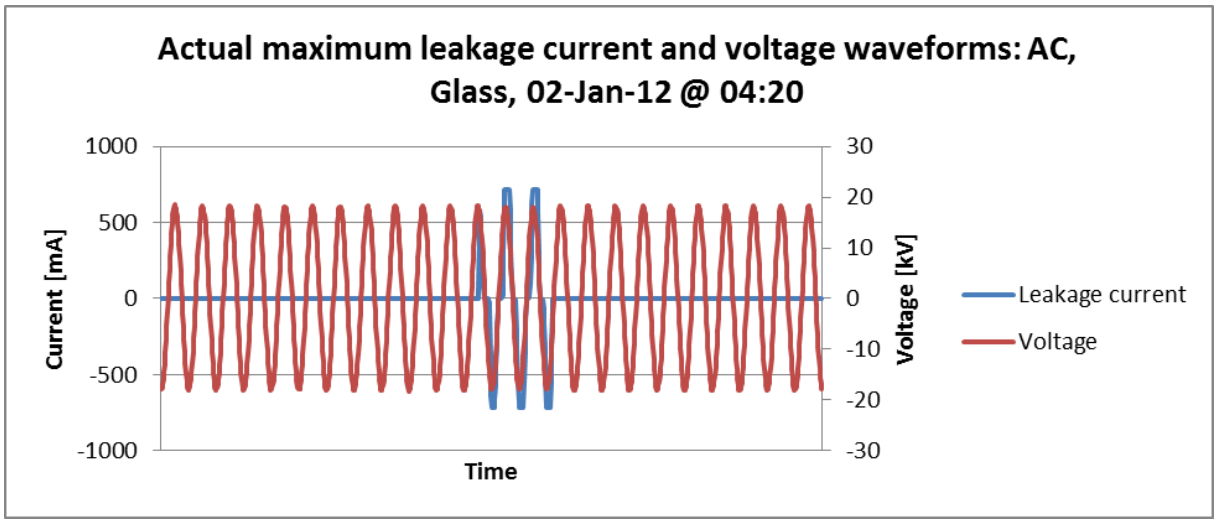

Figure 5-69: Actual maximum leakage current and voltage waveforms of the AC_Glass insulator

It is observed in Figure 5-69 that the AC leakage current has a non-sinusoidal waveform, which implies that the AC leakage current consists of higher harmonic content as well. It is further observed that the maximum peak leakage current saturated at a value of 716 mA.

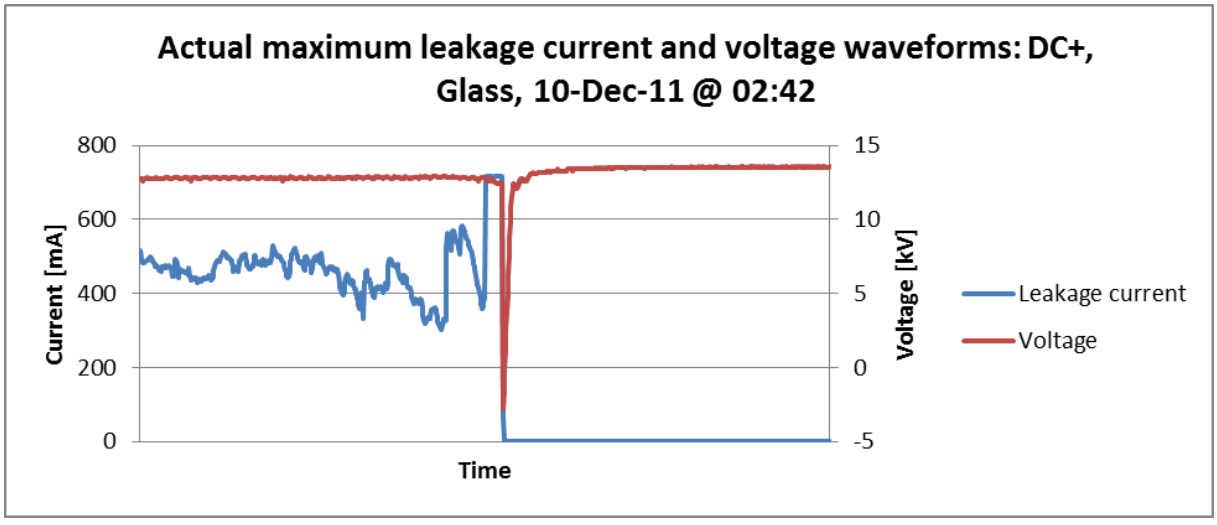

Figure 5-70: Actual maximum leakage current and voltage waveforms of the DC+_Glass insulator

It is observed in Figure 5-70 that the leakage current of the DC+_Glass insulator had a non-linear waveform with an approximate value of 500 mA at the beginning of the graph. It fluctuated around that value with small steep increases and decreases. The steep increases

became larger nearby the instance when the fuse exploded. The steep increases in the leakage current were caused by electrical discharge activity where the small steep increases represents weak electrical discharge activity (small, faint discharges) and the large steep increases represent prominent electrical discharge activities (visible discharges).

In the middle of the graph, the maximum peak leakage current saturated at 717.8 mA and then reduced instantaneously to 0 mA. This happened because the Mace fuse exploded and opened the circuit. The transient response of the smoothing capacitor and the capacitors in parallel with the voltage divider resistors of the AC-to-DC converters reduced the system voltage to -3 kV at the moment the fuse exploded as seen in Figure 5-70. The voltage then recovers immediately to the value it had before the fuse exploded.

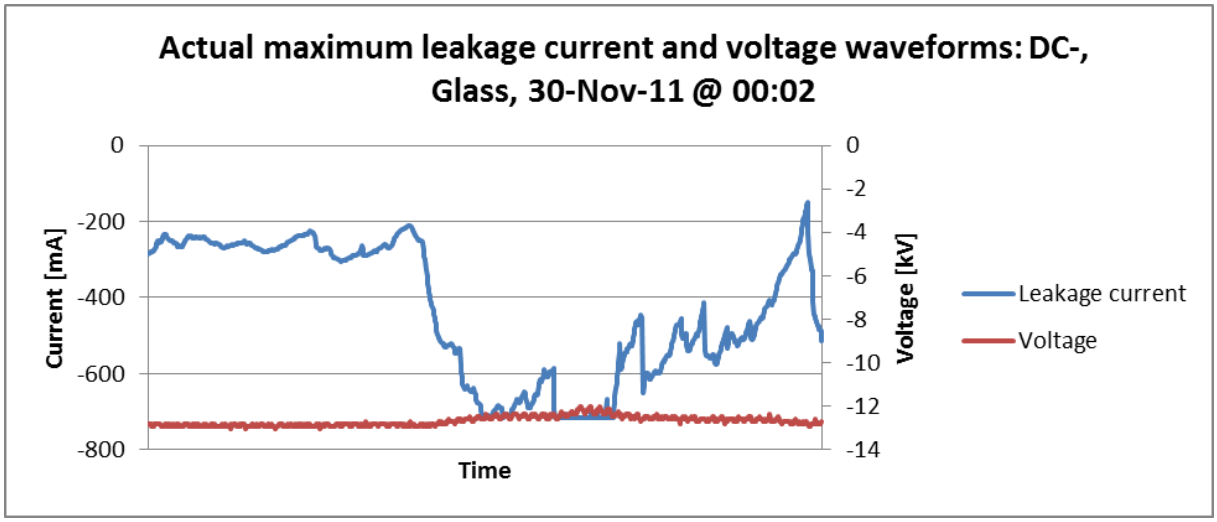

Figure 5-71: Actual maximum leakage current and voltage waveforms of the DC-_Glass insulator

It is observed in Figure 5-71 that the leakage current of the DC-_Glass insulator had a non-linear waveform with an approximate value of -250 mA at the beginning of the graph. It fluctuated around that value with small steep increases and decreases. The steep decreases became large nearby the maximum negative peak leakage current. The steep decreases in the leakage current were caused by electrical discharge activity. The small steep decreases represent weak electrical discharge activity (small, faint discharges) and the large steep decreases represent prominent electrical discharge activities (visible discharges). The steep increases in the graph represent the extinguished electrical discharge activities and the approximate linear increases near the end of the graph represent the evaporation process of the solution layer responsible for the leakage current paths. In the middle of the graph the

maximum peak leakage current saturated at -717 mA and it should be noted that no fuse explosion activity occurred in this graph.

5.4.4.2 Statistical leakage current analysing method

The insulator peak leakage current data were measured and recorded with the OLCA and the recorded data was divided into bins as explained in section 4.4 and plotted as illustrated in Figure 5-72. The peak leakage current measured data of the AC voltage were divided into positive peaks and negative peaks, so as to observe if there is a significant difference between AC positive and AC negative peak leakage currents. AC positive peak leakage currents are referred to as AC+ and AC negative peak leakage currents are referred to as AC- in Figure 5-72 and Table 5-47 up to Table 5-50.

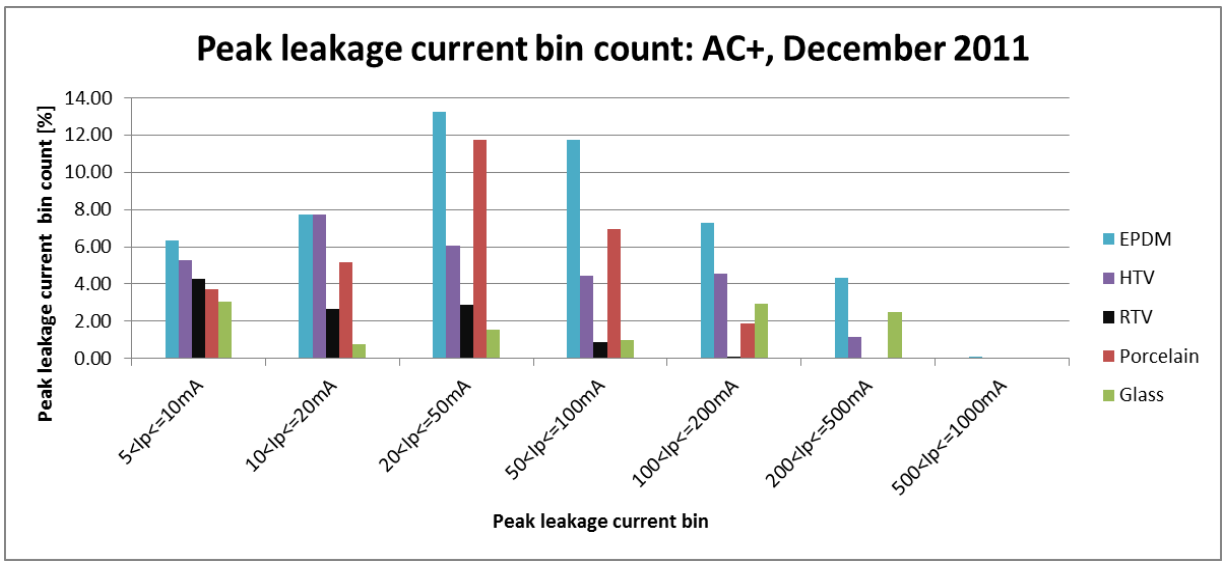

Figure 5-72: AC positive peak leakage current bin count for December 2011

The Plots of bin counts as illustrated in Figure 5-72 were compiled for each excitation voltage and for each month. Please refer to Annex C for a complete set of leakage current bin count graphs.

These graphs were used to compare the leakage current performance of different insulators per excitation voltage. The leakage currents were compared for low peak leakage current values, from 0 mA up to 100 mA, and for high peak leakage current values, from 100 mA up to 1000 mA. The reason for this comparison split is that the electrical discharge activity

responsible for low peak leakage current values are more consistent on the surface of the insulators and mostly responsible for material erosion.

The EPDM and HTV insulators were compared to each other and the RTV, Porcelain and Glass insulators were compared to each other per excitation voltage. The split in comparison was mainly because of the different installation dates as explained in section 3.3.

A ranking system was used to compare the leakage current performance of the insulators. The insulator which showed the best leakage current performance per specific criteria was ranked first and received a 1. The insulator with the second best leakage current performance received a 2 and so forth. The term best leakage current performance refers to the insulator with the lowest absolute peak leakage current values and worst leakage current performance refers to the insulator with the highest absolute peak leakage current values. If two or more insulators had the same leakage current performance, all of them received the same ranking and the insulator with the next best leakage current performance, received the ranking n+1 where n represents the number of insulators with the same leakage current performance. These values are summarised in Table 5-47 up to Table 5-50. The ranking that occurred most frequently per insulator, in the above tables, was used as the final ranking for that insulator. If more than one insulator had the same ranking as their most frequent ranking, then their other rankings were taken into account in order to determine the overall ranking of those insulators.

It is observed from Table 5-47 that the HTV insulators had better leakage current performance than the EPDM insulators for low peak leakage current values for all excitation voltages. This result correlates with the light erosion and erosion observations result given in Table 5-20 where it is evident that the HTV insulators had fewer light erosion and erosion observations than the EPDM insulators for all excitation voltages.

It is observed from Table 5-48 that the HTV insulators had better leakage current performance than the EPDM insulators for high peak leakage current values for all excitation voltages. This result also correlates with the light erosion and erosion observations result given in Table 5-20 where it is evident that the HTV insulators had fewer light erosion and erosion observations than the EPDM insulators for all excitation voltages.

Table 5-47: Comparison between EPDM and HTV insulators in terms of the bin counts for $I_p \leq 100$ mA

Comparison between EPDM and HTV insulators in terms of the bin counts for Ip ≤ 100 mA								
Month	**AC+**		**AC-**		**DC+**		**DC-**	
	EPDM	**HTV**	**EPDM**	**HTV**	**EPDM**	**HTV**	**EPDM**	**HTV**
Feb-11	Not connected		Not connected		Not connected		Not connected	
Mar-11	Not connected		Not connected		Not connected		Not connected	
Apr-11	Not connected		Not connected		Not connected		Not connected	
May-11	2	1	2	1	2	1	2	1
Jun-11	2	1	2	1	2	1	2	1
Jul-11	2	1	2	1	2	1	2	1
Aug-11	2	1	2	1	2	1	2	1
Sep-11	2	1	2	1	2	1	2	1
Oct-11	2	1	2	1	2	1	2	1
Nov-11	2	1	2	1	2	1	2	1
Dec-11	2	1	2	1	2	1	2	1
Jan-12	1	2	1	2	1	2	1	2
Feb-12	2	1	2	1	1	2	2	1
Overall ranking	**2**	**1**	**2**	**1**	**2**	**1**	**2**	**1**
Ranking interpretation	**Worst**	**Best**	**Worst**	**Best**	**Worst**	**Best**	**Worst**	**Best**

Table 5-48: Comparison between EPDM and HTV insulators in terms of the bin counts for $I_p > 100$ mA

Comparison between EPDM and HTV insulators in terms of the bin counts for Ip > 100 mA								
Month	**AC+**		**AC-**		**DC+**		**DC-**	
	EPDM	**HTV**	**EPDM**	**HTV**	**EPDM**	**HTV**	**EPDM**	**HTV**
Feb-11	Not connected		Not connected		Not connected		Not connected	
Mar-11	Not connected		Not connected		Not connected		Not connected	
Apr-11	Not connected		Not connected		Not connected		Not connected	
May-11	1	1	1	1	2	1	1	1
Jun-11	2	1	2	1	2	1	2	1
Jul-11	1	1	1	1	1	1	1	1
Aug-11	2	1	2	1	1	1	1	1
Sep-11	2	1	2	1	2	1	1	1
Oct-11	2	1	2	1	2	1	2	1
Nov-11	2	1	2	1	2	1	2	1
Dec-11	2	1	2	1	2	1	2	1
Jan-12	2	1	2	1	1	2	2	1
Feb-12	2	1	2	1	1	2	2	1
Overall ranking	**2**	**1**	**2**	**1**	**2**	**1**	**2**	**1**
Ranking interpretation	**Worst**	**Best**	**Worst**	**Best**	**Worst**	**Best**	**Worst**	**Best**

Table 5-49: Comparison between Porcelain, RTV and Glass insulators in terms of the bin counts for $I_p \leq 100$ mA

Comparison between Porcelain, RTV and Glass insulators in terms of the bin counts for Ip ≤ 100 mA												
Month	**AC+**			**AC-**			**DC+**			**DC-**		
	Porcelain	**RTV**	**Glass**	**Porcelain**	**RTV**	**Glass**	**Porcelain**	**RTV**	**Glass**	**Porcelain**	**RTV**	**Glass**
Feb-11	3	2	1	3	2	1	3	2	1	3	1	2
Mar-11	3	2	1	3	2	1	3	1	2	3	1	2
Apr-11	3	2	1	3	2	1	1	2	3	3	1	2
May-11	3	2	1	3	2	1	2	1	3	2	1	3
Jun-11	3	2	1	3	2	1	2	1	3	2	1	3
Jul-11	3	2	1	3	2	1	2	1	3	3	1	2
Aug-11	3	2	1	3	2	1	2	1	3	2	1	3
Sep-11	3	2	1	3	2	1	2	1	3	3	1	2
Oct-11	3	2	1	3	2	1	2	1	3	3	1	2
Nov-11	3	2	1	3	2	1	2	1	3	3	2	1
Dec-11	3	2	1	3	2	1	Glass and porcelain disconnected			Glass and porcelain disconnected		
Jan-12	2	3	1	2	3	1	Glass and porcelain disconnected			Glass and porcelain disconnected		
Feb-12	3	2	1	3	2	1	Glass and porcelain disconnected			Glass and porcelain disconnected		
Overall ranking	**3**	**2**	**1**	**3**	**2**	**1**	**2**	**1**	**3**	**3**	**1**	**2**
Ranking interpretation	**Worst**	**2nd Best**	**Best**	**Worst**	**2nd Best**	**Best**	**2nd Best**	**Best**	**Worst**	**Worst**	**Best**	**2nd Best**

Table 5-50: Comparison between Porcelain, RTV and Glass insulators in terms of the bin counts for I_p > 100 mA

Comparison between Porcelain, RTV and Glass insulators in terms of the bin counts for Ip > 100 mA												
Month	**AC+**			**AC-**			**DC+**			**DC-**		
	Porcelain	**RTV**	**Glass**	**Porcelain**	**RTV**	**Glass**	**Porcelain**	**RTV**	**Glass**	**Porcelain**	**RTV**	**Glass**
Feb-11	3	1	1	3	1	1	3	1	2	3	1	1
Mar-11	3	1	1	3	1	1	3	1	2	3	1	2
Apr-11	3	1	1	3	1	1	3	1	2	2	1	3
May-11	1	1	1	1	1	1	1	1	1	1	1	1
Jun-11	1	1	1	1	1	1	1	1	1	1	1	3
Jul-11	1	1	1	1	1	1	1	1	1	1	1	1
Aug-11	1	1	1	1	1	1	1	1	1	1	1	1
Sep-11	1	1	1	1	1	1	1	1	1	1	1	3
Oct-11	1	1	3	1	1	3	2	1	3	3	1	2
Nov-11	3	1	2	3	1	2	3	1	2	2	1	3
Dec-11	2	1	3	2	1	3	Glass and porcelain disconnected			Glass and porcelain disconnected		
Jan-12	3	2	1	3	2	1	Glass and porcelain disconnected			Glass and porcelain disconnected		
Feb-12	3	1	1	3	1	1	Glass and porcelain disconnected			Glass and porcelain disconnected		
Overall ranking	**3**	**1**	**2**	**3**	**1**	**2**	**3**	**1**	**2**	**2**	**1**	**3**
Ranking interpretation	**Worst**	**Best**	**2nd Best**	**Worst**	**Best**	**2nd Best**	**Worst**	**Best**	**2nd Best**	**2nd Best**	**Best**	**Worst**

It is observed from Table 5-49 that the Glass insulator had the best low peak leakage current performance for the AC excitation voltage and the RTV insulators had the best low peak leakage current performance for DC+ and DC- excitation voltages. Furthermore, it is observed that the Porcelain insulators had the worst low peak leakage current performance for AC and DC- excitation voltages where the Glass insulator had the worst low peak leakage current performance for the DC+ excitation voltage. If the light erosion and erosion results for Porcelain insulators, as given in Table 5-21, are not included, then the low peak leakage current result correlates with the light erosion and erosion observations result as given in Table 5-21. The reason for excluding Porcelain insulators from this comparison is that they normally do not erode.

It is observed from Table 5-50 that the RTV insulators had the best high peak leakage current performance for all excitation voltages. Furthermore, it is observed that the Porcelain insulators had the worst high peak leakage current performance for AC and DC+ excitation voltages where the Glass insulator had the worst high peak leakage current performance for the DC- excitation voltage. The high peak leakage current results do not correlate with the light erosion and erosion observations even if the light erosion and erosion results for Porcelain insulators, as given in Table 5-21, were not included.

The ranking of the excitation voltages in terms of their leakage current performance per insulator material was also considered important. For this reason, plots of bin counts as illustrated in Figure 5-73 were compiled for each insulator material per month, wherein the leakage currents generated by the different excitation voltages were compared. Please refer to Annex C for a complete set of leakage current bin count graphs.

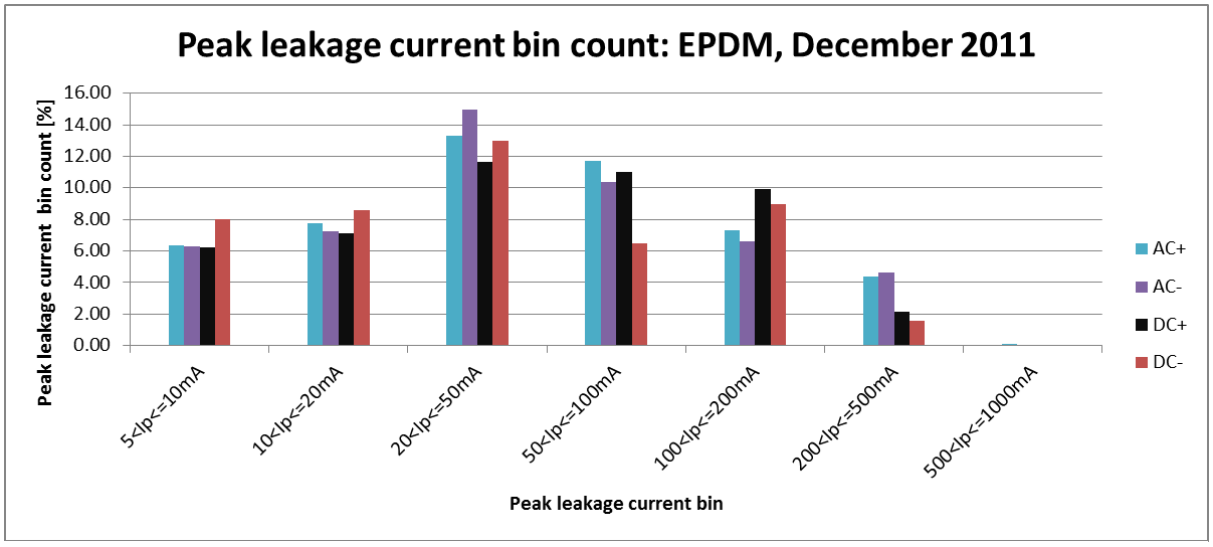

Figure 5-73: Peak leakage current bin count for EPDM insulators during December 2011

These graphs were used to compare the leakage current performance of the three different excitation voltages on the different insulator materials. The leakage currents were compared for low peak leakage current values, from 0 mA up to 100 mA, and for high peak leakage current values, from 100 mA up to 1000 mA. The reason for this comparison split is that the electrical discharge activity responsible for low leakage current peak values are more consistent on the surface of the insulators and mostly responsible for material erosion.

The same ranking system used to compare the leakage current performance on the different insulators per excitation voltage, was used to compare the leakage current performance of the three different excitation voltages on the different insulator materials. The excitation voltage that had the best leakage current performance per specific criteria was ranked first and received a 1. The excitation voltage with the second best leakage current performance received a 2 and so forth. The term best leakage current performance refers to the excitation voltage with the lowest absolute peak leakage current values and worst leakage current performance refers to the excitation voltage with the highest absolute peak leakage current values. If two or more excitation voltages had the same leakage current performance, all of them received the same ranking and the excitation voltage with the next best leakage current performance, received the ranking n+1 where n represents the number of excitation voltages with the same leakage current performance. These values are summarised in Table 5-51 and Table 5-52. The rating that occurred most frequently per excitation voltage was used as the final rating for that excitation voltage.

Table 5-51: Comparison between different excitation voltages in terms of the bin counts for peak leakage currents smaller than or equal to 100 mA

Comparison between different excitation voltages in terms of the bin counts for Ip ≤ 100 mA																				
Month	EPDM				HTV				RTV				Porcelain				Glass			
	AC+	AC-	DC+	DC-	AC+	AC-	DC+	DC-	AC+	AC-	DC+	DC-	AC+	AC-	DC+	DC-	AC+	AC-	DC+	DC-
Feb-11									2	3	4	1	2	1	3	4	2	1	4	3
Mar-11									2	3	4	1	2	1	3	4	1	2	4	3
Apr-11									2	1	4	3	2	1	4	3	2	1	4	3
May-11	3	2	4	1	3	4	1	2	4	3	2	1	3	2	4	1	1	2	4	3
Jun-11	3	2	4	1	4	3	1	2	4	3	2	1	2	1	4	3	1	1	4	3
Jul-11	3	2	4	1	4	3	2	1	3	4	2	1	1	2	4	3	1	1	4	3
Aug-11	4	3	2	1	3	4	1	2	3	4	2	1	4	3	2	1	1	1	3	4
Sep-11	4	3	1	2	3	4	2	1	2	3	4	1	4	3	2	1	1	1	4	3
Oct-11	3	2	1	4	2	1	3	4	2	3	4	1	1	2	3	4	1	2	4	3
Nov-11	3	2	1	4	2	1	3	4	2	3	4	1	2	1	4	3	1	1	4	3
Dec-11	4	3	1	2	2	1	3	4	4	3	1	2	0	0	***Removed***		0	0	***Removed***	
Jan-12	3	2	1	4	1	2	3	4	3	4	1	2	0	0	***Removed***		0	0	***Removed***	
Feb-12	3	4	1	2	3	2	4	1	2	1	3	4	0	0	***Removed***		0	0	***Removed***	
Overall ranking	**4**	**3**	**1**	**2**	**4**	**3**	**2**	**1**	**2**	**3**	**4**	**1**	**2**	**1**	**4**	**3**	**1**	**2**	**4**	**3**
Ranking interpretation	**Worst**	**2nd Worst**	**Best**	**2nd Best**	**Worst**	**2nd Worst**	**2nd Best**	**Best**	**2nd Best**	**2nd Worst**	**Worst**	**Best**	**2nd Best**	**Best**	**Worst**	**2nd Worst**	**Best**	**2nd Best**	**Worst**	**2nd Worst**

Table 5-52: Comparison between different excitation voltages in terms of the bin counts for peak leakage currents greater than 100 mA

Comparison between different excitation voltages in terms of the bin counts for Ip > 100 mA																				
Month	**EPDM**				**HTV**				**RTV**				**Porcelain**				**Glass**			
	AC+	**AC-**	**DC+**	**DC-**	**AC+**	**AC-**	**DC+**	**DC-**	**AC+**	**AC-**	**DC+**	**DC-**	**AC+**	**AC-**	**DC+**	**DC-**	**AC+**	**AC-**	**DC+**	**DC-**
Feb-11									1	1	1	1	1	1	3	4	1	1	3	4
Mar-11									1	1	4	1	2	1	3	4	1	1	3	4
Apr-11									1	1	4	3	2	1	4	3	1	1	3	4
May-11	1	1	1	1	2	2	2	1	1	1	1	1	1	1	1	1	1	1	1	1
Jun-11	4	3	1	1	3	3	1	1	1	1	1	1	1	1	1	1	1	1	3	4
Jul-11	1	1	1	1	1	1	1	1	1	1	1	1	1	1	1	1	1	1	1	1
Aug-11	3	3	1	1	1	1	1	1	1	1	1	1	1	1	1	1	1	1	1	1
Sep-11	3	4	2	1	1	1	1	1	1	1	1	1	1	1	1	1	1	1	1	1
Oct-11	3	4	1	2	2	3	4	1	1	1	4	1	1	1	4	3	3	2	4	1
Nov-11	3	4	2	1	4	3	2	1	2	3	4	1	1	2	4	3	1	1	3	4
Dec-11	3	4	2	1	3	4	2	1	4	3	1	1	0	0	***Removed***		0	0	***Removed***	
Jan-12	4	3	1	2	3	2	4	1	2	3	1	4	0	0	***Removed***		0	0	***Removed***	
Feb-12	3	4	1	2	4	3	2	1	1	1	1	4	0	0	***Removed***		0	0	***Removed***	
Overall ranking	**3**	**4**	**1**	**1**	**4**	**3**	**2**	**1**	**1**	**2**	**4**	**3**	**2**	**1**	**4**	**3**	**2**	**1**	**3**	**4**
Ranking interpretation	**2nd Worst**	**Worst**	**Best**	**Best**	**Worst**	**2nd Worst**	**2nd Best**	**Best**	**Best**	**2nd Best**	**Worst**	**2nd Worst**	**2nd Best**	**Best**	**Worst**	**2nd Worst**	**2nd Best**	**Best**	**2nd Worst**	**Worst**

If more than one insulator had the same ranking as their most frequent ranking, then their other rankings were taken into account in order to determine the overall ranking of those insulators.

It is observed from Table 5-51 that the DC+ excitation voltage had the best low peak leakage current performance for the EPDM insulators and the DC- excitation voltage had the best low peak leakage current performance for HTV and RTV insulators where the AC excitation voltage had the best low peak leakage current performance for Porcelain and Glass insulators. Furthermore, it is observed that the AC excitation voltage had the worst low peak leakage current performance for EPDM and HTV insulators where the DC+ excitation voltage had the worst low peak leakage current performance for RTV, Porcelain and Glass insulators. Thus, the low peak leakage current results do not correlate with the light erosion and erosion observations. As observed in Table 5-20 and Table 5-21, the AC excitation voltages had the fewest light erosion and erosion observations for all the insulators, but in the above discussions it was mentioned that the AC excitation voltage had the worst low peak leakage current performance for EPDM and HTV insulators.

It is observed from Table 5-52 that the DC+ and DC- excitation voltages had the best high peak leakage current performance for the EPDM insulators and the DC- excitation voltage had the best high peak leakage current performance for HTV insulator where the AC excitation voltage had the best high peak leakage current performance for RTV, Porcelain and Glass insulators. Furthermore, it is observed that the AC excitation voltage had the worst high peak leakage current performance for EPDM and HTV insulators and the DC+ excitation voltage had the worst high peak leakage current performance for RTV and Porcelain insulators where DC- excitation voltage had the worst high peak leakage current performance for the Glass insulators. Thus, the high peak leakage current results do not correlate with the light erosion and erosion observations, as observed in Table 5-20 and Table 5-21, where it is evident that the AC excitation voltages had the fewest light erosion and erosion observations for all the insulators.

In summary, it is observed that there exists a correlation between low peak leakage current observations and light erosion and erosion observations when the insulators are compared within a specific excitation voltage. However, no correlation exists when the insulators are compared across excitation voltages. This is due to the prominent light erosion and erosion

observations on the DC excitation voltages. Furthermore, it is observed that a generalization regarding leakage current performance of the different excitation voltages on the insulator materials is not possible, because all three excitation voltages have best and worst leakage current performances. It is also observed that the AC- leakage current performance is better than the AC+ leakage current performance; however the difference is not significant.

5.5 Electrical discharge activity observations

The electrical discharge activity observations were conducted during the night time, as explained in section 4.5 with the CoroCAM 1 and Sony camcorder. The features of these cameras were listed in sections 3.4.2 and 3.4.3 respectively. The activities observed with the CoroCAM 1 camera will be discussed in this section. The CoroCAM 1 camera captured all electrical discharge activities present on the insulators, visible or not visible to a human eye, whereas the Sony camcorder captured only the electrical discharge activities visible to a human eye. Because of this duplication it was decided not to include the activities observed by the Sony camcorder in this section.

For this research, it was important to know which insulator had the first electrical discharge activity and the development of the electrical discharge activity leading up to dry band discharges (DBD). In Table 5-53 and Table 5-54, this criterion was answered where all the first electrical discharge activity observations per insulator, as defined in section 4.5, were listed. The comparisons were split into two groups, namely EPDM and HTV insulators as one group and RTV, Porcelain and Glass insulators as another group, because of the different installation dates of these groups. The detail of the first electrical discharge activity observations per insulator is presented in Annex D.

Table 5-53: First electrical discharge activity observation on EPDM and HTV insulators

			First observation date						
Electrical activity	**Voltage excitation**	**Insulator**	**17-May-11 (Day 2)**	**18-May-11 (Day 3)**	**19-May-11 (Day 4)**	**27-May-11 (Day 12)**	**28-May-11 (Day 13)**	**29-May-11 (Day 14)**	**02-Jun-11 (Day 18)**
Water drop corona (WDC)	AC	EPDM		√					
		HTV			√				
	DC+	EPDM	√						
		HTV							
	DC-	EPDM							
		HTV							
Spot discharge (SD)	AC	EPDM			√				
		HTV							
	DC+	EPDM	√						
		HTV						√	
	DC-	EPDM	√						
		HTV					√		
Dry band corona (DBC)	AC	EPDM	√						
		HTV				√			
	DC+	EPDM							
		HTV							
	DC-	EPDM				√			
		HTV							
Dry band discharge (DBD)	AC	EPDM					√		
		HTV						√	
	DC+	EPDM				√			
		HTV							√
	DC-	EPDM					√		
		HTV							√

Table 5-54: First electrical discharge activity observation on RTV, Porcelain and Glass insulators

			First observation date								
Electrical activity	**Voltage excitation**	**Insulator**	**06-Feb-11 (Day 4)**	**12-Feb-11 (Day 10)**	**14-Feb-11 (Day 12)**	**15-Feb-11 (Day 13)**	**17-Feb-11 (Day 15)**	**18-Feb-11 (Day 16)**	**22-Feb-11 (Day 20)**	**24-Feb-11 (Day 22)**	**08-Mar-11 (Day 34)**
Water drop corona (WDC)	AC	RTV				√					
		Porcelain		√							
		Glass									
	DC+	RTV									
		Porcelain									
		Glass									
	DC-	RTV									
		Porcelain									
		Glass									
Spot discharge (SD)	AC	RTV									
		Porcelain			√						
		Glass									
	DC+	RTV									
		Porcelain	√								
		Glass									
	DC-	RTV									
		Porcelain									
		Glass									
Dry band corona (DBC)	AC	RTV						√			
		Porcelain				√					
		Glass									
	DC+	RTV									
		Porcelain			√						
		Glass									
	DC-	RTV									
		Porcelain									
		Glass									
Dry band discharge (DBD)	AC	RTV							√		
		Porcelain					√				
		Glass									√
	DC+	RTV						√			
		Porcelain				√					
		Glass								√	
	DC-	RTV									√
		Porcelain			√						
		Glass								√	

It is evident from Table 5-53 that the EPDM insulators had the first electrical discharge activities in the form of water drop corona (WDC) under DC+ excitation, spot discharge (SD) under DC+ and DC- excitation and dry band corona (DBC) under AC excitation. These activities were observed on the second night. The first electrical discharge activity observed on the HTV insulators, was on the insulator under AC excitation on the fourth night and it was in the form of WDC. Further, it is observed that the DC+_EPDM insulator had the first dry band discharge (DBD) activity on night 11 and on night 13 was the first DBD activity observed on the HTV insulator under the AC excitation voltage. The insulator that displayed the latest electrical discharge activity was the DC+_HTV insulator on night 14 in the form of SD. The sequence of first occurrences of electrical discharge activities on the EPDM and HTV insulators are given in Table 5-55.

Table 5-55: Sequence of first occurrences of electrical discharge activity on EPDM and HTV insulators

Sequence of first occurrences of electrical discharge activity on EPDM and HTV insulators				
AC_EPDM	Dry band corona	Water drop corona	Spot discharge	Dry band discharge
AC_HTV	Water drop corona	Dry band corona	Dry band discharge	
DC+_EPDM	Water drop corona	Spot discharge	Dry band discharge	
DC+_HTV	Spot discharge	Dry band discharge		
DC-_EPDM	Spot discharge	Dry band corona	Dry band discharge	
DC-_HTV	Spot discharge	Dry band discharge		

From Table 5-55 it is observed that the only consistency in the sequence of first occurrences of electrical discharge activity, is displayed by the DC+_HTV and DC-_HTV insulators in the form of SD and DBD observations. The other insulators displayed a random sequence of first occurrences of electrical discharge activity.

It is evident from Table 5-54 that the DC+_Porcelain insulator had the first electrical discharge activity in the form of spot discharge (SD) on the fourth night. The first electrical discharge activity observed on the RTV insulators was on the insulator under AC excitation voltage on night 13 and it was in the form of WDC. The first electrical discharge activity observed on the Glass insulators was on the insulators under DC+ and DC- excitation voltages on night 22 and it was in the form of DBD. Furthermore, it is observed that the DC-_Porcelain insulator had the first dry band discharge (DBD) activity on night 12, on night 16 was the first DBD activity observed on the RTV insulators under the DC+ excitation voltage and on night 22 was the first DBD activity observed on the Glass insulators under the DC+

and DC- excitation voltages. The insulators that displayed the latest electrical discharge activities were the DC-_RTV and AC_Glass insulators on night 34 in the form of DBD. The sequence of first occurrences of electrical discharge activities on the RTV, Porcelain and Glass insulators are given in Table 5-56.

Table 5-56: Sequence of first occurrences of electrical discharge activity on RTV, Porcelain and Glass insulators

Sequence of first occurrences of electrical discharge activity on RTV, Porcelain and Glass insulators				
AC_RTV	Water drop corona	Dry band corona	Dry band discharge	
AC_Porcelain	Water drop corona	Spot discharge	Dry band corona	Dry band discharge
AC_Glass	Dry band discharge			
DC+_RTV	Dry band discharge			
DC+_Porcelain	Spot discharge	Dry band corona	Dry band discharge	
DC+_Glass	Dry band discharge			
DC-_RTV	Dry band discharge			
DC-_Porcelain	Dry band discharge			
DC-_Glass	Dry band discharge			

From Table 5-56 it is observed that all of the insulators energized under DC- excitation voltage and AC_Glass, DC+_Glass and DC+_RTV insulators progressed straight to the DBD activity. The other insulators displayed a random sequence of first occurrences of electrical discharge activity.

Chapter 6: Conclusions and Recommendations

6.1 Overview

The objectives of this research were to:

- Determine the site pollution severity (SPS) index and climatic conditions at KIPTS, in order to put the results of the research in context.
- Determine which insulator material performed better under HVAC and both polarities HVDC excitation voltages, respectively, in terms of visual material degradation, peak leakage currents, hydrophobicity properties and the starting sequence of electrical discharge activity.
- Determine which excitation voltage performed better per specific insulator material in terms of visual material degradation, peak leakage currents and the starting sequence of electrical discharge activity.

These objectives were achieved by following the research procedures and methodologies as outlined in Chapter 4 to obtain the results as discussed in Chapter 5. A concise summary of the results as discussed in Chapter 5 will be given in this chapter, to answer the abovementioned objectives.

It should be noted that any conclusion made in this thesis, is only applicable to the specific sample of insulators tested during this research, which were exposed to the climatic and pollution conditions experienced at KIPTS. More tests, as conducted during this research, should be carried out before any firm conclusions are made. Therefore, the results cannot be generalized or regarded as conclusive with reference to the materials used in the research.

At the end of this chapter, some recommendations to enhance future similar researches will be rendered.

6.2 Conclusions

From the research it is evident that KIPTS has a class e, i.e. very heavy, site pollution severity (SPS) index. It is also observed that KIPTS has strong winds with wind speeds up to 14.08 m/s. It was noted that the average wind speed over the winter months is lower than that of the summer months and the dominant wind direction in the winter is NE and SE during summer months. Furthermore, it has wet, cold winter seasons and dry, warm summer seasons with very high average relative humidity percentages throughout the year. A correlation was observed between the maximum peak leakage current values recorded per insulator and high relative humidity conditions of above 80%. Thus, it may be concluded that the high relative humidity conditions (> 75%) at KIPTS played a significant role in the forming of leakage current paths over the insulator surfaces. It is also observed that the highest average UV-B radiation occurs during the summer months with the highest average value of 125.81 $\mu W/cm^2$ recorded during December 2011.

From the metal end fitting corrosion results, it appears that hot dipped galvanizing does not provide sufficient protection for the metal end fittings against electrolytic corrosion for insulators under HVDC excitation voltages. A sacrificial zinc sleeve or zinc ring is thus recommended for all metal end fittings of insulators under HVDC excitation voltages.

The results of the comparison of insulator surface conditions, peak leakage currents and electrical discharge activities, as obtained from sections 5.3, 5.4 and 5.5 respectively, are summarized in Table 6-1 to Table 6-8. From these results, the overall comparison is done by considering all testing criteria, in order to determine the insulator material which performed best per excitation voltage and which excitation voltage performed best per insulator material. It should be noted, from the tables below, that the insulator material comparison was split into two groups, because of the different installation dates of these insulator groups.

Please note that N/A in the tables below means ‘Not Applicable’ and it is used when there is no information regarding a specific evaluation criterion. The only exception to this rule applies to the Hydrophobicity criterion for Porcelain, RTV and Glass insulators where RTV has hydrophobicity information, but it would not be correct to use it as a criterion to compare these materials, because porcelain and glass materials do not have hydrophobic characteristics. Furthermore, the insulator material or excitation voltage that appeared the

most frequent per category becomes the overall performer for that category. The counting started from the 'Best' category and the insulator materials or excitation voltages that did not become the overall performer in the 'Best' category, are then counted together with the insulator materials or excitation voltages in the next best category, in order to determine the overall performer for that category. This process repeats itself until all the overall performers are identified for each category. If an instance occurs where a category has two different insulator materials or two different excitation voltages as the most frequent, then factors like flashovers will be taken into account to determine the overall performer for that category; where the specific insulator material or excitation voltage that had a flashover event, will not become the overall performer for that category.

Table 6-1: Insulator material performance comparison for insulators energized under AC voltage

Insulators energized under AC excitation voltage					
Testing criteria	**EPDM and HTV insulators**		**Porcelain, RTV and Glass insulators**		
	Best	**Worse**	**Best**	**2nd Best**	**Worst**
Light erosion and erosion	HTV	EPDM	Glass, Porcelain		RTV
Minor splitting or cutting	HTV	EPDM	N/A	N/A	N/A
Hydrophobicity	HTV	EPDM	N/A	N/A	N/A
Flashover events	N/A	N/A	RTV, Porcelain		Glass
Maximum absolute peak leakage currents	HTV	EPDM	RTV	Porcelain	Glass
Leakage current (Ip ≤ 100 mA)	HTV	EPDM	Glass	RTV	Porcelain
Leakage current (Ip > 100 mA)	HTV	EPDM	RTV	Glass	Porcelain
Electrical discharges	HTV	EPDM	Glass	RTV	Porcelain
Overall performer	**HTV**	**EPDM**	**RTV**	**Glass**	**Porcelain**

Table 6-2: Insulator material performance comparison for insulators energized under DC+ voltage

Insulators energized under DC+ excitation voltage					
Testing criteria	**EPDM and HTV insulators**		**Porcelain, RTV and Glass insulators**		
	Best	**Worse**	**Best**	**2nd Best**	**Worst**
Light erosion and erosion	HTV	EPDM	Porcelain	RTV	Glass
Minor splitting or cutting	N/A	N/A	N/A	N/A	N/A
Hydrophobicity	HTV	EPDM	N/A	N/A	N/A
Flashover events	HTV	EPDM	RTV	Glass	Porcelain
Maximum absolute peak leakage currents	HTV	EPDM	Saturation band	Saturation band	Saturation band
Leakage current (Ip ≤ 100 mA)	HTV	EPDM	RTV	Porcelain	Glass
Leakage current (Ip > 100 mA)	HTV	EPDM	RTV	Glass	Porcelain
Electrical discharges	HTV	EPDM	Glass	RTV	Porcelain
Overall performer	**HTV**	**EPDM**	**RTV**	**Glass**	**Porcelain**

Table 6-3: Insulator material performance comparison for insulators energized under DC- voltage

Insulators energized under DC- excitation voltage					
Testing criteria	**EPDM and HTV insulators**		**Porcelain, RTV and Glass insulators**		
	Best	**Worse**	**Best**	**2nd Best**	**Worst**
Light erosion and erosion	HTV	EPDM	Porcelain	RTV	Glass
Minor splitting or cutting	N/A	N/A	N/A	N/A	N/A
Hydrophobicity	HTV	EPDM	N/A	N/A	N/A
Flashover events	N/A	N/A	RTV	Glass	Porcelain
Maximum absolute peak leakage currents	HTV	EPDM	RTV	Glass, Porcelain	
Leakage current (Ip ≤ 100 mA)	HTV	EPDM	RTV	Glass	Porcelain
Leakage current (Ip > 100 mA)	HTV	EPDM	RTV	Porcelain	Glass
Electrical discharges	HTV	EPDM	RTV	Glass	Porcelain
Overall performer	**HTV**	**EPDM**	**RTV**	**Glass**	**Porcelain**

It is observed in Table 6-1, Table 6-2 and Table 6-3, that the insulators made from HTV silicone rubber, performed better than the insulators made from EPDM silicone alloy rubber under all excitation voltages. This result was expected because the HTV silicone rubber insulators had shown a better hydrophobicity characteristic than the EPDM silicone alloy rubber insulators. Furthermore, it is observed that the RTV silicone rubber coated porcelain insulators performed best under all excitation voltages and the Porcelain insulators performed worst under all excitation voltages. This result was expected because of the hydrophobicity characteristic of the RTV silicone rubber and the anti-fog profile of the Glass cap-and-pin insulators in comparison to the open profile of the Porcelain long rod insulators.

Table 6-4: Excitation voltage performance comparison on EPDM insulators

EPDM insulators			
Testing criteria	**AC, DC+ and DC- excitation voltages**		
	Best	**2nd Best**	**Worst**
Light erosion and erosion	AC	DC+	DC-
Minor splitting or cutting	DC-, DC+		AC
Colour changes	N/A	N/A	N/A
Chipped glazing	N/A	N/A	N/A
End fitting corrosion	AC	DC-, DC+	
Flashover events	DC-, AC		DC+
Maximum absolute peak leakage currents	DC-	AC	DC+
Leakage current (Ip ≤ 100 mA)	DC+	DC-	AC
Leakage current (Ip > 100 mA)	DC-, DC+		AC
Electrical discharges	DC-, AC		DC+
Overall performer	**DC-**	**AC**	**DC+**

Table 6-5: Excitation voltage performance comparison on HTV insulators

HTV insulators			
Testing criteria	**AC, DC+ and DC- excitation voltages**		
	Best	**2nd Best**	**Worst**
Light erosion and erosion	AC	DC+	DC-
Minor splitting or cutting	N/A	N/A	N/A
Colour changes	N/A	N/A	N/A
Chipped glazing	N/A	N/A	N/A
End fitting corrosion	AC	DC+, DC-	
Flashover events	N/A	N/A	N/A
Maximum absolute peak leakage currents	DC-	DC+	AC
Leakage current (Ip ≤ 100 mA)	DC-	DC+	AC
Leakage current (Ip > 100 mA)	DC-	DC+	AC
Electrical discharges	DC+	DC-	AC
Overall performer	**DC-**	**DC+**	**AC**

Table 6-6: Excitation voltage performance comparison on RTV insulators

RTV insulators			
Testing criteria	**AC, DC+ and DC- excitation voltages**		
	Best	**2nd Best**	**Worst**
Light erosion and erosion	AC	DC-	DC+
Minor splitting or cutting	N/A	N/A	N/A
Colour changes	AC	DC+	DC-
Chipped glazing	N/A	N/A	N/A
End fitting corrosion	AC	DC-, DC+	
Flashover events	AC, DC-		DC+
Maximum absolute peak leakage currents	AC	DC-	DC+
Leakage current (Ip ≤ 100 mA)	DC-	AC	DC+
Leakage current (Ip > 100 mA)	AC	DC-	DC+
Electrical discharges	DC-	DC+	AC
Overall performer	**AC**	**DC-**	**DC+**

Table 6-7: Excitation voltage performance comparison on Porcelain insulators

Porcelain insulators			
Testing criteria	**AC, DC+ and DC- excitation voltages**		
	Best	**2nd Best**	**Worst**
Light erosion and erosion	AC, DC+		DC-
Minor splitting or cutting	N/A	N/A	N/A
Colour changes	N/A	N/A	N/A
Chipped glazing	AC	DC-	DC+
End fitting corrosion	AC	DC-, DC+	
Flashover events	AC	DC+, DC-	
Maximum absolute peak leakage currents	AC	DC-, DC+	
Leakage current (Ip ≤ 100 mA)	AC	DC-	DC+
Leakage current (Ip > 100 mA)	AC	DC-	DC+
Electrical discharges	DC-	AC	DC+
Overall performer	**AC**	**DC-**	**DC+**

Table 6-8: Excitation voltage performance comparison on Glass insulators

Glass insulators			
Testing criteria	**AC, DC+ and DC- excitation voltages**		
	Best	**2nd Best**	**Worst**
Light erosion and erosion	AC	DC-	DC+
Minor splitting or cutting	N/A	N/A	N/A
Colour changes	N/A	N/A	N/A
Chipped glazing	N/A	N/A	N/A
End fitting corrosion	N/A	N/A	N/A
Flashover events	AC	DC+, DC-	
Maximum absolute peak leakage currents	Saturation band	Saturation band	Saturation band
Leakage current (Ip ≤ 100 mA)	AC	DC-	DC+
Leakage current (Ip > 100 mA)	AC	DC+	DC-
Electrical discharges	AC	DC+, DC-	
Overall performer	**AC**	**DC-**	**DC+**

Extra evaluation criteria were included in Table 6-4 up to Table 6-8 which are Colour changes, Chipped glazing and End fitting corrosion. This was done because Colour changes and Chipped glazing are only applicable to RTV silicon rubber coated insulators and Porcelain insulators respectively. Thus, it would have been not correct to include these criteria when evaluating the performance of different insulator materials, as done in Table 6-1, Table 6-2 and Table 6-3. End fitting corrosion criterion was added because it conveys more information in the excitation voltage comparison tables by indicating that both DC polarity

voltages were responsible for end fitting corrosion. Furthermore, Hydrophobicity classification was removed from Table 6-4 up to Table 6-8, because the hydrophobicity tests were conducted on different dates per excitation voltage group and thus a valid comparison was not possible.

It is observed in Table 6-4 and Table 6-5 that the DC- voltage performed best on EPDM silicone alloy rubber and HTV silicone rubber insulators and DC+ voltage performed worst on EPDM silicone alloy rubber insulators where the AC voltage performed worst on HTV silicone rubber insulators. From Table 6-6, Table 6-7 and Table 6-8 it is observed that the AC voltage performed best on RTV silicone rubber coated porcelain, Porcelain and Glass insulators. Furthermore, it is observed that the DC+ voltage performed worst on RTV silicone rubber coated porcelain, Porcelain and Glass insulators. The performance difference of the excitation voltages between the abovementioned insulator groups might be due to the fact that the EPDM silicone alloy rubber and HTV silicone rubber insulators were energised for a shorter period than the RTV silicone rubber coated porcelain, Porcelain and Glass insulators. It is observed in Table 5-20 and Table 5-21 that the DC voltages have the most light erosion and erosion observations which indicates that the DC voltages have a greater ageing effect on the insulators than the AC voltage. Thus, if the EPDM silicone alloy rubber and HTV silicone rubber insulators were energized for the same period as the RTV silicone rubber coated porcelain, Porcelain and Glass insulators, then the results in Table 6-4 and Table 6-5 might have looked the same as in Table 6-6, Table 6-7 and Table 6-8.

6.3 Recommendations

The following recommendations are offered to enhance future similar researches:

- A different type of DC current sensor is needed for the measurement of DC leakage currents that do not generate offset fluctuations. This will allow the use of the accumulative charge parameter during evaluations of leakage current measurements, which is an important parameter, because it provides an indication of the duration of the leakage current flowing events.
- The use of three ESDD insulators that are energised with the three different excitation voltages respectively, to research the electrostatic pull forces of the DC electric fields more scientifically.

- The same tests as described in this document should be conducted, but instead of using insulators made of EPDM silicone alloy rubber, insulators made of pure EPDM rubber should be used. Previous laboratory tests have proven that insulators made of pure EPDM rubber perform better than HTV silicone rubber on DC- excitation voltage and this observation is worth further exploration [2, 3].
- Further research on the electrostatic pull forces on charged pollution particles caused by the HVDC electric fields, to verify that the DC- voltage electrostatic pull force is stronger than the DC+ voltage electrostatic pull force as assumed in this thesis.

References

[1] CIGRE, "Caprivi Link HVDC Interconnector: Site Selection, Geophysical Investigations, Interference Impacts and Design of Earth Electrodes," 2010.

[2] G. Heger *et al.*, "A Comparative Study of Insulator Materials Exposed to High Voltage AC and DC Surface Discharges," *IEEE Trans. Dielectr. Electr. Insul.*, vol. 17, no. 2, pp. 513–520, Apr. 2010.

[3] J. P. Holtzhausen *et al.*, "Insulator Aging Tests with HVAC and HVDC Excitation using the Tracking Wheel Tester," *2010 Int. Conf. High Voltage Engineering and Application (ICHVE)*, New Orleans, LA, 2010.

[4] A. I. Elombo, "An Evaluation of HTV-SR Insulators with Different Creepage Lengths under AC and Bipolar DC in Marine Polluted Service Conditions," M.Sc. thesis, Dept. Elect. and Electron. Eng., Univ. of Stellenbosch, Stellenbosch, South Africa, March 2012.

[5] A. I. Elombo *et al.*, "Evaluation of the Relative Ageing Performance of Power Line Insulators under AC and DC Voltage in a Coastal Pollution Environment: Planning and Early Results," *Southern African Universities Power Engineering Conf. (SAUPEC 2011)*, Cape Town, South Africa, 2011.

[6] P. J. Pieterse *et al.*, "A Coastal Insulator Pollution Test Station for the Evaluation of the Relative Ageing Performance of Power Line Insulators under AC and DC Voltage," *17th Int. Symp. High Voltage Engineering (ISH 2011)*, Hannover, Germany, 2011.

[7] *EPRI AC Transmission Line Reference Book – 200 kV and Above*, 3rd ed., EPRI, Palo Alto, CA, 1011974, 2005.

[8] J. Looms, "Insulators for High Voltages", *IEE Power Eng.*, no. 7, 1988.

[9] W. L. Vosloo *et al.*, *Practical Guide to Outdoor High Voltage Insulators*, Johannesburg, South Africa: Crown Publications CC., 2004.

[10] *EPRI Polymer Insulator Survey 2002: Utility Field Experience and In-service Failures*, EPRI, Palo Alto, CA, 1007752, 2003.

[11] *Polymeric Insulators for Indoor and Outdoor Use with a Nominal Voltage Greater than 1000 V – General Definitions, Test Methods and Acceptance Criteria, First Edition*, IEC Standard 62217, 2005.

[12] W. L. Vosloo, "A Comparison of the Performance of High Voltage Insulator Materials in a Severly Polluted Coastal Environment," Ph.D. dissertation, Dept. Elect. and Electron. Eng., Univ. of Stellenbosch, Stellenbosch, South Africa, March 2002.

[13] *Selection and Dimensioning of High Voltage Insulators Intended for Use in Polluted Conditions, Part 1: Definitions, Information and General Principles, First Edition*, IEC Standard 60815-1, 2008.

[14] J. M. George and Z. Lodi, "Design and Selection Criteria for HVDC Overhead Transmission Line Insulators," presented at CIGRE Canada Conference on Power Systems, Toronto, ON, 2009.

[15] T. Imakoma et al., "Electrical and Mechanical Characteristics of Non-ceramic Phase-to-Phase Spacers and Akimbo Insulator Assemblies," presented at SEE Conference, Paris, France, 1994.

[16] *EPRI Application Guide for Transmission Lines*, EPRI, Palo Alto, CA, NCI. TR. 111-566, 1998.

[17] D. L. Armentrait *et al.*, "Baron-free Fibers for Prevention of Acid Induced Brittle Fracture of Composite Insulator GRP Rods," *IEEE Trans. Power Del.*, vol. 18, pp. 684–693, Jul. 2003.

[18] R. Gorur *et al.*, *Outdoor Insulators*, Phoenix, AZ: S. Ravi, Grour Inc., 1999.

[19] L. H. Meyer *et al.*, "The Role of Inorganic Fillers in Silicone Rubber for Outdoor Insulation – Aluminum Tri-hydrate or Silica," *IEEE Electr. Insul. Mag.*, vol. 20, no. 4, Jul. / Aug. 2004.

[20] A. J. Phillip *et al.*, "Ageing of Non-ceramic Insulators due to Corona from Water Drops," *IEEE Trans. Power Del.*, vol. 14, pp. 1080–1086, 1999.

[21] A. J. Phillips *et al.*, "Water-drop Corona Effects on Full-scale 500 kV Non-ceramic Insulators," *IEEE Trans. Power Del.*, vol. 14, pp. 258–263, 1999.

[22] *EPRI Non-Ceramic Insulator End Fitting Analysis*, EPRI, Palo Alto, CA, 1001744, 2002.

[23] B. Mobasher *et al.*, "Mechanical Aspects of Crimped Glass Reinforced Plastic (GRP) Rods," *IEEE Trans. Power Del.*, vol. 18, pp. 852–858, Jul. 2003.

[24] CIGRE, "The Measurement of Site Pollution Severity and its Application to Insulator Dimensioning for AC Systems," Working Group 33.04, Electra, ref. no. 64, pp. 101–116, 1979.

[25] S. M. Fikke *et al.*, "Long Range Transported Pollutants and Conductivity of Atmospheric Ice on Insulators," *IEEE Trans. Power Del.*, vol. 18, no. 3, Jul. 1993.

[26] Y. Taniguchi *et al.*, "Natural Contamination Test of Insulators at Noto Testing Station Near Japan Sea," *IEEE Trans. Power App. Syst.*, vol. PAS-98, no. 1, pp. 239–245, Jan. / Feb. 1979.

[27] J. Wang *et al.*, "Combined Effect of Different Fields on the Motion Characteristics of Dust Particles around the Insulators," *17th Int. Symp. High Voltage Engineering (ISH 2011)*, Hannover, Germany, 2011.

[28] I. Kimoto *et al.*, "Antipollution Design Criteria for Line and Station Insulators," *IEEE Trans. Power App. Syst.*, vol. PAS-91, pp. 311-316, Jan. / Feb. 1972.

[29] K. Naito *et al.*, "Test Methods and Results for Recent Outdoor Insulation in Japan," *IEEE Trans. Dielectr. Electr. Insul.*, vol. 6, pp. 732–743, Oct. 1999.

[30] R. G. Houlgate *et al.*, "The Performance of Insulators at Extra and Ultra High Voltages in a Coastal Environment," *CIGRE 29th Session*, Paris, France, 1982, Paper no. 47-15.

[31] K. Chrzan, *et al.*, "Hygroscopic Properties of Pollutants on HV Insulators," *IEEE Trans. Electr. Insul.*, vol. EI-24, no. 1, pp. 107–112, Feb. 1989.

[32] G. Ramos *et al.*, "A Study on the Characteristics of Various Conductive Contaminants Accumulated on High Voltage Insulators," *IEEE Trans. Power Del.*, vol. 8, no. 4, Oct. 1993.

[33] M. T. Campillo *et al.*, "Conductivity and Flashover Voltage of Low Soluble Materials Deposited on High Voltage Insulators," *9th Int. Symp. High Voltage Engineering (ISH 1995)*, Graz, Austria, 1995, paper 3217.

[34] R. Matsuoka *et al.*, "Influence of Non-soluble Contaminants on Flashover Voltages of Artificially Contaminated Insulators," *IEEE Trans. Power Del.*, vol. 11, pp. 420–430, Jan. 1996.

[35] P. J. Lambeth, "Effect of Pollution on High-Voltage Outdoor Insulators," *Proc. IEE. IEE Reviews*, vol. 118, no. 9R, pp. 1107–1130, Sep. 1971.

[36] K. L. Chrzan, "Concentrated Discharges and Dry Bands on Polluted Outdoor Insulators," *13th Int. Symp. High Voltage Engineering (ISH 2003)*, Delft, Netherland, 2003.

[37] R. S. Gorur *et al.*, "Sudden Flashover of Non-ceramic Insulators in Artificial Contamination Tests," *IEEE Trans. Dielectr. Electr. Insul.*, vol. 4, pp. 79–87, Feb. 1997.

[38] G. G. Karady, "Flashover Mechanism of Non-ceramic Insulators," *IEEE Trans. Dielectr. Electr. Insul.*, vol. 6, pp. 718–723, Oct. 1999.

[39] A. Goldman *et al.*, "Analysis of Air Corona Products by Means of Their Reactions in Water," *Proc. 9th Int. Symp. Plasma Chemistry*, Pugnochiuso, Italy, 1989, pp. 1654–1658.

[40] *EPRI 230 kV Accelerated Ageing Chamber: Condition of NCI after 2 Years of Ageing*, EPRI, Palo Alto, CA, 1001746, 2003.

[41] S. M. Gubanski, "Research Findings on the Ageing Factors of Silicone Rubber," *Proc.: World Conf. & Exhibition Insulators, Arrestors and Bushings*, Marbella, Spain, 2003, pp. 285–296.

[42] *EPRI 230 kV Accelerated Ageing Chamber: Description of Test and Condition of NCI after One Year of Ageing*, Palo Alto, CA, 01001745, 2002.

[43] *EPRI Field Guide: Visual Inspection of NCI*, revision 1, EPRI, Palo Alto, CA, 1008739, 2004.

[44] CIGRE, "Failure of Cap-and-pin Insulators subjected to HVDC," Task Force 33.04.02 of Study Committee 33, Electra, no. 153, pp. 22 – 31, Apr. 1994.

[45] STRI Guide 5, "Guide for Visual Identification of Deterioration & Damages on Suspension Composite Insulators," STRI LAB, Ludvika, Sweden, 2005.

[46] P. J. Pieterse, "Operating Procedure for Test Rig at KIPTS," unpublished.

[47] G. Heger, "A Comparative Study of Insulator Materials Exposed to High Voltage AC and DC Surface Discharges," M.Sc. thesis, Dept. Elect. and Electron. Eng., Univ. of Stellenbosch, Stellenbosch, South Africa, March 2009.

[48] CT LAB (Pty) Ltd. (2012, Sep. 30). *OLCA101 Product Brochure* [Online]. Available: http://www.ctlab.co.za

[49] UVIRCO Technologies (Pty) Ltd. (2012, Sep. 30). *Technical Brochure of CoroCAM 1 and Sony GV-HD700 Portable Video Recorder* [Online]. Available: http://www.uvirco.com

[50] Sony India Pvt. Ltd. (2012, Sep. 30). *Technical Brochure of Sony HDR-XR550E Camcorder* [Online]. Available: http://www.sony.co.in/support/product/HDR-XR550E

[51] Greisinger Electronic GmbH. (2012, Sep. 30). *Operating Manual of GMH 3410* [Online]. Available: http://www.greisinger.de

[52] Radwag Wagi Elektroniczne. (2012, Sep. 30). *Technical brochure of AS 220/C/2 Balance* [Online]. Available: http://www.radwag.com

[53] STRI Guide 1, "Hydrophobicity Classification Guide," STRI LAB, Ludvika, Sweden, 1992.

[54] *Selection and Dimensioning of High Voltage Insulators Intended for Use in Polluted Conditions, Part 3: Polymer Insulators for AC Systems, First Edition*, IEC 60815-3, 2008.

[55] *Selection and Dimensioning of High Voltage Insulators Intended for Use in Polluted Conditions, Part 2: Ceramic and Glass Insulators for AC Systems, First Edition*, IEC 60815-2, 2008.

[56] J. F. Anthoni. (2012, Sep. 30). *The Chemical Composition of Seawater* [Online]. Available: http://www.seafriends.org.nz/oceano/seawater.htm

[57] NGK Insulators Ltd. (2012, Sep. 30). *Technical Information HVDC* [Online]. Available: http://www.ngk.co.jp/english/products/power/technical/hvdc/zinc.html.

[58] Corrosion Doctors. (2012, Sep. 30). *Rust Chemistry* [Online]. Available: http://corrosion-doctors.org/experiments/rust-chemistry.htm

[59] CIGRE, "Field and Laboratory Testing for the Choice of Optimum Composite Insulator Design for a Marine-desert Environment," Work Group 33-202, 2000.

Appendix A: Data capturing forms

Samples of data capturing forms for insulator surface condition observations, hydrophobicity observations and electrical discharge observations used during this project will be presented in this appendix.

A.1 Data capturing form for insulator surface conditions

Table A-1: Surface condition observation form

Surface Condition Observations				
Date:		**Time:**		
Identity:				
	A (Land, East)	**B (Sea, West)**	**C (UV, North)**	**D (South)**
1S				
1T				
1B				
2S				
2T				
2B				
3S				
3T				
3B				
4S				
4T				
4B				
5S				
5T				
5B				
6S				
6T				
6B				
7S				
7T				
7B				
8S				
8T				
8B				
9S				
1 - Live, 9 - Dead, S - Sheath, B - Shed Bottom, T - Shed Top				

A.2 Data capturing form for Hydrophobicity observations

Table A-2: Hydrophobicity classification form

Hydrophobicity Classifications Form

Date: Time:

Date of Installation:

Weather at time of measurement:

	Date and time as above	
Temperature [deg C]:		
Wind speed [m/s]:		
Humidity [%]:		

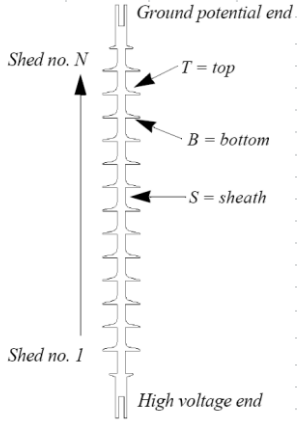

Comments:

Hydrophobisity Classification (HC) Measurements

Identity:

Shed No	Position					
	Side of insulator: Sea			Side of insulator: Land		
	Top	Bottom	Sheath	Top	Bottom	Sheath
1						
2						
3						
4						
5						
6						
7						
8						
9						

Hydrophobisity Classification (HC) Measurements

Identity:

Shed No	Position					
	Side of insulator: Sea			Side of insulator: Land		
	Top	Bottom	Sheath	Top	Bottom	Sheath
1						
2						
3						
4						
5						
6						
7						
8						
9						

Hydrophobisity Classification (HC) Measurements

Identity:

Shed No	Position					
	Side of insulator: Sea			Side of insulator: Land		
	Top	Bottom	Sheath	Top	Bottom	Sheath
1						
2						
3						
4						
5						
6						
7						
8						
9						

Hydrophobisity Classification (HC) Measurements

Identity:

Shed No	Position					
	Side of insulator: Sea			Side of insulator: Land		
	Top	Bottom	Sheath	Top	Bottom	Sheath
1						
2						
3						
4						
5						
6						
7						
8						
9						

A.3 Data capturing forms for electrical discharge activity

Table A-3: CoroCAM 1 observation form

COROCAM MARK I VIDEO TAPE RECORDING														
Video Tape #	Insulator samples energized under AC voltage					Observation Point		Tape Position		Starting Time	Date	Comments	Day	Week
	EPDM	*HTV*	*RTV*	*Porcelain*	*Glass*	*Land Side*	*Sea Side*	*From*	*To*					

Table A-4: Sony 0-lux camcorder observation form

0-lux Sony VIDEO RECORDING: *Night time observations*												
Insulator samples energized under AC voltage					Observation Point		Video File Name	Starting Time	Date	Comments	Day	Week
EPDM	*HTV*	*RTV*	*Porcelain*	*Glass*	*Land Side*	*Sea Side*						

Appendix B: Hydrophobicity classification results

B.1 Results under AC excitation

Table B-1: Hydrophobicity classification results of AC_RTV insulator

Hydrophobicity Classification (HC) Results							
Identity: AC_RTV							
Date	Position No	Position					
		Side of insulator: Sea			Side of insulator: Land		
		Top	Bottom	Sheath	Top	Bottom	Sheath
2011/03/03 (Day 29)	1	4	3	4	5	4	3
	3	4	4	4	5	4	4
	5			3			4
	6	4	4		4	4	
2011/04/05 (Day 62)	1	3	4	7	4	7	7
	3	5	7	7	6	7	4
	5			7			4
	6	5	7		6	7	
2011/05/04 (Day 91)	1	4	6	4	7	6	4
	3	7	7	7	7	7	7
	5			7			6
	6	7	7		7	6	
2011/07/07 (Day 155)	1	4	3	5	7	5	7
	3	5	7	3	7	5	3
	5			7			7
	6	7	7		7	7	
2011/08/25 (Day 204)	1	4	5	7	5	7	5
	3	4	5	7	5	7	4
	5			7			5
	6	5	7		4	5	
2011/11/29 (Day 300)	1	7	7	7	7	7	7
	3	7	7	7	7	7	7
	5			7			7
	6	7	7		7	7	
2012/02/08 (Day 371)	1	7	7	7	6	7	7
	3	7	7	7	7	7	7
	5			7			7
	6	7	7		7	7	

Table B-2: Hydrophobicity classification results of AC_EPDM insulator

Hydrophobicity Classification (HC) Results							
Identity: AC_EPDM							
Date	Position No	Position					
		Side of insulator: Sea			Side of insulator: Land		
		Top	Bottom	Sheath	Top	Bottom	Sheath
2011/07/06 (Day 52)	1	7	7	7	7	7	7
	4	7	7	7	7	7	7
	8	7	7		7	7	
	9			7			7
2011/08/25 (Day 102)	1	7	7	7	7	7	7
	4	7	7	7	7	7	7
	8	7	7		7	7	
	9			7			7
2011/11/29 (Day 198)	1	7	7	7	7	7	7
	4	7	7	7	7	7	7
	8	7	7		7	7	
	9			7			7
2012/02/06 (Day 267)	1	7	7	7	7	7	7
	4	7	7	7	7	7	7
	8	7	7		7	7	
	9			7			7

Table B-3: Hydrophobicity classification results of AC_HTV insulator

Hydrophobicity Classification (HC) Results							
Identity: AC_HTV							
Date	Position No	Position					
		Side of insulator: Sea			Side of insulator: Land		
		Top	Bottom	Sheath	Top	Bottom	Sheath
2011/07/06 (Day 52)	1	5	4	7	7	5	4
	4	7	4	7	7	5	5
	8	7	4		7	4	
	9			4			4
2011/08/25 (Day 102)	1	7	6	7	7	6	7
	4	7	7	7	7	7	6
	8	7	7		7	5	
	9			7			7
2011/11/29 (Day 198)	1	7	7	7	7	7	7
	4	7	7	7	7	7	7
	8	7	7		7	7	
	9			7			7
2012/02/08 (Day 269)	1	7	7	7	7	7	7
	4	7	7	7	7	7	7
	8	7	7		7	7	
	9			7			7

B.2 Results under DC+ excitation

Table B-4: Hydrophobicity classification results of DC+_RTV insulator

Hydrophobicity Classification (HC) Results							
Identity: DC+_RTV							
Date	Position No	Position					
		Side of insulator: Sea			Side of insulator: Land		
		Top	Bottom	Sheath	Top	Bottom	Sheath
2011/02/21 (Day 19)	1	5	3	3	5	4	3
	3	4	5	4	4	6	3
	5			4			3
	6	5	5		6	7	
2011/03/24 (Day 50)	1	4	7	7	3	3	7
	3	6	7	7	5	5	7
	5			7			7
	6	6	6		5	7	
2011/04/19 (Day 76)	1	7	7	7	6	6	7
	3	7	7	7	5	6	7
	5			7			7
	6	7	6		7	7	
2011/06/07 (Day 125)	1	5	4	7	4	5	7
	3	5	4	7	6	7	7
	5			7			7
	6	7	7		7	7	
2011/08/03 (Day 182)	1	4	4	7	4	5	4
	3	5	5	7	6	4	5
	5			7			7
	6	7	6		7	7	
2011/10/26 (Day 266)	1	6	5	7	5	7	6
	3	6	5	7	6	7	7
	5			7			7
	6	7	6		7	7	
2012/02/08 (Day 371)	1	7	7	7	7	7	7
	3	7	7	7	7	7	7
	5			7			7
	6	7	7		7	7	

Table B-5: Hydrophobicity classification results of DC+_EPDM insulator

Hydrophobicity Classification (HC) Results							
Identity: DC+_EPDM							
Date	Position No	Position					
		Side of insulator: Sea			Side of insulator: Land		
		Top	Bottom	Sheath	Top	Bottom	Sheath
2011/06/07 (Day 23)	1	7	7	7	7	7	7
	4	7	7	7	7	7	7
	8	7	7		7	7	
	9			7			7
2011/08/03 (Day 80)	1	7	7	7	7	7	7
	4	7	7	7	7	7	7
	8	7	7		7	7	
	9			7			7
2011/10/26 (Day 164)	1	7	7	7	7	7	7
	4	7	7	7	7	7	7
	8	7	7		7	7	
	9			7			7
2012/02/08 (Day 269)	1	7	7	7	7	7	7
	4	7	7	7	7	7	7
	8	7	7		7	7	
	9			7			7

Table B-6: Hydrophobicity classification results of DC+_HTV insulator

Hydrophobicity Classification (HC) Results							
Identity: DC+_HTV							
Date	Position No	Position					
		Side of insulator: Sea			Side of insulator: Land		
		Top	Bottom	Sheath	Top	Bottom	Sheath
2011/06/07 (Day 23)	1	7	4	7	7	4	7
	4	5	4	7	7	4	4
	8	7	4		7	4	
	9			7			7
2011/08/03 (Day 80)	1	7	3	7	7	3	7
	4	7	4	7	7	5	4
	8	7	5		7	6	
	9			7			7
2011/10/26 (Day 164)	1	7	7	7	7	7	7
	4	7	7	7	7	6	6
	8	7	7		7	6	
	9			7			7
2012/02/08 (Day 269)	1	7	7	7	7	7	7
	4	7	7	7	7	7	7
	8	7	5		7	5	
	9			7			7

B.3 Results under DC- excitation

Table B-7: Hydrophobicity classification results of DC-_RTV insulator

Hydrophobicity Classification (HC) Results							
Identity: DC-_RTV							
Date	Position No	Position					
		Side of insulator: Sea			Side of insulator: Land		
		Top	Bottom	Sheath	Top	Bottom	Sheath
2011/02/10 (Day 08)	1	3	2	2	2	2	2
	3	2	2	3	2	2	2
	5			3			2
	6	3	2		2	2	
2011/03/11 (Day 37)	1	6	4	7	6	3	4
	3	5	6	3	6	6	3
	5			6			4
	6	5	4		4	3	
2011/04/13 (Day 70)	1	6	6	7	4	5	4
	3	5	7	7	4	7	4
	5			7			7
	6	5	6		6	7	
2011/05/19 (Day 106)	1	7	6	7	6	7	5
	3	7	6	7	6	6	6
	5			7			5
	6	6	6		5	6	
2011/07/26 (Day 174)	1	6	6	7	6	7	5
	3	3	4	7	4	4	3
	5			7			5
	6	7	5		5	5	
2011/09/05 (Day 215)	1	7	7	7	7	7	7
	3	7	5	7	7	7	7
	5			7			7
	6	7	6		7	7	
2011/12/01 (Day 302)	1	7	7	7	7	7	7
	3	7	7	7	5	5	7
	5			7			7
	6	7	7		7	7	
2012/02/13 (Day 376)	1	7	7	7	7	7	7
	3	7	7	7	7	7	7
	5			7			7
	6	7	7		7	7	

Table B-8: Hydrophobicity classification results of DC-_EPDM insulator

Hydrophobicity Classification (HC) Results							
Identity: DC-_EPDM							
Date	Position No	Position					
		Side of insulator: Sea			Side of insulator: Land		
		Top	Bottom	Sheath	Top	Bottom	Sheath
2011/05/19 (Day 4)	1	7	6	6	6	6	6
	4	6	6	7	6	6	7
	8	6	6		7	6	
	9			6			7
2011/07/26 (Day 72)	1	7	6	7	7	6	7
	4	7	6	7	7	6	7
	8	7	6		7	6	
	9			7			7
2011/09/05 (Day 113)	1	7	7	7	7	7	7
	4	7	7	7	7	7	7
	8	7	7		7	7	
	9			7			7
2011/12/01 (Day 200)	1	7	7	7	7	7	7
	4	7	7	7	7	7	7
	8	7	7		7	7	
	9			7			7
2012/02/10 (Day 271)	1	7	7	7	7	7	7
	4	7	7	7	7	7	7
	8	7	7		7	7	
	9			7			7

Table B-9: Hydrophobicity classification results of DC-_HTV insulator

Hydrophobicity Classification (HC) Results							
Identity: DC-_HTV							
Date	Position No	Position					
		Side of insulator: Sea			Side of insulator: Land		
		Top	Bottom	Sheath	Top	Bottom	Sheath
2011/05/19 (Day 4)	1	4	3	4	4	3	3
	4	4	4	5	4	3	3
	8	4	3		3	3	
	9			5			4
2011/07/26 (Day 72)	1	6	5	7	7	6	7
	4	7	5	7	7	6	4
	8	7	6		7	6	
	9			7			3
2011/09/05 (Day 113)	1	7	7	7	7	6	6
	4	7	7	7	7	7	7
	8	7	6		7	7	
	9			7			7
2011/12/01 (Day 200)	1	7	5	7	7	7	7
	4	7	7	7	7	7	5
	8	7	7		7	7	
	9			7			7
2012/02/10 (Day 271)	1	7	7	7	7	7	7
	4	7	7	7	7	7	7
	8	7	7		7	7	
	9			7			7

Appendix C: Peak leakage current plots

C.1 Linearity test plots of current sensors

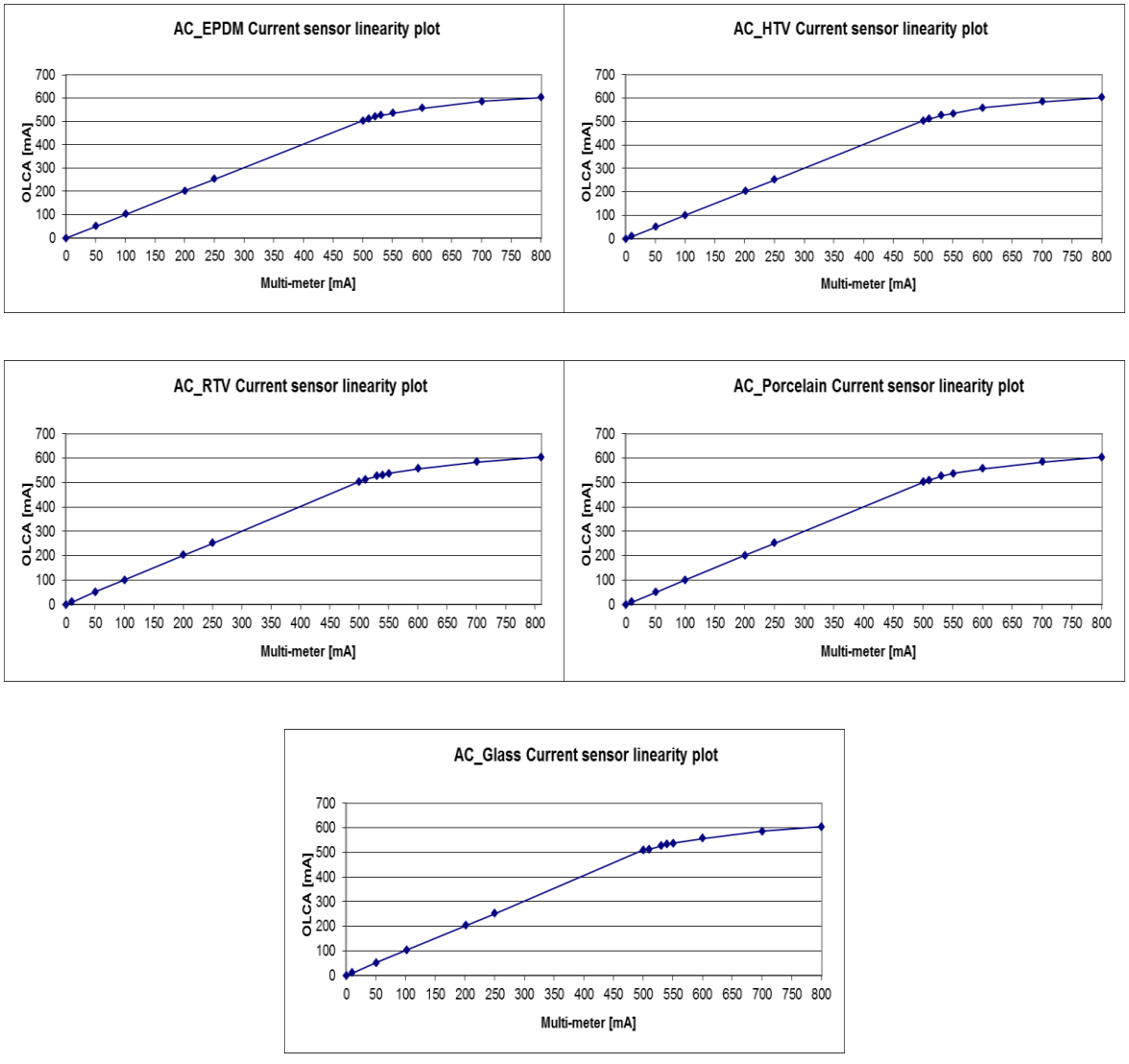

Figure C-1: AC current sensors linearity test plots

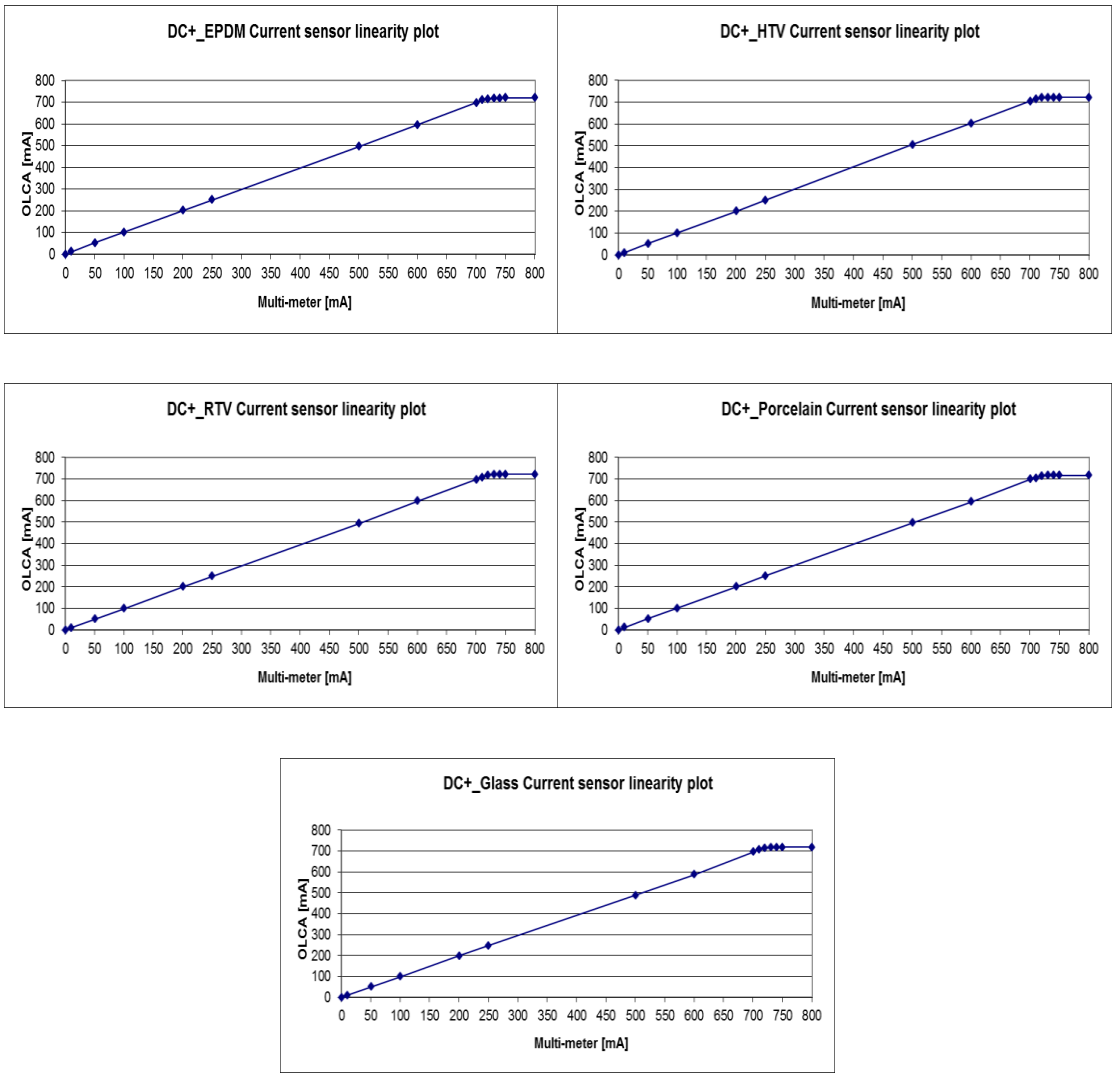

Figure C-2: DC+ current sensors linearity test plots

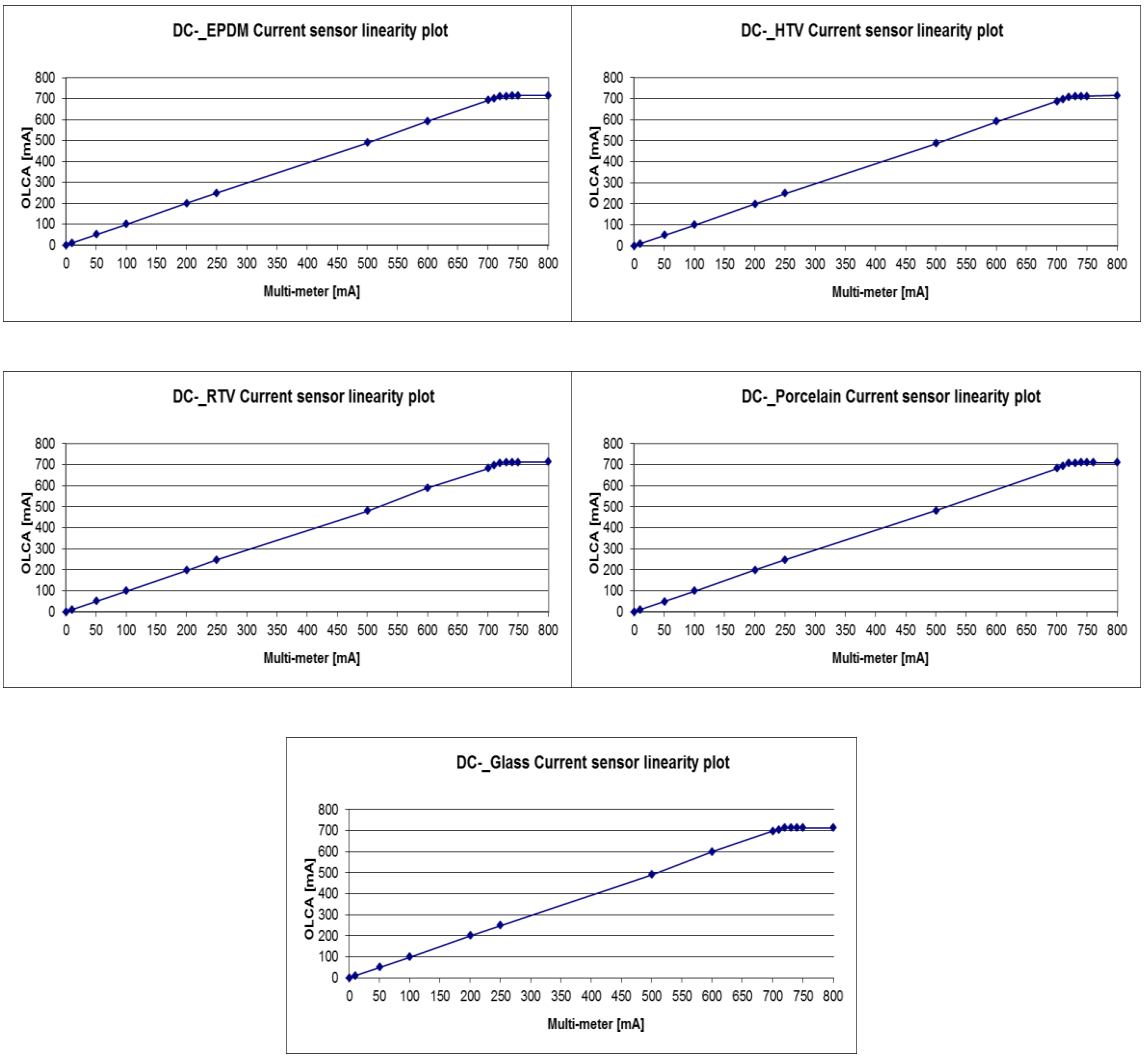

Figure C-3: DC- current sensors linearity test plots

C.2 Peak leakage current bin count: material comparison

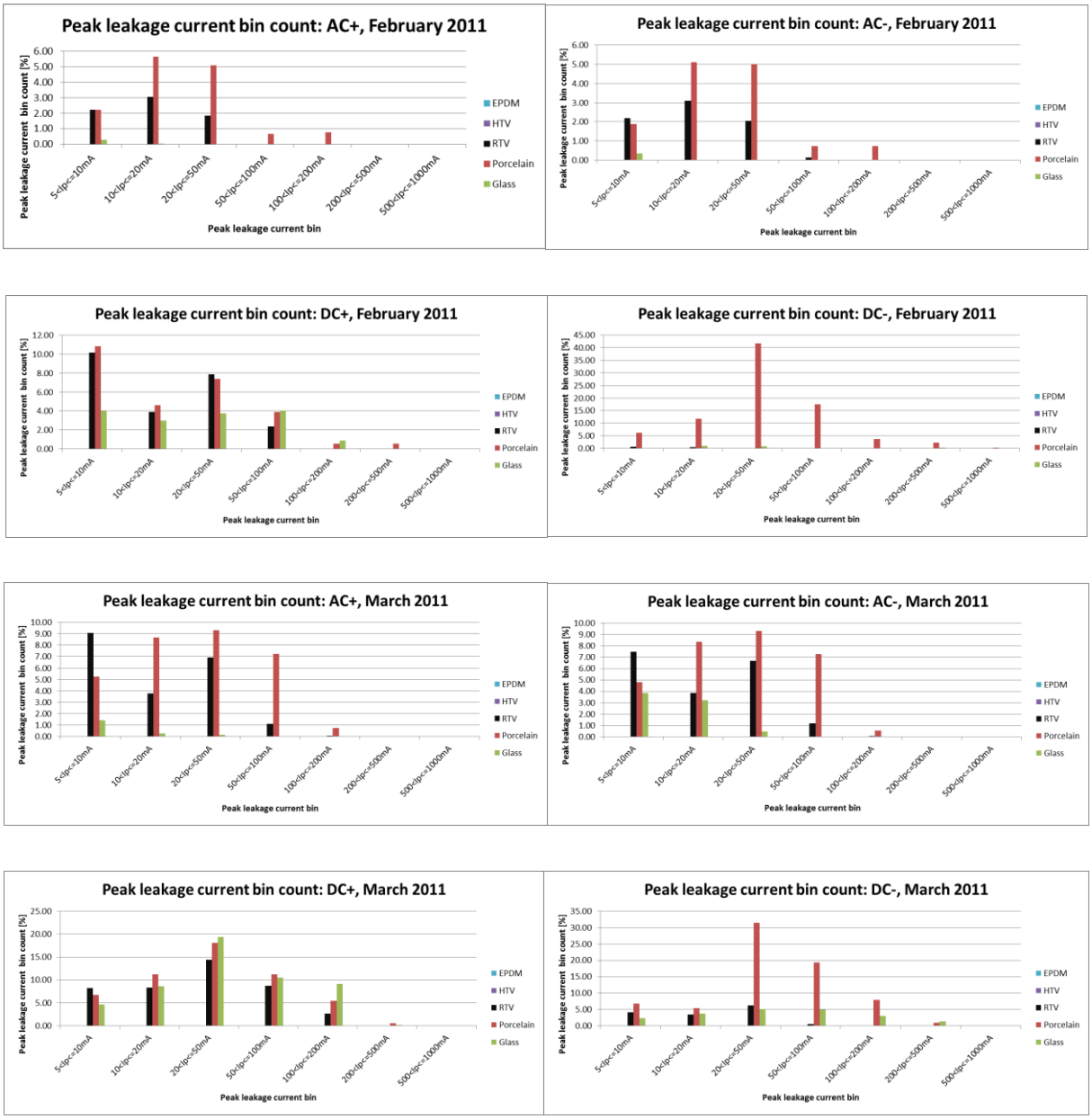

Figure C-4: Peak leakage current bin count comparison for different materials; February, March 2011

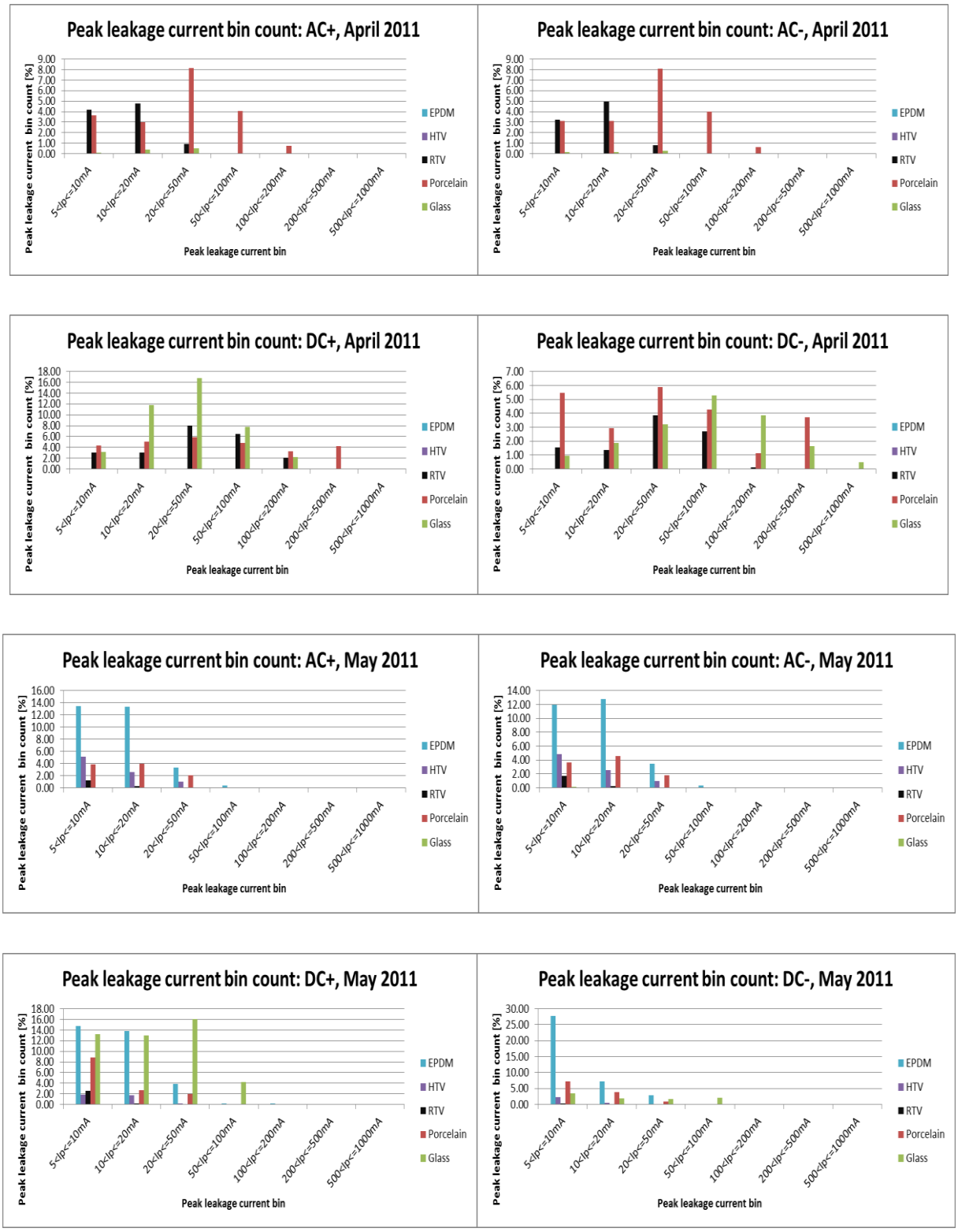

Figure C-5: Peak leakage current bin count comparison for different materials; April, May 2011

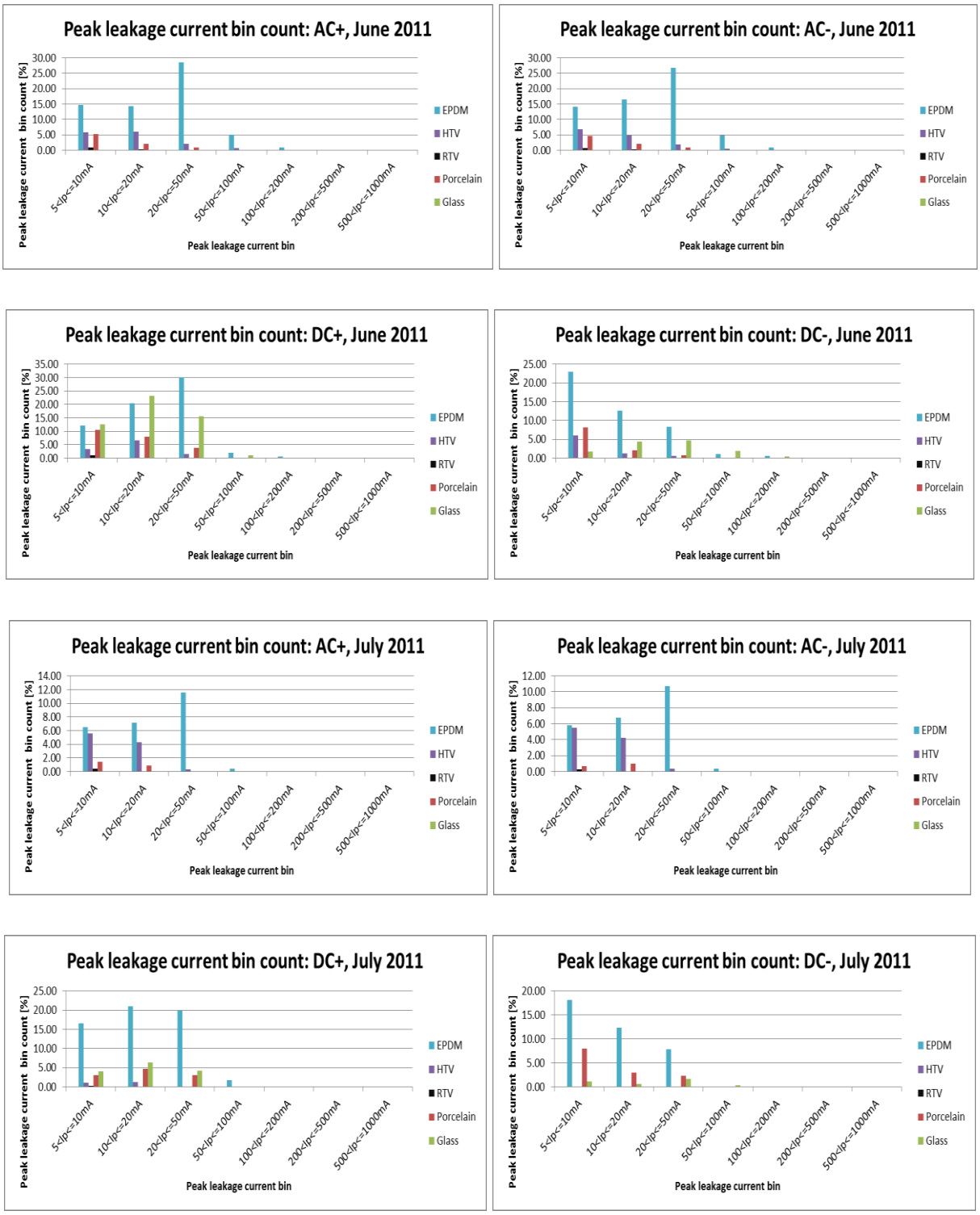

Figure C-6: Peak leakage current bin count comparison for different materials; June, July 2011

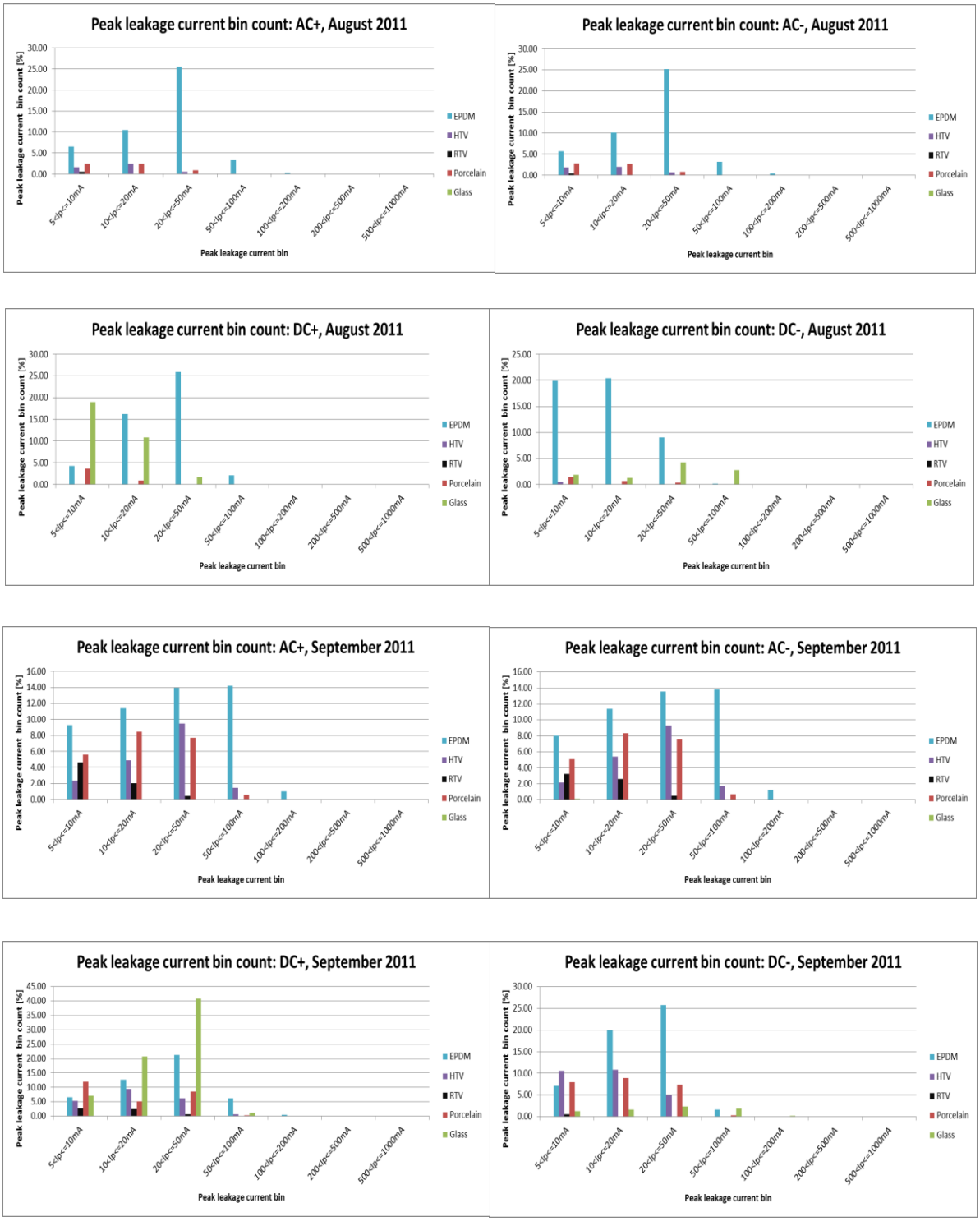

Figure C-7: Peak leakage current bin count comparison for different materials; August, September 2011

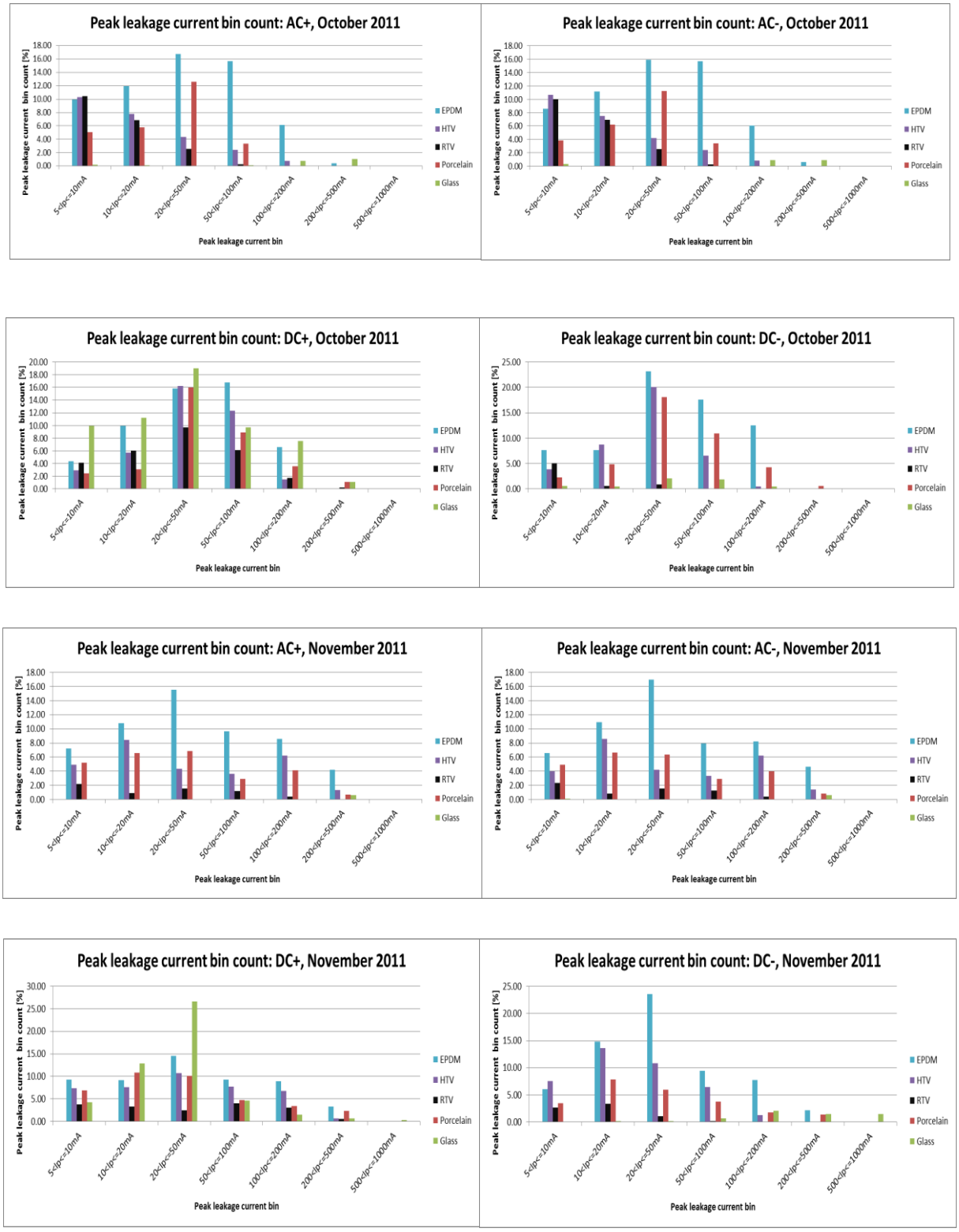

Figure C-8: Peak leakage current bin count comparison for different materials; October, November 2011

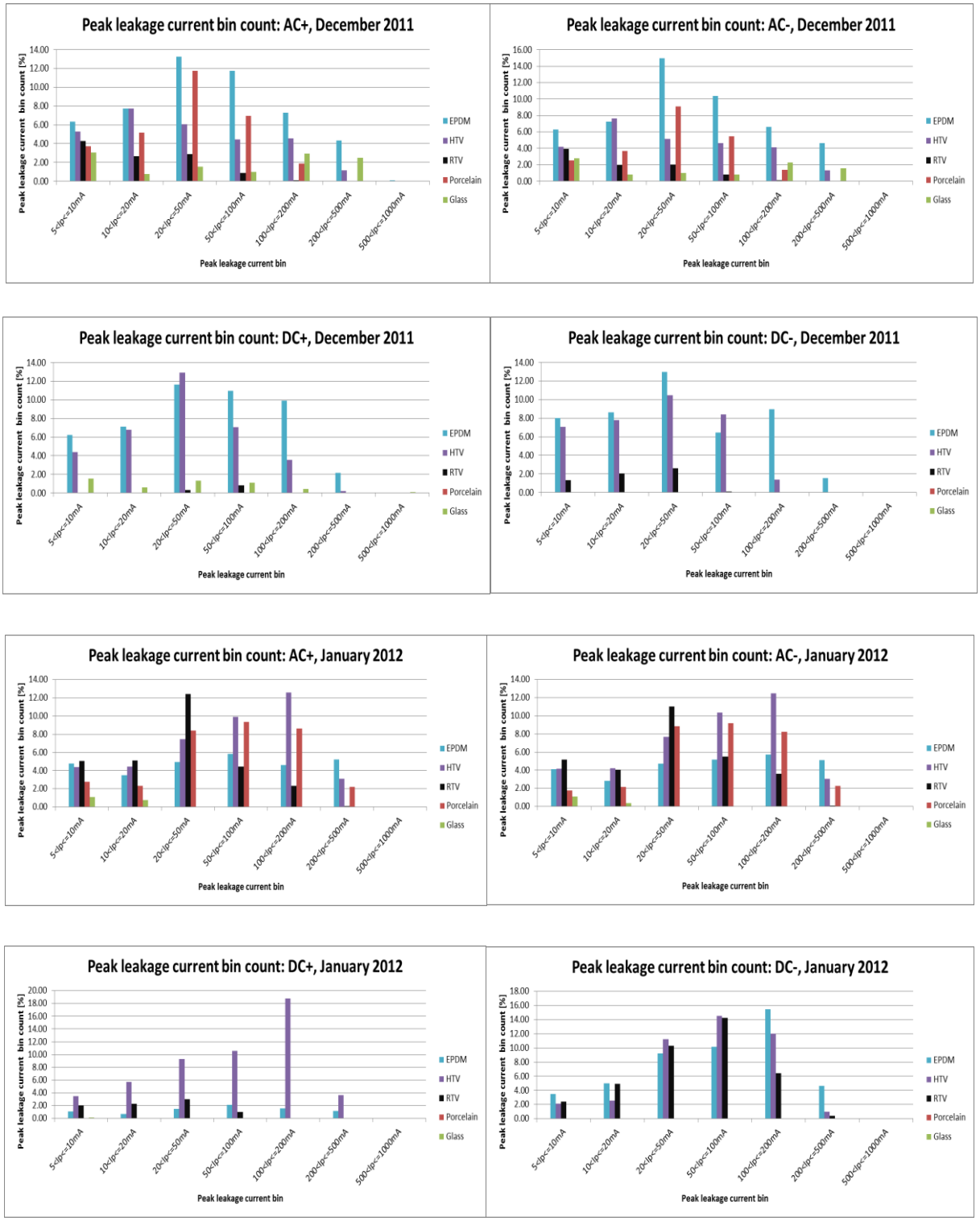

Figure C-9: Peak leakage current bin count comparison for different materials; December, January 2011

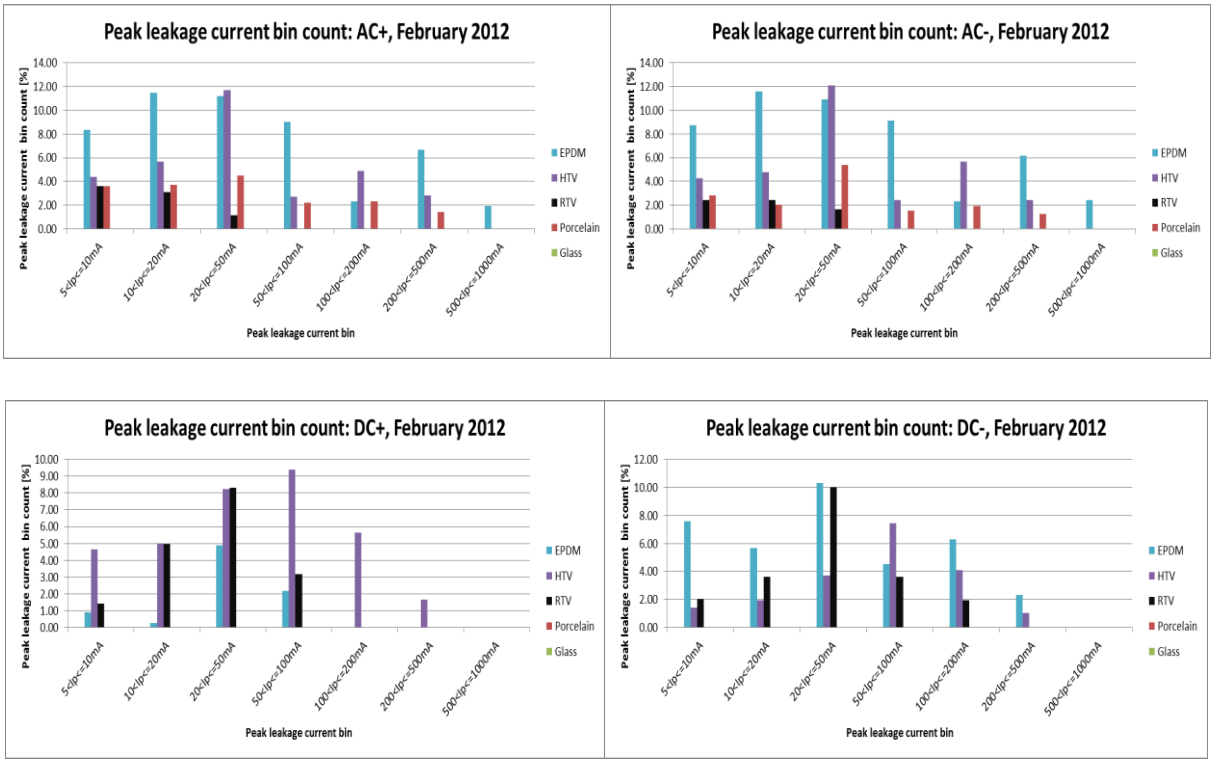

Figure C-10: Peak leakage current bin count comparison for different materials; February 2012

C.3 Peak leakage current bin count: voltage comparison

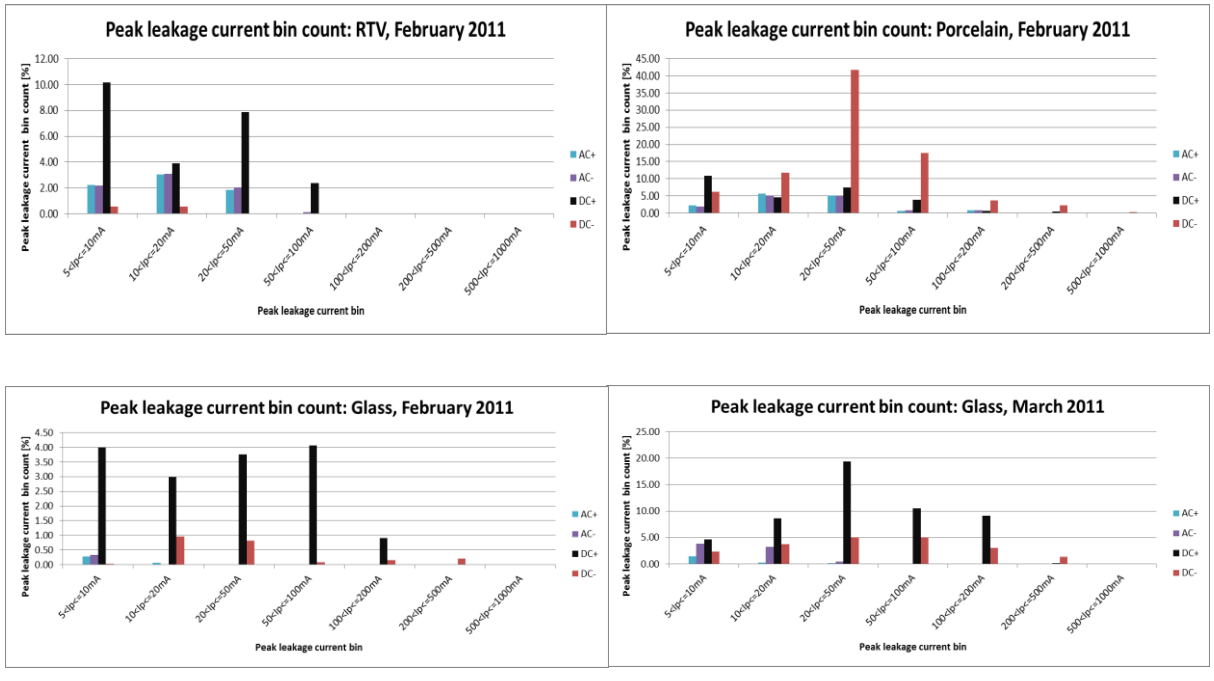

Figure C-11: Peak leakage current bin count comparison for different voltages; February, March 2011

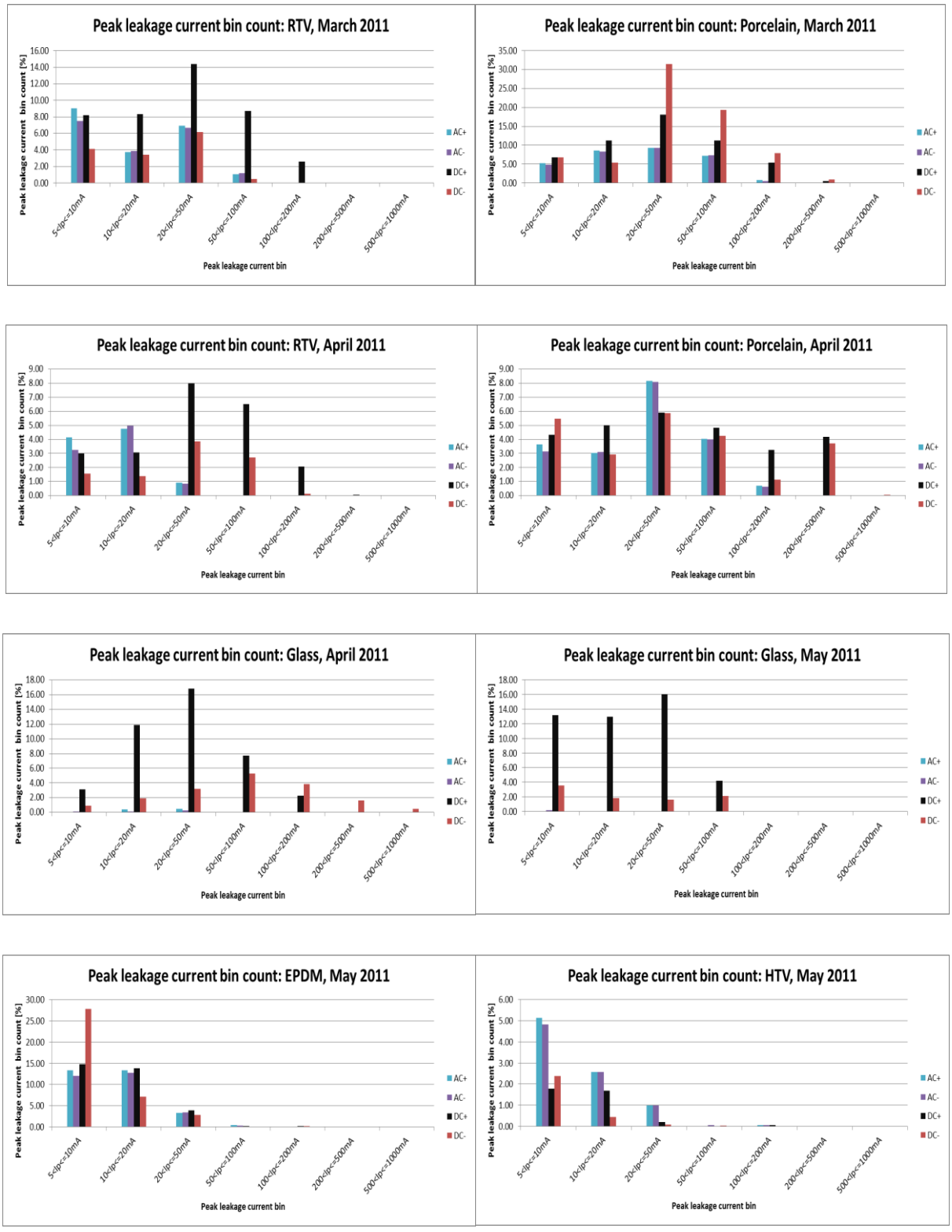

Figure C-12: Peak leakage current bin count comparison for different voltages; March - May 2011

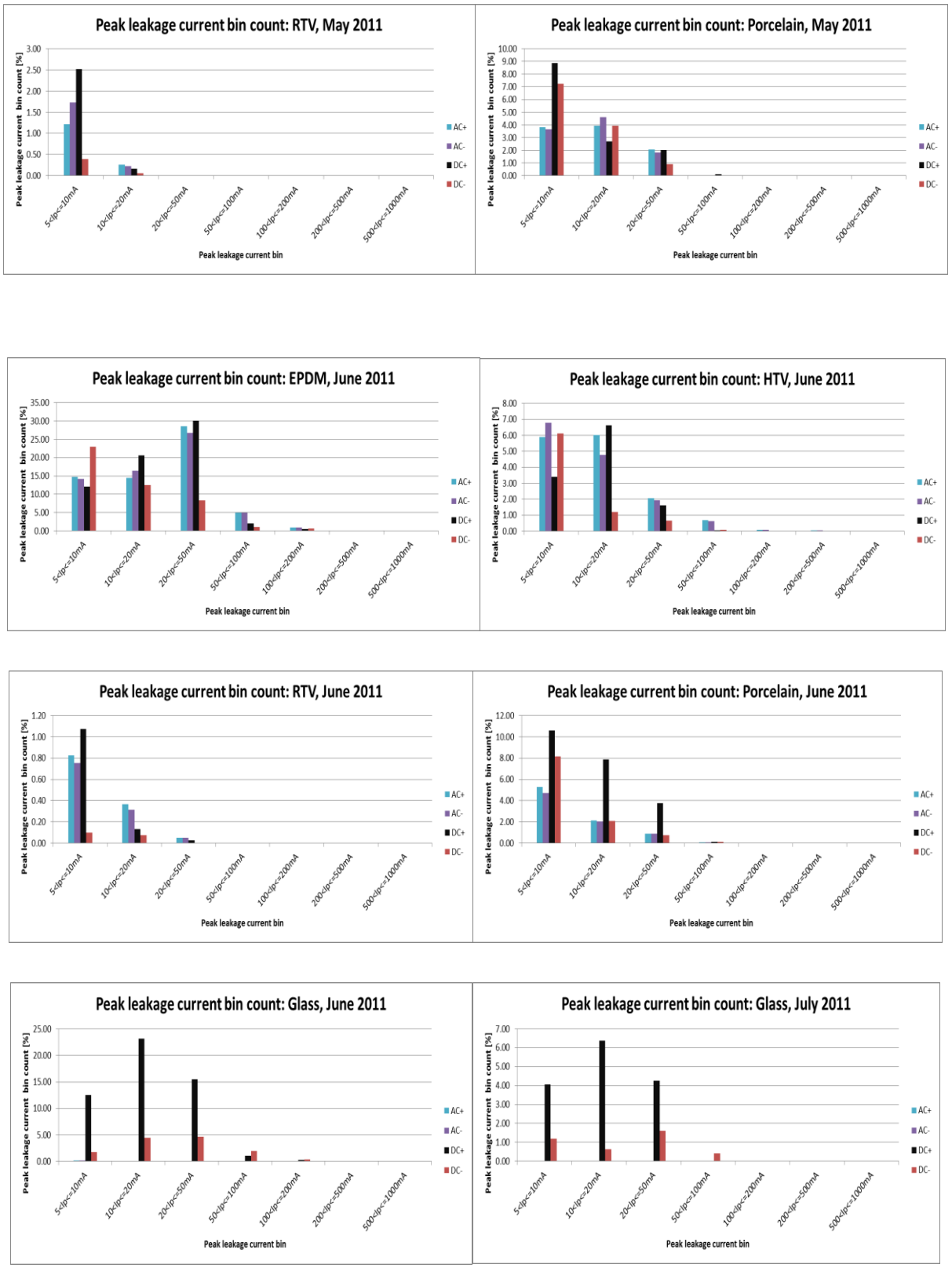

Figure C-13: Peak leakage current bin count comparison for different voltages; May - July 2011

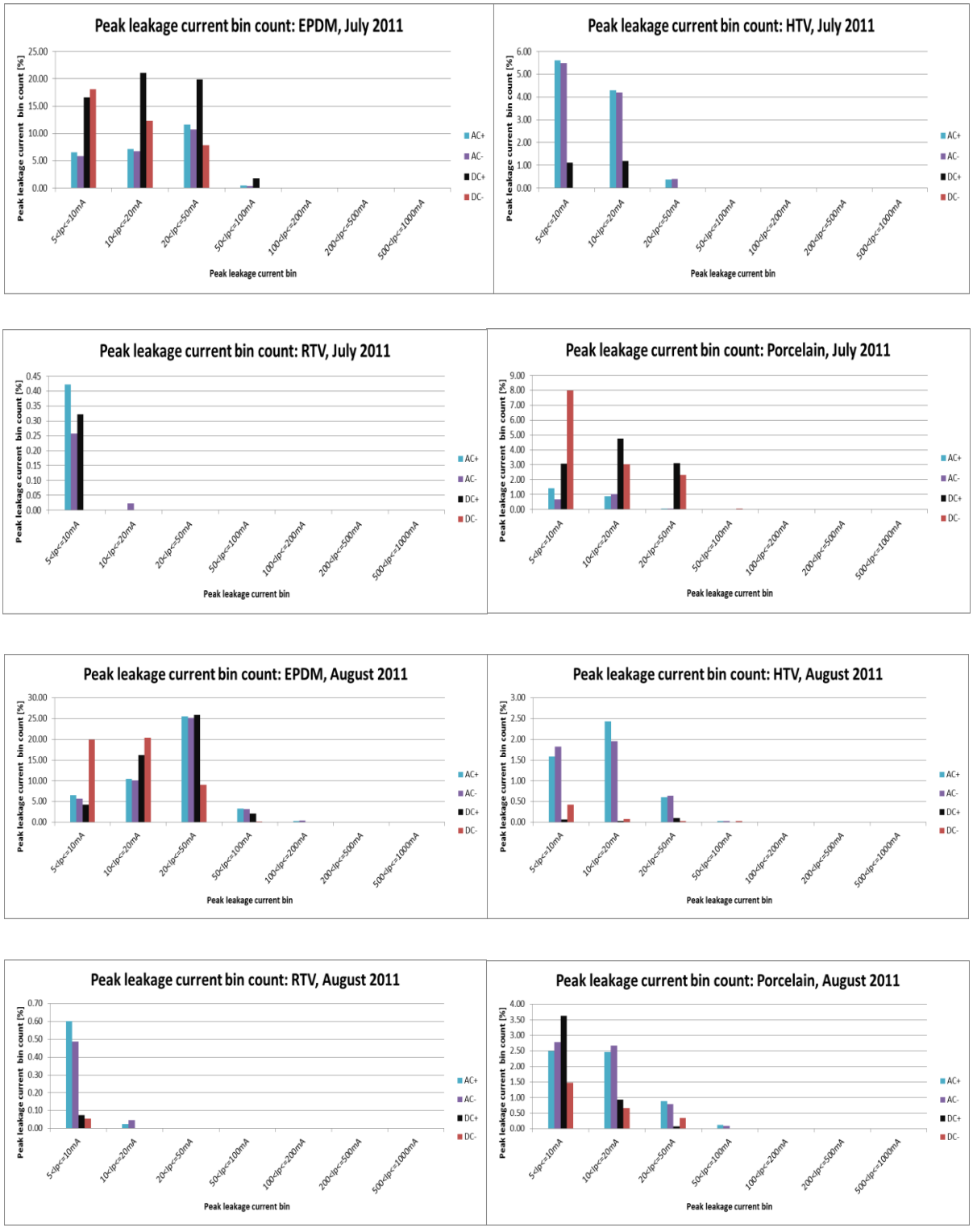

Figure C-14: Peak leakage current bin count comparison for different voltages; July - August 2011

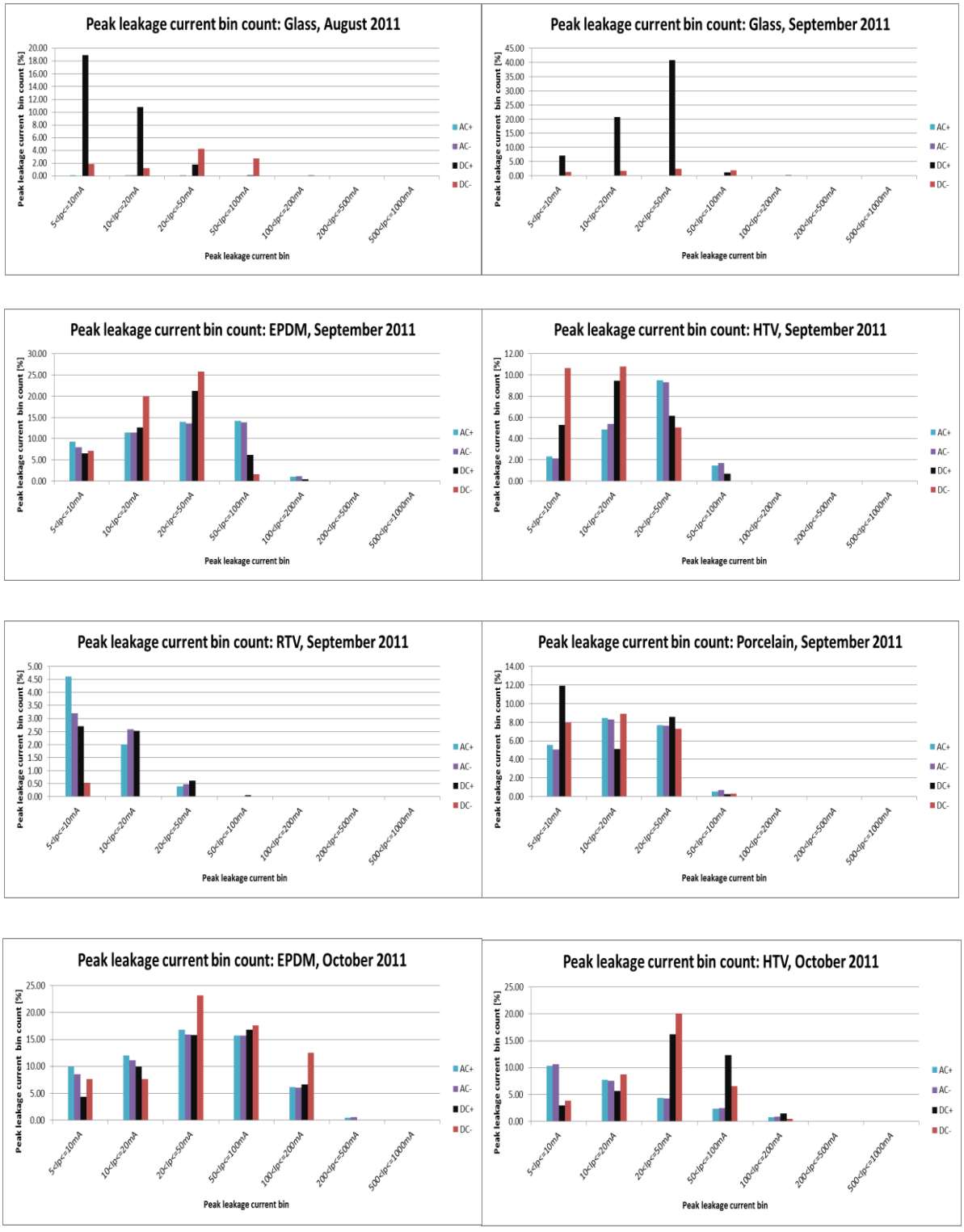

Figure C-15: Peak leakage current bin count comparison for different voltages; August - October 2011

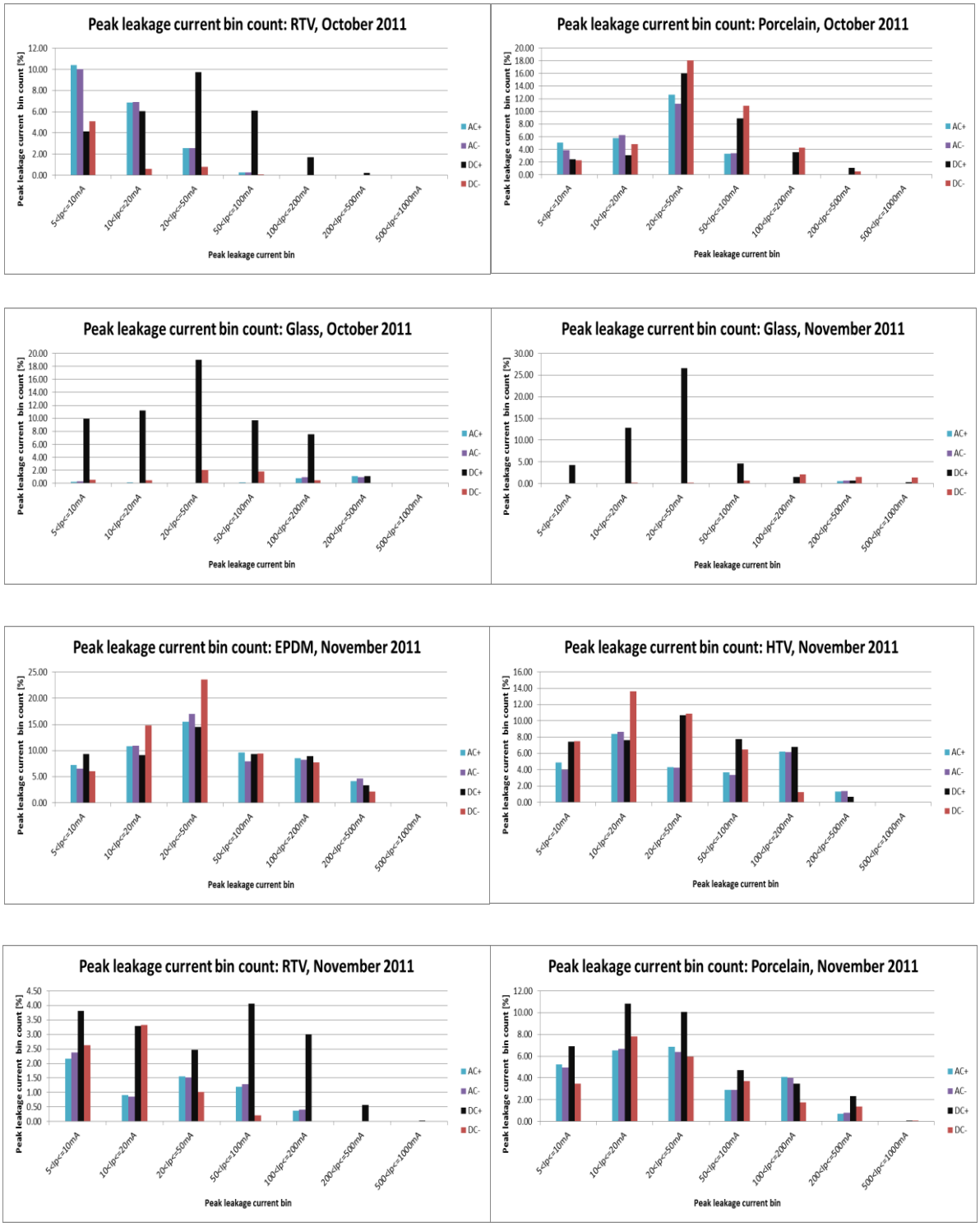

Figure C-16: Peak leakage current bin count comparison for different voltages; October - November 2011

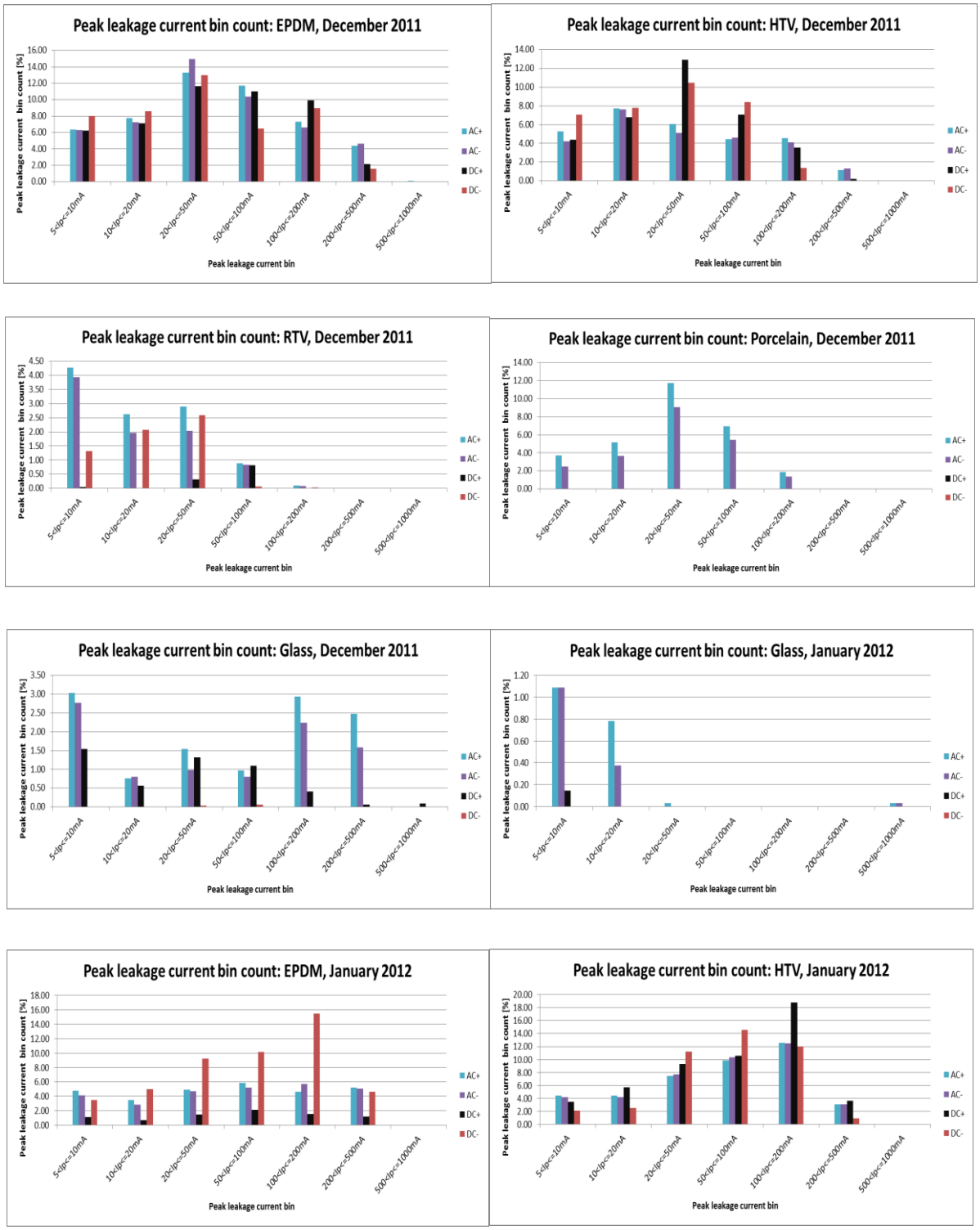

Figure C-17: Peak leakage current bin count comparison for different voltages; December - January 2012

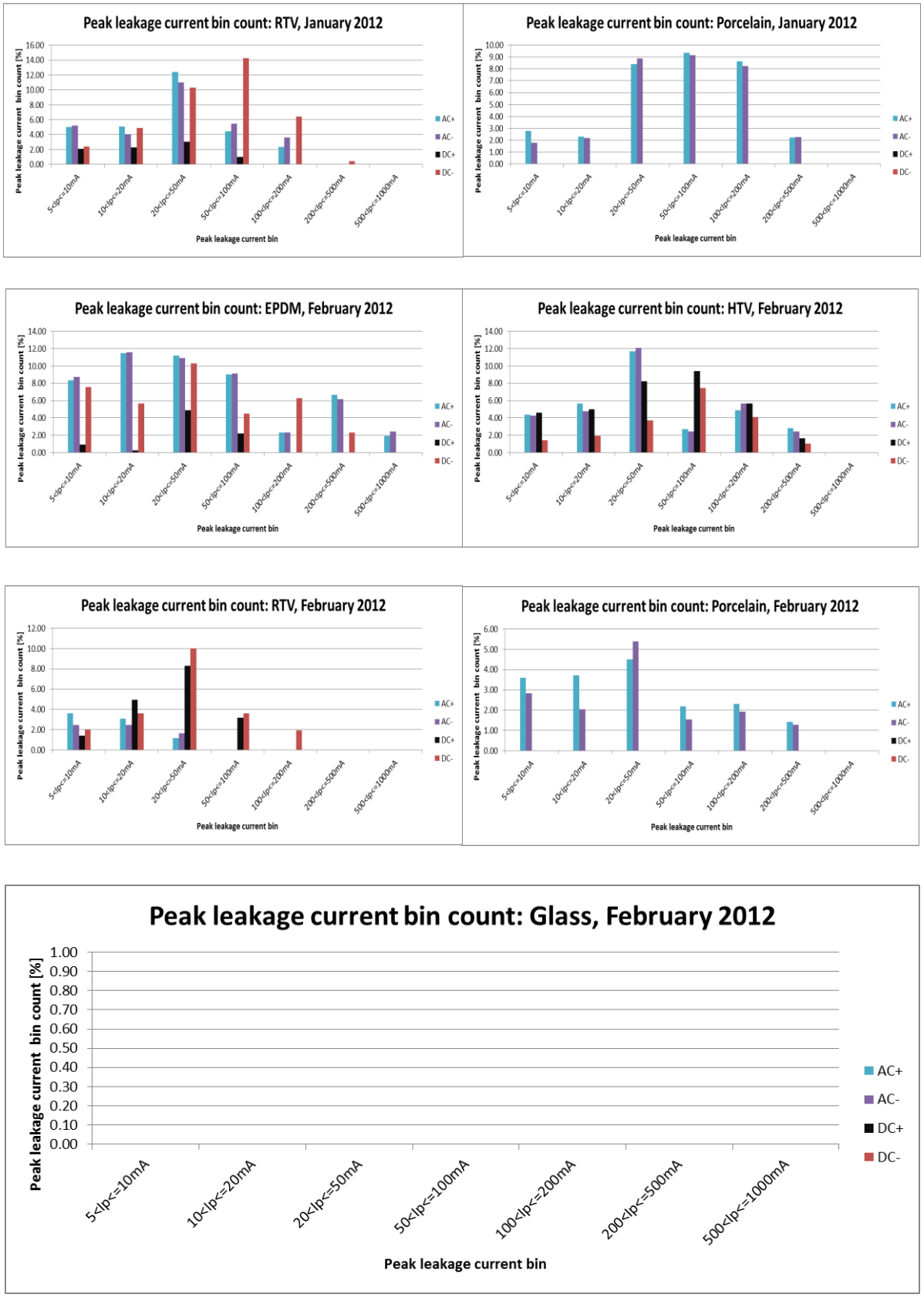

Figure C-18: Peak leakage current bin count comparison for different voltages; January - February 2012

C.4 Peak leakage current bin count: month comparison

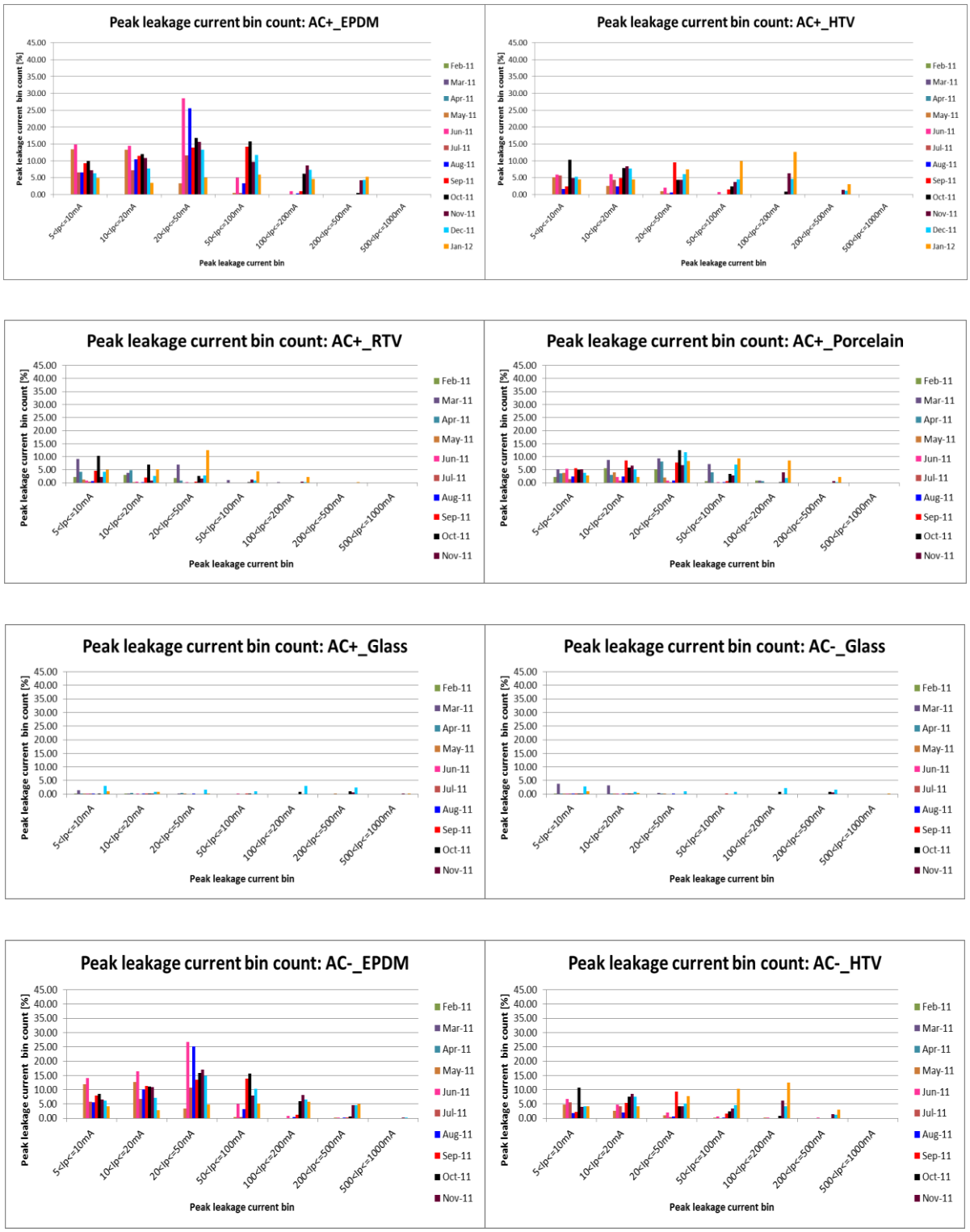

Figure C-19: Peak leakage current bin count comparison for different months; AC- and AC+ voltages

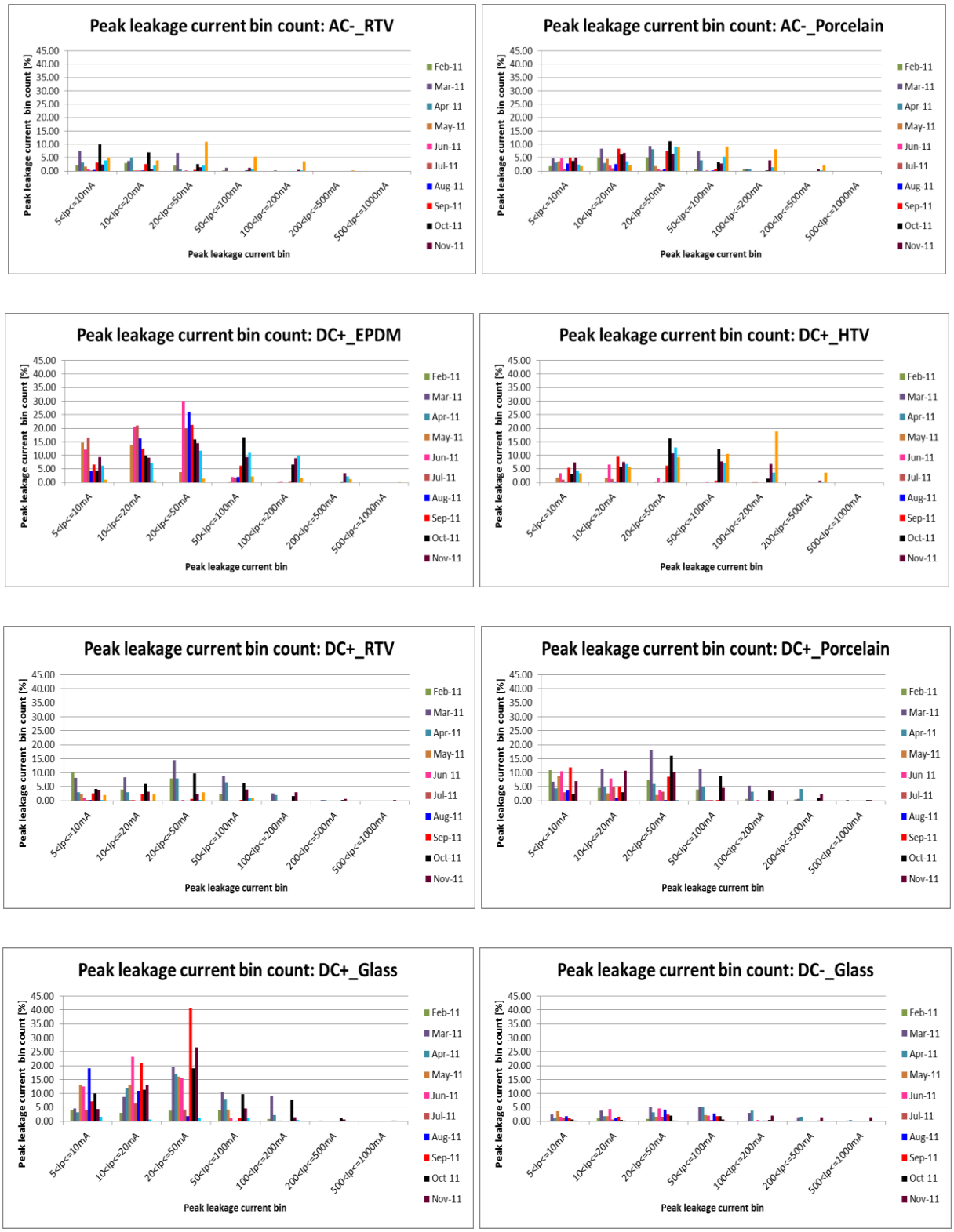

Figure C-20: Peak leakage current bin count comparison for different months; AC-, DC+ and DC- voltages

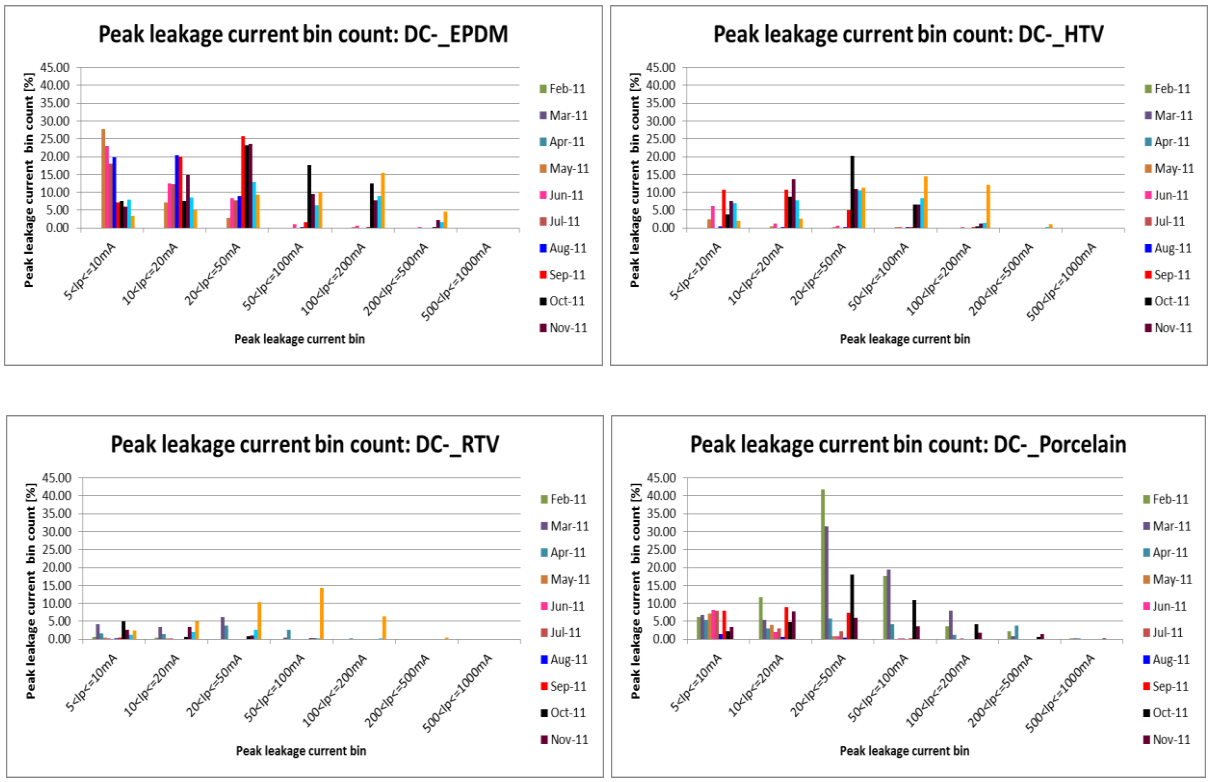

Figure C-21: Peak leakage current bin count comparison for different months; DC- voltage

Appendix D: Electrical discharge activity observations

D.1 Observations on EPDM and HTV insulators

Table D-1: Initial electrical discharge activity observations on EPDM and HTV insulators

		Date						
		2011/05/17 (Day 2)	2011/05/18 (Day3)	2011/05/19 (Day 4)	2011/05/27 (Day 12)	2011/05/28 (Day 13)	2011/05/29 (Day 14)	2011/06/02 (Day 18)
AC	EPDM	DBC on sheath 6, all directions (very foggy conditions experienced)	DBC on top of shed 8, E-direction + WDC on the bottom of shed 8, W-direction	DBC on bottom of shed 2, E-direction + Spot discharge on bottom of shed 8, N & E directions		DBD on sheaths 2 and 9, all directions		
	HTV			WDC on bottom of sheds 1 & 7, N-direction	DBC on bottom of shed 2, all directions		DBD on sheath 3, all directions + Spot discharge on sheath 9, E-direction	
DC+	EPDM	WDC + Spot discharge on bottom of shed 1, NW-direction (very foggy conditions experienced)			DBD on sheath 8, all directions			
	HTV						Spot discharge on bottom of sheds 4, 5, 7 & 8, all directions	DBD on sheath 8, NW-direction
DC-	EPDM	Spot discharge on sheaths 2, 4 & 5, E-direction + Spot discharge on bottom of shed 3, E-direction (Very foggy conditions experienced)			SD on sheath 1, all directions + DBC on bottom of shed 2, all directions	DBD on sheath 8, all directions		
	HTV					Spot discharge on bottom of sheds 2, 4 & 6, E-direction		DBD on sheath 1, all directions

D.2 Observations on RTV, Porcelain and Glass insulators

Table D-2: Initial electrical discharge activity observations on RTV, Porcelain and Glass insulators

		Date								
		2011/02/06 (Day 4)	2011/02/12 (Day 10)	2011/02/14 (Day 12)	2011/02/15 (Day 13)	2011/02/17 (Day 15)	2011/02/18 (Day 16)	2011/02/22 (Day 20)	2011/02/24 (Day 22)	2011/03/08 (Day 34)
AC	RTV				WDC on the rim of shed 1, S-direction		Dryband corona on the bottom of shed 2, W-direction	DBD on the bottom of shed 5, W-direction		
	Porcelain		WDC on the bottom of shed 5, N-direction	Spot discharge on the bottom of shed 4, W-direction	DBC on the ground end-fitting, SW-direction	Dryband discharge on the bottom of shed 5, W-direction				
	Glass									DBC on interface of Glass and cap (ground end-fitting) + DBD on bottom of Glass
DC+	RTV						DBD on the bottom of shed 2, all directions			
	Porcelain	Spot discharge at the interface of shed 1 and the live-side end-fitting, W-direction		Dryband corona on the rim of shed 5, N-direction + Dryband discharge on sheath 5 and shed 5 bottom, N-direction	Dryband discharge on sheath 2, SW-direction					
	Glass								DBD on the bottom of Glass	
DC-	RTV									DBD on sheath 5 E-direction and spot discharge on bottom shed 1 SW-direction
	Porcelain			Dryband discharge on the bottom of shed 5, E-direction	Spot discharge on the top of shed 1, SE-direction	DBD on the bottom of shed 6, top of shed 3 & sheath 3, E-direction				
	Glass								DBD inside Glass, all directions	